UNIVERSITY OF BIRMINGHAM

MECHANICAL AND ELECTRO-MECHANICAL RELIABILITY OF TRANSPARENT OXIDE THIN FILMS FOR FLEXIBLE ELECTRONICS APPLICATIONS

by

DILVEEN WAHEED MOHAMMED

A thesis submitted to the University of Birmingham

for the degree of Doctor of Philosophy

School of Metallurgy and Materials

University of Birmingham

December 2016

Abstract

Flexible electronic devices such as solar cells, touch panels and wearable displays have developed industrially and commercially in recent years because they are flexible and light weight at low cost. Since such devices constitute a brittle oxide layer applied to a polymer substrate, the cracking and/or film damage of the brittle inorganic coating when the device is under different mechanical and environmental loading during processing and service is one of the most important problems in the flexible electronic industry. This can lead to degradation and reduction in electrical functionality of the entire device; therefore, it is important to assess the behaviour of such layers under different mechanical deformation and environmental loads and to develop new mechanical testing for predicting reliability.

This research focusses on the investigation of the reliability of two types of flexible components; indium gallium zinc oxide (IGZO), and Ag-alloy based indium tin oxide (ITO/Ag-alloy /ITO), that are typically used as a channel layer, and as an anode in thin film transistor and solar cell applications respectively. IGZO was deposited on both polyethylene terephthalate (PET) and polyethylene naphthalate (PEN) substrates for investigation including uniaxial tensile and buckling tests coupled with *in situ* confocal laser scanning microscopy. *Ex situ* scanning electron microscopy (SEM) and atomic force microscopy (AFM) were performed to investigate the cracking morphology of the IGZO films after testing. Characterisations of uncoated PET and PEN was also performed.

Furthermore, the electro-mechanical performance and corrosion resistance of ITO/Ag-alloy /ITO were investigated using *in situ* twisting tests, twisting fatigue, corrosion by aggressive salt environments, bending fatigue, bending fatigue-corrosion and long term bending under different temperature and humidity conditions. The changes in electrical resistance was

monitored *in situ* to investigate the relationship between the electrical continuity and the load and as a consequence of failure. In some case spectrophotometer tests were also conducted on the ITO/Ag-alloy /ITO samples. During this work it was found that the IGZO/PEN films can function at up to 2.9% strain which is higher than that of IGZO/PET. Different applied loads and deformation lead to different failure modes.

In twisting test, cracks start to occur at angle of 39° ± 1.7°. The higher applied angles, higher number of cycles and higher temperatures applied were found to cause a higher percentage change in electrical resistance of the ITO/Ag-alloy/ITO during twisting fatigue. The corrosion studies of ITO/Ag-alloy/ITO showed that the increase in NaCl concentration led to the rapid degradation of conductivity and transmittance of such structure. Furthermore, it is shown that the Ag agglomerations are promoted by presence of defects in the deposited films.

During long term bending of ITO/Ag-alloy/ITO high it was found that high humidity was the most important factor enhancing degradation. It is therefore of major importance to consider mechanical reliability and structural integrity of films on flexible substrates in designing devices. It is to be hoped that the experimental study of thin-film electrodes in flexible optoelectronics will contribute to the design of more reliable devices.

Acknowledgments

I would like to express my extreme gratitude to my supervisor Dr Stephen Kukureka for his guidance, patience and research support throughout my PhD studies. I would also like to extend my sincere gratitude to Dr Kostas Sierros at West Virginia University for his inspiring discussions and valuable thoughts on the project.

I am extremely grateful to my collaborator Dr Andrew Flewitt for giving me the opportunity to fabricate IGZO film in the Department of Engineering at the University of Cambridge.

I would like to specially thank Mr Frank Biddlestone for his technical support and ideas during my experiments and I also thank Mr Warren Hay for his help in the workshop.

My thanks go out to Dr James Bowen (now of the Open University) and Miss Chiara Busa for their help with atomic force microscopy in the School of Chemical Engineering.

In addition, I would like to thank DuPont-Teijin for donating polymer samples. My thanks also go to Dr Grzegorz Potoczny for providing ITO/Ag-alloy/ITO/PET samples.

I would like to give my special thanks to my family for their patience and encouragement. In particular, I would like to thank my husband who always gave me his support and understanding during my studies.

Financial support from the Kurdistan Regional Government HCDP programme is gratefully acknowledged.

This thesis is dedicated to

the loving memory of my mother Dian and my father Waheed and

my husband Rayan

and my kids Shayan and Shadiyar.

Contents

1. Introduction

1.1. Background to flexible electronics systems

Flexible electronic technology is delivered by having small-scale structures consisting of thin films that are assembled on a compliant substrate (e.g. polymers) to make the devices suitable for various applications. Flexible electronics date back to the 1960s - silicon solar cells were the first generation of flexible electronics made by a reduction in the thickness of single crystal silicon wafer cells to around 100 μm and then mounting them on a flexible substrate [1,2]. After further development, processes such as roll-to-roll manufacturing (aiming to replace batch processing) and the various thin-film coating methods such as magnetron sputtering were further advanced. Optoelectronic materials on flexible substrates for large-area applications including solar cells, touch panels, liquid crystal displays (LCDs), flexible organic light-emitting diodes (OLED) and biomedical devices were also developed. These devices offer a number of advantages such as light weight, the capability of conforming to the shapes different structures, robustness and being amenable to low cost (roll-to-roll) manufacturing processes [3]. Figure 1-1 gives examples of flexible optoelectronic devices. In particular, flat-panel displays and solar cells are visible examples of flexible electronic devices at present and will be discussed in greater detail in the next section.

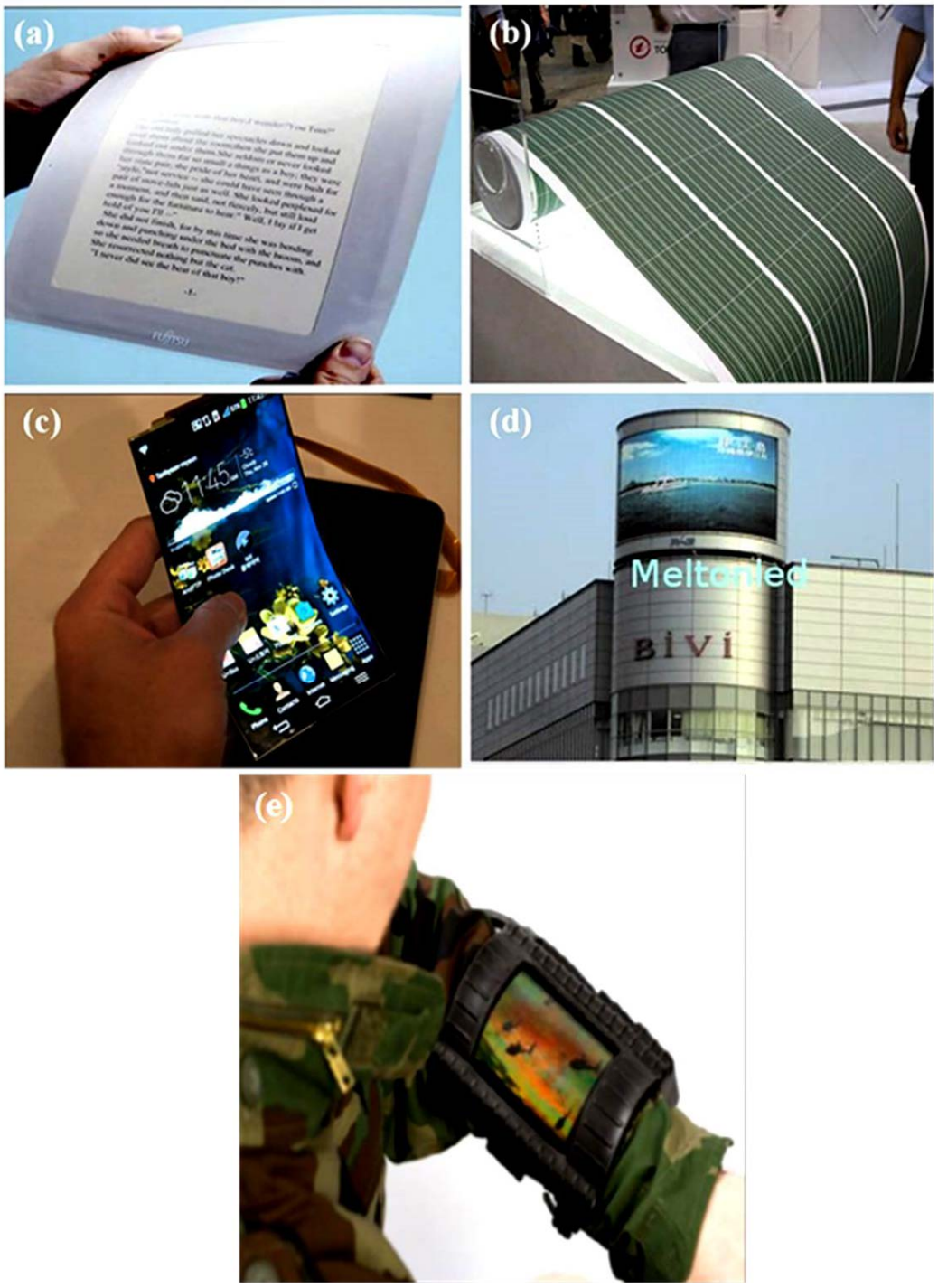

Figure 1-1 Examples of flexible displays: (a) Flexible tablet [4](b) Flexible solar cell [5](c) bendable smart phone [6](d) LED display screen [7](e) Display worn on sleeve [8].

Flat-panel displays (FPDs) have been commercially used as the displays of choice in various applications replacing cathode ray tubes in flat-panel TV, and cellular phones since 2000.

FPDs are expected to overtake other electronic devices in sales over the next few years. The current FPDs available in the market use glass as a substrate [9]. However, the market opportunities for FPDs fabricated on flexible plastic substrates have rapidly grown so that several research groups and electronics companies are investing in the development of new generation displays. For instance, in 2005 Philips presented the first prototype of a rollable electronic display and Samsung have demonstrated flexible liquid-crystal panels [10].

In addition, the small size and light weight of flexible and rollable displays will make them very valuable for military applications [11]. For instance, a 101.6 cm display on a 0.2 mm thick plastic substrate would only weigh approximately 500 g. It is lighter by two order of magnitude compared with cathode ray tube displays [12]. Another flexible optoelectronics device that is becoming possible at low cost is a regenerative energy source and inexpensive alternative to traditional photovoltaic cells in the form of a flexible solar cell. Recent progress in roll-to-roll manufacturing processes has made it possible to fabricate solar cells on flexible substrates at low cost.

In addition, it has been suggested that if solar cells covered an area of 100 x 100 km in the deserts of Arizona then they would meet the whole electricity requirements of the United States [13]. Robust plastic sheets are much less likely to break than glass panels therefore that can reduce the cost of applications in the desert. So far, the power conversion efficiency which flexible solar cells have achieved is up to 10% [14]. Figure 1-2 shows market prospects for the solar industry. The structure of flexible optoelectronic devices usually comprises a substrate, transparent oxide inorganic anode, thin-film transistor (TFT) layer, electro-optic materials, metal cathode, and barrier layers as shown in Figure 1-3 [15]. In terms of a substrate material, polymers are being considered as good alternatives as substrates materials for flexible electronic devices. They can replace traditional brittle glass substrates that are

currently utilized in FPDs such as plasma discharge panels and LCDs [15]. This is because of their satisfactory optical transmittance, mechanical flexibility, light weight, low cost and they can be rolled away when not required [16]. However, the physical properties of polymers substrates have a significant influence on the flexible electronic device efficiency and performance. In addition, organic polymer substrates cannot meet all the requirements of commercial success for flexible electronic devices such as solvent resistance, scratch resistance, barrier properties and low coefficient of thermal expansion (CTE) coupled with a smooth surface. Therefore, polymers are likely to need an additional barrier layer when applied in the fabrication of TFTs and displays such as OLEDs for protection against oxygen and moisture [17].

Among the materials which are used inside these flexible electronics devices, transparent semiconductive and conductive oxides, such as indium tin oxide (ITO), zinc oxide (ZnO), gallium doped zinc oxide (GZO), indium gallium zinc oxide (IGZO) and zinc tin oxide (ZTO), have attracted many researchers. Firstly, due to their low electrical resistivity and high optical transmittance they are used as transparent anodes in OLEDs and LCDs as shown in Figure 1-3 [18]. Secondly because of their high electron mobility, processing compatibility with plastic substrate materials, good-uniformity, and transmittance in the visible spectrum (400-700 nm) they are used as a channel layer alternative to hydrogenated amorphous silicon (a-Si:H) in TFTs as shown in Figure 1-4 [19,20]. However, the high cost of indium encourages the reduction of the quantities employed in fabrication. It is difficult to reduce thickness to under 150 nm in the case of single ITO films because of the decreased electrical connectivity with thickness decrease [21]. Therefore, a very thin metal film can be inserted between ITO films to show higher conductivity than of a single ITO layer of the same

thickness [21]. Such a multilayer system has been shown to be effective in achieving electrically conductive and optically transparent electrodes by optimising the thickness of the ITO layer [22]. Usually, silver (Ag) film is used as the metal layer because Ag thin films exhibit the highest conductivity in comparison with all other metals [23].

A large differential thermal expansion and mechanical mismatch between the brittle ceramic layer and organic polymer substrate is a significant challenge to manufacturing processes of reliable flexible electronic devices, as well as their use and maintenance. In particular, during the fabrication processes the depositing of a high modulus ceramic layer on a polymer substrate will subject it to thermo-mechanical loads, that may cause cracking and/or buckling delamination [10,24,25]. In use, flexible electronic devices will suffer from different mechanical loading such as stretching, bending and twisting repeatedly and also will suffer from environmental loading for example temperature changes and corrosion. This can lead to rapid degradation of optoelectronic device performance [26]. Therefore, failure mechanisms and the influence of cracks on the electrical properties of brittle inorganic thin film materials on organic polymer substrates become important parameters to design new devices that can be used without losing their functional properties under mechanical loading.

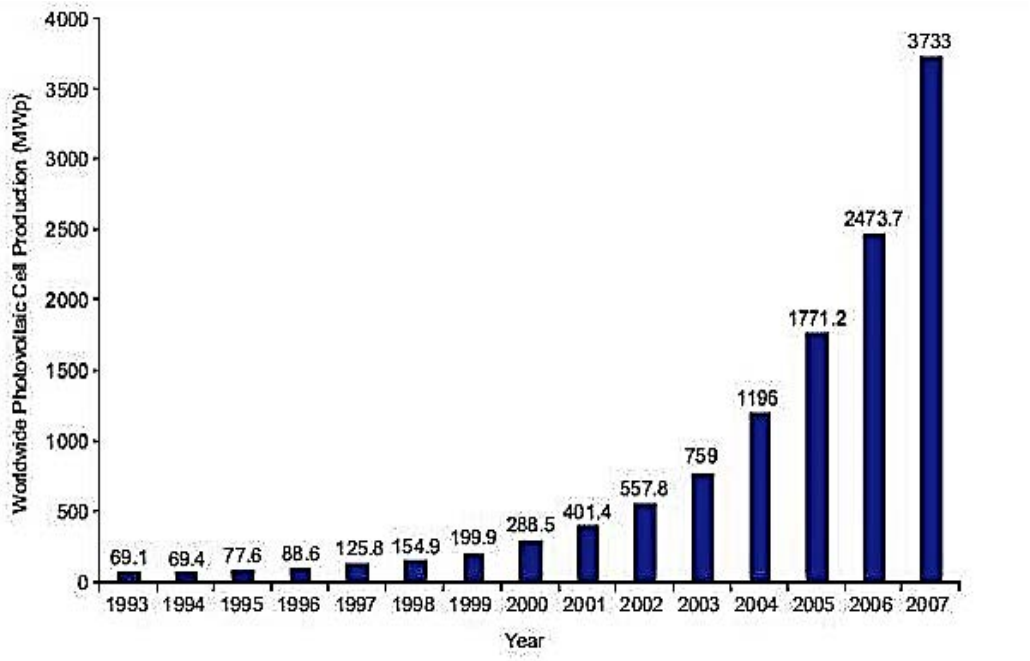

Figure 1-2 Early photovoltaics production worldwide [27].

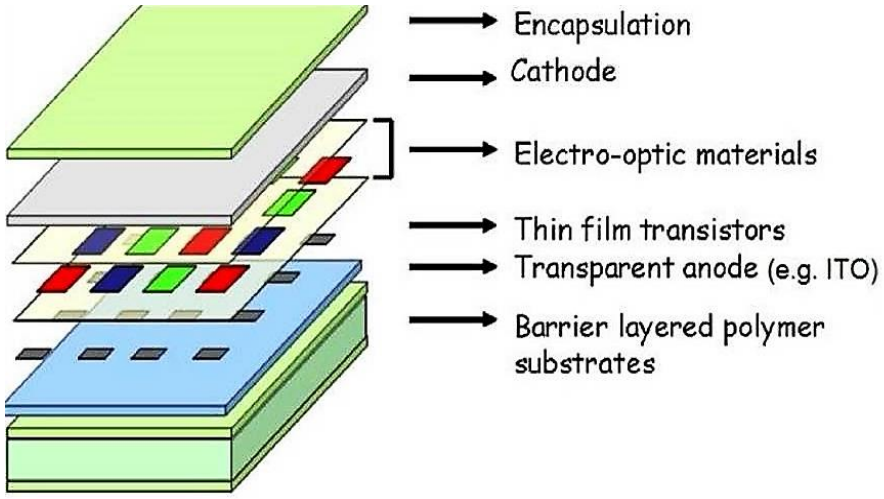

Figure 1-3 Cross-sectional structure of electronic device on a flexible substrate [15].

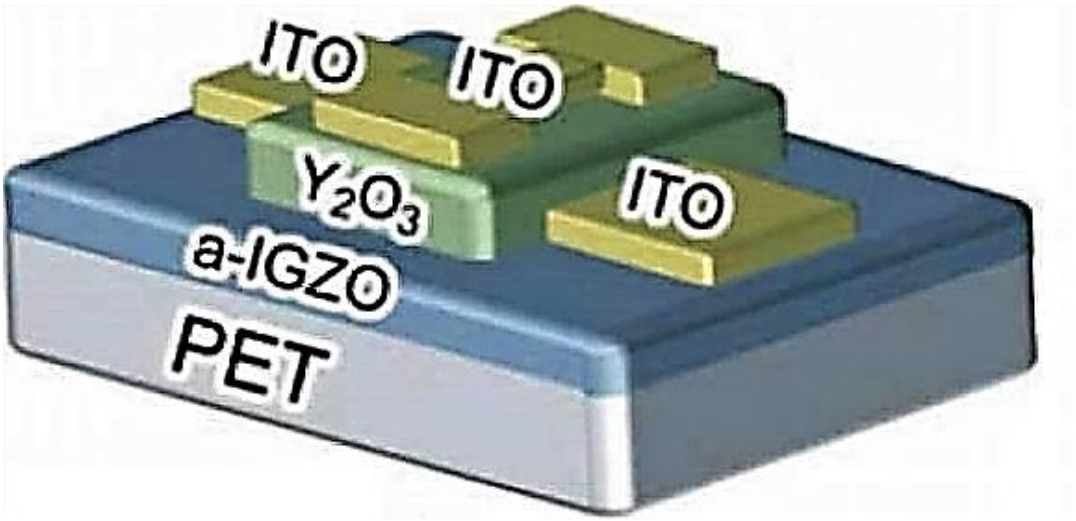

Figure 1-4 Schematic cross-section of TFT with channel layer and source/drain electrodes and gate of IGZO and ITO and Y_2O_3 respectively [28].

1.2. Scope of this work

There are currently new developments in the use of thin films for optoelectronic applications based on IGZO and ITO/Ag-alloy /ITO that are used respectively as a channel layer and as an anode in TFT and solar cell applications. However, there are significantly fewer studies on the performance of IGZO and ITO/Ag-alloy/ITO coated polymer substrates under mechanical and environmental loading than of other materials. Most studies focus purely on functional performance rather than on mechanical and electro-mechanical reliability of flexible optoelectronics components and devices. Some reviews and studies on mechanical reliability have been published and there have been some research studies developing this area. The present work aims to develop the understanding of mechanical and electromechanical reliability of flexible optoelectronics components and of test methods for these materials and

components. In addition, this research will aid materials and parameter selection to help optimise flexible electronic devices.

1.3. Outline of the Thesis

Chapter 2 will begin with introduction to polymer substrate and in particular the production and characterization of PET and PEN are reviewed. In the next section transparent thin films on polymer substrates for optoelectronic device applications will be introduced. Then there is an overview of the literature on mechanical and electromechanical properties of thin film under different loading and environmental condition.

Chapter 3 will present the materials, experimental setup and methodologies used in this project.

Chapter 4 will provide results of characterization of the PET and PEN.

Chapter 5 will report the results of characterization of sputtered IGZO on PET and PEN substrates followed by description and discussion of the results of IGZO/polymer subjected to uniaxial tensile and buckling tests.

Chapter 6 will discuss the results of twisting and cyclic twisting experiments conducted using ITO/Ag-alloy/ITO films coated PET substrates.

Chapter 7 will present the results and discussion of corrosion and corrosion-fatigue experiment studies of ITO/Ag-alloy/ITO films. In addition, the result of long term bending durability of ITO/Ag-alloy/ITO under different temperature and humidity conditions will be discussed in detail.

Chapter 8 will provide the conclusions of the thesis and recommendations for future work.

2. Materials for flexible electronic devices

2.1. Substrates for use in flexible electronic devices

The mechanical flexibility of electronic devices is significantly dependent on the choice of substrate material. Substrate materials which have been considered include thin glass as well as metal foils and polymers. By reducing the thickness to 100 μm, thin glass films can be made flexible. Glass is currently used as standard substrate material for FPD fabrication [10], exhibiting good moisture and oxygen barrier properties, and offering a high transmission rate in the visible range and a low CTE [29]. Thin glass, however, is brittle and this limits its ability to be used in large-scale manufacturing processes [3].

Metal foils can withstand high temperature processes resulting in excellent barrier layer properties against moisture and oxygen without problems of breakability [30]. Foil could provide an ideal substrate for TFT fabrication used to make top-emitting active matrix OLED devices. However, foil can only work for applications where transparency is not required and cannot function with multiple bends. Also, metal foil substrates are expected to have higher cost compared to polymer substrates [10]. Therefore, polymer materials offer the best option as a substrate in flexible electronic devices, because of their satisfactory optical transmittance, mechanical flexibility, light weight, low cost and suitability of mass production via the roll-to-roll manufacturing process [15].

2.1.1. Polyethylene terephthalate and polyethylene naphthalate

In 1941 Whinfield and Dickson discovered polyethylene terephthalate (PET) [31]. Shortly after the discovery of PET, polyethylene naphthalate (PEN) was developed by Cook, Huggill and Lowe in 1948 [32]. Both PET and PEN thermoplastics are almost ideal substrates for flexible electronic applications. They have good mechanical properties, good surface quality, high resistance to most environments and they are suitable for roll-to-roll fabrication processes [33]. As a result, they have been used to meet the demanding requirements of flexible applications such as (OLEDs) [32].

In addition, PET and PEN are semicrystalline polymers from the same polyester family but have different characteristics including chemical, physical, mechanical, and thermal properties which result from their chemical structure [34,35]. The structure is shown in Figure 2-1.The substitution of the phenyl ring of PET by the naphthalene double ring of PEN gives PEN some attractive features, for example: high glass transition temperature, good mechanical properties such as high modulus and tensile strength and excellent dimensional stability [31] even when exposed to temperatures up to 180 ^{o}C [36]. The glass transition temperature is the temperature at which the mechanical behaviour of the amorphous part of the polymer changes from glassy to tough and leathery behaviour. Table 2.1 shows some important parameters for (PET and PEN) flexible substrates. Furthermore, PET and PEN polyester films can achieve both excellent surface smoothness and increased scratch resistance (required for many flexible electronic applications) by using planarization coatings [35], and both PET and PEN also show a good optical transmission of above >85% in the

visible light range and haze of less than 0.7%. These are desirable for display applications [34].

(a) **(b)**

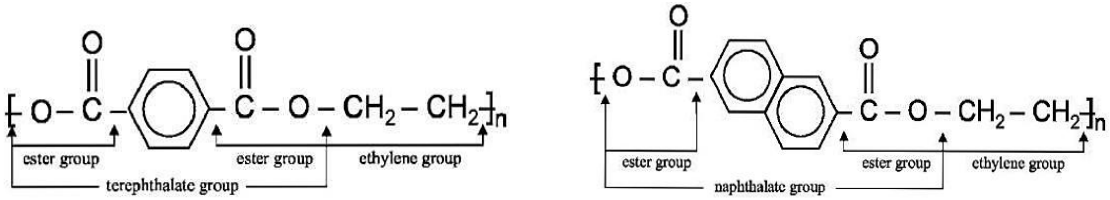

Figure 2-1 the structure of (a) polyethylene terephthalete (PET) (b) polyethylene naphthalate (PEN) [37].

Table 2.1 properties of PET and PEN substrates.

Property	**PET**	**PEN**
Young's modulus, E/ (GPa)	4.5, 4.9 at 25 °C 1.4 at 120 °C [38]	5.0 at 20 °C [36]
Melting temperature, $T_{m/}$ /(°C)	256 [38]	263 [35]
Glass transition temperature, T_g/(°C)	78 [38]	120 [32]
Coefficient of thermal expansion (up to 150 °C), CTE (ppm/°C)	20-25 [35]	18-20 [35]

2.1.2. Drawing behaviour of PET and PEN films

Molecular orientation and drawing during uniaxial or biaxial industrial processing has a great influence on the final polyester film product. As reported by De *et al*. [39] , at a low degree of crystallinity the mechanical properties of semicrystalline polymers seems to be predominately affected by orientation in the amorphous regions. They also conclude that the amount of uniaxial or biaxial orientation not only has an effect on mechanical behaviour but it also affects other properties such as thermal properties and transparency.

Figure 2-2 shows processing to produce PEN and PET film. In the first stage the polymer is extruded as a sheet at a temperature above its melting point (T_m). It is then quenched to form an amorphous film before biaxial drawing. In the second stage the film is heated to temperature of 85 – 90 °C and aligned in the machine direction (MD). Oriented and crystalline film of up to 10-30%, can be achieved, which causes the film to exhibit higher modulus and strength. Then the film is heated to above 100 °C and stretched in the transverse direction (TD). After drawing in both machine and transverse directions the film becomes crystalline by 25 - 40%. In order to reduce the shrinkage, the polymer films are usually heat stabilized. A planarizing coating (the details of this coating are commercially sensitive and so not available) can also be applied to control the surface quality which is required for subsequent depositing layers [36].

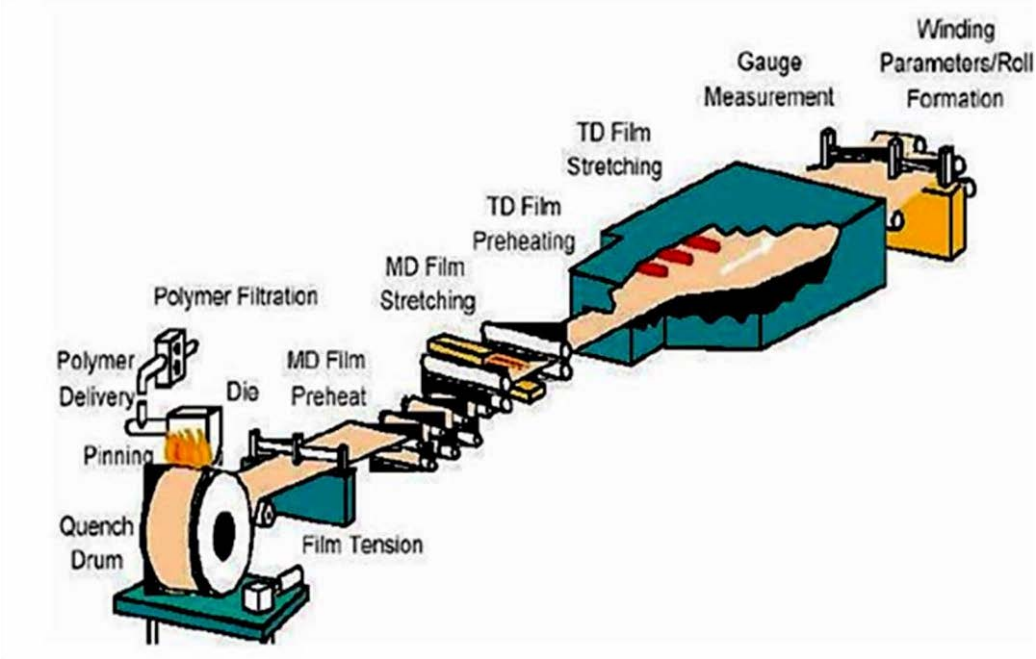

Figure 2-2 A typical PEN and PET film manufacturing process [40].

Kim et al. [41] studied the effect of biaxial deformation on the optical, thermal and mechanical properties of PEN films as well as a blend of PEN with polyetherimide (PEI). They pointed out that the refractive indices in the normal direction decreased as an areal expansion ratio (the product of the draw ratios in the both the transverse and machine directions) increases. This observation is attributed to the preferential orientation of flat naphthalene groups parallel to the film surface at high expansion ratio. They also found that the biaxially stretched PEN films exhibited a bimodal orientation behaviour with one population oriented in the MD and the other in the TD. This orientation behaviour causes the PEN film to exhibit lower modulus in the direction between MD and TD. However, they conclude that bimodal orientation is eliminated and biaxially stretched film was observed to show mechanical isotropy properties when PEN blended with 10 to 20% concentration of PEI.

Cakmak *et al.* [42] observed necking behaviour when PEN was stretched between 117 ^{o}C Tg (glass transition temperature) and 195 °C T_c (cold crystallization temperature). They pointed out that in order to achieve high quality PEN film, high stretching at temperature range 135-150 °C should be applied. They also conclude that mechanical properties such as yield strength, modulus and tensile strength of PEN film can be improved by biaxial stretching [42].

Bauer [43] reported the influence of the degree of stretching and heat setting on density, shrinkage and oxygen permeability of biaxially stretched PET, PET modified copolymers and blends. The density increased with both degree of stretching and also with the heat-set temperature, regardless of composition for the samples tested. The density of all films was independent of the degree of stretching at high heat-set temperature of 180^{o}C. It was found that by increasing naphthalate content in PET films and increasing heat set temperature, shrinkage and oxygen permeability decreased. Also, shrinkage was found to increase while oxygen permeability decreased with the increase in degree of stretching for all films.

Sharma and Misra [44] investigated the stress-induced crystallization of amorphous PET film by varying the stretch condition such as stretching rates ranging from 100-600 % per minute at 85 °C. A decrease of elongation at break and increase of elastic modulus and yield stress were observed with the increase in stretching rate. They found that birefringence, and amorphous orientation values increased as the stretching rate increased. The authors also showed that the amount of film relaxation is reduced at high stretching rates, and hence gives high strength and orientation to the film. However, a significant amount of relaxation takes place at low stretching rates, resulting in low strength and orientation of the film.

Maruhashi and Asada [45] examined the effect of various parameters of the stretching process on the shrinkage behaviour of PET sheet. More thermal stability was found when PET was stretched with high speed at high temperature in comparison to that stretched with low speed and low temperature. They point out that this is due to high crystallinity and relaxation of molecular chains in the amorphous state. Until the draw ratio reached 2.0, the shrinkage increased as draw ratio increased while above that the shrinkage decreased as draw ratio increased.

Mody *et al.* [46] studied the thermal shrinkage of sheet PET (homopolymer and copolymer) as a function of parameters of the stretching process. It was observed that percent shrinkage of both homopolymer and copolymer samples stretched in both biaxial and uniaxial modes increased with increasing stretching speed. Amorphous orientation and crystallinity orientation function were found to increase with increase in stretching speed and extension ratio. This observation was similar to that reported by Sharma and Misra [44]. They finally concluded that the biaxially oriented samples exhibit higher activation energies of shrinkage in comparison to those measured for uniaxially oriented samples, thus providing good dimensional stability as compared with those uniaxially oriented.

2.1.3. Thermal properties

Polymers have two main transition temperatures which are the glass transition temperature (T_g) at which the movement of polymer chains segments increases, and melting temperature (T_m) at which the chains move out of their crystal structures. In the case of PEN the structure containing a naphthalene double ring provides significant rigidity and hence has a significant

effect on T_g while having an extremely slight effect on T_m only by ~10 °C as shown in Table 2.1 Therefore, PEN shows a high T_g of 120 °C when compared to that of PET (70 °C).

Dimensional and thermal stability of the polymer substrate is particularly necessary to be able to withstand elevated temperatures during device manufacturing and processing in order to achieve high levels of integration of the different layers in the final product [47]. It is necessary because, for instance, problems may occur with deposition of the electrode, barrier coatings, patterning and TFT fabrication. T_g and CTE of a polymer are important factors for controlling dimensional stability. Because of molecular relaxation and shrinkage or expansion during the processes, polymer films undergo a significant change in their dimensions at T_g. In this regard PEN, with a 120 ^oC T_g can be a better option in comparison to PET in applications when exposed to elevated temperatures [34]. However, PET and PEN films can be subjected to a thermal relaxation process to enhance further their dimensional stability for OLED display applications. Some shrinkage occurs because of the relaxation of the molecular orientation in the amorphous regions [32]. In addition, the low CTE of the substrate, relatively close to the inorganic layer is an advantage for fabricating devices with dimensional stability. Polymer substrates have much higher CTEs than inorganic layers used for electrode layers or barrier layers, therefore at high deposition temperature the large CTE mismatch induces high stress levels in the layers and cracks them under thermal cycling during manufacturing processes [15].

Heat stabilised PEN film has shrinkages of lower than 0.1% after 5 minutes at 180 ^oC but heat stabilised polyethylene terephthalate possesses low shrinkage up to a temperature of 150 ^oC [34].

2.1.4. Optical Properties

Biaxially oriented PET and PEN perform extremely well in applications where transparency over 85% in the 400 - 800 nm range coupled with a haze of less than 0.7% are required such as bottom-emissive displays [36]. PEN exhibits high absorption up to wavelengths of 380 nm in comparison to PET's absorption up to a wave-length of 313 nm that contribute to or from the naphthalene ring which possesses a more extended chromophore. For applications requiring high UV absorption, PEN is the ideal option [31]. Both PET and PEN are optically birefringent, as noted by MacDonald [36]. Anisotropic optical properties of PET and PEN are highly dependent on the orientation process, thus they are unsuitable for LCDs use because the birefringent film would change the polarization state of the LCD (and LCD displays need to control the polarization). However amorphous substrates, such as polycarbonate (PC) and polyethersulfone (PES), that are more likely to be used in LCDs are not birefringent substrates [48].

2.1.5. Crystal structure

Semi-crystalline polymers consist of an amorphous part where molecular chains are randomly arranged in space, and a crystalline part where the molecular chains have a regular form and orientation. On cooling from the liquid state, spherulites can be formed. Spherulites grow from the inside of the crystal nucleus to the outside with free space in between the various individual units. The free space is filled with amorphous polymer as shown in Figure 2-3, where a layer format referred to as lamella is formed.

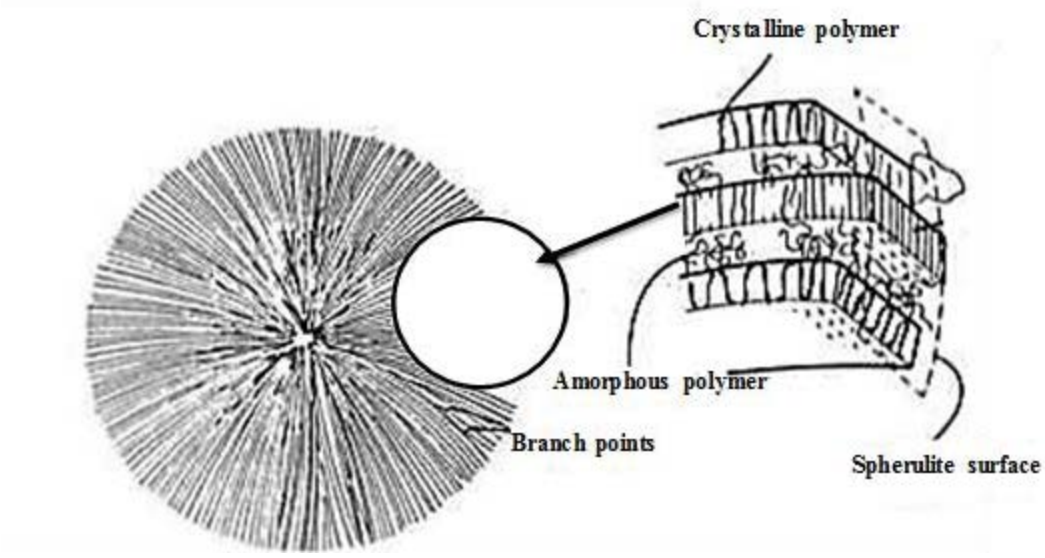

Figure 2-3 Schematic illustration of the spherulitic semi-crystalline polymers [49]**.**

The degree of crystallinity and the size and arrangement of the crystallites in a semi-crystalline polymer has a profound impact on the mechanical and physical properties of polymers [50]. Polymers with a high level of crystallinity exhibit a higher T_g, higher modulus, higher tensile strength, higher toughness, and greater resistance to solvents [51]. Various experimental techniques such as measurements of density, differential scanning calorimetry (DSC) and X-ray diffraction (XRD) are used for determination of the degree of crystallinity [52]. DSC is a rapid method for measuring polymer crystallinity based on heat of fusion measurements which is the amount of energy required to accomplish the solid-to- melt phase change. Therefore, DSC was also used in this work.

2.1.6. Surface properties

The surface quality of both PET and PEN polyester films can be controlled to an extent by close control of the polymer recipe, film processing and web-cleaning techniques. However, sporadic surface peaks from internal contamination may still remain in the polymer film due to manufacturing of films in a non-clean environment [34,36]. Therefore, to eliminate these types of defects and to satisfy requirements of various flexible electronic devices, a planarising coating is necessary. For providing low level of intrinsic and extrinsic contamination the planarising coating process is carrying out in a clean room. These coatings provide not only surface smoothness but also hardness to prevent surface scratches during further processing and handling [34,35]. (The details of these coatings are subject to commercial confidentiality and are not available).

2.1.7. Chemical resistance and barrier properties

During manufacturing processes for flexible electronic devices such ink-jet printing, polymer substrates will be subjected to several solvents as well as chemical solutions, therefore high chemical resistance is another important factor to be considered when choosing substrate materials for OLED display applications. Amorphous polymers possess poor solvent resistance whereas semicrystalline polymers such as PEN and PET have a high resistance to many acids and organic solvents, thus a hard coat is necessary to provide solvent resistance for amorphous polymers [53].

Electronic devices, such as OLEDs are highly sensitive to moisture and oxygen, in comparison with LCDs because the thickness of the layers in an OLED is in the range of 100

to 200 nm, and any defect that protrudes from the surface is likely to have deleterious effects on the device performance [54]. Low work function metals including Ca, Li and Mg have been utilized as cathodes in OLEDs which are unstable in the air and moisture atmosphere compare to higher work function materials such as Al and Ag that would also accelerate the degradation process [15].

Water vapour transmission rates (WVTR) and oxygen transmission rates (OTR) of 10^{-6} g/m^2/day and 10^{-5} cm^3/m^2/day respectively are required for OLEDs [33]. PET and PEN, have barrier properties of the order 10^{-1}–10^{2} cm^3/m^2/day OTR and g/m^2/day WVTR. To improve permeation-barrier performance significantly and to match OLED display requirements [55] , polymer based substrates will be multilayer composite structures [47,54]. As shown by Affinito *et al*. when they deposited polymer and aluminium oxide layers on polyethylene terephthalate substrate (polymer / Al_2O_3 / PET) oxygen and water vapour permeation rates for (polymer / Al_2O_3 / PET) structures are lower by four orders of magnitude than for PET substrates alone and lower by three orders of magnitude than for (Al_2O_3 /PET) structures [56].

2.1.8. Mechanical properties

Mechanical properties are another significant factor for polymer substrates. During roll-to-roll manufacturing processes polymer substrates will undergo various stress states and mechanical deformation modes. Flexible electronic devices such as OLEDs usually contain polymer substrates, brittle inorganic anodes and a TFT layer. There is significant mechanical mismatch between the organic substrate and inorganic layer which causes mechanical failure in devices.

Therefore, understanding the mechanical properties of polymer substrates is essential to achieving the performance required of substrates for flexible optoelectronic applications.

The higher draw ratio capacity of PEN yields highly oriented film with better mechanical properties compared with PET film [31]. As mentioned before, the high rigidity of PEN results from the double ring in its main structure. Macdonald *et al*. [47] found that the stiffness of both PEN and PET decreased as temperature increased. However, PEN is stronger and stiffer with a Young's modulus almost twice than that of PET at a temperature range from 120-160 ^{o}C.

2.2. Thin film for use in flexible electronic devices

2.2.1. Indium Tin Oxide (ITO)

Indium tin oxide is one of the most common transparent conductive oxides (TCO) used as anode material in optoelectronic applications including FPDs, solar cells and TFT [57–59]. ITO is a compound of indium (III) oxide (In_2O_3) and tin (IV) oxide (SnO_2), typically 90% In_2O_3, 10% SnO_2 by weight [60].

ITO is produced by substituting Sn as the dopant in In2O3; it replaces the In3+ atoms in the indium oxide cubic bixbyite structure. Tin thus forms an interstitial bond with oxygen as SnO or SnO2. The conductivity of ITO is influenced by the valency state. A low valence and a low Sn levels creates hole which acts as a trap and decreases conductivity due to a decrease in the carrier concentration [61]. On the other hand, high valence state and high Sn content results in an increase of conductivity as a result of Sn+4 acting as an n-type donor releasing electrons to the conduction band [61]. A crystalline form of the semiconducting ceramic film exhibits free

electrons created within the grains and electrons trapped at the grain boundaries [62], whereas the amorphous form of ITO is less conductive. The thermal expansion coefficient of ITO is $7.2\times10^{-6}\ °C^{-1}$ [63], so that thermal stresses would develop when ITO is deposited on flexible polymer substrates at high temperature.

ITO films demonstrate a wide band-gap energy approximately between 3.5 and 4.3 eV resulting in a high optical transparency in the visible region (1.7–3.1 eV). However, defects such as grain boundaries, vacancies, etc. that exist in the deposited film are detrimental to the transmittance of ITO film [18].

High optical transmittance (>90%) and low electrical resistivity $\sim7\times10^{-4}$ ($\Omega.\mathrm{cm}$) enable ITO to be a good candidate material for optoelectronic device applications [59]. However, two drawbacks of ITO limit its application in flexible electronics. The first limitation is the rarity of indium that results in increasing the price of ITO [64] and contributes to the reduction of the quantities employed for films fabrication. The second limitation is the brittle nature of ITO that make it susceptible to cracking and delamination when it is under mechanical deformation during manufacturing and in service conduction [25]. Therefore, finding films with low cost and more sustainable alternatives are important research aims.

2.2.2. Indium gallium zinc oxide (IGZO)

IGZO is a compound of indium, gallium, zinc and oxygen. When combined in the proper ratios these elements form a semiconductor thin film than can be used as an extremely promising alternative to a-Si:H for TFTs [65]. This is because IGZO exhibits high saturation mobility μ_{sat} in the range of (10-50 $cm^2/V.s$), processing compatibility with plastic substrates,

good-uniformity and high transparency in the visible wavelength region (400−700 nm) [19,65,66]. High transmittance of IGZO facilitates another promising application for IGZO as an alternative transparent anode to ITO which is an important part in photovoltaic devices [66]. However, further improvements of its physical properties are still required for practical applications.

2.2.3. ITO/metal/ITO multilayer structures

Currently, TCO based on a single layer structure of ITO or ZnO are commonly used, however TCO electrodes with higher conductivity and transmittance are required for new and advanced devices.

TCO/metal/TCO multilayer structures could potentially offer high conductivity at reasonable transmittance and with a decrease in film thickness. This means that multilayer performance would be superior in comparison to single-layer electrodes [67]. Both uniform and continuous metal thin film are key factors in achieving both low sheet resistance and high transmission in TCO/metal/TCO structures. The typical thickness of metal layer is in the range of 5–20 nm. Thicker layer thickness would address the continuity issue but would cause a significant reduction in transparency [67].

To achieve the desired properties, it means that less of the TCO is required in a multilayer structure. This is particularly important for ITO since there is increasing interest in the reduction of the indium quantities employed for ITO film fabrication due to the high cost of indium. It is difficult to reduce the thickness under 150 nm in the case of a single ITO film owing to the decrease in the electrical connectivity with the thickness decrease. Therefore, a

very thin metal film can be inserted between the ITO film to show higher conductivity than that of a single ITO layer of the same thickness [21] and can take the advantage of the mechanical properties of a ductile metallic interlayer [68]. Such a multilayer system has been shown to be effective in achieving electrically conductive and optically transparent electrodes by optimising the thickness of the ITO layer [22]. As mentioned earlies, Ag is the most commonly used middle layer for TCO/Ag/TCO multilayers since Ag thin film has the lowest resistivity of approximately 2×10^{-6} Ω. cm in comparison with all other metals [23]. Copper (Cu) is close behind as it only exhibits slightly higher resistivity [69]. Also, Ag-based alloys including Cu, Au and Pd have been used for interlayers. Such metallic elements may improve stability to heat and moisture of the ITO/Ag-based alloy/ITO electrodes [67].

It has also been reported by Park et al. [70] that an ITO/Ag/ITO multilayer electrode deposited on polyethersulphone (PES) substrate by roll-to-roll sputtering system at room temperature showed lower resistivity and superior flexibility when compared with a single ITO electrode. Lewis et al. [71] also found good performance in conductivity, transmission, and bending for Ag films with thickness in the range 8–12 nm .

2.3. Deposition methods for flexible transparent electrodes

It is possible to produce TCOs using various techniques, for example pulsed laser deposition, sputtering, evaporation, spray pyrolysis, chemical vapour deposition, and sol-gel processing [72]. Among these, the magnetron sputtering technique which can be operated with radio frequency (RF) or a direct current is the most attractive applied process used to deposit TCOs for optoelectronic application because it has the following advantages: high-quality film adhesion, low deposition temperature allowing the use of polymer and glass substrates, high deposition rate,

excellent control over coating thickness, uniformity and film density, capability of co-deposition of metallic elements to form alloy layers and is a very low cost method to utilise [73]. During magnetron sputtering, once the required base pressure is attained in a vacuum system, argon atoms are continuously introduced to the chamber, which are ionised by the applied voltage and become positively charged in front of the target. The negative charged target is bombarded by argon ions at high speed and this ion bombardment ejects the target material which is then condensed on to the desired substrate as a thin film [74]. The bombardment also causes emitted secondary electrons from the target surface and these secondary electrons are important in sustaining the glow discharge [74]. The sputtering process is limited by high substrate heating, low deposition rates and low ionization efficiency; however, by applying a magnetic field during glow discharge sputter deposition, these limitations can be overcome. The applied magnetic field causes the electrons to spend longer circulating near the target hence the probability of ionising electron-atom collisions increases and consequently increases the plasma density which in turn increases the ion bombardment of the target and further results in higher deposition rates. The increased ionisation efficiency also allows the discharge to be sustained at lower operating pressures (10^{-3} mbar) [74]. A schematic of the magnetron sputtering system is shown in Figure 2-4.

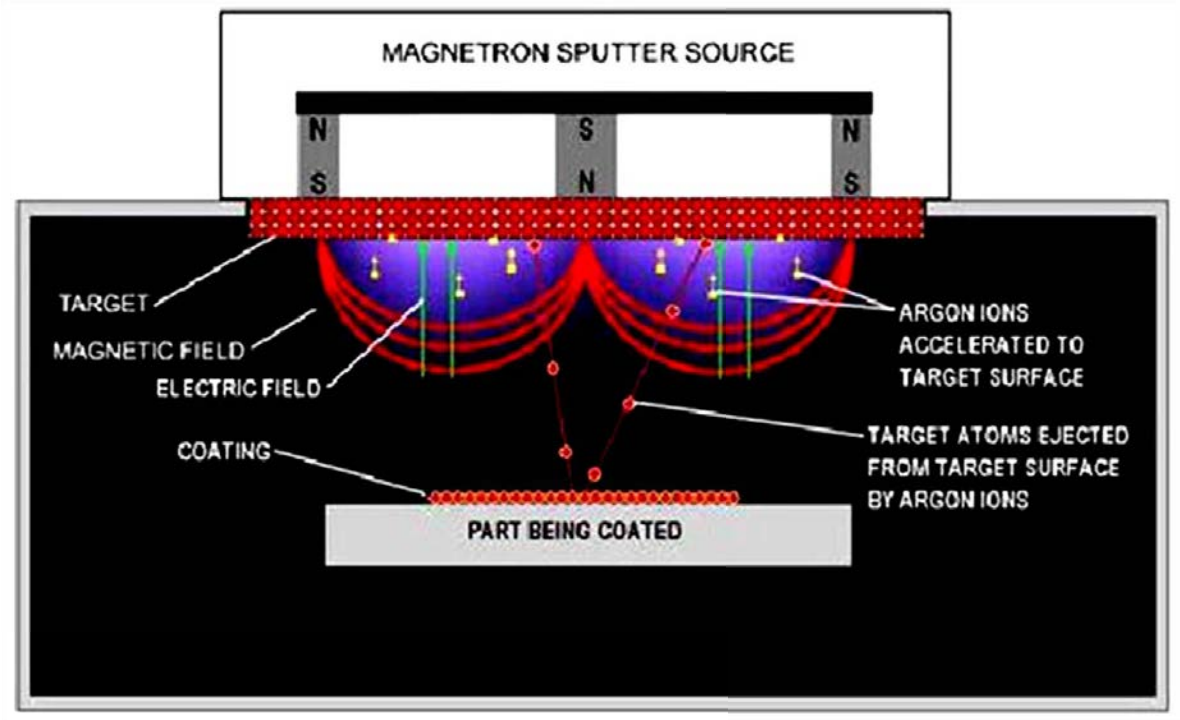

Figure 2-4 Schematic diagram of a d.c. magnetron sputtering process [75].

Antony *et al*. [76] studied the effect of target to-substrate spacing and annealing temperature on the electrical, optical and structural properties of ITO films grown on a glass substrate by RF magnetron sputtering. They found lower resistivity, better transparency and higher crystallinity for the films deposited at target-to-substrate distance 4 cm compared to those at 6 and 8 cm.

Han *et al*. [77] deposited ITO films with excellent electrical and optical properties on PEN substrates at room temperature using RF sputtering. It was found that higher oxygen atoms content in the ITO lead to increased resistivity, possibly because of fewer oxygen vacancies and a lower carrier concentration. Also it was noted that the surface roughness of ITO grown on 200 μm film was 3.2 nm and this was lower than the value on 125 μm PEN. This

discrepancy is due to the roughness of the polymer substrate itself. The resistivity of ITO film grown on 200 μm thick was also lower compared to that deposited on 125 μm thickness due to electron scattering. This indictates that the electrical properties of the ITO films are also influenced by surface roughness.

Yabuta *et al*. [78] fabricated TFTs using a-IGZO films deposited on a glass substrate at room temperature by RF magnetron sputtering. They showed that with increasing total deposition pressure oxygen/(argon + oxygen) for RF magnetron sputtering from 3.1% to 3.7% the conductivity of the a-IGZO films significantly decreased from 10^{-3} to 10^{-6} S cm^{-1}.

Shi *at al*. [79] investigated the influence of oxygen partial pressure on the structural, surface morphology, electrical and optical properties of IGZO thin film deposited on glass substrates using the RF-magnetron sputtering method. Under 1.5 sccm (sccm denotes standard cubic centimetre per minute at STP conditions) of oxygen partial pressure, the lowest electrical resistivity of $8.5 * 10^{-5}$ Ω .cm was obtained. They also observed an increase in optical transmission by increasing the oxygen flow. They indicated that RF-magnetron sputtering is a possible method of obtaining high quality IGZO thin films.

For this work sputtering conditions were chosen to optimise the TFT behaviour as explained in Section 5.2.

Guillen and Herrero [80] investigated the optical and electrical characteristics of single ITO layers and ITO/Ag/ITO multilayer structures deposited on glass substrates by sputtering at room temperature. They showed that thickness of the Ag film strongly influences the transmittance and sheet resistance values; and the maximum transmittance can be achieved by careful control of the ITO films thickness. They achieved sheet resistance below 6 Ω/sq for Ag layer thicknesses above 10 nm and ITO film thicknesses ranging from 30 to 50 nm.

2.4. Roll-to-roll manufacturing

The development of flexible electronic devices such as solar cells and flexible displays often requires the development of new processing equipment and techniques that provide significant productivity enhancements, such as roll-to-roll processing. A schematic of the roll-to-roll process for fabrication of a TFT is shown in Figure 2-5. There are three main steps in the roll-to-roll manufacturing: (i) deposition (ii) patterning and (iii) packaging [81]. In the deposition step, a TCO is grown on a top of the flexible substrate to act as the gate electrode for the TFT (see Figure 2-6).

In subsequent patterning steps, before printing the organic semiconductor layer, a dielectric layer of SiO_2 and the source and drain metal electrodes are produced. Finally, in order to prevent oxygen and moisture contamination of the organic layer, the devices must be packaged in a barrier layer [81].

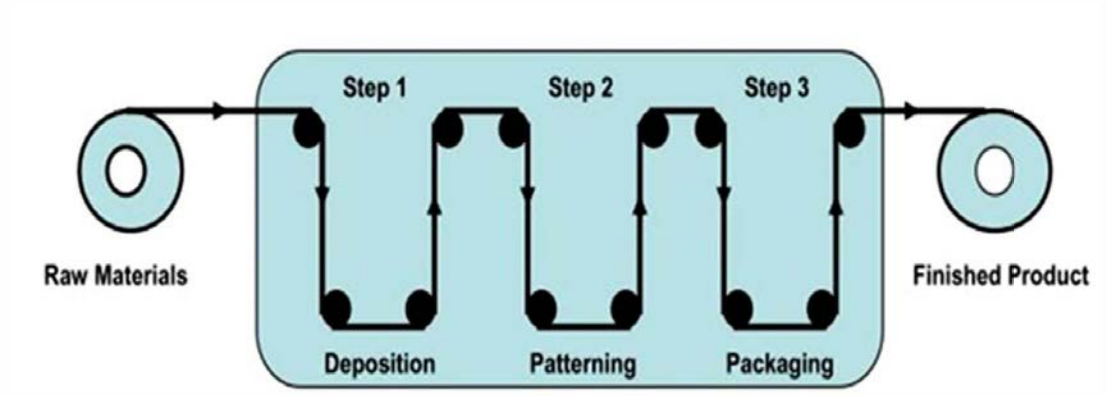

Figure 2-5 Schematic diagram of roll-to-roll manufacturing of flexible displays [82].

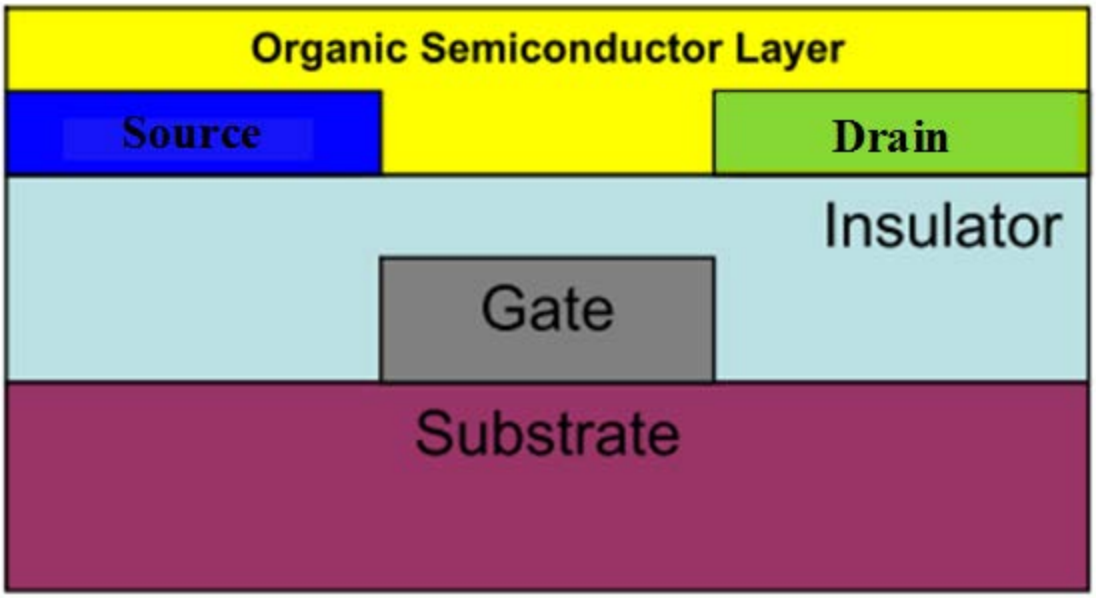

Figure 2-6 Schematic illustration of TFT device structure [81].

The process of roll-to-roll manufacture offers the following advantages [82]:

- It provides continuous production of thin, lightweight and durable appliances.
- It can help reduce equipment costs, reduce display part costs, whilst increasing throughput and eliminate component supply issues.
- It provides a high yield output due to a reduction in human contact in processing.
- It allows devices to be fabricated automatically in large quantities.

However, there are some disadvantages in employing these system as there is limited availability of equipment and therefore it requires custom-built tools which in turn cause a

high initial set up cost [82]. However, these costs can often be recovered through the economic advantages during production. Furthermore, because of the extreme temperatures used, the thermal process cycling involved can be problematic for some substrates [82]. Also, impurities or particles which results from chemical steps in a roll-to-roll fabrication process may form nuclei for crack initiation and surface damage [83]. This in turn leads to degradation in the performance of the device [84].

Chio *et al*. [85] used a specially designed roll-to-roll sputtering system as shown in Figure 2-7 to ITO on PET substrates for organic solar cells. They demonstrated the ability of the roll-to-roll sputtering technique to be a used as an alternative to conventional DC and RF sputtering for deposition of ITO on PET substrate. It was found that the argon/oxygen flow ratio during this roll-to-roll sputtering strongly influences both the electrical and optical properties of the flexible ITO electrode and even at low deposition temperatures films can be obtained with a sheet resistance of 47.4 Ω/square and with an average optical transmittance of 83.46 % in the green region at 500-550 nm wave length.

In addition, Park *et al*. [70] successfully deposited ITO/Ag/ITO electrode on a polyethersulfone (PES) substrate at room temperature using a specially designed roll-to-roll sputtering system. They pointed out that high transmittance 89.28% and low sheet resistance of 4.28 Ω/square was for an optimum Ag thickness of 12 nm.

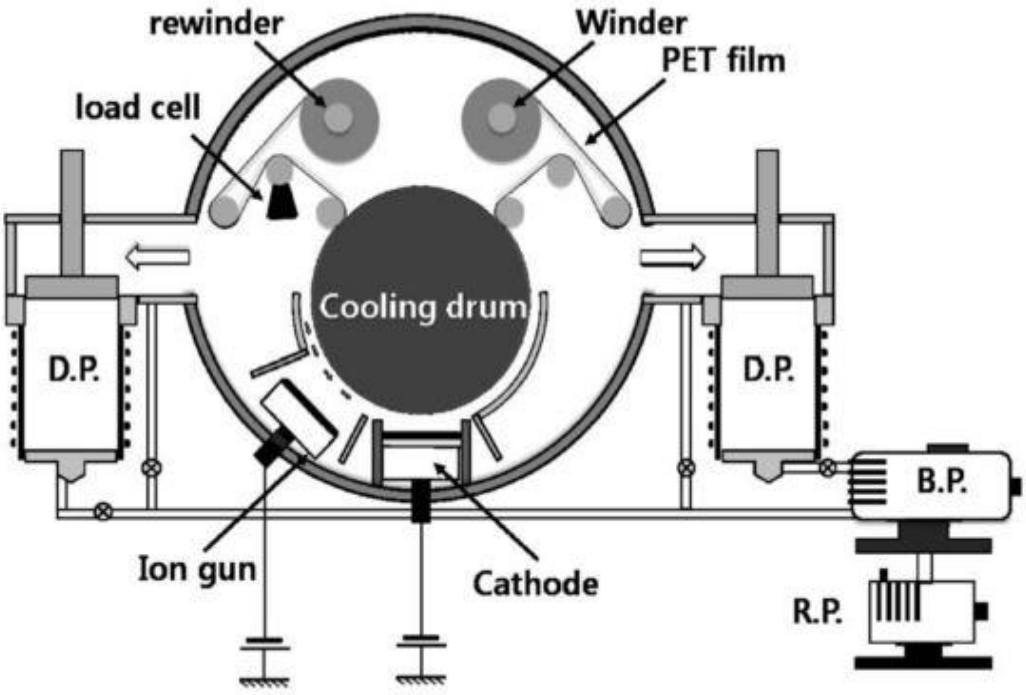

Figure 2-7 a specially designed roll-to-roll sputtering system [85].

2.5. Electromechanical characterization of thin composite system

2.5.1. Failure of brittle layers on a compliant substrate

The performance of the thin film on a flexible substrate under different mechanical and environmental conditions is a challenge to the functionality and reliability of flexible and electronic devices. For example, during both manufacturing and in-service conditions, a flexible thin component is subjected to different deformation loads that cause loss of device functionality. In addition, higher concentrations of chlorine in the surrounding atmosphere where the flexible solar cells are sometimes used, such as marine environments can cause corrosion and degradation of transparent electrodes. Also, hydrogen chloride (HCl)solutions

that are used in photolithographic patterning processes for thin films in the fabrication of electronic displays [86] may contribute to corrosion processes and losses in device functionality. Furthermore, during both the manufacturing process and in-service under changes in temperature, the difference in the CTEs of the thin layer and the polymer substrate results in a thermal stress that may lead to tensile failure of the coating. The misfit stress σ_o which is generated during the deposition process when the temperature of the polymer substrate increases as a result of the highly energetic particle bombardment [87], is given by the following equation [88]:

$$\sigma_o = \frac{E_f}{1-\nu_f}(\alpha_s - \alpha_f)\Delta T \qquad 2\text{-}1$$

where E_f is the Young's modulus of the film, ν_f is the Poisson's ratio of the film, α_s and α_f are the thermal expansion coefficients of the substrate and film respectively and ΔT is the change in temperature. Next, after deposition, the coated polymer substrate cools down and shrinks. Thus, compressive stress can be induced into the thin film which in turn leads to bending in the coated substrate [87] with a radius of curvature r defined by Stoney's equation [89].

$$r = \frac{E_s^* t_s^2}{6 t_f \sigma_o} \qquad 2\text{-}2$$

where E_s^* is the biaxial modulus of the substrate, t_s and t_f are thickness of the substrate and film respectively and ν_s is the Poisson's ratio of the substrate. It is important to underline the

long time period which is required for deposition of a thick film which contributes to an increase in thermal stress [90].

2.5.2. Failure mechanisms of brittle thin film cracking and delamination as a result of induced stress

The stresses in the multilayer inorganic coating/organic substrate resulting from thermal or mechanical loading may cause fracture of the inorganic layer (cohesive failure) or may delaminate the inorganic layer from the organic substrate (adhesive failure) [91]. Upon tension loading a crack is more common, while delamination, buckling and cracking in a tunnelling motion are more common for films under compression load [92]. The cracking mechanism of brittle thin film on polymer substrate has been described in [92,93]. As a background, the theory is that a crack starts from a pre-existing defect (flaw), either in the deposited film or at the edge, and runs across the film and may arrest at the film-substrate interface [8], as shown in Figure 2-8. These cracks then extend laterally in the film until they emerge at the edge of the film or another crack. This type of cohesive fracture mode for thin films under tension is commonly known as channel cracking [8]. This because the film is likely to have a number of flaws and when subjected to large deformation, many channel cracks are produced [93]. When the channel crack length exceeds a few times the thickness of the film, the crack approaches a steady state in which the crack advances without affecting the initial opening width or the crack-face profile [94]. This is for a thin brittle coating on a polymer substrate under uniform stress. The level of stress and strain at the front of a propagating crack is not influenced by crack length so that the crack front shape and the rate

of release of energy is constant. The energy release is related to the elastic strain energy G_{ss} and is given by the following equation [95]:

$$G_{ss} = \frac{1}{2}\,\bar{E}_f\, h_f\, \epsilon^2 g(\alpha;\beta) \qquad 2\text{-}3$$

where h_f is the thickness of the thin film, $\bar{E}_f = \frac{E_f}{1-\nu_f^2}$ is the plane strain modulus of the coating, E_f and ν_f are the Young's modulus and Poisson's ratio of the thin film and $g(\alpha;\beta)$ is a function of Dundurs elastic mismatch parameters α and β and its magnitude depends on the crack type and the elastic mismatch between the coating and substrate. The two Dundurs elastic mismatch parameters α and β [96,97]:

$$\alpha = \frac{E_f - E_s}{E_f + E_s}\ , \qquad \beta = \frac{\mu_f\,(1-2\nu_s) - \mu_s\,(1-2\nu_f)}{2\mu_f\,(1-\nu_s) + 2\mu_s\,(1-\nu_f)} \qquad 2\text{-}4$$

where E , ν , and $\mu = \frac{E}{2+2\,\nu}$ are the Young's modulus, Poisson's ratio and shear modulus respectively; subscript s and f refer to the substrate and film, respectively. For substrate having the same properties as their coating, $\alpha = \beta = 0$. For a stiff coating on a compliant substrate the value of $\alpha \to 1$, while for a soft coating on a rigid substrate the value of $\alpha \to -1$ [98]. As reported by Waller *et al*. [97] the dependence of g function on parameter α is relatively significant, hence it is more representative of elastic mismatch between the film and the substrate rather than parameter β. Furthermore, for most thin film/polymer systems the value of β lies between $\beta = 0$ and $\beta = \frac{\alpha}{4}$, and, therefore $\beta = 0$ is also used in this work.

Cracking occurs when this release of energy becomes equal to, or larger than the energy required for film cracking (crack resistance energy G_c). By equating G_{ss} from equation 2-3 to crack resistance energy G_c , the critical strain ϵ_c , becomes inversely proportional to the square root of the coating thickness [95] .

$$\epsilon_c = \sqrt{\frac{2G_c}{\bar{E}_f h_f g(\alpha;\beta)}} = C\frac{1}{\sqrt{h_f}} \qquad 2\text{-}5$$

where C is a combined constant of proportionality.

Thin film/ substrate systems under compression may show delamination by buckling. The stored elastic energy of the system is released when the thin film buckles. This energy is used to form the new free surface by peeling the film from the substrate surface and also might be used to create cracks from a buckled film [91].

Figure 2-9 shows the buckling pattern morphology which consists of a closed or open tip buckles [40]. Chen *et al*. [92] investigated fracture of the film under both tension and compression. They observed by using SEM and AFM that the coating failure under compression was buckling delamination then film cracking. The rate of release of energy under compression G_{com} depends on the delamination area and is given by [92]:

$$G_{com} = G_d + \left(\frac{h_f}{2b}\right) G_c \qquad 2\text{-}6$$

where G_d and $2b$ is the delamination energy and delamination width respectively.

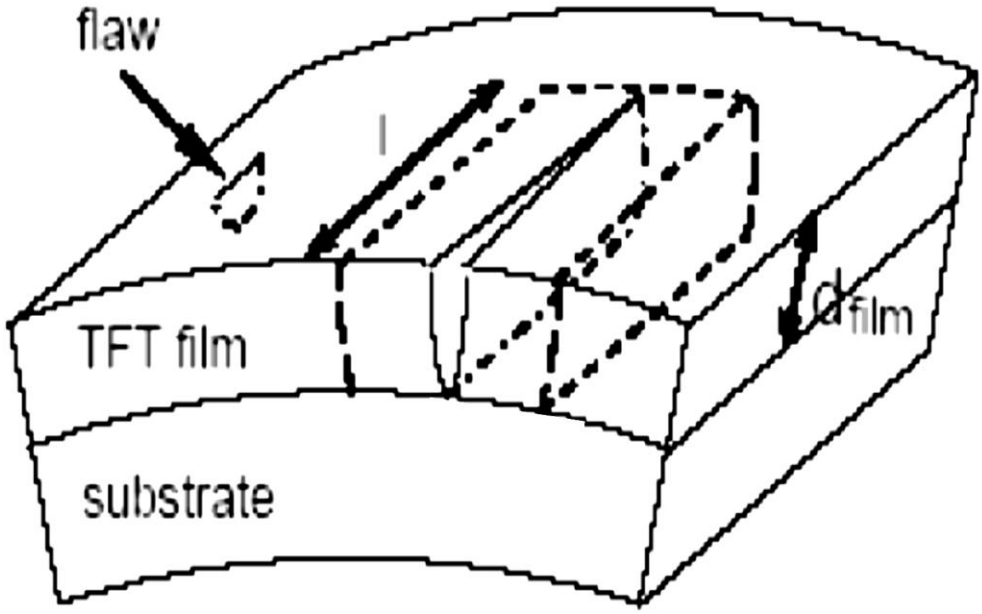

Figure 2-8 Schematic cross section of initial flow and growth of crack in thin film under tensile stress [8].

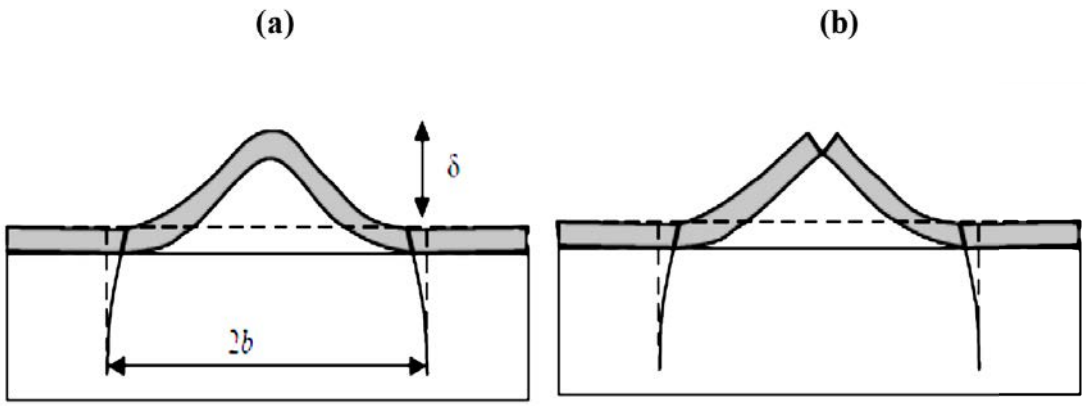

Figure 2-9 Schematic cross section of (a) closed (b) open buckling patterns [91].

2.5.3. Uniaxial tensile testing of thin films on compliant substrate

Uniaxial tensile tests, coupled with *in situ* optical microscopy are commonly used to determine the failure strains of thin coatings adhering to a compliant substrate, in which the crack density (CD) evolution is monitored *in situ* as a function of applied strain [99]. The crack onset strain (COS) is defined as the specific value of strain at which the first crack initiates in the film [100]. For a conductive coating COS is defined as the strain at which the change in electrical resistance reaches 10% [91] as shown graphically in Figure 2-10. The COS is not only dependent on thickness of the coating but also when a coating defect resulting from deposition or service leads to a concentration of stresses in the film, the COS is dependent on the size and the type of defect [91].

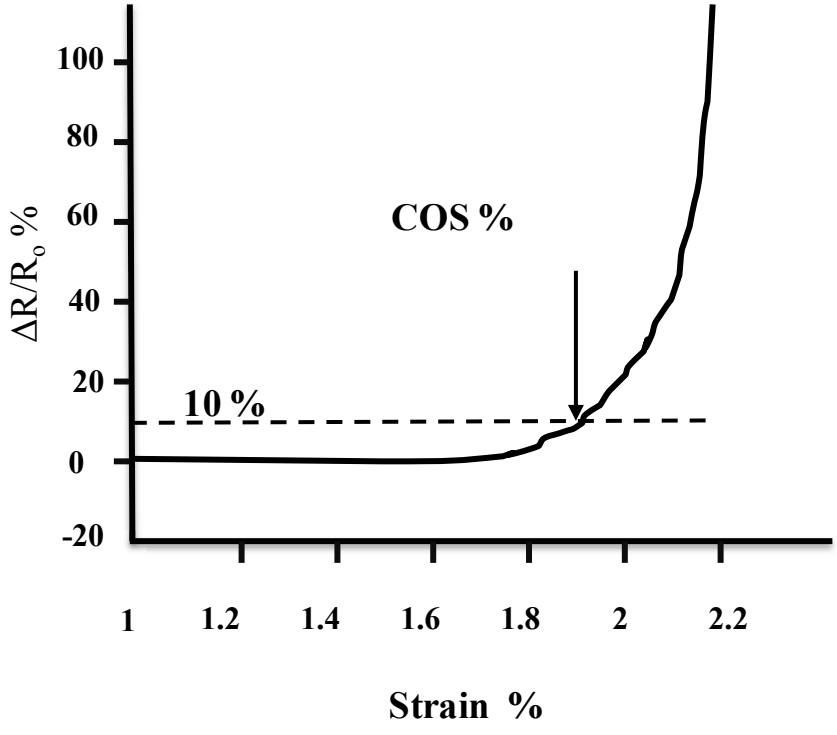

Figure 2-10 Graphical representation of crack onset strain.

Several studies have been performed to characterize the behavior of different thin films under tensile stress. Leterrier *et al*. [101] studied the influence of substrate properties on silicon oxides coated PET substrates using uniaxial tensile tests coupled with *in situ* optical microscopy. It was shown that recovery of the polymer substrate occurred, thus leading to closure of the microcracks when samples were strained to less than 4% of the strain when unloaded. At 1.2% strain the COS of coating was identified. With further increase of strain many fine cracks were observed and propagated perpendicularly to the straining direction and extended across the sample. At around 6% strain, secondary cracks were formed and developed parallel to the loading direction due to lateral contraction of sample. At 10% strain, tertiary cracks were observed and the direction of these cracks was parallel to the direction of primary cracks. Their growth across the sample width stopped when these tertiary cracks met the secondary cracks or buckling zones.

Leterrier *et al*. [102] performed uniaxial fragmentation tests on PET films coated with silicon oxides, in order to investigate the influence of coating thickness ranging from 30 to 156 nm on adhesive and cohesive strengths. They observed that the adhesive strength modelled, using crack density at saturation according to the Kelly-Tyson approach [103], was found to be independent of thickness of the coating in the range from 30 to 156 nm and equal to the substrate shear stress. It was finally concluded that the cohesive strength is proportional to the crack onset strain of the coating, which also depends on the layer thickness.

The increase in electrical resistance of ITO films deposited on PET as a function of applied uniaxial tensile strain was first reported by Cairns *et al*. [104]. It was observed that the crack onset strain of between 2 and 2.5% correlates strongly with a significant increase of electrical resistance. It was pointed out that the resistance remains finite even after cracks propagate across the entire sample width due to the presence of a conducting interfacial layer bridging

the crack width and connecting neighbouring ITO film fragments. They also proposed a physical model that describes the observations of increasing resistance as a function of strain and the effect of cracks. This model states that at some threshold strain the first crack is initiated and spans the whole sample width. For each crack there is gap (crack width) between two sides of ITO fragments, but some conducting material bridges it (see Figure 2-11). The volume of this material is assumed to be constant in each crack and to undergo plastic deformation. They also assumed the bridging length to be zero in each crack at the instant the crack forms and then the crack width increase is assumed to be proportional to the increase in strain.

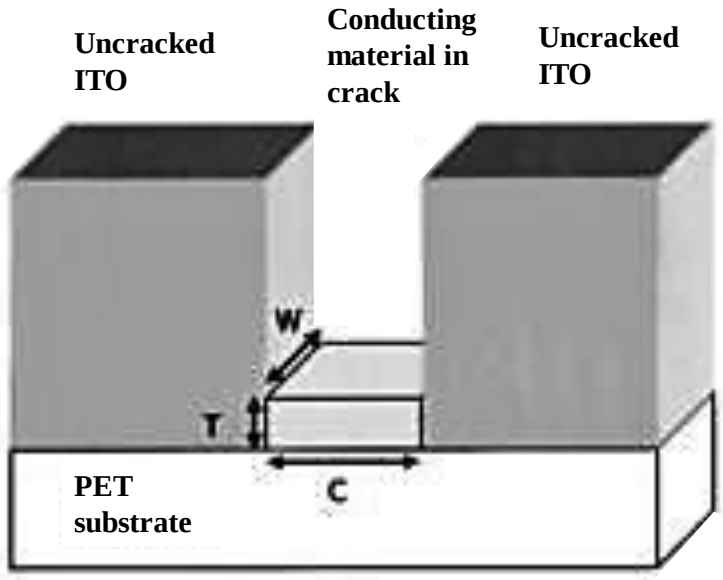

Figure 2-11 A schematic diagram showing bridging material inside a crack [104].

Leterrier [87] also studied the electromechanical behavior of ITO deposited on to a high temperature aromatic polyester. Under uniaxial tensile loading condition, the sample was electrically and optically monitored *in situ*. They observed that the cracks in the ITO begin to initiate from microscopic defects such as pinholes in the coating and surface defects on the underlying polymer substrates. Cracks then grow in a stable manner up to their length which was about 100–500 times the film thickness. They pointed out that the crack propagation was responsible for significant increase in electrical resistance and related loss of device functional performance. In addition, the mechanical resistance against crack initiation was reduced due to the formation of large surface grains during deposition which increased local stress concentration. They also concluded that the most important factor influencing the cohesive ITO properties is the improvement of the substrate surface quality such as that obtained with a hard coat (acrylate-silica hybrid materials).

Changji *et al.* [105] reported fragmentation tests carried out on ZnO, deposited by the cathodic vacuum arc technique, on a polyimide foil substrate in order to study the influence of deposition pressure on the adhesion of ZnO thin films. They observed that cracking of a ZnO film deposited at 0.9 Pa began at 0.53% strain. They also found that the number of cracks increased and the cracks become wider immediately after the first crack appeared. Secondary cracks appeared at 5.5% applied strain and were parallel to the stretching direction. They concluded that samples deposited at a pressure of 0.9 Pa exhibited good adhesive properties.

Kim *et al*. [106] studied the effect of substrate on cracking and buckling resistance of uniaxially-strained ITO films deposited by DC magnetron sputtering. They used PET, and PET which was treated by O_2 plasma surface treatment. They observed, using *in situ* strain in an SEM, that both on bare and treated PET, 50 nm thick ITO had very low crack onset strain of between 1.0 and 2.0%, but was not affected by the surface treatment. On the other hand,

the buckling onset strain for different thicknesses of ITO coated on plasma-treated PET substrates was significantly improved due to improved adhesion between the ITO film and polymer substrate. Therefore, the use of O_2 plasma treatment was found to highly improve the adhesion strength between ITO and PET and hence improved the mechanical resistance against buckling of the film.

The influence of cohesive and adhesive properties of the ITO film by inserting ductile metal interlayers, such as Ag has been reported by Yang and Park [107]. They found that over a certain thickness of Ag interlayers, the crack and delamination resistances were improved against the uniaxial tensile strains. They observed that the improved crystallinity of ITO by the Ag interlayers was contributed to the enhancement of the cohesive strength of ITO on PET substrate.

However, relatively little research to date has been reported about the mechanical behaviour in tension of IGZO coated on polymers. Kim *et al.* [108], investigated the mechanical characteristics of a stretchable a-IGZO TFT. They optimized the device structure by using numerical simulation in order to improve the mechanical stability and evaluated the stress and strain distribution near the silicon dioxide (SiO_2) bridge. They observed from experimental results that the new model was not fractured or cracked when stretched by a total of 5% of its length along the x-axis while the fracture occurred in the reference model at the vertical edge of the SiO_2 bridge when stretched under the same conditions (see Figure 2-12). They also found the maximum stress and strain values at the corner of the SiO_2 bridge in both models. These finding were acquired from a simulation. The mechanical stability of the device's new design was validated by both experimental and simulation results.

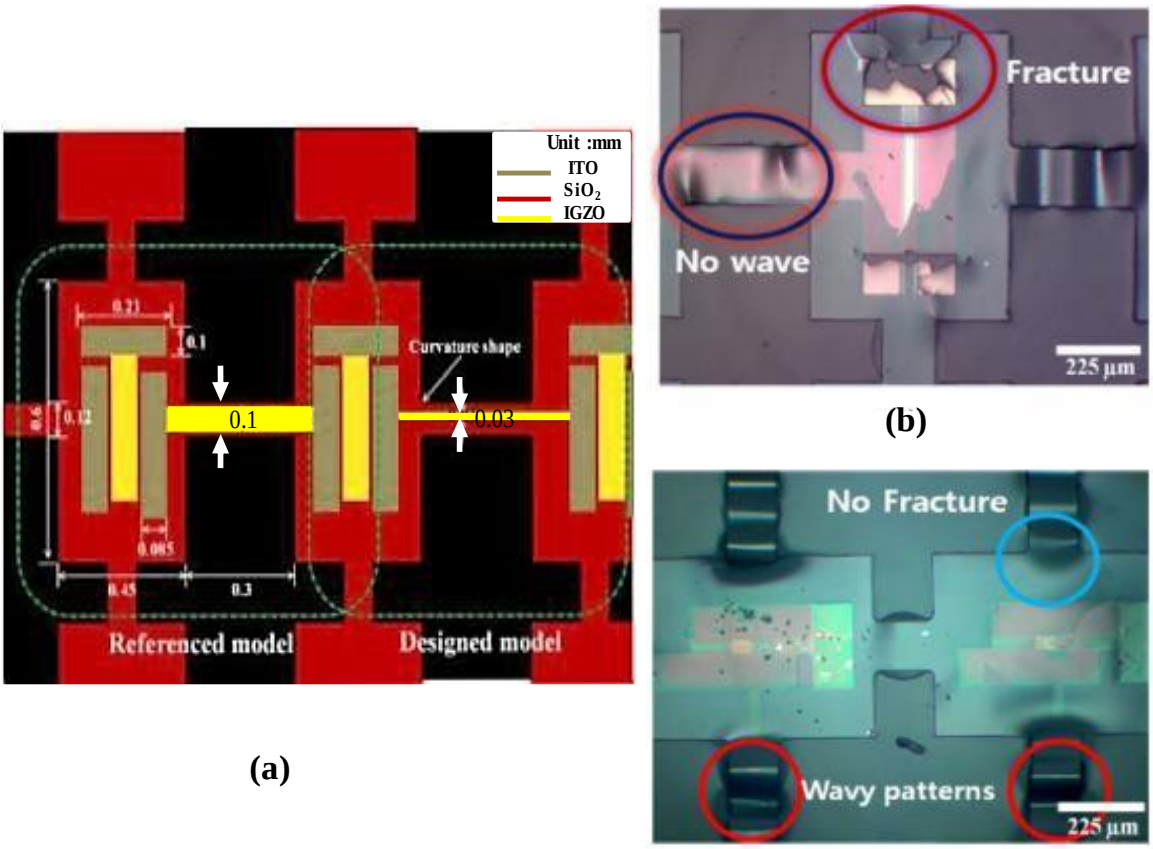

(a)

(b)

(c)

Figure 2-12 (a) Schematic showing the structure of the referenced and newly designed models for simulation, (b) and (c) Optical microscope images showing the surface of referenced and designed model of TFT device after expermintlly tested [108].

2.5.4. Bending and buckling tests on thin films

Beside the uniaxial tensile test, other experiments that characterize fracture of thin film are bending and controlled buckling experiments. When a thin flexible electronic device component is subject to bending during fabrication or in service, further mechanical complications arise. As a thin film on compliant substrate is bent to a specific radius of curvature R, with the film deposit on the top surface, it will be in tensile strain while the inner surface (substrate) will be in compressive strain, as shown in Figure 2-13. When the thin film thickness t_f is very small compared with the substrate thickness t_s , a plane of zero strain which is well known as the neutral axis is located at the mid-plane of the substrate [95]. In such case, the induced strain ϵ in the film can be calculated using the following equation [92,109].

$$\epsilon = \frac{t_s + t_f}{2R} \qquad 2\text{-}7$$

Therefore, the minimisation of the strain of film is possible by placing the most critical component close the neutral axis (i.e. reducing the device thickness) and thus the flexibility of the device will be higher [92].

Similar to the tensile test, in this test the influence of the tensile and compressive strain on the thin film can be monitored *in situ* by the use of optical microscopy and by measuring the electrical resistance if the specimen is conductive. Chen *et al*. [92] studied the fracture behaviour of the ITO film on PET under both tension and compression buckling deformation. Lower strain values were obtained for films under tension compared with film under compression. They also showed that the failure mode in tension was due to film cracking while in compression it was due to buckling delamination and cracking.

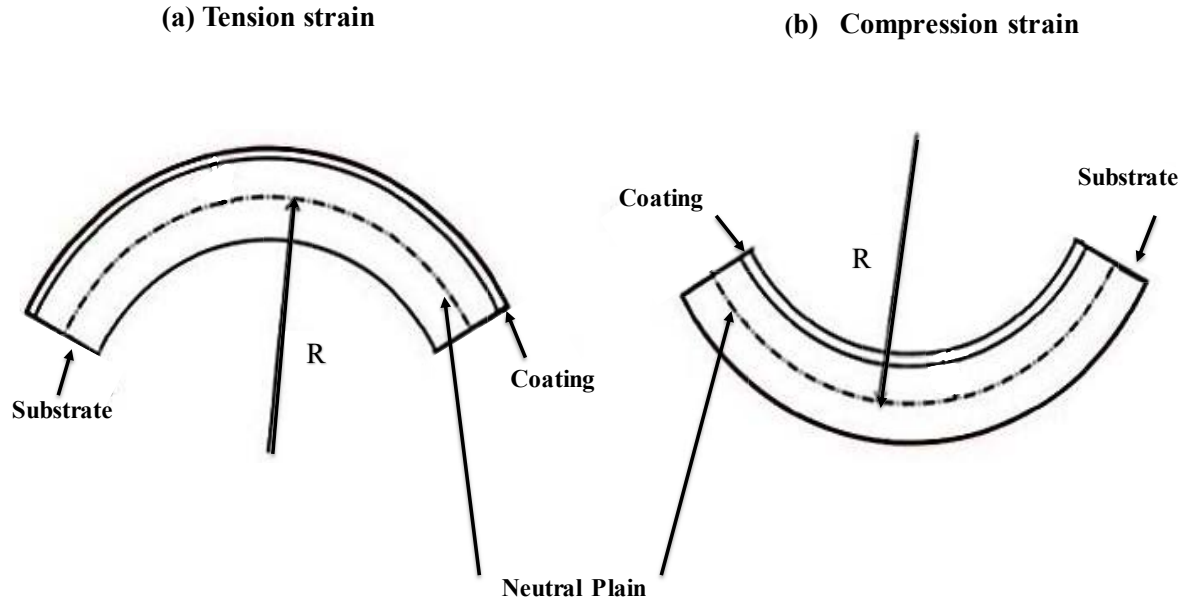

Figure 2-13 Schematic diagram of a bending state (a) in tension (b) in compression.

Gleskova *et al*. [110] fabricated a-Si:H TFTs on a 25 μm thick polyimide foil. They investigated electrical properties of the TFTs including the on current, off-current, leakage current, mobility, source-gate and the threshold voltage of the transistor in the bent state under mechanical stress at various radii of curvature. They found that when transistors are under compression, they can function down to R=0.5 mm, which corresponds to a strain of 1.25% and when transistors are under tension, they can function down to R=1 mm, which corresponds to a strain of 0.51% without any change in their electrical performance. Finally, they conclude that the TFT's failure under high tensile strains is by cracks in the TFT channel layers which are perpendicular to the loading direction, as shown in Figure 2-14.

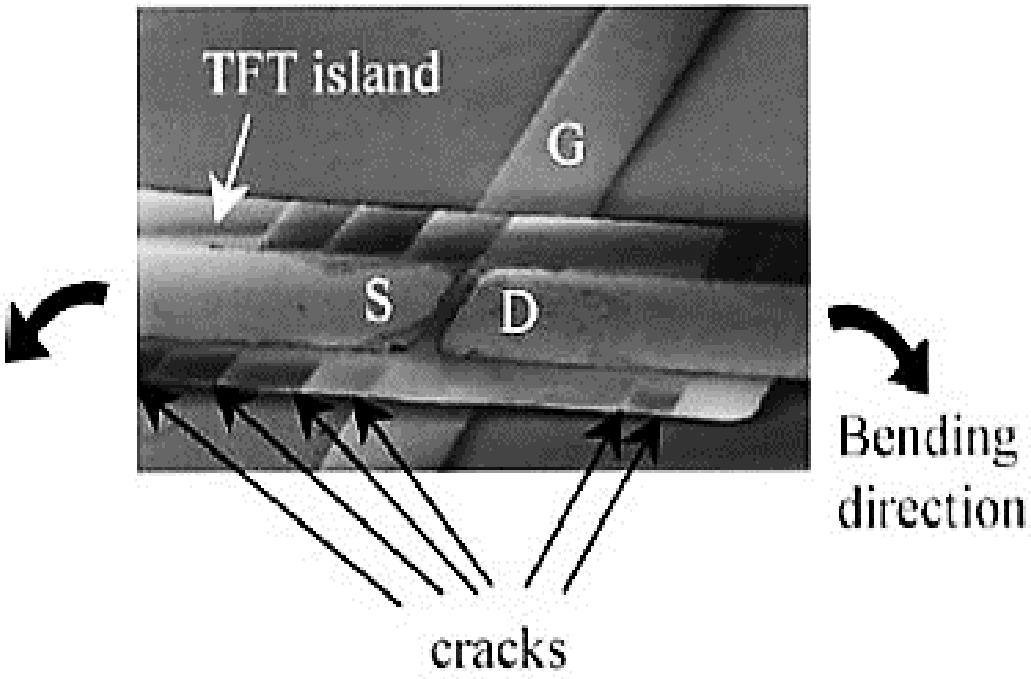

Figure 2-14 SEM image showing mechanical failure of a TFT. TFT bent in tension down to R=2 mm [110].

Ramji *et al*. [111] reported that the crack density for patterned ITO when wrapped around a mandrel to 3% strain was more than seven times higher than of the un-patterned ITO. They observed that the cracks of pattern ITO-PET initiated at the micro-cracks caused by the patterning process, as Figure 2-15 shows.

(a)

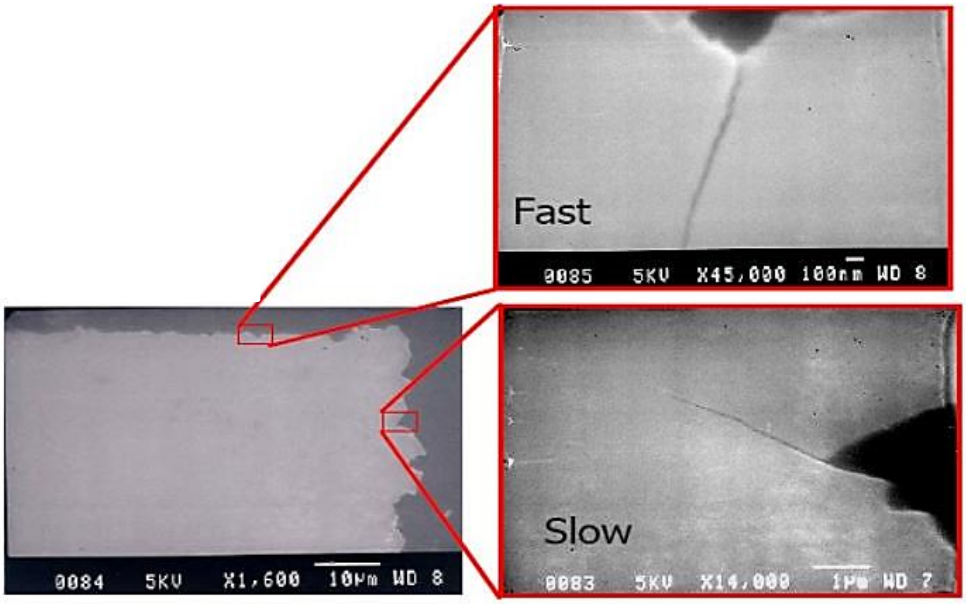

(b)

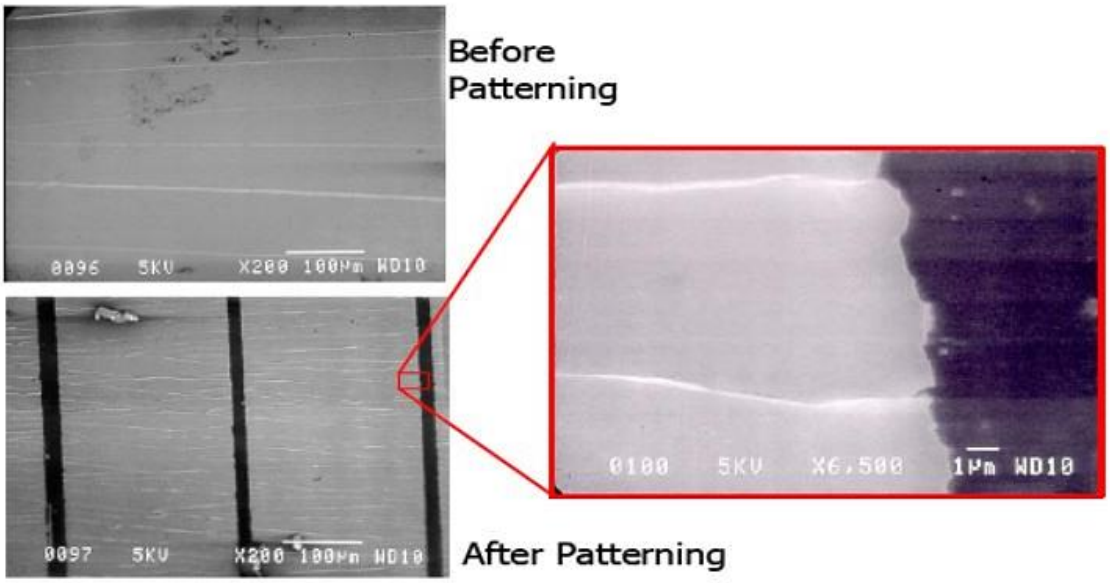

Figure 2-15 SEM micrographs image of (a) patterned ITO coated PET substrate showing microcracks at sharp edges. (b) ITO coated PETsubstrates under applied bending strain 3% [111].

Bejitual *et al*. [112] used the controlled buckling experiment to investigate the failure behaviour of various patterned ITO shapes and sizes coated on a PET substrate. The smaller size patterns were found to exhibit highest crack onset strain. In addition, lowest crack onset strain was observed for square-shaped pattern. Also, it was found that failure under tensile and compression buckling mode is driven by micro-cracks initiating from the pattern edge.

Ni *et al.* [113] investigated the fracture properties of AZO-coated on PET substrates under simply-supported bending conditions. It was reported that the coating damage, under tensile strain, is caused by the creation of channel cracks, while under compression the film specimen may first delaminate from the polymer substrate and then buckle before the initiation of a crack. They explained that in tension, on the outer surface, the stored elastic energy went solely into crack formation; however, in compression the elastic energy was distributed between crack formation and delamination, so the crack density is usually lower for bend-testing on the compression side.

Sierros *et al*. [96] investigated mechanical behaviour of ZnO films with different thicknesses coated on PET and PEN by sputtering. They used compression and scratch tests. During compression, the crack onset strain of ZnO films, using *in situ* optical microscopy was found to be approximately 2% and to depend on the film thickness. During scratch testing, and by observing the crack's morphology, it was shown that the secondary cracks appear in the form of buckles due to impregnation of film debris into the polymer substrates at high scratch loads.

Cherenack *et al*. [114] fabricated TFTs using IGZO and ZnO coated polyimide substrates for comparison purpose. They investigated the electrical performance of TFTs at different bending radii starting from a flat substrate down to 10 mm in a custom-built bending tester.

No significant degradation of the properties was observed for IGZO TFTs as compared to the unloaded case and ZnO TFTs. For example, both linear mobility and saturation mobility of bent ZnO TFTs were almost two order of magnitude lower than that of un-deformed ZnOTFTs. They concluded that the IGZO is the best material choice for development of robust flexible TFTs.

Also, Munzenrieder *et al*. [115] investigated the performance of a-IGZO TFTs on 50-µm-thick (Kapton E polyimide) substrate. It was found that the saturation mobility and other parameters like threshold voltage were considerably influenced by mechanical stress induced by bending (tensile and compressive).

Khan *et al*. [116] investigated the performance of a-IGZO TFTs fabricated on stainless steel foils when flexed to different bending radius of tensile and compressive deformation. It was reported that under tensile strain a-IGZO TFTs remained functional until applied strain equal to 0.8%. It was found out that the a-IGZO TFT displayed higher flexibility under compressive strain than that under tensile strain. In order to improve mechanical robustness, some materials have been suggested as promising alternatives to ITO electrodes such as oxide–metal–oxide (OMO) multilayer including, ITO/Ag/ITO, IZO/Ag/IZO, ZTO/Ag/ZTO and AZO/Ag/AZO. However, few studies have been reported about mechanical properties of these electrode grown on polymer substrate. Lim *et al*. [117] conducted lab-made outer/inner bending tests in order to investigate the mechanical integrity of ZnO-doped tin oxide (ZTO/Ag/ZTO) multilayer electrodes deposited on PET by roll-to-roll sputtering. The fracture behaviour of the films was monitored using *in situ* optical microscope observations and electrical resistance measurements. They found that the critical radius of curvature was 3 and 4.5 mm of the ZTO/Ag/ZTO film in the outer and inner bending tests. The crack density increased with decreasing bending radius. They concluded that the difference between the

points of crack initiation and changes of the electrical resistance during inner bending were due to the overlapping films during crack generation which provided a conducting path.

2.5.5. Twisting test of thin film on compliant substrates

Besides tensile and bending deformation, the twisting deformation is expected as another frequent deformation to which flexible displays or other flexible electronics devices may be subject to during their operation. To date, however, such deformation has not been considered in detail where brittle thin films are concerned and so investigation of this films by means of twisting deformation is a particularly interesting area of research.

Choa *et al*. [118] studied the mechanical integrity of the roll-to-roll -deposited (ZnO-doped In_2O_3) and IZO/Ag/IZO multilayers on PET substrate under twisting loading. A lab-made twisting test machine was mounted under an optical microscope. They found that the crack started to initiate at the twisting angle of 26^o and no change in electrical resistance of the IZO/Ag/IZO multilayer electrodes was observed up to angle of 28^o compared to that single IZO layer (~ 20^o). The crack density and electrical resistance was found to increase with increasing twisting angle. Optical microscope images showed broken IZO/Ag/IZO film and crack overlapping each other which contributes to the formation of a conduction path and delayed changes in the electrical resistance. They conclude that the ductile Ag interlayer improves the flexibility of IZO/Ag/IZO multilayer.

Additionally, Jung *et al*. [119] investigated the effect of inserting a poly(3,4-ethylenedioxythiophene):poly(styrenesulfonate) (PEDOT: PSS) buffer layer on the electro-mechanical stability of 20 nm thick ITO film coated PET substrate. When a PEDOT:PSS

layer was inserted between ITO and PET, the sheet resistance was decreased from 270 Ω/square to 57 Ω/square. They found that the ITO/PEDOT:PSS/PET films can be deformed to a twisting angle of 50° and the resistance remains constant. They conclude that the ITO/PEDOT:PSS electrode is a promising alternatives to the ITO electrode for the next-generation of flexible electronic devices.

Finally, Lim *et al*. [120] fabricated a transparent Ag nanowire (NW) network electrode on colorless polyimide substrates with better values of a sheet resistance and an optical transmittance compared to the values obtained from a conventional flexible amorphous ITO film. They investigated the mechanical integrity and flexibility of the AgNW electrode under twisting deformation. They observed that the change in the electrical resistance of the AgNW electrode was very small, even though the sample was twisted to an angle of 40^{o}. In contrast, for ITO film there was a slightly greater increase in resistance after twisting to an angle of 40^{o}.

2.5.6. Cyclic-fatigue tests of thin films on compliant substrates.

Since flexible electronics need to remain functional after a load is repeatedly applied to the structure, repeated mechanical loading of brittle layers under bending and twisting conditions is also vital. As reported in [121] repeated loading forces for a large number of cycles can cause structures to fail at stresses less than those needed for failure under static loads. Lechat *et al*. [122] showed that the cyclic loading stress was the cause of PET failure as it led to crack propagation at low stress.

Gorkhali *et al*. [123] reported results for the electro-mechanical properties of repeated loading of ITO coated PET substrates using mandrel-bending over varying diameters ranging between 8 to 24 mm and the resistance changes were continuously monitored. They observed that a

rapid increase in electrical resistance was due to the dimensional change of the polymer substrate until an equilibrium size was attained, then a gradual increase in resistance was found due to cracking of the ITO. After, 50,000 cycles catastrophic conductive failure occurred due to severe cracking.

Lewis *et al*. [71] added a thin silver layer between two of 35-nm ITO layers and found that the electrical resistance increased by only 1.2- 2.7 times the original value where subjected to 10,000 repeated bending cycles at 3 mm radius of curvature. They suggested that this response was due to the Ag ductile layer that remains conducting even after the failure strain of the ITO (~0.8%).

Alzoubi *et al*. [124] studied the influence of bending diameter, bending frequency, and sample width on the bending fatigue behaviour of ITO coated PET. Crack development and the electrical resistance were monitored during the experiments at a specific number of cycles. A high crack density was observed at the middle area across the sample width and then propagated toward the edges. A high change in electrical resistance was observed at smaller bending diameters and higher bending cycles. The results indicated that the size of bending diameter and number of bending cycles greatly affect the electrical resistance of ITO thin film.

Hsu *et al*. [125] investigated the stability of an (20 nm) ITO film coated on PET substrate under tensile and compressive fatigue bending. They observed that both tensile and compressive stress can cause ITO failure and an increase in electrical resistance and transparency. In addition, tensile stress increased electrical resistance more easily compared with compressive stress. Moreover, the sheet resistance and optical transmittance were found

to increase with increasing PET thickness regardless of if it was under tensile or compressive stress.

Chen *et al*. [126] assessed the reliability of the STN (super-twisted nematic) display under twisting fatigue condition. The sample was placed between the bottom jig which was fixed with ground and top one which is mobile with a rotational driver. The top jig was twisted in a clockwise and anti-clockwise direction. Functional failure was found after it twisted to 30^{o}. For this reason, the twisting limitation angle was set to 20^{o} during experiment. They found that five samples from nine survived up to 20,000 cycles of the twisting fatigue test.

Cho *et al*. [127] conducted cyclic loading experiments in the twisting mode. Poly(3,4-ethylenedioxythiophene): poly(styrenesulfonate) (PEDOT:PSS) films printed on PET substrate were repeatedly twisted and untwisted from both sides of the samples at an angle of 30° and the change in electrical resistance monitored *in situ*. It was observed that the change in electrical resistance was constant after 2,000 cycles, this indicating that such structures can provide high levels of twistability and flexibility.

In addition to external repeated mechanical stress, the thin film anode may also be subject to high temperature such as 100 °C during the manufacturing process and perhaps up to 40 °C during the use of devices. The temperature is likely to change the mechanical, physical and electrical properties of the thin film over time for a wide range of materials and to increase the oxidation of the metal film when used as intermediate layer between TCO layer. Because of the mismatches in the CTEs of the substrate and the thin film, both of them do not respond to temperature in term of elongation by the same percentage and the thin film is either stretched out or compressed and this results cracking or/and delamination of the coating layer. Despite the importance of high temperature issues combined with repeated mechanical stress for

reliable long-term operation, to the best of my knowledge no systematic investigation of the electro-mechanical behaviour of TCO film coated PET under the combination of twisting fatigue stress and harsh environmental condition has been published. However, Alzoubi *et al*. [128] studied the influence of temperature on the bending fatigue behaviour of copper thin film deposited on a PET substrate. They showed that high temperature caused a more rapid degradation of the conductive surface.

2.5.7. Corrosion and mechanical stress of thin film on compliant substrates

Because of the wide application of flexible electronic devices, it is expected that such devices may require to effectively function with exposure to a harsh outdoor environment such as in solar cell panels. The long-term stability of solar energy is still limited by the instability of Ag/Ag-alloy based TCO electrodes such as ITO/Ag/ITO and ZnO/Ag/ZnO which are very sensitive to the surrounding atmosphere such as, chlorine, acids, ozone [129] as well as high temperature and moisture environments [130]. Silver atoms aggregate around chlorine atoms which exist in the ambient atmosphere such as marine environments, as Figure 2-16 shows. This causes corrosive white spot to appear on the multilayer sputter coatings after exposure to ambient atmosphere for long period of time.

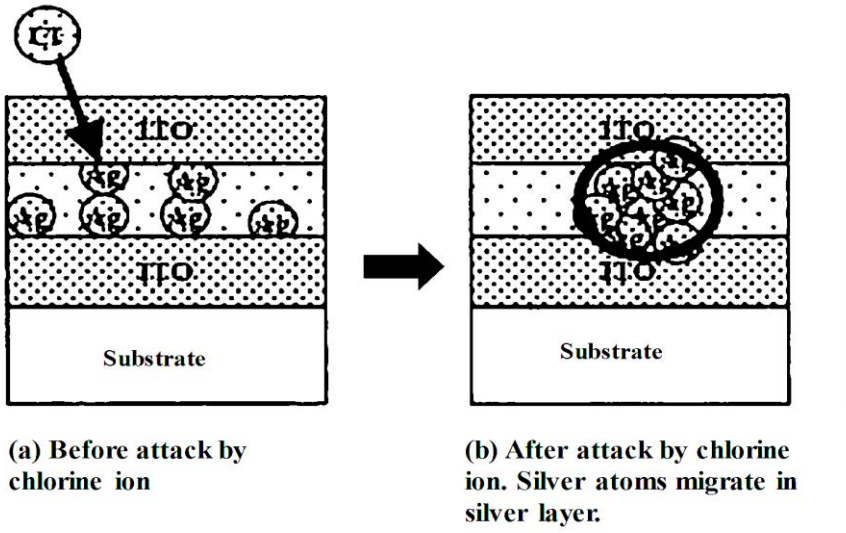

Figure 2-16 Cross-sectional schematic illustration of multilayer film showing process of silver migration [131]**.**

However, few studies have been reported on Ag/Ag-alloy based TCO corrosion. Nadel *et al*. [132] found film cracking, peeling of the ZnO top layer, and agglomeration using SEM after a 24-hour of exposure of ZnO/Ag/ ZnO to water including sodium chloride. The agglomerated material was analyzed by energy dispersive X-ray spectroscopy in SEM and was identified as silver. They conclude that the high level of chlorine concentrations which may be introduced from fingerprints or other direct contamination can cause corrosion through cracking and delamination of the top zinc oxide layer.

The durability of the multilayer sputter coating including silver layer as intermedia layer was investigated by Kioke *et al.* [131]. After immersion in 0.1 mol/ l of salt water for 17 h, white spots were found on the surface of the multilayer sputter coating resulting from the migration of silver atoms in the silver layer. In order to improve the corrosion resistance of the multilayer coatings, they also sputtered 0.5-2 nm thick transition metals such as titanium, vanadium, tantalum, and zirconium on the top surface of the multilayer coatings, and then the appearance, electrical resistance and transmittance of the multilayer coatings was evaluated.

They observed that durability against salt-water exposure was dramatically improved by deposition of titanium and tantalum to the top surface multilayer coatings (ITO/Ag/ITO/Ag/ITO/Ag/ITO/PET substrate) without a significant decrease in transmittance.

Ando and Miyazaki [133] investigated the moisture deterioration of zinc oxide/silver/zinc oxide on glass substrates. It was found that the moisture penetration through the top zinc oxide layer enhanced Ag migration and resulted in decreasing the interface bonding between the top ZnO and Ag and also peeling of top ZnO layer was observed to be due to weakened adhesive forces and high internal stresses in the top oxide layer. In order to improve the moisture durability of Ag based TCO and to reduce white dots appearance, they also have proposed two methods. One of the methods was adding metal elements to the Ag layer to suppress Ag migration [130] and the other one was reduction of the internal stress of the oxide top layer to avoid crack occurring [134].

Chen *et al.* [135] reported that the many corrosive spots appear when an ITO/Ag/ITO multilayer is exposed for 144 hours to 323 K with a relative humidity of 90%, and these spots are related to the corrosion of Ag. However, there are no spots observed on the surface of ITO/AgTi/ITO (see Figure 2-17) due to the greater corrosion resistance of Ag-Ti alloy as compared to pure Ag. It is also observed that the conductivity and the transmittance at wave length of 550 nm of ITO/Ag/ITO were significantly decreased after the durability test but no change was found for ITO/AgTi/ITO. They conclude that ITO/AgTi/ITO is a promising candidate for transparent conductive electrodes.

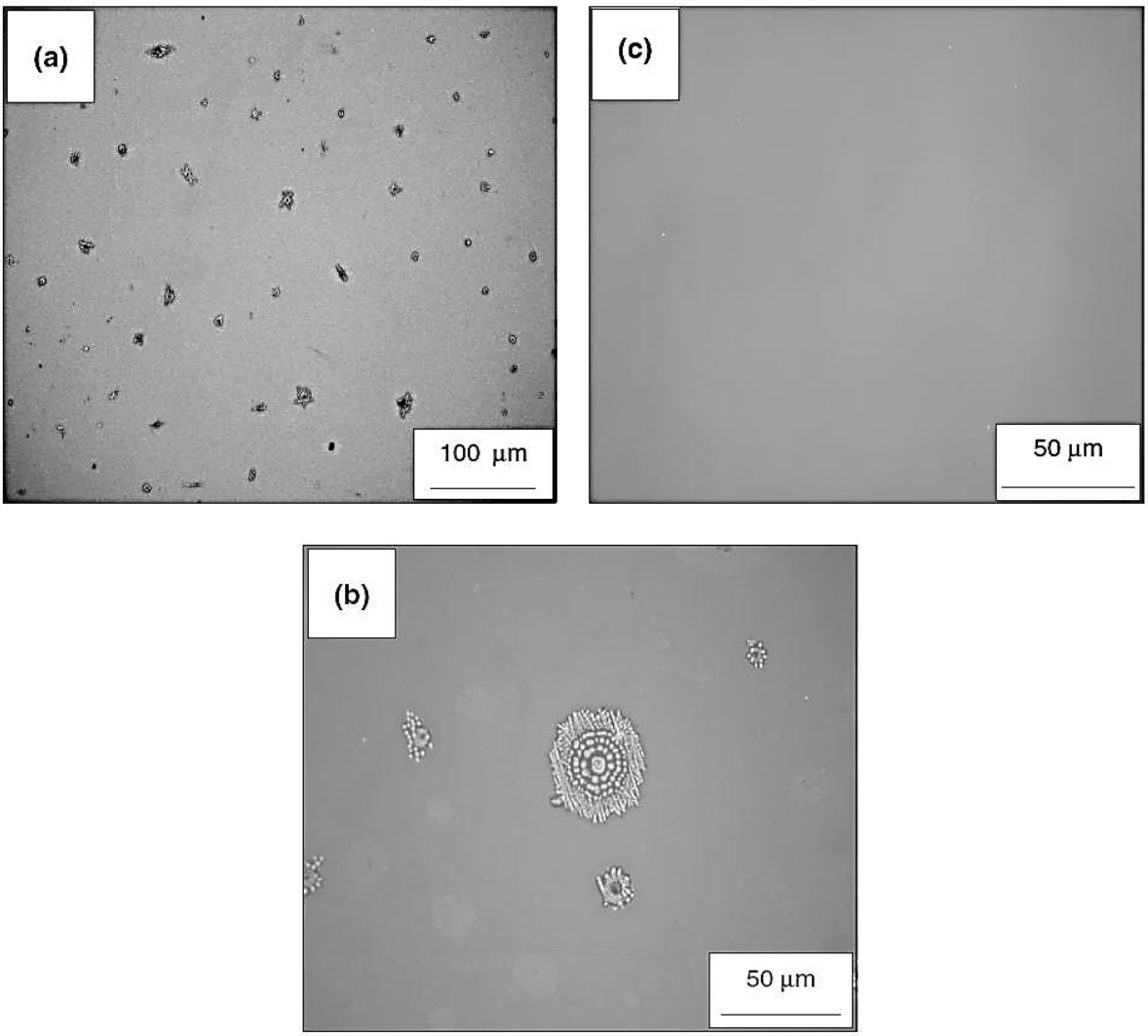

Figure 2-17 Surface observation of (a) –(b) ITO–Ag–ITO and (c)) ITO–AgTi–ITO film ,after exposure to 323K with a relative humidity of 90% for 144 h [135].

Chen *et al.* [136] also investigated the mechanism of degradation of ITO/Ag/ITO in humid environments. They reported that the moisture penetrated through pre-existing defects in the oxide top layer and then was absorbed by the Ag layer and decreased the interfacial sticking force between the top ITO layer and Ag layers. This induces silver migration and promotes the Ag aggregation. After that the ITO top layer cracked and peeled off as the internal stresses

relaxed. Defects resulting from moisture penetration can cause the hazy spots formation and scattering of light which thereby reduces the transmittance.

In addition to the degradation of transparent electrodes when subjected to a corrosive environment, they may fail when subjected to the combination of mechanical stress and corrosion during manufacture and use and so this can lead to stress corrosion cracking. A few other studies have paid attention to the effect of combination of stress and corrosion on the transparent conductive electrodes.

Sierros *et al.* [137] stated that the primary cause of premature failure of ITO is stress corrosion cracking. They wrapped ITO-coated PET specimen around mandrels with various diameters and then submerged them in a corrosive environment provided by acrylic acid. It was found that the combination of both applied stress and corrosion can cause cracking to occur at strains below a quarter of those needed for ITO electrical failure with no corrosion. It was also noted that the corrosion is observed to form in rough specimen areas thus suggesting that substrates with smooth surfaces are important for avoiding extreme corrosion.

Hamasha [138] reported the influence of different temperatures and relative humidity on the electrical resistance of ITO film with and without cyclic bending. The electrical resistance of samples cycled at 20 °C of temperature and 20% relative humidity did not exceed 1% of the original value, while it exceeded 2% for samples cycled at 70 °C and 20 % relative humidity as well as samples that were cycled at 20 °C and 80% relative humidity. However, the electrical resistance for the sample cycled at 70 °C and 80% relative humidity increased significantly by 17% and severe cracking and moisture damage (spots) were observed on the surface. They concluded that without involving bending fatigue, temperature and relative

humidity have no significant influence on the electrical resistance of the ITO film. They conclude that cyclic bending is the dominant factor in ITO electrical failure.

Bejitual *et al.* [139] applied cyclic bending on ITO coated PET under (0.05 M concentration) acrylic acid solution and measured *in situ* the change in electrical resistance. Acrylic acid is contained in many pressure-sensitive adhesives that are included in optoelectronic stacks. They found that the percent increase in electrical resistance when specimens were under corrosion-fatigue was significantly greater than that under fatigue or corrosion alone. In addition, crack density values were higher for specimens under corrosion-fatigue as compared to samples with no corrosion. For example, under fatigue–corrosion after 500,000 cycles at 0.9% applied strain, the crack density was found to be 1.7 times that of the no-corrosion case, indicating that the combined action of fatigue and corrosion is significant.

In particular, the specific objectives are:

- Investigation of the mechanical, optical and morphological properties of uncoated PET and PEN substrates in order to understand the role they play when IGZO is deposited on polyesters.

- According to the literature review as mentioned earlier there is relatively little research reported about the mechanical behaviour of a-IGZO coated on polymers. Therefore, the general characterization and mechanical properties of IGZO films both coated PET and PEN substrates was discussed.

- The electrical resistance changes under tensile and bending deformation have been studied by several research groups [101,104,112]. However, twisting deformation is expected as another common deformation type in flexible display or other flexible

electronics devices. Therefore, new mechanical testing methods and apparatus such as a twisting and cyclic twisting device were developed for the characterization of thin film components for flexible electronic devices.

- Since Ag is sensitive to salt environments, chlorine presents in the marine environments can influence the stability of ITO/Ag-alloy /ITO, which can negatively impact on the lifetime of the flexible solar cells device. In addition, the residual Cl^- after the roll-to-roll etching processes can cause degradation of ITO/Ag-alloy/ITO functional properties. However, this issue has been little researched in the past. Therefore, the impact of exposure of aggressive salt environments on electrical, optical and morphological properties of ITO/Ag-alloy /ITO films was investigated and also bending fatigue and bending fatigue-corrosion behaviour of ITO/Ag-alloy /ITO films were studied.

- In use, solar cells are usually bent around the surface on which the devices are laid (i.e under stress) and can be in service in hot and humid climates for long times in the summer. This can cause cracks in TCO film and corrosion Ag layer and with subsequent loss of device functionality. Early work [138] evaluated the bending fatigue behavior of TCO film under different temperature and humidity. However, data on the long term bending of TCO in various environments including temperature and humidity conditions has not been reported. Therefore, in this project the bending behaviour of ITO/Ag-alloy/ITO film over time under different temperature and humidity conditions was investigated.

3. Materials and experimental methods

In each case, the test was conducted on at least five test specimens and the average values were calculated. The research flow for the overall methodology is illustrated in Figure 3-1

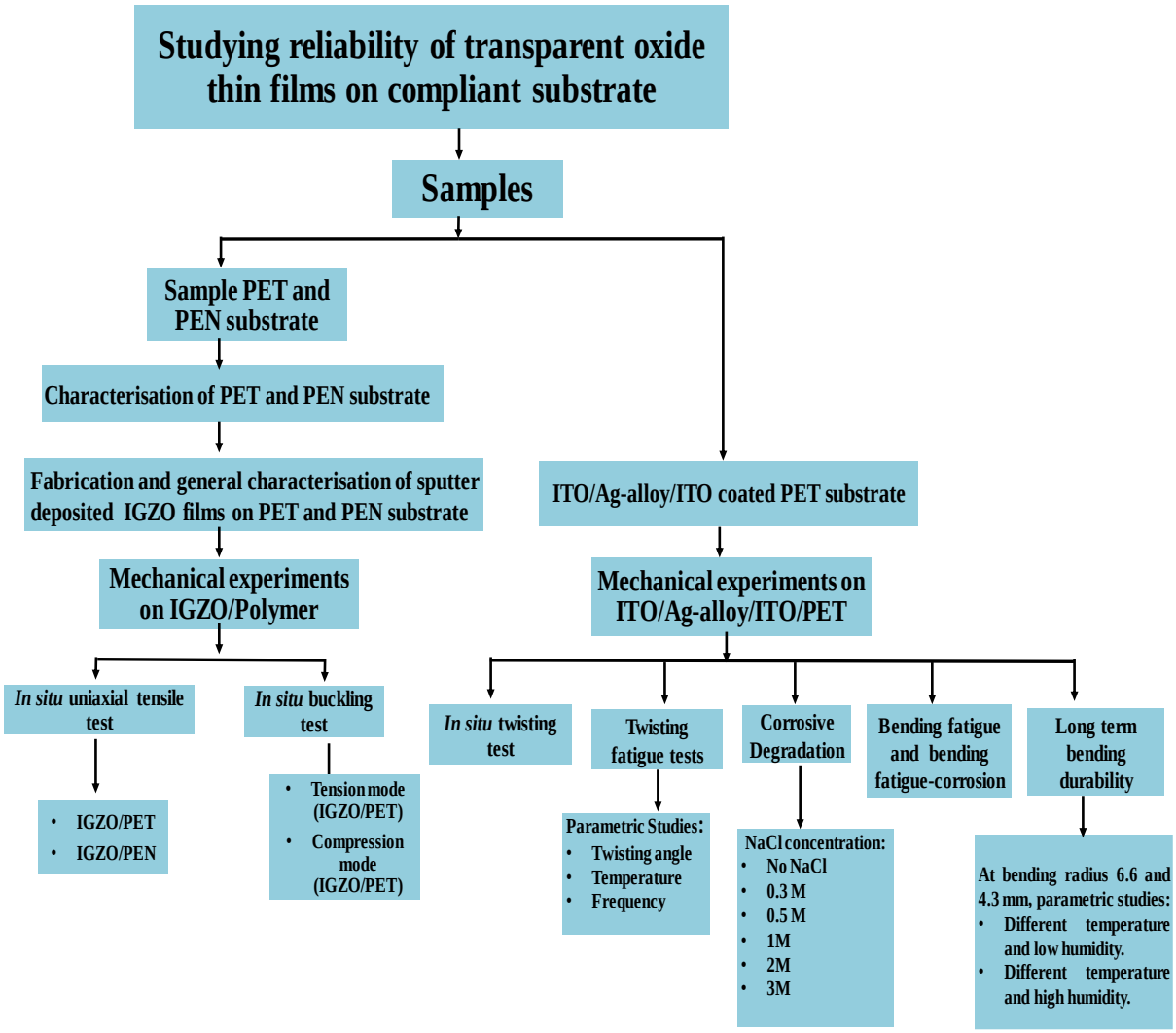

Figure 3-1 Systematic research flow for this study.

3.1. Sample Production and Preparation

3.1.1. Polymer substrates

The polymer substrates that were used are two semi-crystalline polyesters, PET (Melinex ST 504) and PEN (Teonex Q65 FA). Samples of both were supplied in the form of A4 sheet by DuPont Teijin Films [140]. Polymer sheets were separated with paper in order to avoid any surface damage to the surface layer. During the manufacturing processes by Du Pont, the PET and PEN were heat-stabilised and pre-treated on one side by an adhesion-promotion coating. The details are commercially confidential and not available. However, adhesion studies of the coating are not a central feature of this work. The thickness of the biaxially - oriented polymer substrate sheets which was measured by micrometer is 0.125mm.

3.1.2. IGZO coated on PEN and PET

IGZO film of thickness ~50 nm was deposited on to the polymer substrates using RF magnetron sputtering from a In_2O_3:Ga_2O_3:ZnO (1:1:1) target (99.99% purity). The substrates having a dog-bone shape (50 mm length, with 18 mm gauge length and 4 mm gauge width) were cut from sheets using a Moore Hydraulic Press. Prior to introduction inside the sputtering chamber, the polymer substrates were ultrasonically cleaned in acetone, ethanol, and then in deionized water for 5 min each. Deposition was performed (without heating the substrate) in an argon atmosphere and without an oxygen feed. A 10.16 cm diameter ceramic target, 20 cm from the substrate, was used under a base pressure of 5.1×10^{-6} Pa; constant RF power of 55 W; deposition pressure of 0.5 Pa; power density of 0.7 W/cm^2; Ar flow rate of 50 sccm and deposition rate of ~3.3 nm/min. In order to remove contaminant on the surface of

the target, the IGZO target was pre sputtered for 5 min before the deposition of the film. The deposited film was estimated to be 50 nm thick by using ellipsometry measurements on the thickness of a typical IGZO film grown on glass. The IGZO deposition conditions were previously optimized to produce TFTs with a high mobility, low threshold voltage and large switching ratio. Examples of TFT characteristics have been reported previously in [141].

3.1.3. ITO/Ag-alloy/ITO coated PET substrate

The ITO(~95nm)/Ag-alloy (~10 nm)/ITO(~95nm) sheets on PET (125μm) substrate, supplied by Dr G. Potoczny were deposited by a commercial magnetron sputtering machine in CSEM (Brazil). The sheet resistance of the ITO/Ag-alloy/ITO layer was 11Ω/sq. Sheet resistance was measured using a four-point probe.

3.1.4. Salt Corrosion

NaCl solutions were used in the corrosion and fatigue–corrosion experiments. Various concentrations of NaCl: 0.3M, 0.5M, 1M, 2M and 3M were prepared from analytical grade sodium chloride (Sigma-Aldrich and Fisher Scientific) and de-ionised water was supplied by an Elix water purification system.

3.2. Experimental Method

3.2.1. Characterisation of uncoated polymer substrate.

- **Differential Scanning Calorimetry (DSC)**: It is a technique that is used to examine the thermal transition of a polymer. For example, the glass transition temperature (T_g),

crystallisation temperature (T_C) and melting temperature (T_m) can be obtained from this method. Experiments were carried out with a DSC Perkin Elmer 7. Samples of around 10 mg were cut directly from the polymer sheets and loaded in one pan while the other pan which used as a reference was left empty. Both pans were held at 25 °C for two minute and then heated to 290 °C at a temperature ramp rate of 10 °C/min. The resulting temperature changes are monitored and converted to a chart recorder where changes such as crystallisation or melting peaks are recorded. The enthalpy of fusion ΔH_f of the samples was calculated from a DSC thermogram (the area under the melting point). From this the degree of crystallinity X_c of the samples can be determined by using the following equation [142]:

$$X_c = \frac{\Delta H_f - \Delta H_c}{\Delta H_f^o} \qquad 3\text{-}1$$

where ΔH_c is the enthalpy of cold crystallization and ΔH_f^o is the enthalpy of fusion of a pure crystalline polymer.

- **Tensile tests:** The mechanical properties of uncoated polymer substrates were obtained with an Instron 5566 mechanical testing machine. Dog-bone samples were cut from polymer substrate sheets by using a Moore Hydraulic Press. The sample dimensions were 50 mm length, 4 mm gauge width and 18 mm gauge length as shown in Figure 3-2. The strain-stress data are collected using Merlin software. The PET and PEN samples were strained at a crosshead speed of 0.5 mm/min in uniaxial tension at room temperature, the parameters that can then be calculated are elastic modulus and

the yield point of the polymer. Elastic modulus is the slope of the straight line portion of the stress-strain diagram as Figure 3-3 illustrates and is represented by E where:

$$E = \frac{\sigma}{\epsilon} \qquad 3\text{-}2$$

where σ and ϵ are the nominal stress and the nominal strain, respectively.

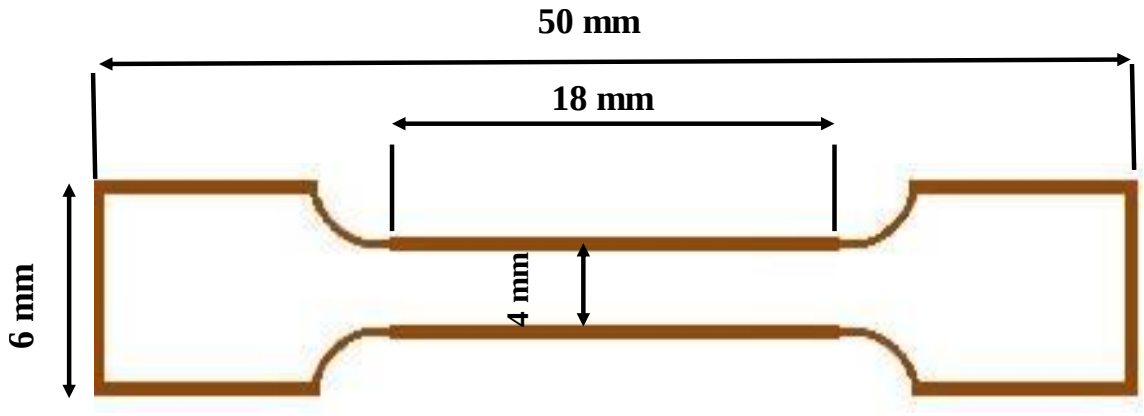

Figure 3-2 Shape and dimensions of dog-bone tensile test sample.

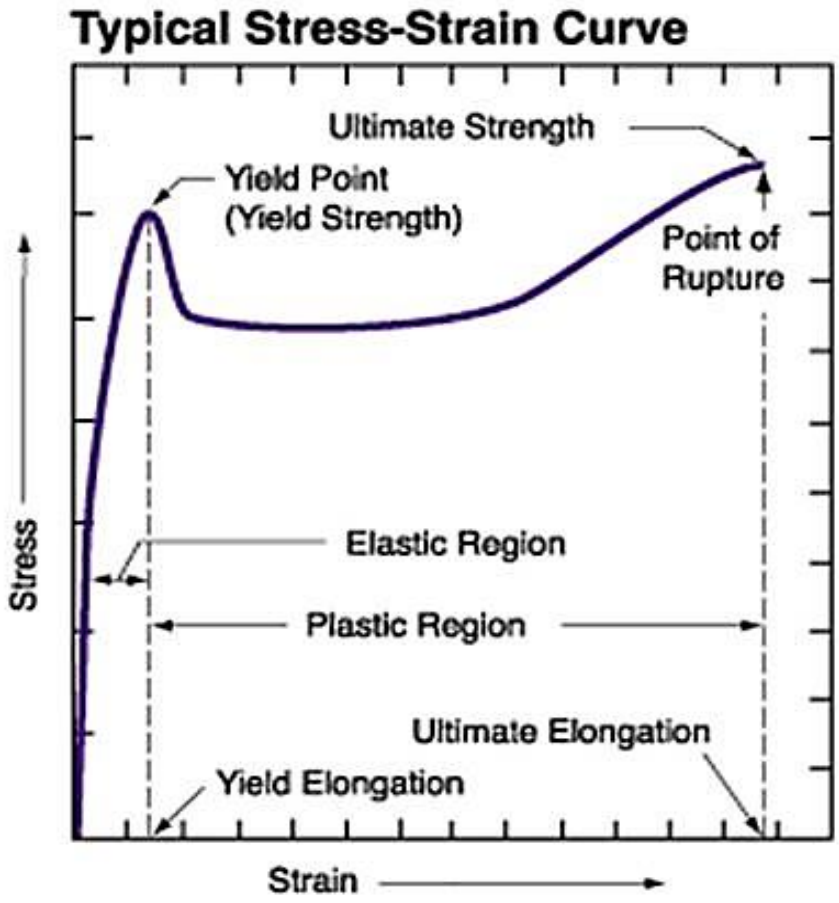

Figure 3-3 Generalized stress-strain curve [143].

- **The Bulge Test:** It was used to study the mechanical behaviour of uncoated polymer samples under biaxial conditions. The biaxial test facility used in this work was designed in a previous project [40] and the experimental set-up can be seen in Figure 3-4. A cylindrical pressure vessel made of brass, of 34 mm inner diameter and 16 cm height is used. A circular sample of diameter 38 mm is clamped on the open orifice of the vessel using a brass ring of 34 mm inner diameter and 38 mm outer diameter. A pressure P is applied, manually, by using the N_2 gas cylinder, and the deflection at the centre of the thin circular sample h, is measured by using a linear voltage displacement transducer (LVDT). It is important to note that the time was monitored,

as 20 KPa of pressure was applied per minute, and this process was repeated until the leak from the failure point takes place. The data are collected and recorded using National Instruments Lab View program.

The initial stress σ_o and biaxial modulus M are important parameters that can affect the performance, efficiency and reliability of thin film devices. The biaxial modulus M can be expressed as follows $M = \frac{E}{1-\nu}$. The biaxial modulus is used because the stress is in a biaxial configuration, therefore the effects of Poisson's ratio ν must be taken into account. M and σ_o could be calculated from the direct fit between the data of P and h , using the generalised bulge equation [144]:

$$P = \frac{h}{a^2} c_1 \sigma_o t + c_2 M t \frac{h^3}{a^4} \quad 3\text{-}3$$

where t is the film thickness , a is the half-width of the membrane, as shown in Figure 3-5, c_1 and c_2 are equal to 4 and 8/3 respectively, and are obtained from the analytical spherical cap mode [40].

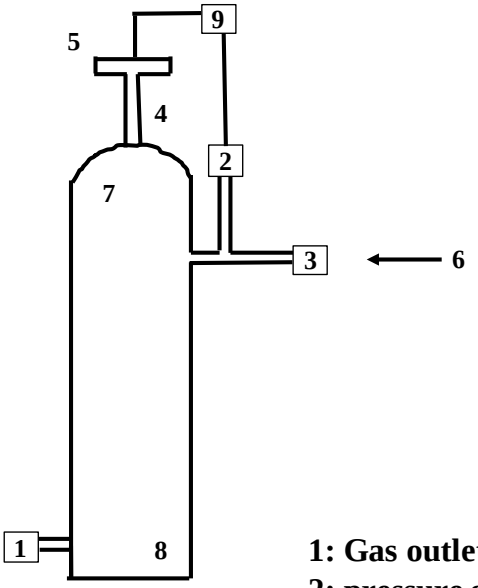

1: Gas outlet valve
2: pressure gauge
3: Gas inlet valve
4: Displacement transducer probe
5:Displacement transducer (LVDT)
6: Nitrogen gas
7: sample
8: pressure vessel
9: PC

Figure 3-4 Schematic of the bulge test system [40].

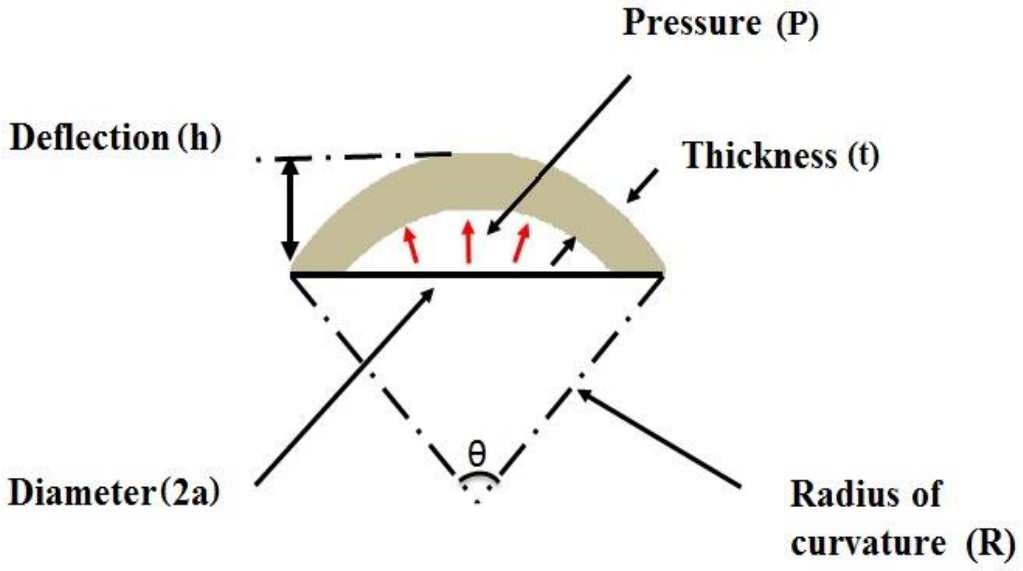

Figure 3-5 Schematic diagram showing geometric deformation of a thin sample using the biaxial bulge test.

- **Dynamic mechanical thermal analysis:** In order to obtain the dynamic mechanical properties of polymers at various temperatures, dynamic mechanical thermal analysis (DMTA) was performed on all samples. This technique measures the deformation of a sample usually by applying an oscillating force in sinusoidal form to a specimen [145].

  The dynamic mechanical properties are described in terms of the storage modulus E' and loss modulus E'' of the sample, which are approximately represented by the elastic and viscous behaviour of the sample respectively. $E'$and $E''$and are the real and imaginary components of the complex dynamic modulus E^*. The strain usually lags

from the stress by an angle δ. The ratio of the loss to the storage defines $tan\delta$ often referred to as the loss tangent [146]:

$$E^* = \frac{\sigma}{\epsilon} \quad 3\text{-}4$$

$$E' = E^* \cos\delta \quad 3\text{-}5$$

$$E'' = E^* \sin\delta \quad 3\text{-}6$$

$$\tan\delta = \frac{E''}{E'} \quad 3\text{-}7$$

The DMTA apparatus was of the type [NETZSCH DMA 242 Cell]. The dimensions of the sample were $30\times4\times0.125$ mm, cut from the dog-bone tensile test sample. Tests were carried out in the tension mode using different vibration frequencies (1, 25) Hz. Samples were heated from 24 °C to 200 °C at 1 °C/min. The storage modulus and $\tan\delta$ were collected as a function of increasing temperature at different vibration frequencies. The T_g was taken as the position of the peak in the temperature of $\tan\delta$ curve [147].

3.2.2. Mechanical experiments on IGZO coated polymer

- **The Uniaxial Fragmentation test** was performed using a miniature tensile testing machine (PL Thermal Sciences) equipped with a 200 N load cell as shown in Figure 3-6 the tensile tester was attached to an optical microscope stage (Leitz Wetzlar model

Epivert) and the images were taken every 3s during the test via a camera (PixeLINK) connected to the microscope in order to monitor the critical onset strain and the development of the cracking of the IGZO-coated PET and PEN as the applied tensile strain increased. The images were collected by a computer using LINK software and can be combined with stress-strain data. The extension and load signals were recorded by National Instruments Lab View software, and treated in order to obtain stress and strain data. Tests were carried out on dog-bone samples at 0.1 mm/min. It is observed that under a continuous loading situation it was difficult to focus the microscope if the loading rate was too fast but that a slow loading rate of 0.1 mm/min allowed us to accurately capture the crack pattern. The development of IGZO cracking was analysed in terms of crack density (CD) at each applied strain increment. The crack density that was defined as the inverse of the average spacing between the cracked IGZO thin film was obtained from optical microscope photographs using image analysis software (Image J).

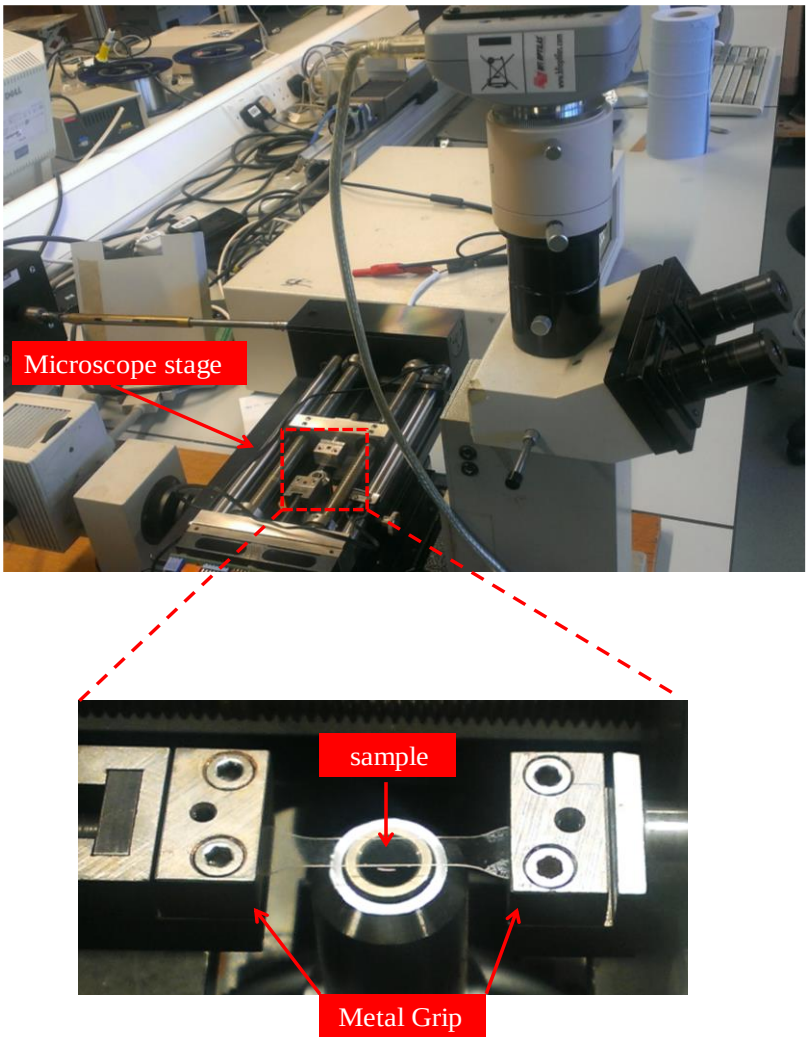

Figure 3-6 Image of miniature tensile testing machine

- **Buckling test :** The equipment which was originally designed to determine the critical failure strain of optical fibres was slightly modified to test the IGZO/polymer samples. Figure 3-7 shows the experimental set-up used in this case.

.

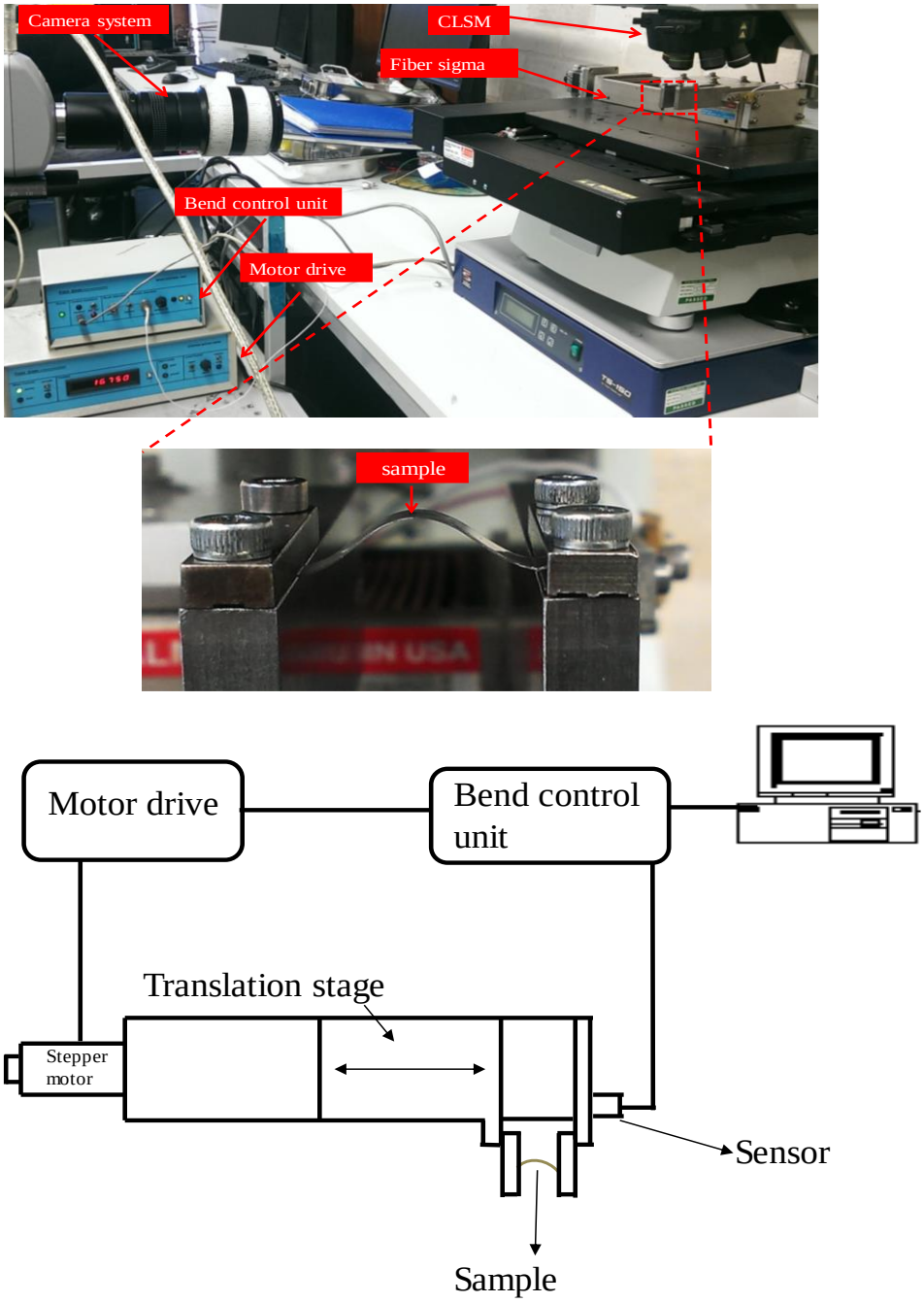

Figure 3-7 Photograph and schematic diagram of the buckling test set-up used in this study.

Metal plates were prepared and attached to the Fiber Sigma rig (ALM WESTBURY, NY). The sample with dimension 30×4 mm, is clamped between the two parallel plates, where one plate is movable causing the sample to bend at crosshead speed set at 0.5 mm/min, while the other plate is fixed. The distance between the two parallel plates *L* (20 mm) was decreased stepwise (0.25 mm) under an applied force driven by a stepper motor until the maximum bending strain value was reached. The image was taken at each loading step during a three-minute holding period. The buckling apparatus was mounted under the CLSM to determine crack onset strains under both tension and compression and to monitor crack propagation. *In situ* optical observation was used as a simple and effective way to determine the crack-initiation strain of the thin film, particularly as the film is non-electrically conductive [148]. CD was obtained in a similar manner to that obtained in the uniaxial fragmentation test**.** The angle of curvature θ was measured using a side-view digital imaging system and image analysis software (Image J). The radius of curvature, R can be written in terms of the axial displacement *e* by using an analytical large deflection solution [149]; the cross-sectional view of buckled specimen is schematically shown in Figure 3-8

$$\frac{\mathrm{e}}{\mathrm{L}} = 2[1 - \frac{\mathrm{E(k)}}{\mathrm{K(k)}}] \qquad 3\text{-}8$$

$$\frac{\mathrm{L}}{\mathrm{R}} = \mathrm{NK(k)\ k} \qquad 3\text{-}9$$

$$\mathrm{k} = \sin\frac{\theta}{2} \qquad 3\text{-}10$$

where K(k) and E(k) and are the complete elliptical integrals of the first and second and N is equal to 8 for clamped ends. Combining equation 3-10 and equation 3-9 with equation 3-8 , R is given by:

$$R = \frac{2L - e}{16E(k) \times \sin\frac{\theta}{2}} \qquad 3\text{-}11$$

where E(k) was obtained based on the Eq (a-1) in [150]. Hence, from R the values of the resulting buckling strain ϵ were calculated by using equation 2-7.

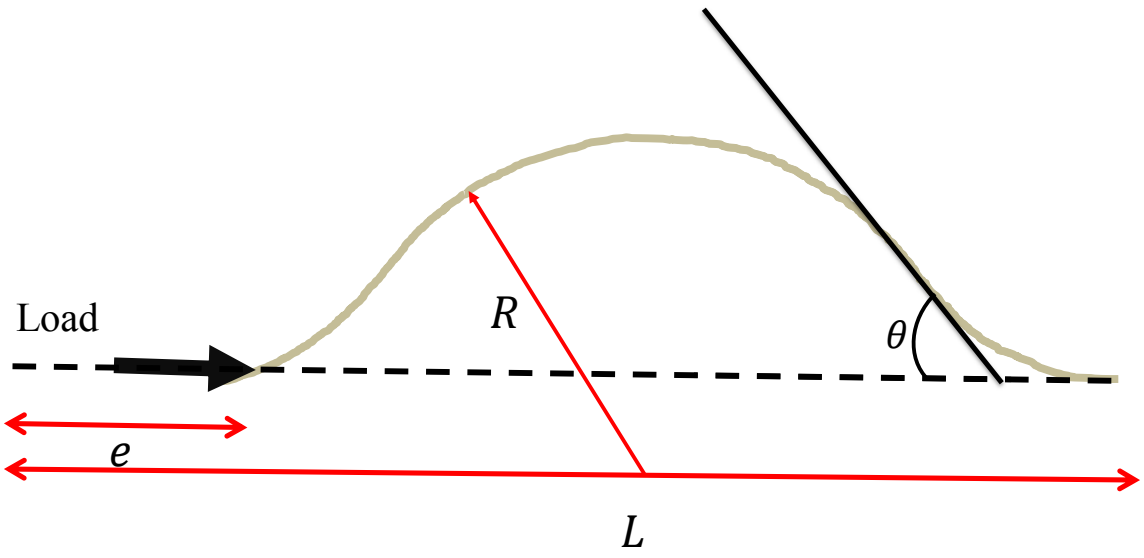

Figure 3-8 Schematic diagram of the buckled specimen - Clamped ends.

3.2.3. Electro-mechanical experiments of ITO/Ag-alloy/ITO coated PET

- **Twisting Test:** It was carried out using a twisting apparatus in order to investigate the twisting durability of the ITO/Ag-alloy/ITO coated polymer. The twisting apparatus as shown in Figure 3-9 was designed in this project and can be operated manually. Goniometers, originally used either to measure the angles between crystal faces in

crystallography or to rotate samples in X-ray diffraction, were used as a torsional device for rotating the ITO/Ag-alloy/ITO coated PET, enabling fine control rotation angle as low as 2°. They were attached into a rigid frame. Metal grips were prepared and connected to both goniometers to clamp the specimen. For *in situ* electrical resistance monitoring purposes, a plastic plate was placed between each metal grip and each goniometer to provide a closed electrical circuit (see Figure 3-9). Then, two copper wires were attached to both grips and connected to a FLUKE 45 multimeter. A computer running National Instruments Lab-View software was used to collect electrical resistance data. The twisting apparatus was placed underneath the CLSM to monitor film crack initiation and propagation. The clamped sample 30×4 mm was twisted in opposite directions by each goniomoter. The twisting angle was increased stepwise to around 62° so that image and change in electrical resistance could be recorded at each twisting step during a 3-minute hold.

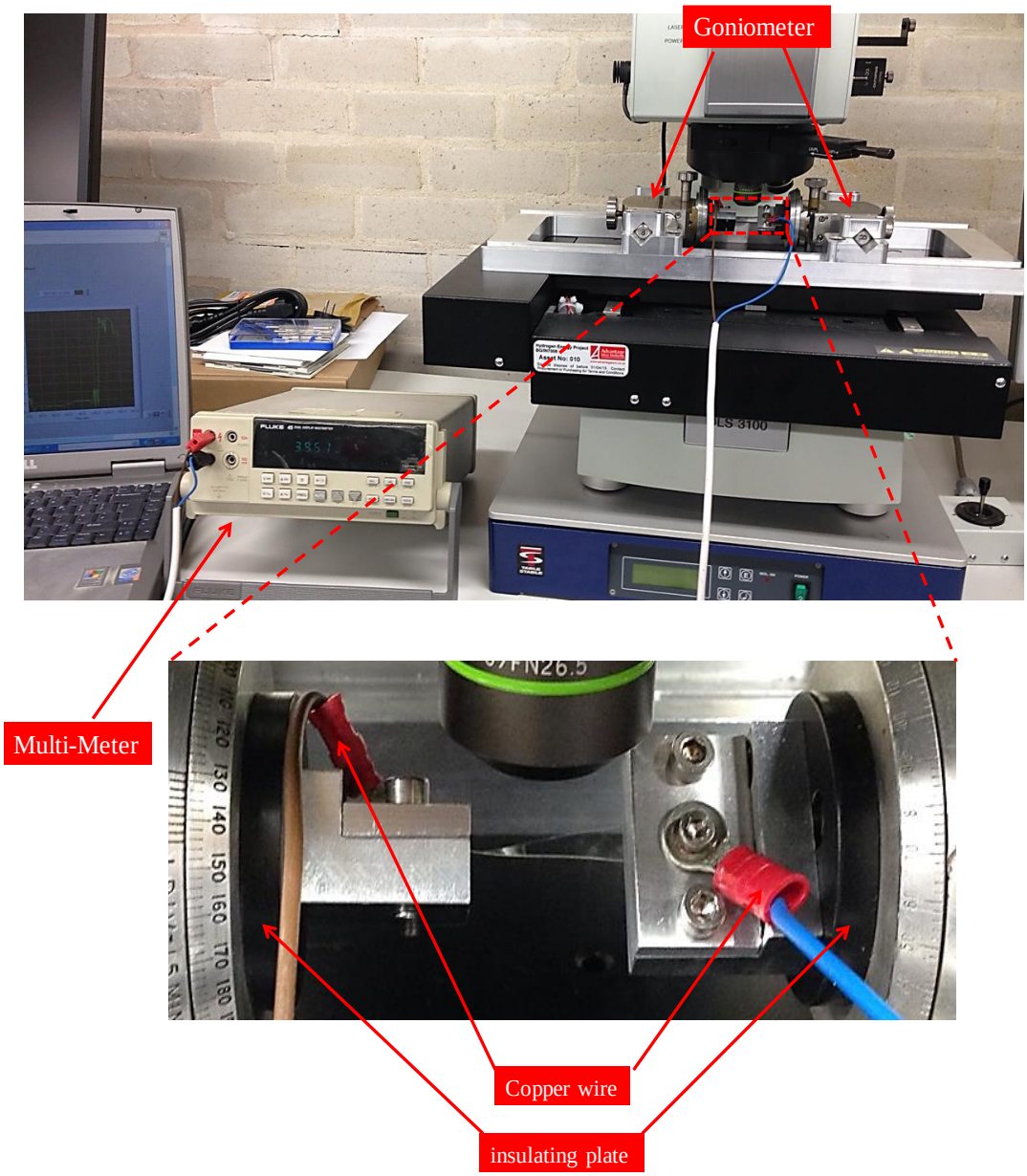

Figure 3-9 Custom -built twisting loading apparatus.

- **Twisting fatigue test:** The commercial rheometer machine (A RES) equipped with a temperature-controlled oven are typically used to measure flow and deformation of rheological materials under applied forces [151]. However, several modifications to the apparatus were used in this project to investigate the twisting fatigue behaviour of

ITO/Ag-alloy/ITO coated PET. First, two grips were prepared and attached to the two jigs that screw in to the crossheads of the rheometer to hold the sample under investigation. The top jig is fixed to the base of the rheometer machines while the other in the bottom, is moving with a rotational driver, as shown in Figure 3-10. During the experiment the lower jig is rotated about the Z - axis causing the specimen to twist in a clockwise and anti-clockwise direction. Similar to the twisting testing experiment, in order to close the electrical circuit and measure the electrical resistance change, the bottom jig is insulated from the base of the rheometer machine by using a polymer plate and also plastic screws as shown in the inset of Figure 3-10. As earlier, electrical resistance is monitored by a multimeter and recorded by Lab View software. In order to keep the sample flat and stable, a small initial load was applied before the starting the test. In addition, a calibration was performed to link the applied strain to the twisting angle. Angle (17.5°, 22.5°, 27.5°), frequency (10 cycles/min and 5 cycles/min) and temperature (RT, 50 °C, 100 °C) were all used as the experiment parameters. The device's limiting twisting angle is 27.5° beyond which the sample does not twist. Also, the maximum temperature used was 100 °C because this allowed measurements either side of the Tg of PET. This set up is controlled by Orchestrator software. Samples of the same dimensions as those used in the twisting experiments were cut from the coated film. The measured torques were (38, 43, 48 g.cm) for an angle of 17.5°, 22.5° and 27.5°, respectively. An air oven was used to heat the sample. 10 minutes were set aside before each material tested to reach the necessary temperatures. At any selected angle, such as at 17.5°, during one complete cycle the sample will twist from 0° to 17.5°, 0°, -17.5°, and then back to 0.

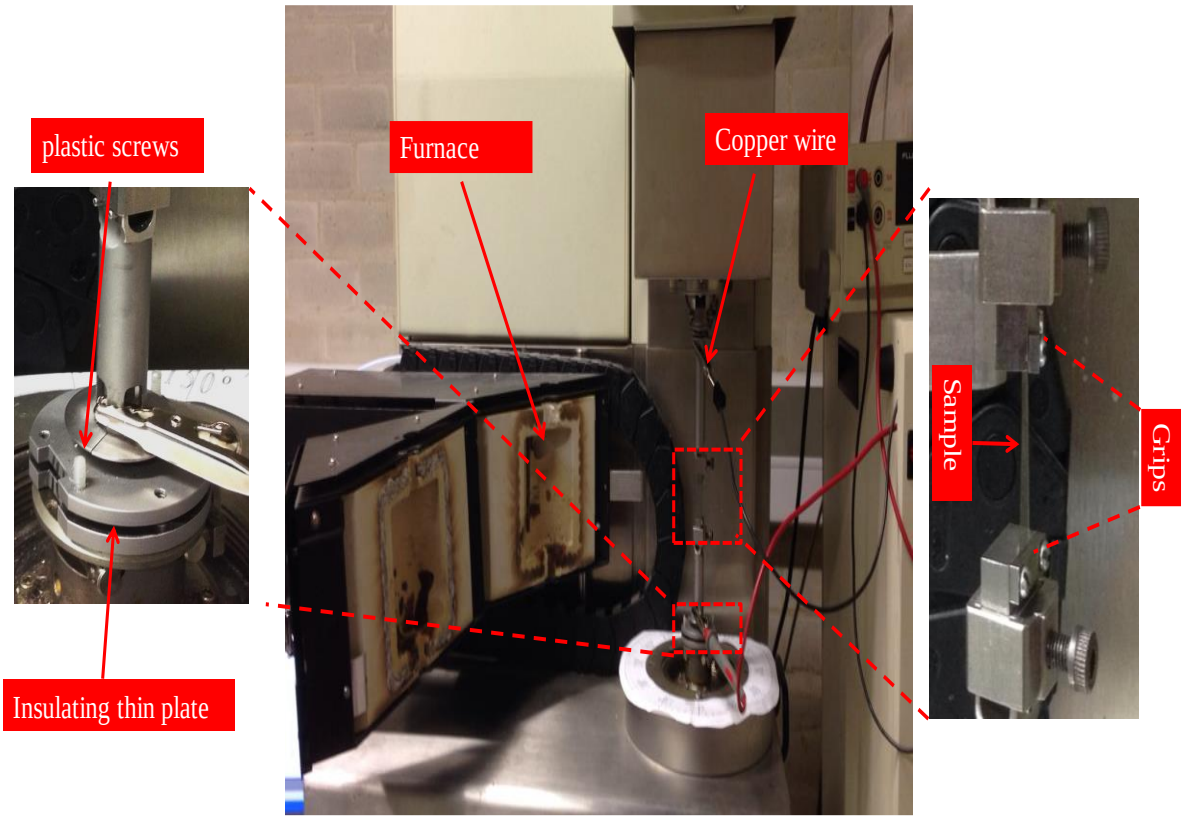

Figure 3-10 The twisting fatigue experiment set-up used.

- **Corrosion testing:** The sample as schematically shown in Figure 3-11 was cut from ITO/Ag-alloy/ITO sheet. The samples were cleaned using distilled water and dried in cold flow air before performing the experiment. The samples with edges clamped using crocodile clips were fitted inside an open plastic container. Then the container was filled with either 0.3,0.5, 1, 2, or 3 M NaCl solution and left for 16,000 and 57,6000 seconds at room temperature and the change in the electrical resistance was monitored *in situ*. The concentrations were chosen because sea-water has salt

concentrations of 0.5 M [152] and the time periods were chosen arbitrarily for experimental convenience. In addition, special care has to be paid in order to prevent stressing the sample when clamping it inside the container using copper conductive tape, the end of each sample was coated by it for electrical resistance measurement. After, the length of time required for immersion, the samples were removed from the NaCl solution, and then they were quickly washed again by distilled water and subsequently dried in air.

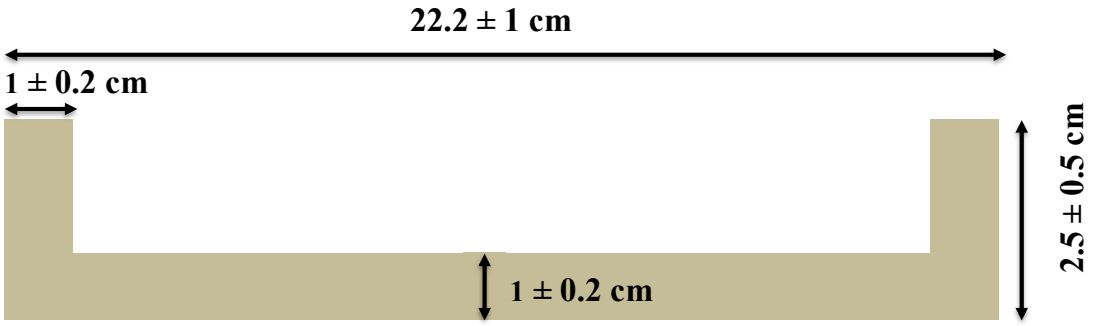

Figure 3-11 Schematic diagram of the ITO/Ag-alloy/ITO coated PET sample used in corrosion experiments.

- **Corrosion-fatigue testing:** Custom-built cyclic uniaxial bending apparatus based on that used in [139] was utilized. A schematic diagram and the setup of this experimental display is shown in Figure 3-12 . The sample was wrapped over a mandrel made from chlorinated polyvinyl chloride (c-PVC) on one end and fixed to a spring balance at the other end. Copper conductive tape was used at each end of the sample to allow electrical contact for resistance measurements. A large c-PVC mandrel (R >> r) supported the sample in the horizontal position and prevented sagging of the sample. Due to the cost of the software that drives the reciprocating rotary

motion in the original, a servo motor was utilized to rotate the mandrel instead of the stepper motor used by Bejitual *et al*. [139]. The reciprocating rotary motion of the servo motor was controlled by an Arduino board driven using Arduino software [153]. Tests were run at fixed reciprocating frequency of 2 cycles/sec. The test was carried out for few hundred thousand of cycles. The response of the film in term of the electrical resistance was monitored *in situ* using multimeter. A high-density polyethylene (HDPE) container was filled with 0.3 M of NaCl solution for the corrosion-fatigue test. Before and after testing, the samples were washed by distilled water and dried using compressed air. The data obtained through this test are the number of cycles to failure and electrical resistance. Note the ITO/Ag-alloy/ITO surface is placed under tension mode. According to the mandrel radius r of 12.5 mm, sample strips of approximately 202 mm in length and 10 mm in width were cut out. The bending tensile stain ϵ from this mandrel was calculated to be 0.5% using equation [92]:

$$\epsilon = \frac{t_s + t_f}{2r} \qquad 3\text{-}12$$

where t_s and t_f are substrate and the film thickness respectively.

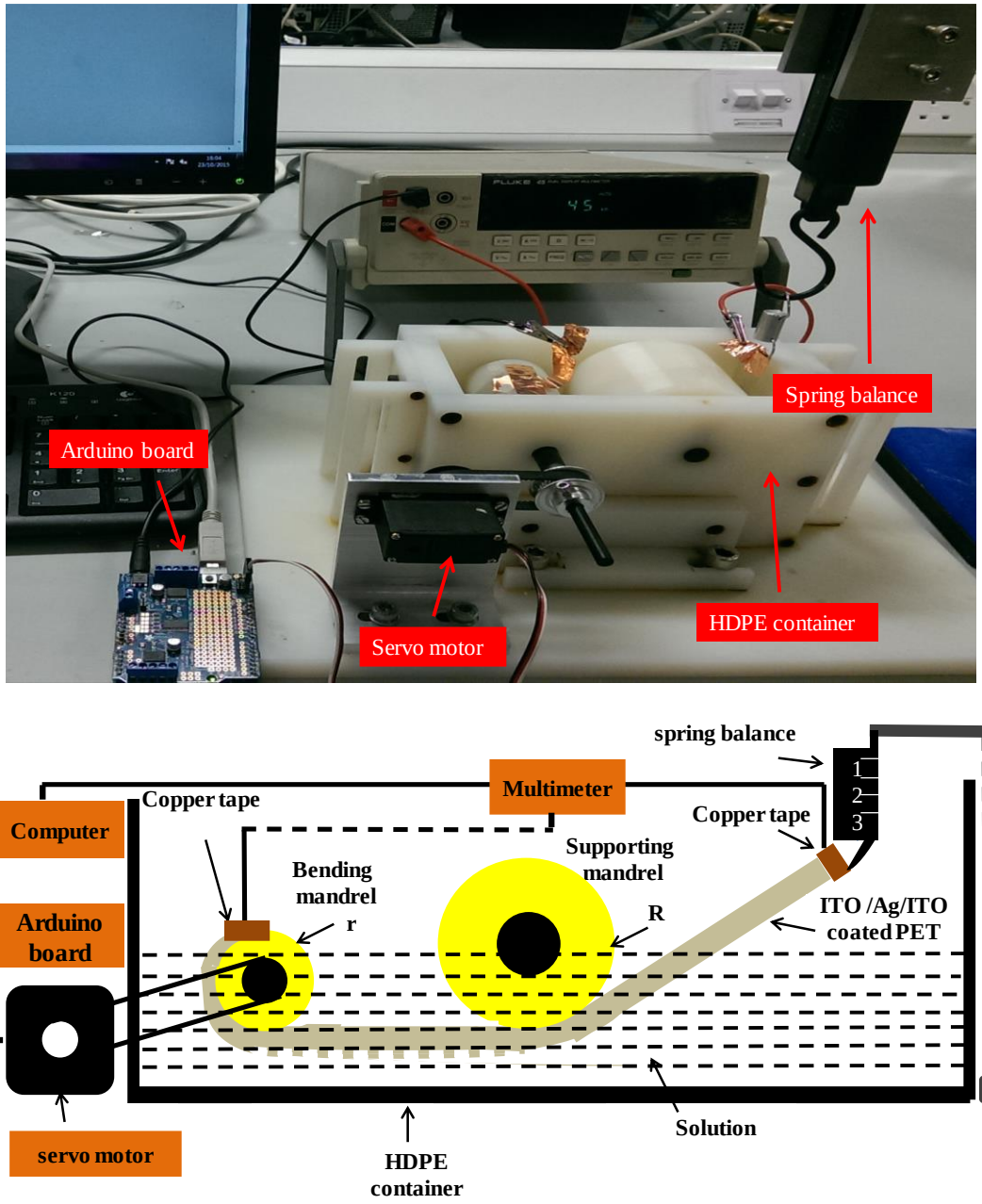

Figure 3-12 Photograph and schematic diagram of the custom--built bending fatigue apparatus.

- **Long term bending under harsh environments:** Long-term bending of ITO/Ag-alloy/ITO coated PET was evaluated using the test apparatus used for the buckling tests on IGZO (see Figure 3-13). Samples with dimension 30×4 mm were clamped in

place between two parallel plates and loaded in steps at speed 0.5mm/min by a computer-controlled stepper motor until they reached the selected radius of curvature (6.6 or 4.3 mm) which is equivalent to strains of 0.94% or 1.44% (determined using the method described above in section 3.2.2). The apparatus was placed underneath the CLSM for photographing the surface of the sample during a 3 min time period. The time period was chosen to allow the machine to scan and photograph the sample. The bend apparatus was unable to be inserted in the environmental chamber, therefore, to remove the two parallel plates from the bending test apparatus and keep the sample under load, an adjustment plate was prepared and attached above the two parallel plates as can be seen in the experimental set up in Figure 3-13. Then the two parallel plates were placed in an environmental chamber. It is necessary to insulate the testing area and to measure the change in electrical resistance *in situ* inside the environmental chamber; hence the adjustment plate was attached to the parallel plates with plastic screws and had thin plastic sheets placed between them and parallel plates. Prior to running the experiment, the environmental chamber was turned on to stabilize the humidity and temperature. After the temperature and humidity reach the chosen values and the environmental chamber has stabilized for approximately 10 mins, the experiment was started and the electrical resistance was measured for 57,600 seconds. Then the load sample was removed from the environmental chamber and the surface was examined again using CLSM. The experiments were performed at 25 and 65 °C combined with low and high relative humidity of (25% and 80%).

(a)

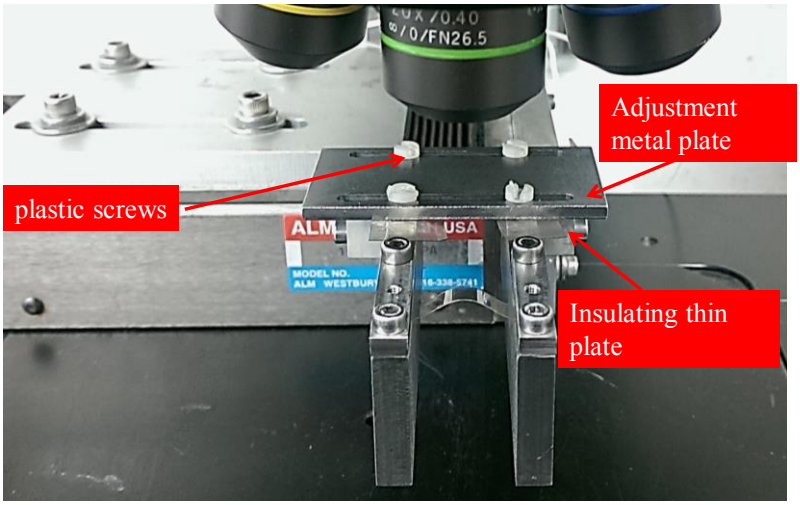

(b)

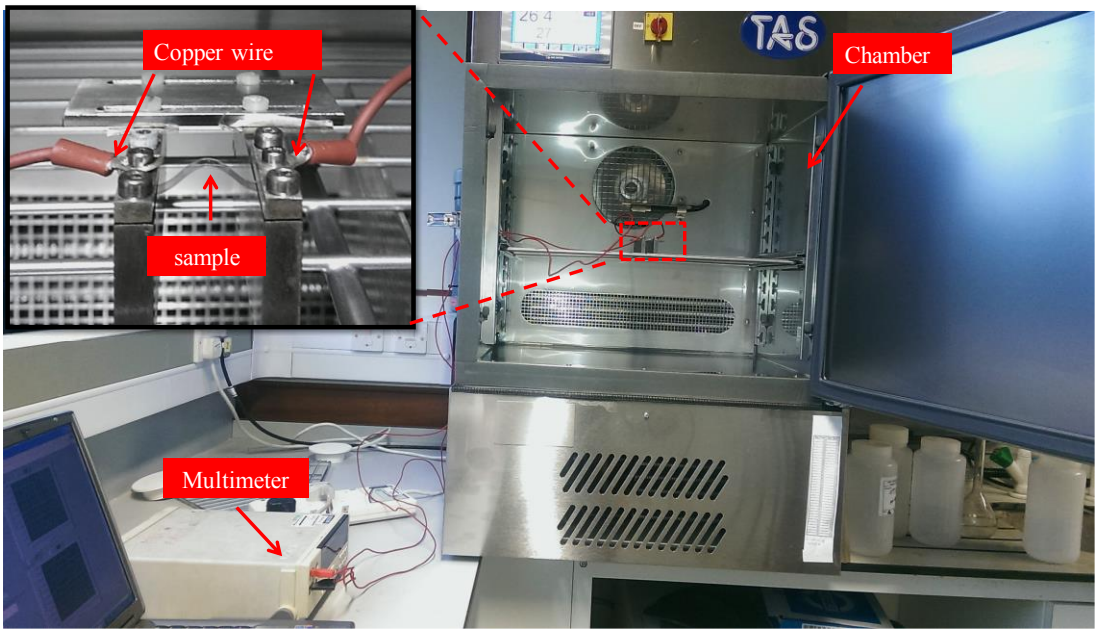

Figure 3-13 (a)The sample secured into bending apparatus attached to CLSM (b) Illustration of experimental set-up.

3.3. Optical transmission measurement

Optical transparency measurements of uncoated polymer substrates, IGZO and ITO/Ag-alloy/ITO coated samples were carried out using a Jenway 6310 spectrophotometer. The absorbance spectrum was recorded as a function of wavelength between 380 nm and 1000 nm, then it was converted to transmittance using the well-known Lambert-Beer's equation [154].

$$A = -\log T \qquad 3\text{-}13$$

where A absorbance and T is transmittance. Five samples were used to determine the average transmittance in the visible range from 400 nm to 800 nm.

3.4. X-ray diffraction

X-ray diffractometry (Bruker D8-Advance) was used in this project in order to study the crystalline structure of the materials. XRD patterns were collected for both the substrate and a-IGZO coated sample and ITO/Ag-alloy/ITO before and after exposure to temperature. Monochromatic CuKα1 radiation (λ = 1.54056 Å) was utilised as radiation source. The samples were scanned over a 2θ range of 20° to 70° angle using an approximate step size of 0.028°.

3.5. Microscopy

Various different types of microscopes were used to investigate surface morphology and the film composition:

- **Scanning Electron Microscopy (SEM):** It is the most commonly selected microscopy in modern laboratories due to its combined properties of both high lateral resolution and good depth of focus. A JEOL JSM – 7000F FE – SEM microscope equipped with a field emission gun was used. Besides imaging the topography, the system was also able to provide information on the chemical composition of the sample through energy dispersive x-ray spectroscopy (EDS). INCA EDS software was used to determine composition. Focused ion beam (FIB) microscopy was also used to produce high magnification and high resolution images. A conductive tape was used to attach samples on to an SEM stub. Prior to SEM observation, the samples were sputtered with gold to dissipate electric charges. The images were taken under an accelerating voltage of 15 kV and working distance of 10 mm.

- **Atomic force microscopy (AFM):** It uses a very sharp tip attached to a cantilever which is using to scan the surface of the sample as shown in Figure 3-14. During the scan, the tip approaches extremely closely to the surface of the sample and van der Waals forces between the surface and atoms of tip can take effect. These forces cause a deflection of the cantilever reflecting the topography of the sample surface. The specific microscope used in this study was of the type Nano Wizard II atomic force microscope (JPK Instruments, UK) operating in contact mode conditions and primarily used to investigate the roughness of PET and PEN samples. Silicon cantilevers with a spring constant of 0.3 N/m were used with an operating frequency of 330 Hz. The average of five values of root mean square roughness (RMS) at different places was taken for each sample.

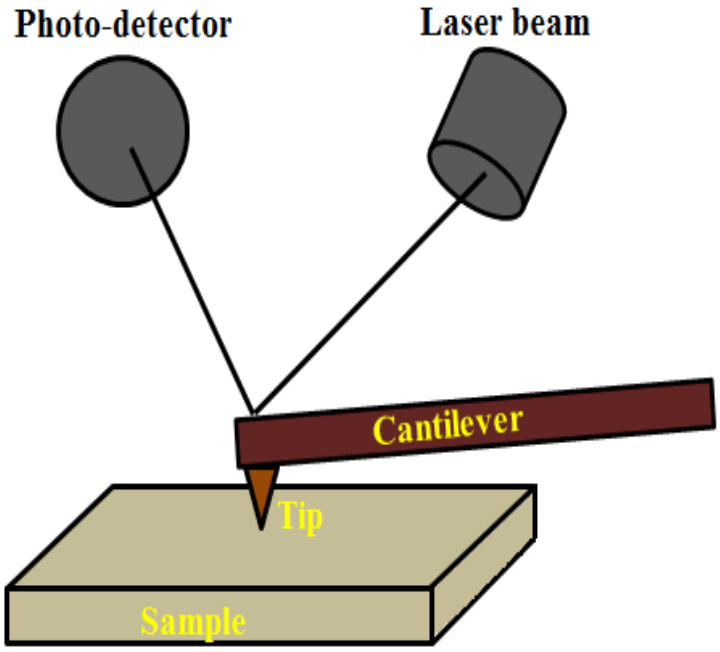

Figure 3-14 Schematic representation of the AFM system. The photo-detector records differences in the reflection angle of the laser resulting from movements of the cantilever.

- **Confocal laser scanning microscopy (CLSM):** It is a scanning imaging technique which can obtaine high resolution images and uses a laser light as a light source that illuminates a small spot on the specimen. A schematic representation of the optical pathway in a CLSM system is shown Figure 3-15. The incident laser light is focussed into a spot on the sample. Hence, by operating an isolated optical system, the reflected light is focussed and transmitted into the special filter (pinhole) on to a detector without any loss. The scattered or emitted light by other planes than the focal plane is deliberately dimmed. It is important to note that no sample preparation is required prior to the investigation and it is relatively easy to use an appropriate testing machine for *in situ* experiments. The microscope was used in this study was an Olympus LEXT OLS3100. Because it has a very stable stand, it is useful for the *in situ*

experiments where the bending and twisting apparatus could be placed on top of the stage and the crack progress viewed.

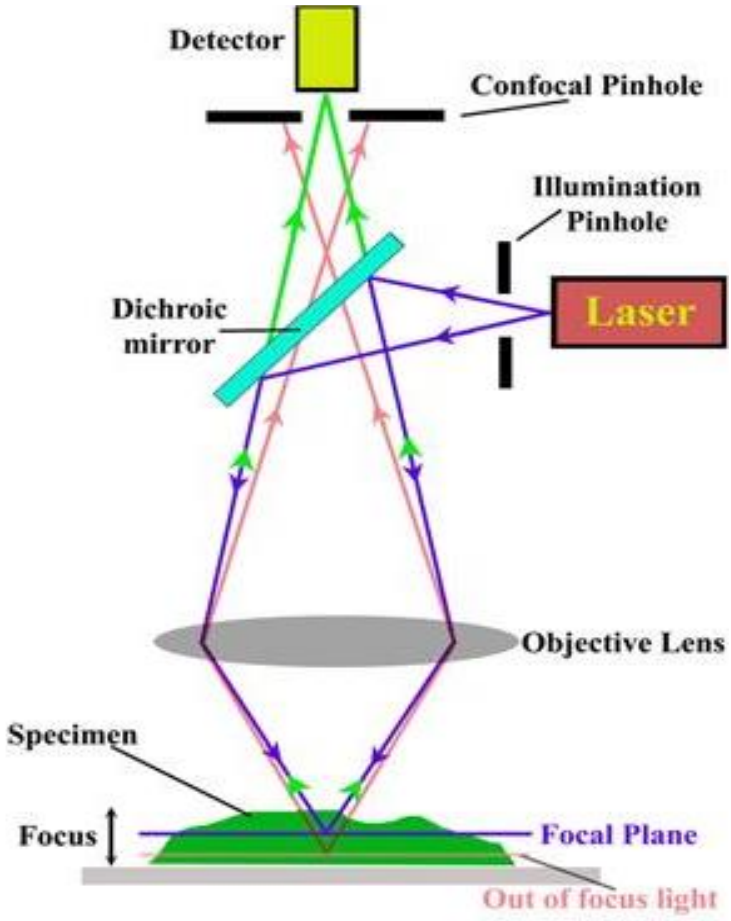

Figure 3-15 Schematic diagram illustration of the working of a CLSM [155].

4. Potential substrate for use in flexible display applications

4.1. Introduction

In this chapter, substrate characterisation methods such as thermal, optical methods and mechanical and surface properties are investigated and discussed for the polymer substrates used as candidates in flexible electronics device.

4.2. Results and discussion

4.2.1. DSC Analysis of PEN and PET

T_g and T_m of PEN and PET were measured by using a differential scanning calorimeter (DSC, Perkin-Elmer DSC-7). Figure 4-1 displays the DSC curves for the PEN substrate. It is observed that the peaks related to the glass transition temperature and the melting temperature are 122.6 and 261.5 °C respectively. In addition, the weak peak appearance at a temperature of 239 °C before the final melting point was attributed to the melting of small or imperfect crystallites produced on heating or orientation processes [156]. The heat of fusion, ΔH_f which is equal to 40.5 J/g was obtained from the area under the melting peak. Thus the degree of crystallinity of the PEN substrate was calculated to be equal to 39.3% by using a previously observed value of heat of fusion of 100% crystalline PEN polymer which is equal to 103.4 J/g [157]. The T_g and T_m values from the DSC measurements for the PET substrate are shown in Figure 4-2. The T_g was observed at 77 °C and the melting peak temperature was observed at 255.5 ^oC. Also, pre-melting starts to appear at a temperature of 220 ^oC similarly to that of PEN substrate. The area under the melting peak which represents the heat of fusion is equal to

44.9 J/g. Alves *et al*. [142] reported that the theoretical value of heat of fusion of 100% crystalline PET is equal to 140 J/g. Consequently, the crystallinity of the PET substrate was obtained to be equal to 32.1%.

The values of T_g, T_m and the degree of crystallinity of PEN and PET are also listed in Table 4.1. The figures and table show that the T_g and T_m of PEN and PET substrate are very close to the values reported in the literature by Robert *et al*. [16] for T_g and by MacDonald *et al.* [32] for T_m . In addition, it is clear to see that the T_g of PEN is higher than the T_g of PET whereas the T_m of PEN is only a few degrees higher than the T_m of PET which can be attributed to the discrepancy in chemical structure between PEN and PET [32]. Also, PEN was found to have a high degree of crystallinity compared to that of PET, which gives it a high elastic modulus.

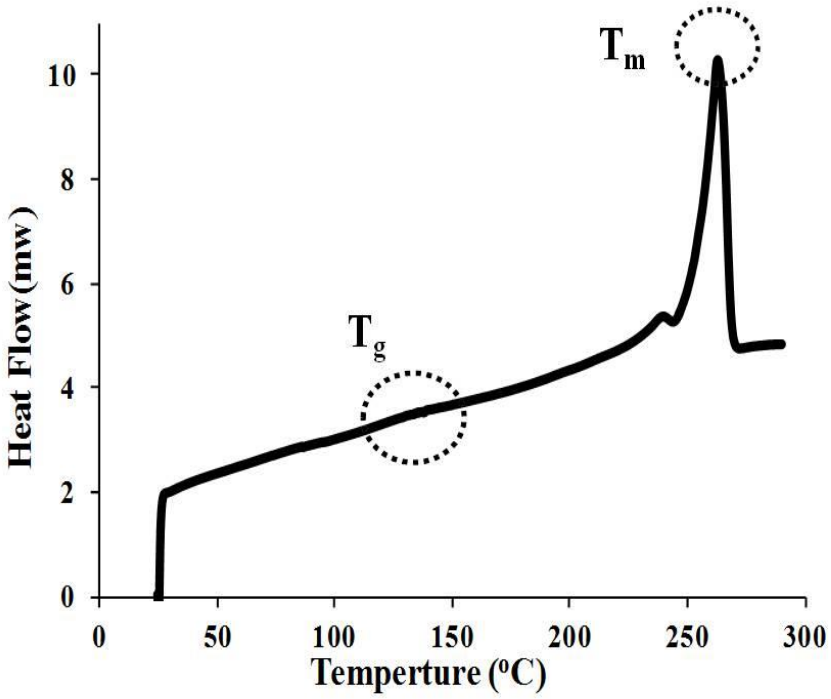

Figure 4-1 DSC graph of PEN Teonex Q65 FA.

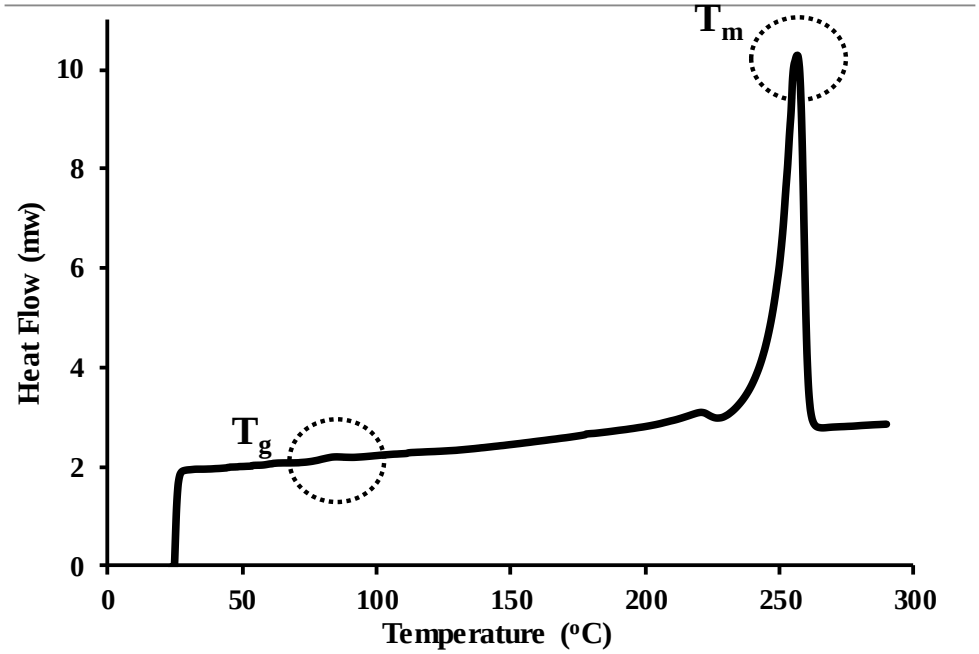

Figure 4-2 DSC graph of PET Melinex ST 505.

Table 4.1 The values of T_g,T_m, X_c and ΔH_f obtained for PEN and PET using the DSC technique.

Property	**PEN**	**PET**
Glass transition temperature, T_g/(°C)	122.9	77
Melting temperature, T_m/(°C)	261.5	255.5
Heat of fusion (J/g)	40.5	44.9
Degree of crystallinity (%)	39.3	32.1

4.2.2. Optical transmission

The optical transmission measurements for PET and PEN substrate were conducted using A Jenway 6315 Spectrophotometer. Figure 4-3 presents the optical transmittance in the wave length range 350-1000 nm for semicrystalline PET and PEN substrates. PEN transmittance started to increase at wavelengths ≥ 380 nm, in comparison to PET's transmittance at wavelengths ≥ 350 nm. This difference is due to the naphthalene ring group in PEN that brought with it a chromophore. It is observed that the average transmittance in the visible wavelength spectrum (400- 800 nm) for both substrates was approximately equal to 86%. These results are in good agreement with the data obtained elsewhere [34].

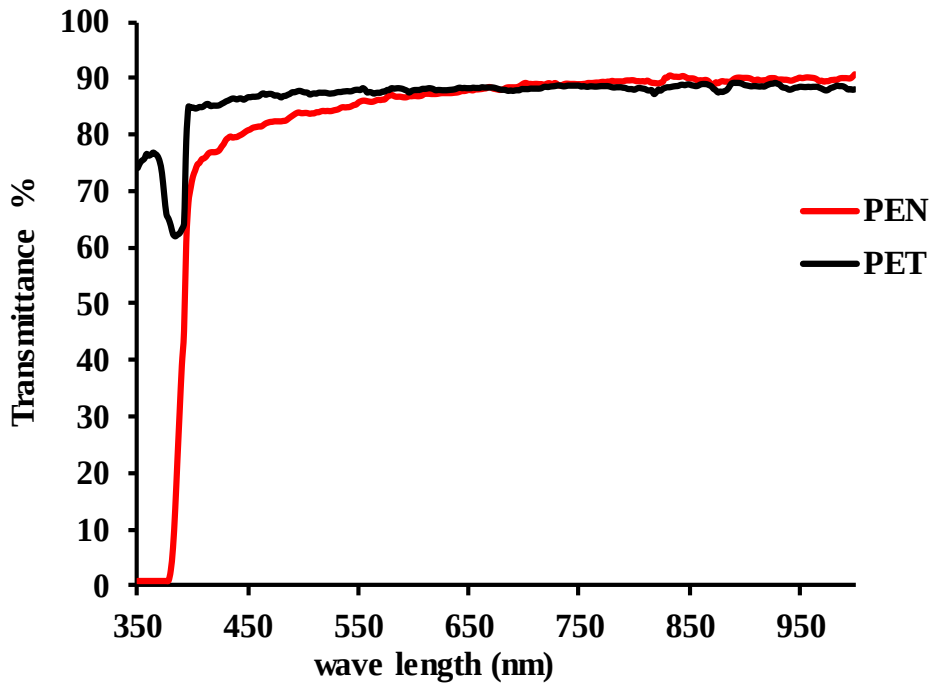

Figure 4-3 Transmittance spectra of semicrystalline PET and PEN.

4.2.3. Surface morphology properties

The surface morphology of polyester substrates was investigated using contact mode AFM techniques in order to understand the role it plays when additional layers such us IGZO are deposited on the polymer.

The top and back of PET and PEN substrates were examined. Figure 4-4 shows surface morphology of the top PET substrate. Several elongated features were observed that protrude on the order of only a few nanometres above the film surface. RMS roughness that is measured over an area of 2×2 μm^2 is relatively small and equal to 1.04 ± 0.03 nm. Beake *et al.* [158] observed similar topography for biaxially-oriented PET by using tapping mode AFM. Their studies suggest that these features are more likely to be plate-like crystallites. Also the RMS roughness parameter was in good agreement with the results by Benmalek *et al.* [159] who reported for biaxially oriented PET films a value of 1.13 nm.

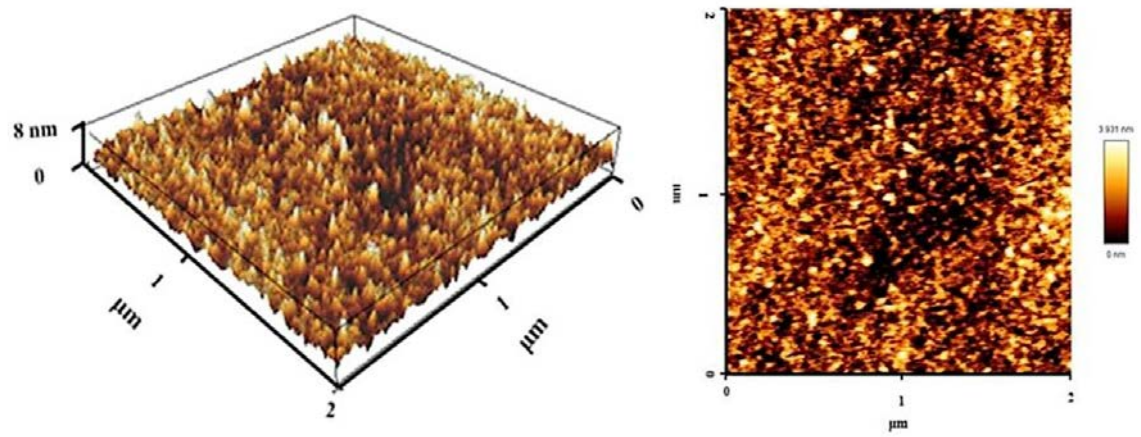

Figure 4-4 AFM (3D) left and (2D) right view images of the top PET substrate.

In addition, Figure 4-5 displays the surface morphology of the back PET. Many lumps were observed. It shows a higher RMS roughness of surface 7.21 ± 0.4 nm, as compared with the top PET surfaces. This difference comes from the adhesion pre-treatment of the top PET substrate.

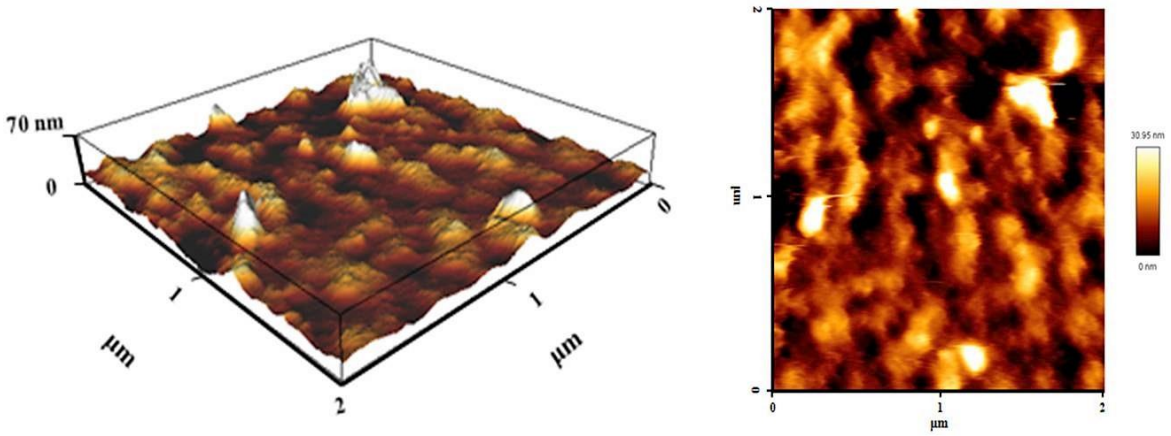

Figure 4-5 AFM (3D) left and (2D) right view images of the back PET substrate.

Furthermore, the surface morphology of the back PEN is presented in Figure 4-6. Extended long surface features similar to those of the top PET were observed. In addition, the back PEN exhibits slightly higher RMS 1.4 ± 0.04 nm as compared to root mean square roughness of the top PET surface.

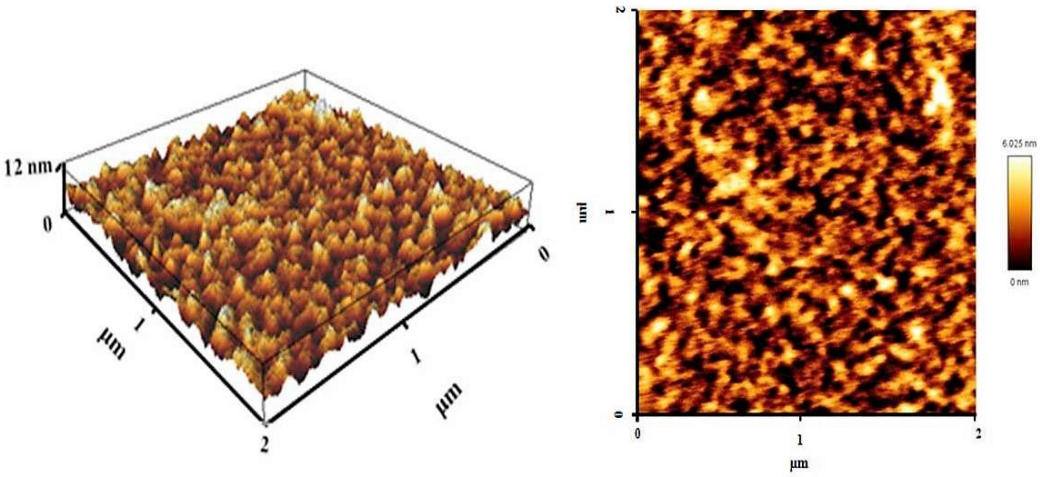

Figure 4-6 AFM (3D) left and (2D) right view images of the back PEN substrate.

Figure 4-7 presents the surface topography of the top PEN substrate. It can be observed that the elongated features are absent in this case. However, some small lumps and few large ones exist. RMS roughness of top PEN surface is approximately equal to 8.1 ± 0.3 nm and it is higher than that of the back PEN. The smoother surface of back PEN is attributed to an adhesion promotion coating.

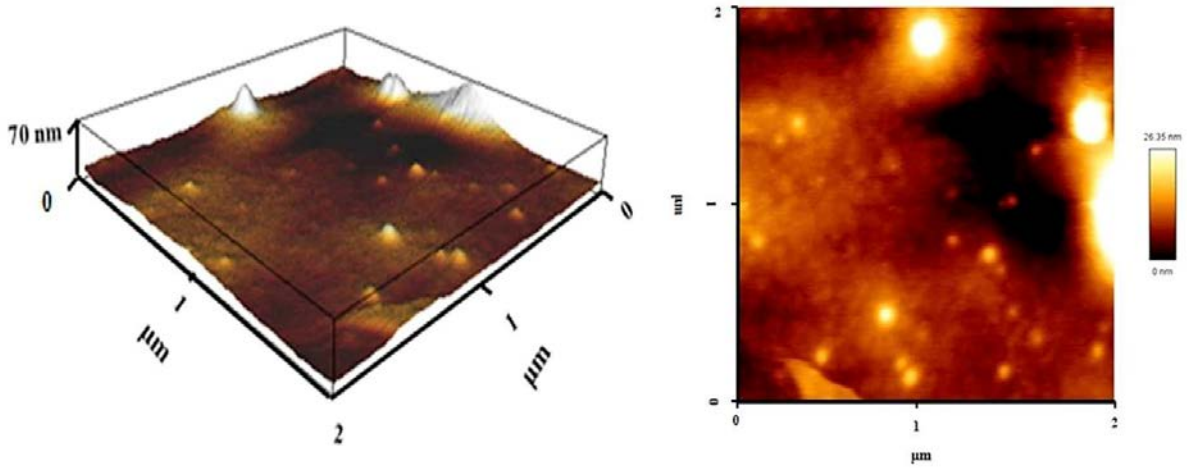

Figure 4-7 AFM (3D) left and (2D) right view images of the top PEN substrate.

The results reveal that the PET substrate exhibits slightly lower surface roughness than the PEN substrate. This is an important factor to be considered to achieve high quality of subsequent layers in display applications. The roughness discrepancy could be related to the slight difference in the degree of crystallinity between PET and PEN (i.e increase in the surface RMS values associated with crystallisation) [160].

4.2.4. Mechanical properties

4.2.4.1. Tensile test analysis

Tensile test for both PET and PEN were conducted with an Instron 5520 mechanical testing machine. The elastic modulus (E)was determined under uniaxial tension and 0.5 mm/min crosshead speed by calculating the slope of the initial linear regime of stress-strain curves. Also, the yield strength was determined by intersection of the two tangents to the initial and final region of stress-strain curves [161] as shown in the Figure 4-8. The samples, 50 mm length, 4 mm gauge width and 18 mm gauge length were cut from A4 sheet at different angles 0, 30°, 45°, 60° and 90° with respect to x–axis, as Figure 4-9 illustrates.

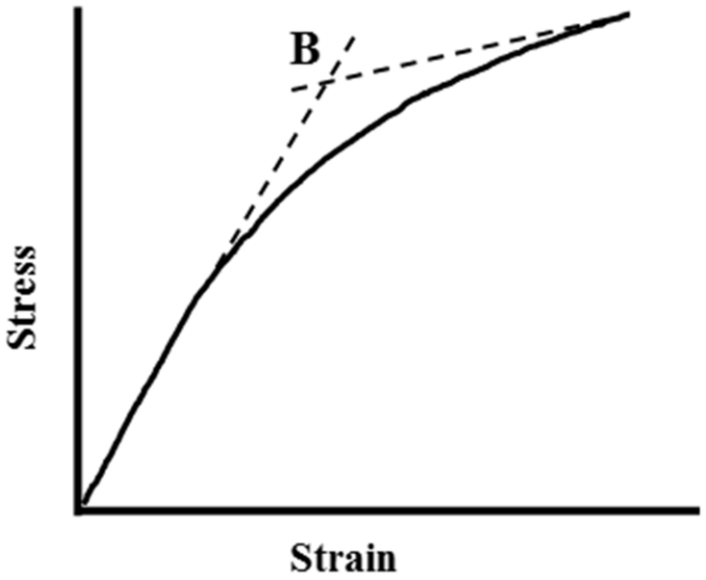

Figure 4-8 Stress- strain curve of polymer, the stress at point B is defined as yield stress.

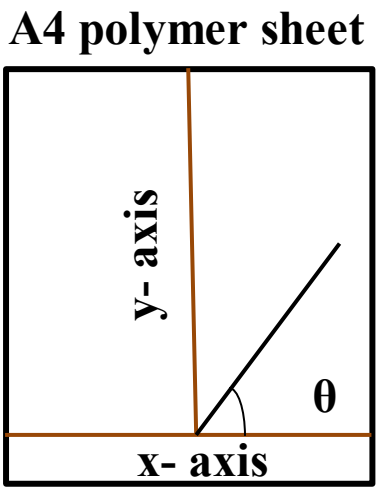

Figure 4-9 Definition of x-axis and angle regarding the polymer.

The Young's modulus and yield strength at different angles for polymer samples with respect to A4 sheet x-axis are shown in Figure 4-10 and Figure 4-11 respectively. PET and PEN biaxial orientation has a great influence on elastic modulus values. Generally, the modulus and yield strength values for PEN are higher as compared to values obtained for PET

substrates at each angle. PEN exhibits highest modulus values 3.76 ± 0.03 GPa and highest yield strength values at 0°, while a slightly lower elastic modulus 2.9 ± 0.26 GPa and lower yield strength 51 ± 14.1 MPa are obtained at 30° for PEN. The results obtained in this work are in agreement with those reported previously for biaxially stretched PEN [41].

From Figure 4-10 and Figure 4-11 it can also be observed that PET samples exhibit similar behaviour to PEN samples with highest Young's modulus value 3 ± 0.24 GPa and highest yield strength 73 ± 21.5 MPa, being at 0° angle. However, PET exhibits lowest modulus value and lowest yield strength at angles 30° and 60° respectively. The modulus value for PET was lower in comparison to those reported in the literature [40,47]. Leterrier *et al.* pointed out that the effect of sample dimension (length over width) ratio on the Young modulus measurements must be taken into account for samples less than 10 mm width [101].

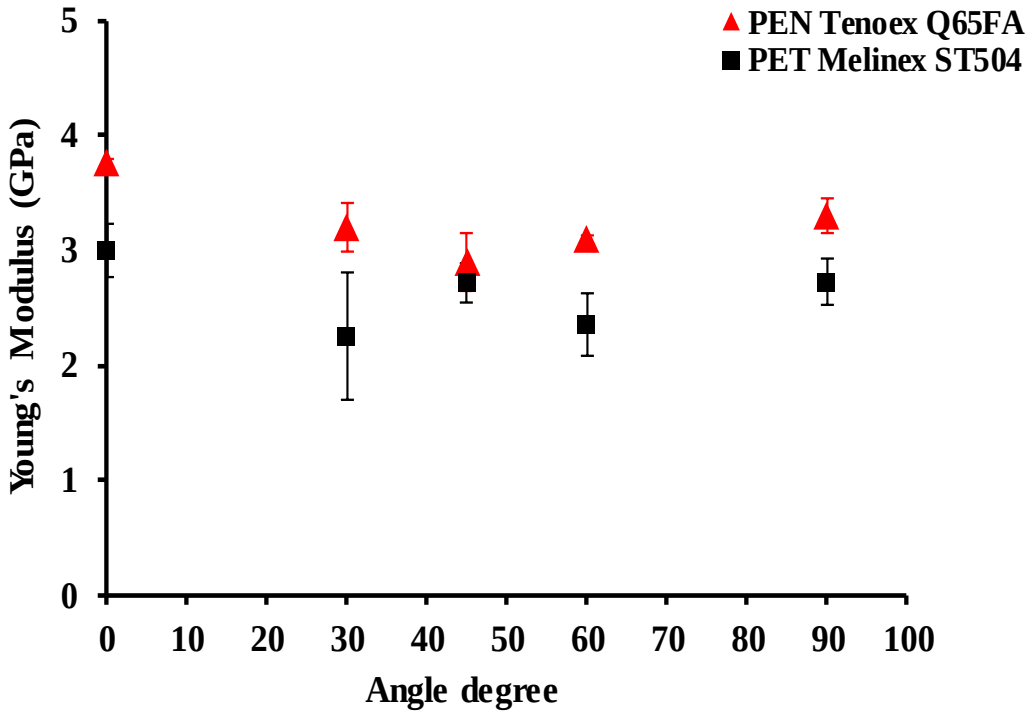

Figure 4-10 Young's modulus versus angle with respect to x-axis of bare PET and PEN substrates.

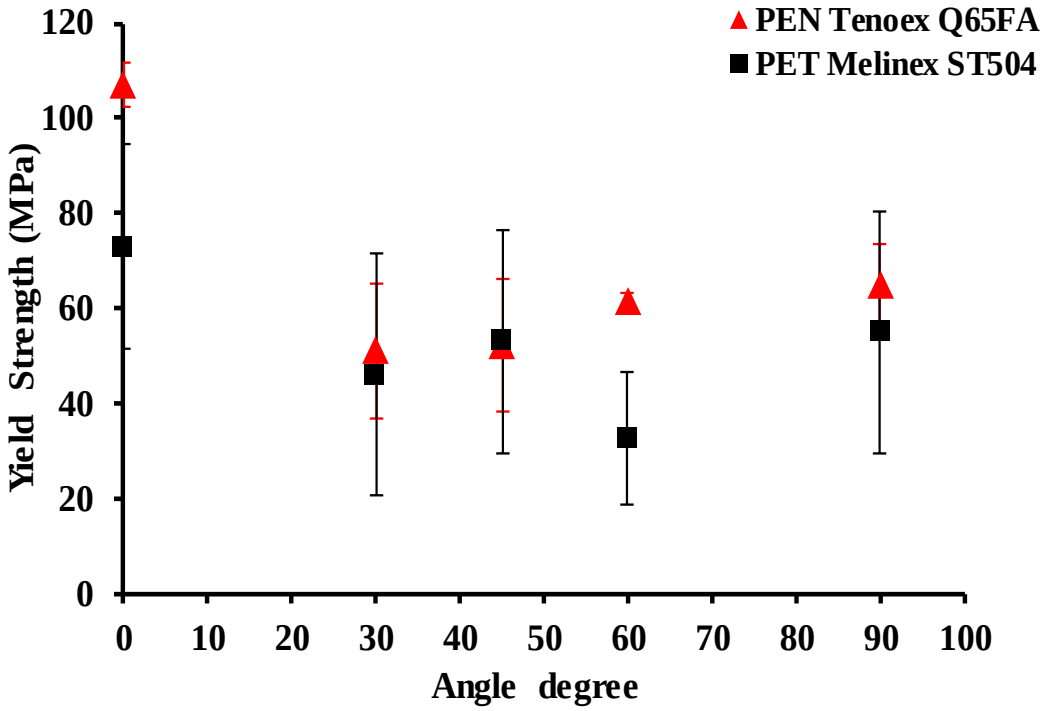

Figure 4-11 Yield strength versus angle with respect to x-axis of bare PET and PEN substrates.

Anisotropy of modulus and yield strength values were observed at 0°, 30°, 60° and 90° angles for both film substrates. This is related to the biaxial orientation of the molecular chains that both films exhibit. Also, the lowest modulus value was observed at intermediate angles such as at 45° for PEN and at 30° for PET sample. This might be related to the bimodal orientation of the molecular chains [41].

In addition, the highest modulus value for PEN and PET was observed at 0° angle. It suggests that the molecular chains for PET and PEN specimen at 0° are aligned parallel to the applied force [162]. Because of this, the zero angle was used to cut the substrates for further experiments.

The effect of strain rate was investigated by stretching PEN and PET samples at different strain rates. Crosshead speeds of (0.1, 0.5 and 5) mm/min which is equivalent to strain rate of ($5.5*10^{-3}$, $2.7*10^{-2}$, $2.7*10^{-1}$) min^{-1} were used.

Figure 4-12 and Figure 4-13 show the stress-strain curves at different strain rates for PEN and PET substrate respectively. The strain rate was found not to affect the elastic modulus, while increases in yield stress were found with increasing strain rate. This is comparable with the results reported by Leterrier *et al.* [101] for PET under uniaxial tension.

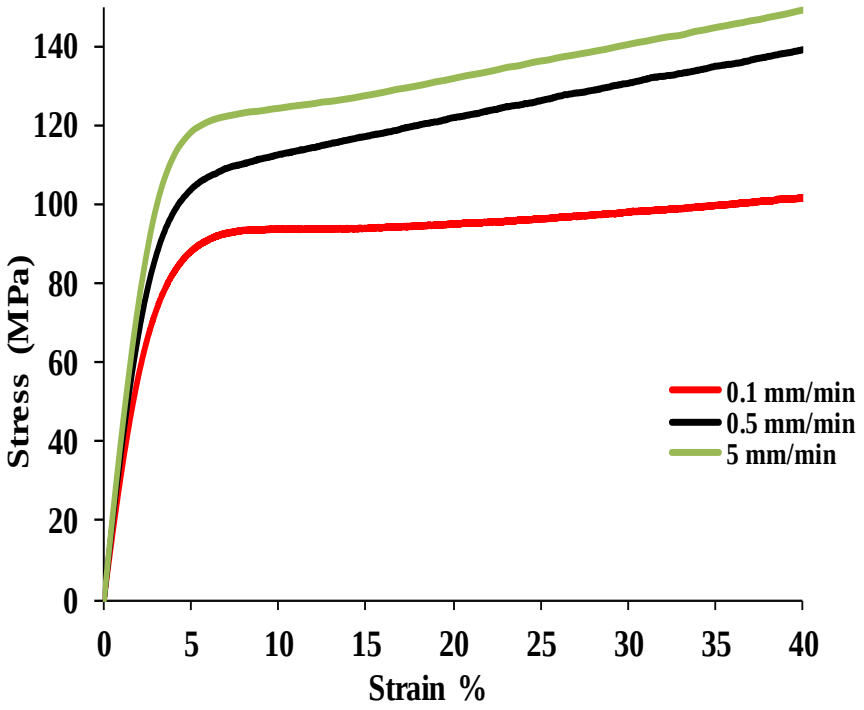

Figure 4-12 Stress- strain curve for PEN samples at different strain rates.

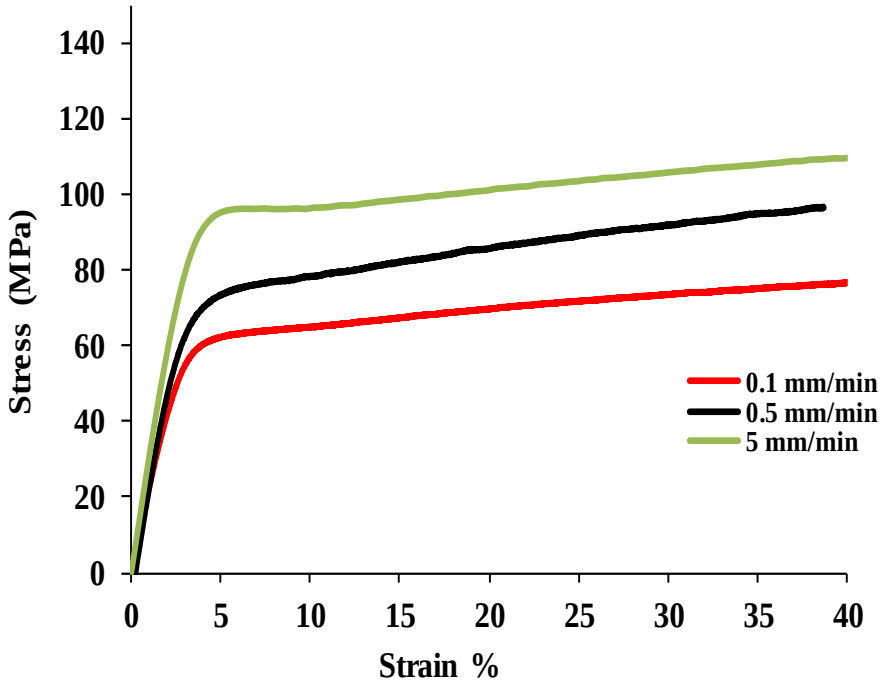

Figure 4-13 Stress- strain curve for PET samples at different strain rates.

4.2.4.2. Bulge Test Analysis

In order to obtain the mechanical properties of polymer substrates under biaxial conditions, the bulge test was used, fitting the pressure - deflection recorded data to Equation 3-3. By rearranging constants from the first and second term of Equation 3-3 and acquiring the A and B parameters as shown in Figure 4-14.

$B = \frac{C_1 \sigma_o t}{a^2}$, $A = \frac{C_2 M t}{a^4}$, the initial stress σ_o and biaxial modulus M are then calculated. It should be noted that the initial linear region of the pressure/deflection against h^2 data must be fitted into Equation 3-3. An underestimation of the biaxial modulus can occur if the whole data is fitted into the generalised equation. Hence, it is important that the bulge pressure gauge must show good resolution during the early stages of the introduction of pressure. As reported

by Lin *et al.* [163] that accuracy in controlling the pressure loading is important for the bulge test. Figure 4-14 shows a typical example of a linear fit of bulge test data for PEN. A biaxial modulus of 2.5 ± 0.3 and 2 ± 0.2 GPa, and initial stress of 1.3 ± 0.3 and 0.28 ± 0.06 MPa were found for PEN and PET substrates respectively. By assuming a Poisson's ratio $\nu = 0.37$ and $\nu = 0.45$ for PEN and PET respectively [97], the Young's modulus for PEN and PET are calculated to be 3.9 ± 0.2 and 3.6 ± 0.5 GPa respectively. The Young's modulus values for PET and PEN are in agreement with values obtained by tensile testing. These agreements demonstrate that the bulge test is suitable for measuring mechanical properties such as biaxial modulus and initial stress.

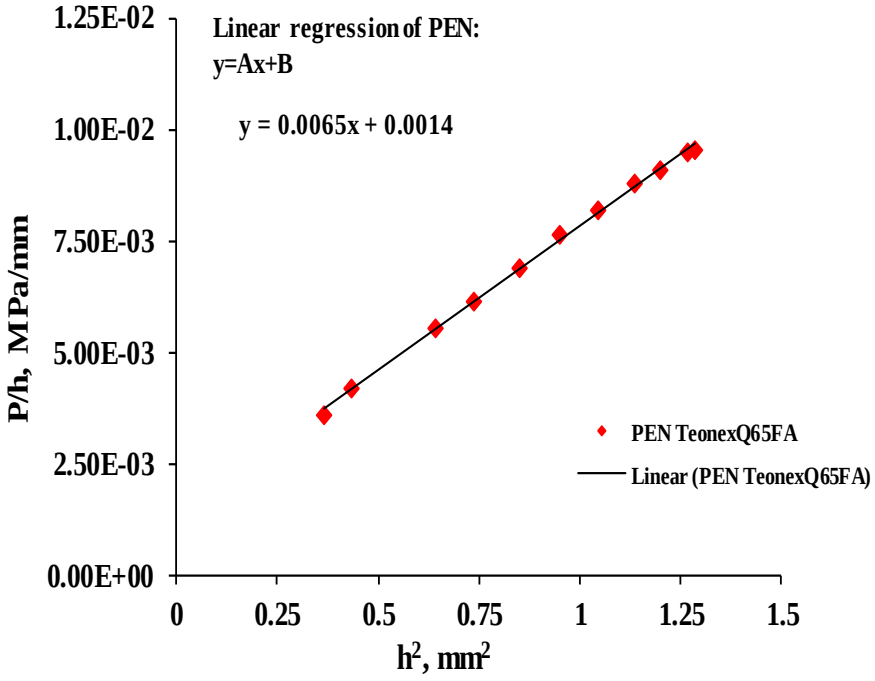

Figure 4-14 Plot used to derive initial stress σ_o and biaxial modulus M for PEN bare substrate.

4.2.4.3. Dynamic Mechanical Thermal Analysis (DMTA)

Dynamic mechanical properties of PET and PEN sample were monitored over a wide range of temperatures by applying a sinusoidal deformation to them at 1 and 25 Hz. Because of their viscoelastic behaviour the response of PET and PEN sample to an imposed deformation will depend on how fast or slow the deformation was applied to the specimen. Results for the temperature dependence of storage modulus for PEN and PET substrate are depicted in

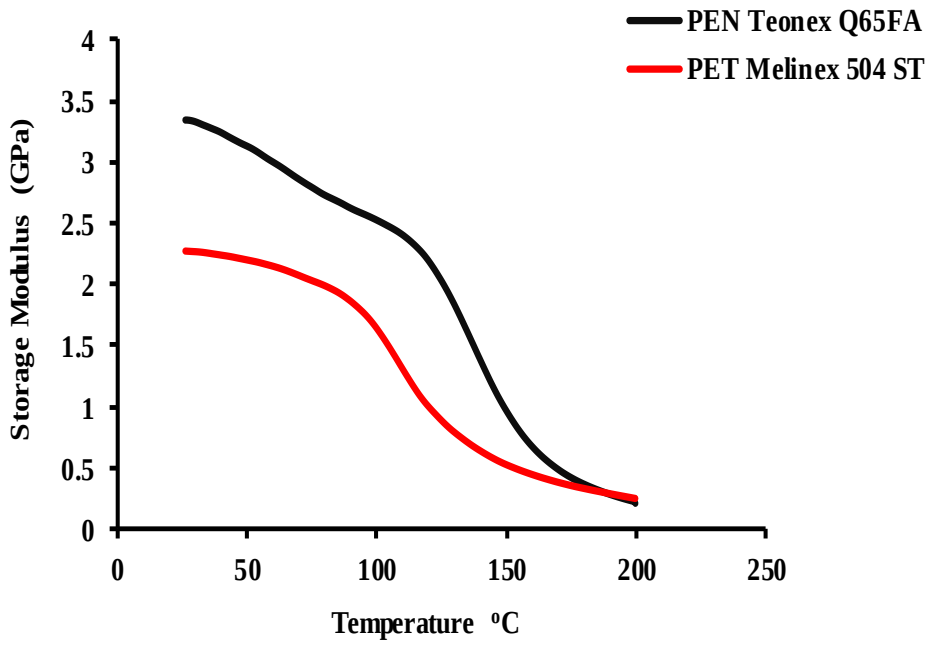

Figure 4-15 Change in storage modulus of PEN and PET with temperature.

It is seen that the storage modulus, E' of both materials decreases as the temperature increases, i.e. both materials become softer or more flexible as they are heated. However, in the region (100 – 140 °C) PEN samples exhibit higher modulus and it is almost twice as great as that of the PET sample. Our results are consistent with results obtained by Macdonald *et al.* for PET and PEN [47]. Figure 4-16 and Figure 4-17 show the dependence of the storage modulus and

mechanical loss ($\tan\delta$) for PEN and PET samples on the temperature at frequencies of 1 Hz and 25 Hz. The storage modulus increased as the temperature decreased and the frequency increased. The peak of the curve, which is the relation between the energy lost and the energy stored E"/ E′ during the transition, was used to determine the T_g of PEN and PET substrate to understand how the polymer behaves under ambient conditions.

At higher frequencies, T_g (α-process) for PEN and PET shifts from ∽146 and ∽114 °C to a higher temperature of ∽156 and∽120 °C respectively. This means that the T_g of the polymer material strongly depends on the time allowed for chain segment rotation. The faster the applied stimulus, the less time the molecules have to respond to it. Therefore, a higher temperature is required to energize the movement of the molecules at higher frequencies.

The T_g values obtained for PET and PEN by this technique are greater than from those obtained by DSC. This finding is consistent with other studies [164] carried out on these polymers. In addition to the T_g, there are other properties of PET and PEN films which are different. For example, in a comparison between PET and PEN in term of the storage modulus versus temperature values, the distance between the 1 Hz and 25 Hz curves for PEN is larger than the PET which suggests that PEN is more highly affected by frequency than that of the PET film.

Also, the peak of β*- relaxation of PEN was observed at around 66 °C and 82 °C at frequencies of 1 Hz and 25 Hz respectively. This process is related to the movement of the naphthalate ring of the PEN. However, this relaxation cannot be found in PET because this type of relaxation is created by the movement of the naphtalate group, which is not present in PET, and phenyl group does not cause this type of relaxation.

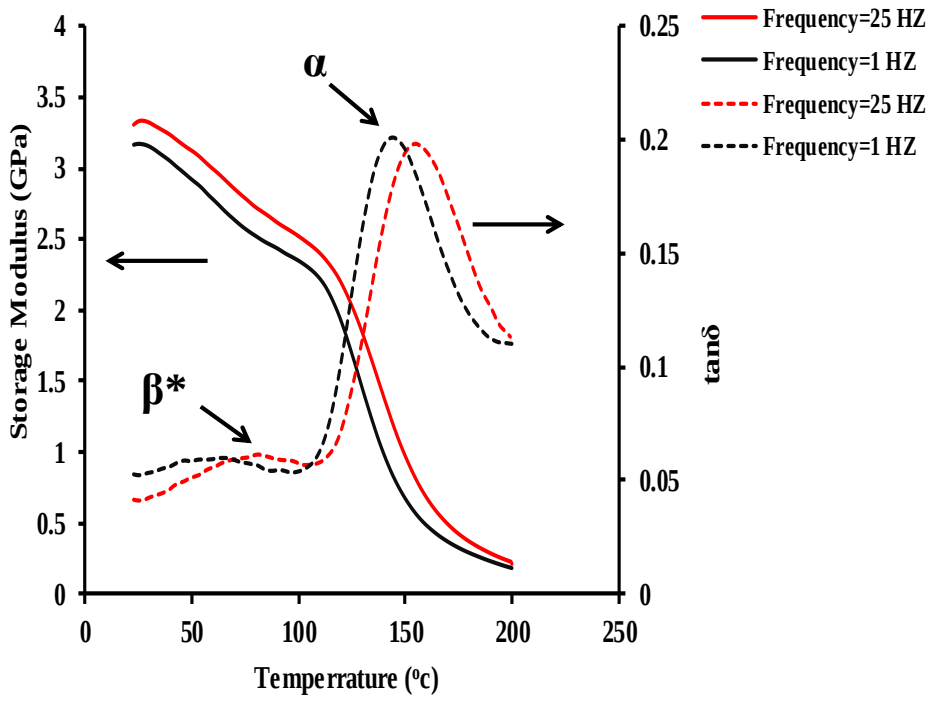

Figure 4-16 Storage modulus and tan δ determined for PEN by DMTA.

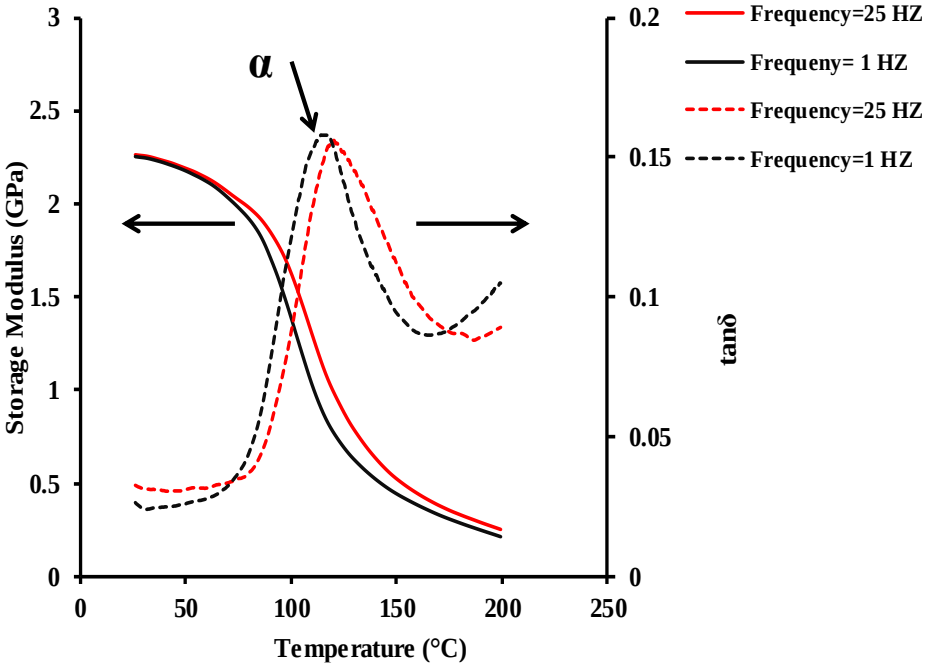

Figure 4-17 Storage modulus and tan δ determined for PET by DMTA.

4.3. Conclusions

The results of this investigation show that PEN substrates exhibit higher T_g and T_m values compared to those of PET which has a significant influence on their utilization for flexible electronics fabrication at high temperatures. Both polymer substrates exhibit high and almost the same transparency in the visible range and low surface roughness; they can be chosen as candidates for bottom – emissive displays. The biaxial orientation of polymer chains has a significant influence on the elastic modulus of semicrystalline polymer samples. The initial stress and biaxial modulus of PET and PEN substrates have been determined by measuring the bulge height versus pressure. It was found that elastic modulus measured by bulge test data is comparable to the elastic modulus measured by uniaxial tensile testing especially in the case of PET. PEN exhibited a higher storage modulus in the region (100 – 140 ^oC) as compared to that of PET, which indicates that PEN may be a better candidate. The results also show that the glass transition is strongly influenced by frequency and PEN has higher frequency dependence when compared to PET.

5. Mechanical properties of flexible transparent thin films

5.1. Introduction

The main issue with transparent brittle material coated on polymer materials is the mechanical mismatch between the brittle layer and the viscoelastic polymer substrate which can lead to cracking or even delamination during processing/service. IGZO has drawn considerable attention as an extremely promising alternative to a-Si:H for TFTs [19]. However, there is little previous work on the mechanical properties of IGZO on polymer substrate. Therefore, this chapter discusses the general characterization and mechanical properties of IGZO films both coated PET and PEN substrates. This work focusses on the failure of coatings adhering to a compliant substrate using several mechanical experiments such as uniaxial tensile and buckling tests coupled with *in situ* optical microscopy. The effects of the polymer substrate on critical onset strain, adhesion and saturated crack spacing of the film are also investigated. The work presented in this chapter has been published in Thin Solid Films ,594 (2015) 197–204.(see Appendix A for full paper manuscript).

5.2. General characterisation of IGZO deposited on polymer substrates

IGZO film was deposited on to polymer substrates using RF magnetron sputtering from a In_2O_3:Ga_2O_3: ZnO (1:1:1) target (99.99% purity) at room temperature as discussed previously in section 3.1.2. The thickness of the films on PET and PEN substrates were measured as ~50 nm by using an ellipsometer (Gaertner He-Ne (633 nm)). Room temperature deposition was performed using the conditions previously used for optimisation to produce amorphous IGZO

TFTs with a high mobility, low threshold voltage and large switching ratio. Examples of TFT characteristics have been reported previously in reference [165].

The optical transmittance was tested by using a Jenway spectrophotometer Figure 5-1 shows the transparency spectra of the IGZO coated PET and IGZO coated PEN. It can be seen that both samples exhibit almost the same transparency ≥ 82% in the visible wavelength spectrum. These values are comparable to the previously reported transparency of IGZO film grown on glass by magnetron sputtering [166].

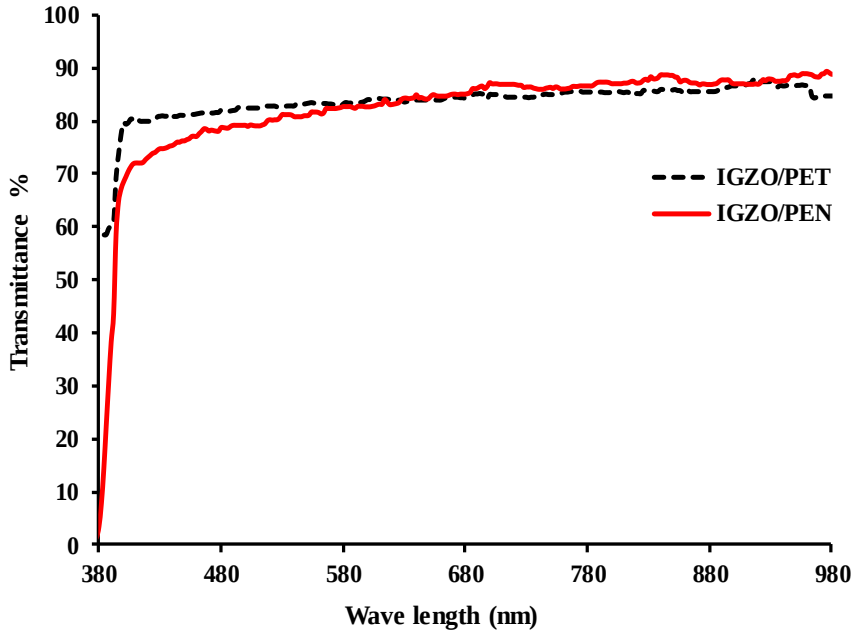

Figure 5-1 Transmittance spectra of IGZO thin film grown on PEN and PET substrate.

Contact-mode AFM was employed in order to examine the surface morphology of IGZO grown by sputtering on different polyester substrates.

Figure 5-2 presents AFM images of the surface morphology of IGZO/PET. The RMS roughness of the films was 0.84 ± 0.12 nm. It shows very small island-like structures on the

surface of the IGZO/PET film, which contributes to the high electrical performance of the proposed device [167,168]. However, these islands can be observed more clearly and become larger in both the lateral and vertical directions when IGZO is deposited on a PEN substrate, as shown Figure 5-3.

The root mean square roughness is equal to 1.13 ± 0.07 nm, a value larger than those measured for the case of IGZO/PET. It is assumed that such a discrepancy can be attributed to the higher surface roughness of the PEN substrate. However, large substrate surface roughness may have a negative impact on the performance of devices. For instance, it is reported by Klauk *et al*. [169] that pentacene organic transistors (OTFT) fabricated on PEN substrates have a higher subthreshold swing and threshold voltage than those fabricated on glass substrates. This is associated with the large surface roughness of the PEN substrate compared to with glass substrate [169]. In addition the analysis by Dhar *et al*. [170] shows that structural and electrical properties of Au thin films are dependent on the surface roughness of the substrate, and the authors reported that thin film deposited on glass exhibited hydrophilic behaviour when compared with thin film fabricated on PEN and better electrical conductivity was observed when thin films were deposited on glass.

The low RMS roughness of IGZO/PET indicates that PET is a promising substrate candidate for flexible electronics application where low RMS of the IGZO is required. RMS values of both IGZO /PET and IGZO/PEN thin film obtained in this work are higher compared with previous results [171], which showed an RMS of 0.23 nm for amorphous IGZO film on a silicon dioxide (SiO_2)/ p-type silicon substrate.

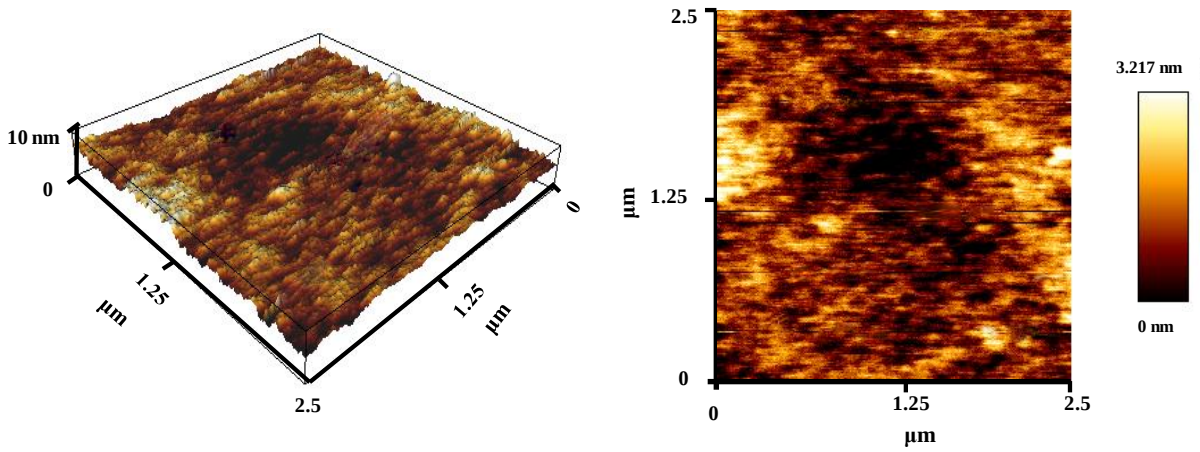

Figure 5-2 AFM (3D) left and (2D) right view images of IGZO thin film coated PET substrate.

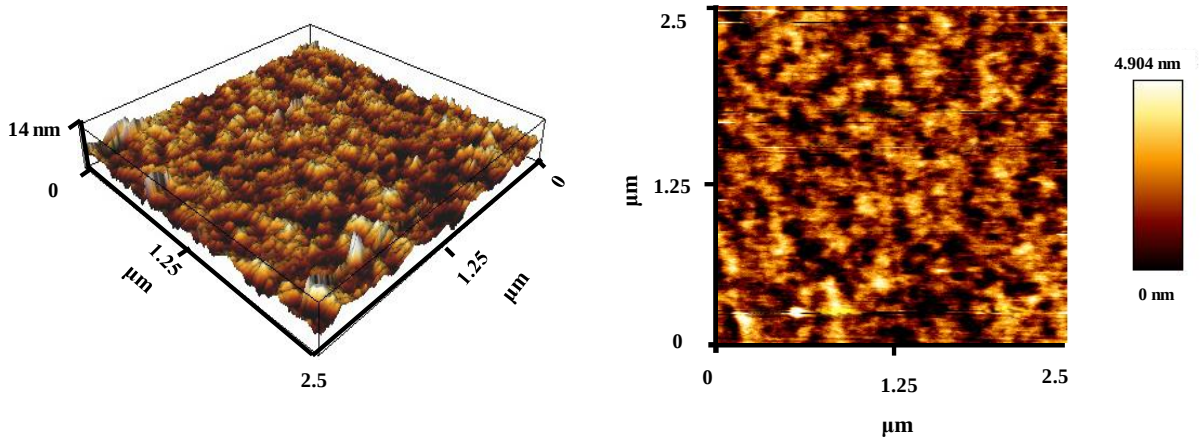

Figure 5-3 AFM (3D) left and (2D) right view images of IGZO thin film coated PEN substrate.

X-ray diffraction was utilized to examine the structural properties of the IGZO films when deposited on both PET and PEN substrates. Figure 5-4 display XRD patterns of IGZO/PET. For comparison, the data for bare PET are also shown in Figure 5-4. Only peaks which were from the semi-crystalline polymer substrate were observed for IGZO/PET. The lack of any

other peaks confirms the amorphous nature of the IGZO. Figure 5-5 shows an XRD spectrum of the IGZO/PEN, which has no diffraction peak corresponding to IGZO film, but peaks that showed the PEN substrate were detected. Thus, the XRD patterns of Figure 5-4 and Figure 5-5 indicate that the room temperature depositions produced amorphous IGZO films. This finding agrees well with result reported previously by Nomura *et al*. [28] for IGZO thin film deposited on glass, and compares with result in Refs. [79] for IGZO films deposited on unheated glass substrates by RF-magnetron sputtering.

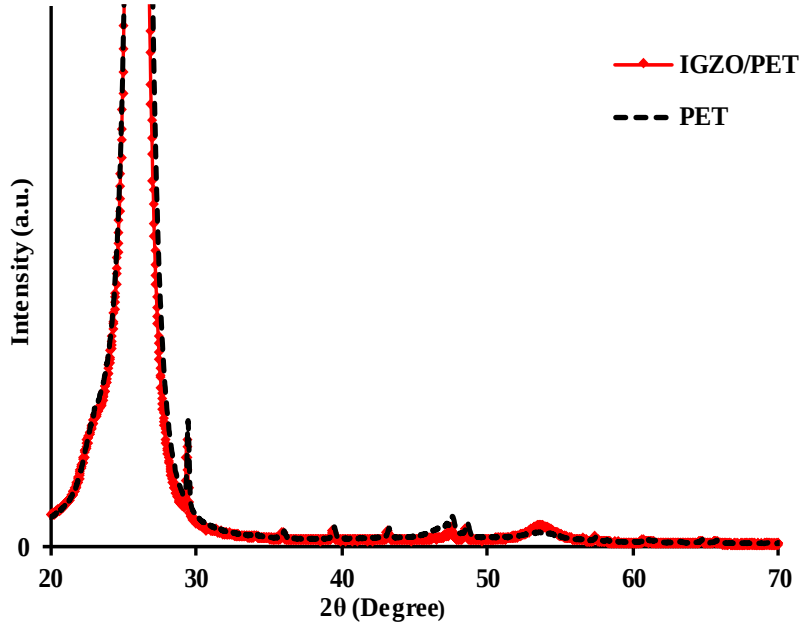

Figure 5-4 XRD plots of IGZO thin film deposited on PET substrate.

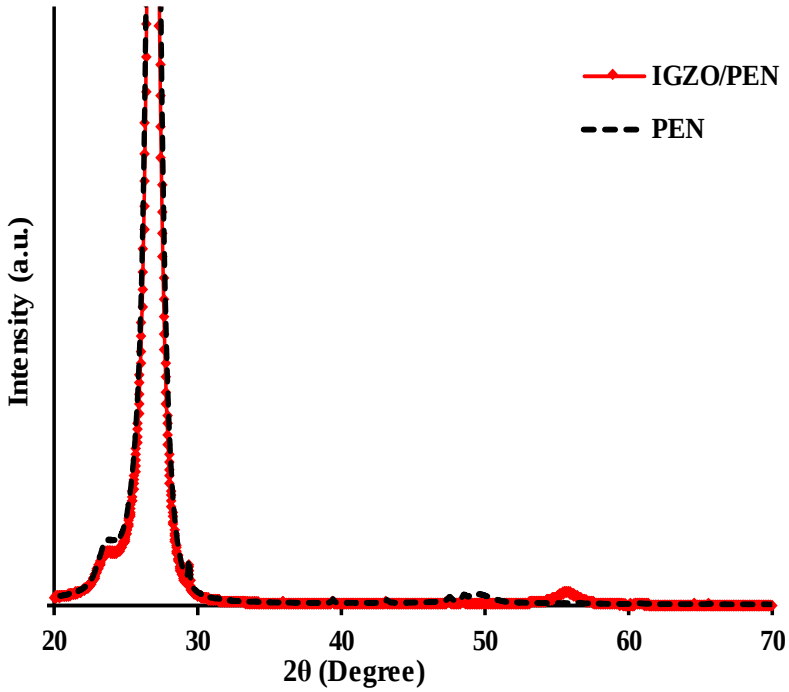

Figure 5-5 XRD plots of IGZO thin film deposited on PEN substrate.

5.3. Mechanical properties of IGZO/polymer system

5.3.1. Tensile tests of IGZO coated polymer substrates

Uniaxial tensile tests were carried out on 50- nm-thick IGZO coated PET and PEN substrates by using an Instron tensile machine at a 0.05 mm/min crosshead speed. Typical examples of the stress-strain curves for coated and uncoated PEN substrates are depicted in Figure 5-6. It is clear to see that the IGZO layer increases the elastic modulus of the coated samples. The elastic modulus of IGZO thin film E_f was assumed to be 200 GPa, by applying the rule of mixtures [40,172] and based on separate measurements of the substrate and composite film modulus. In addition, the first Dundur's parameter α, which describes the mechanical

mismatch between the substrate and the coating, was calculated from substrate modulus values and coating modulus data as measured above; using in equation 2-4, (~0.96) α for IGZO on PEN was observed, which is slightly lower than that of IGZO on PET (~0.97). This indicated a lower mismatch in mechanical properties of the oxide coating on a PEN substrate compared with a PET substrate, which leads, in turn, to a higher crack onset strain.

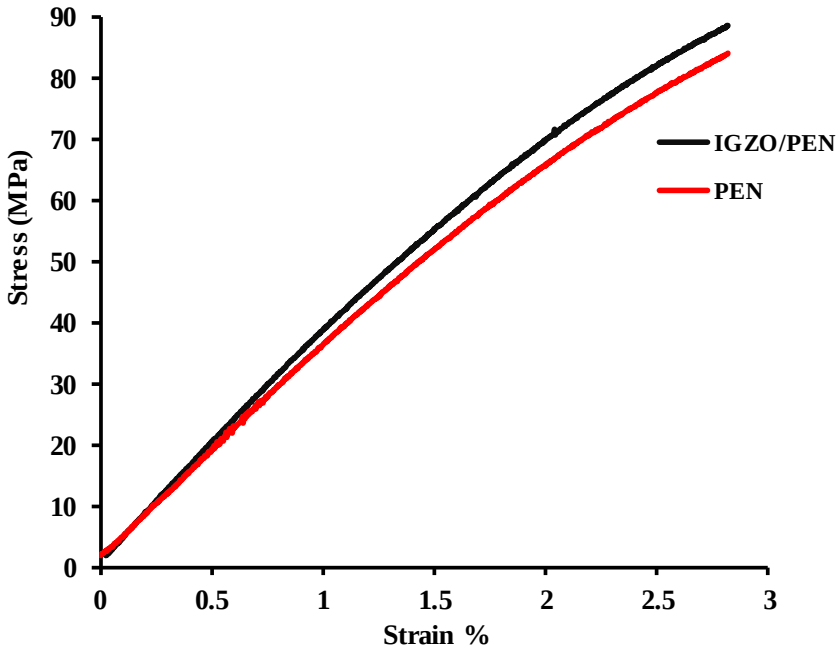

Figure 5-6 Typical stress-strain curves of uncoated and IGZO coated PEN.

5.3.2. *In situ* uniaxial tensile test investigation

The uniaxial fragmentation test was performed using a Miniature Material testing machine at a crosshead speed 0.1mm/min. The sample was prestrained in tension to provide good alignment. The test was coupled with *in situ* optical microscopy; images were taken every 3 s during the test in order to monitor the critical onset strain and development of the cracking of the IGZO-coated PET and PEN when the applied tensile strain was increased. Figure 5-7(a)

and (b) show a series of representative optical microscopy images of crack progression for the IGZO coating on PEN and PET substrates, respectively. These were optically monitored *in situ* during the tensile tests. The cracks can channel across the film and may arrest at the film-substrate interface. The channel crack initiation and evolution processes in the IGZO/PEN films are quite similar to those in the IGZO/PET samples. Upon loading, the initial channel cracks begin to initiate from microscopic defects such as pinholes in the coating and surface defects on the underlying polymer substrates. The cracks then grow to span the whole sample width direction, and propagate perpendicular to the loading direction. However, the IGZO/PEN sample exhibits a higher COS of ~2.9% (resulting in an applied stress of 67.07 ± 0.85MPa) than that for IGZO/PET at ~2.4% (resulting in an applied stress of 48.4 ± 2.5 MPa). Such a slight difference in critical strain for the IGZO layer deposited on the two types of substrates may be due to the lower mechanical mismatch between the IGZO coating and the PEN. It is seen that the channel crack in IGZO thin film is uniformly distributed along the direction of the sample length. This could be due to the uniform stress state in uniaxial loading as mentioned previously for ITO in [173].

As the strain level increases, at almost ~6.8% (resulting in an applied stress of 98.8 ± 2.2 MPa) and ~5.4% strain (resulting in an applied stress of 66.1 ± 8.2 MPa) of IGZO coated PEN and PET respectively, an adhesion-related failure appears in the form of buckling of the IGZO film.

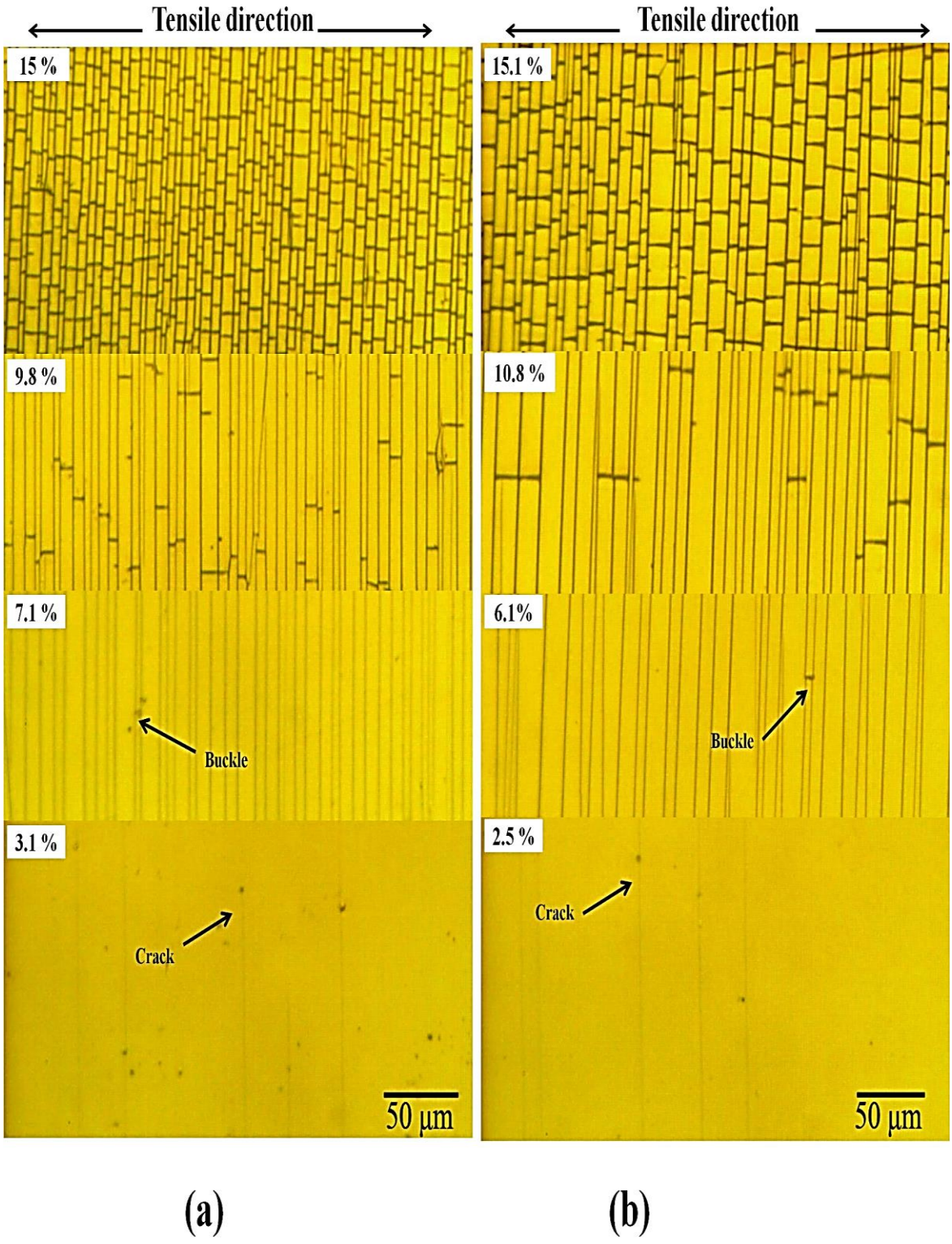

Figure 5-7 Progressive cracking in the IGZO (50 nm) coating on PEN substrate (a) and on PET substrate (b) at different applied tensile strains. The arrows show failure initiation on the coating. The images were displed in yellow backgrounds for better contrast visualization.

Leterrier *et al.* [101] found that at approximately 6% strain, transverse cracking of silicon oxide film occurred. Furthermore, Changji *et al.* [105] reported that the transverse cracks parallel to the stretching direction start to initiate after straining a ZnO / polyimide foil specimen to 5.50% strain.

In this study, cracks on the buckle top were not visible during *in situ* optical microscopy observations indicating buckle delamination. However, FIB-SEM images show that there are cracks present on the top of the buckle, parallel to the applied tensile strain (see Figure 5-10 (b) and Figure 5-11 (b)). The secondary cracks and buckling of the film appear to be due to the lateral contraction mismatch between the substrate and the brittle IGZO which result from Poisson's ratio [107,174,175].

It should be mentioned that the internal stress or thermal residual stress of the IGZO thin film on PET/or PEN can be assumed to be negligible as the sample was flat due to the small thickness of the film and room temperature deposition.

Based on the optical images, the crack initiation and crack development behaviour of IGZO film under uniaxial tensile tests which were observed in this study are consistent with other studies reported in the literature for thin ceramic coatings on compliant polymer substrates. For example Leterrier *et al.* [87] conducted fragmentation tests on ITO thin films coated onto a high temperature aromatic polymer substrate. They observed that surface defects on the underlying polymer substrate and pin-holes remaining after sputtering act as crack initiation sites. It has also been reported by Rochat *et al.* [176] that the failure of silicon oxide coatings SiO_x on semi-crystalline PET originated at coating defects such as pinholes. Furthermore, the likely explanation for fragmentation patterns is that when the specimen is subjected to external tensile stress it relieves that stress in the IGZO at points adjacent to the crack path.

The stress remains unrelaxed at some distance from the crack channel due to the constraint of the substrate. This causes the initiation of long cracks parallel to the previous crack formed [177]. Cordill *et al*. [100] observed that the crack initiation direction of Au(gold) /Cr (chromium) film on polyimide substrate under uniaxial fragmentation test was diagonal to the straining direction as shown Figure 5-8. These cracks were a consequence of scratches in the substrate. They reported that proper preparation of the substrate is an important factor influencing the crack onset strain and consequent tension reliability of flexible electronic device.

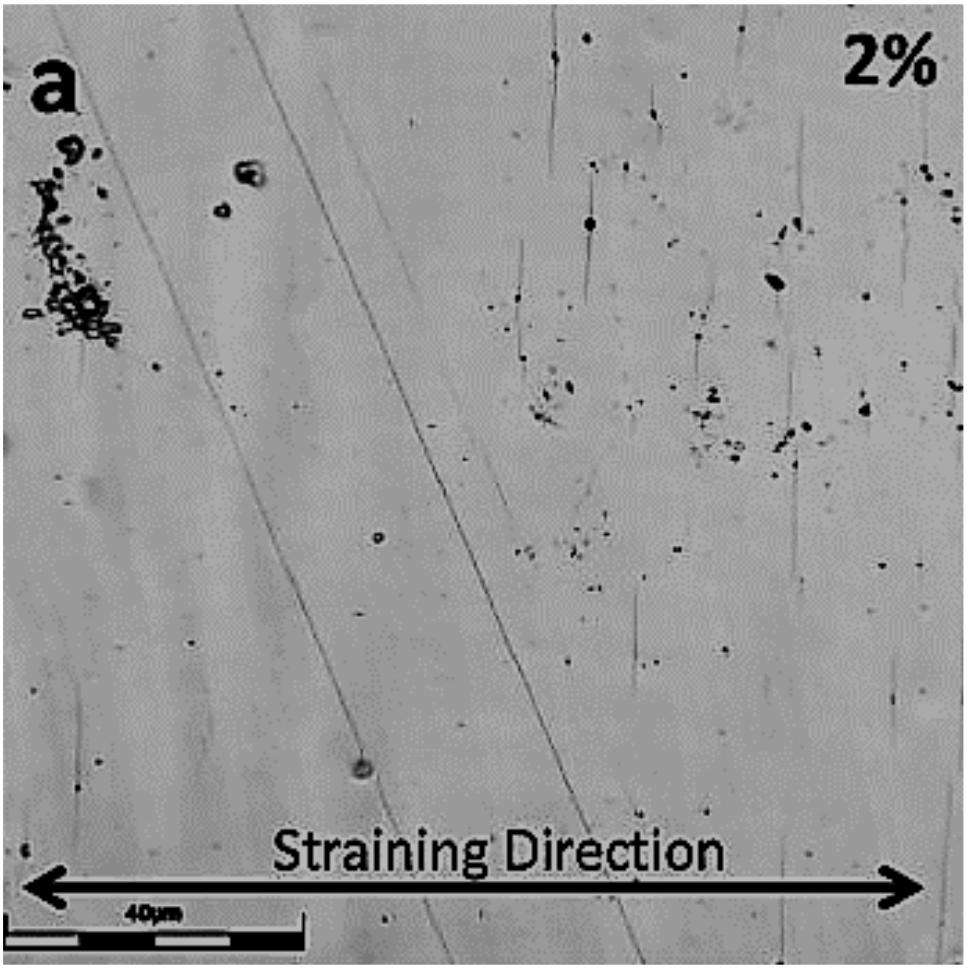

Figure 5-8 CLSM image of cracked 50-nm Au film with a 10-nm Cr adhesion layer under unaxial fragmentaion test. Applied strain is 2% [100].

The IGZO cracking was quantitatively characterized under tensile strain, in terms of CD, defined as the number of channel cracks per unit length in the strain direction [176]. The CD was determined as the inverse of the average spacing between the cracked IGZO thin film obtained from different random locations on the micrograph. The standard deviation of CD and COS were calculated, based on averages for five samples. Figure 5-9 shows the evolution of the coating crack density as a function of the applied strain for both IGZO/PEN and IGZO/PET samples. It is observed that there is a significant increase in crack density as the applied strain increases. However, with further increases in strain, the crack density gradually saturates at certain value, above which no new cracks can form. The saturation in crack density is strongly related to buckling delamination of the IGZO film on the PEN and PET substrate, which eventually leads to a reduction in the tensile stress transferred from the compliant substrate to the IGZO film [25]. This case is evident in Figure 5-7; it shows that the buckling of the IGZO/PET and IGZO/PEN takes place at strains close to their saturation strain state.

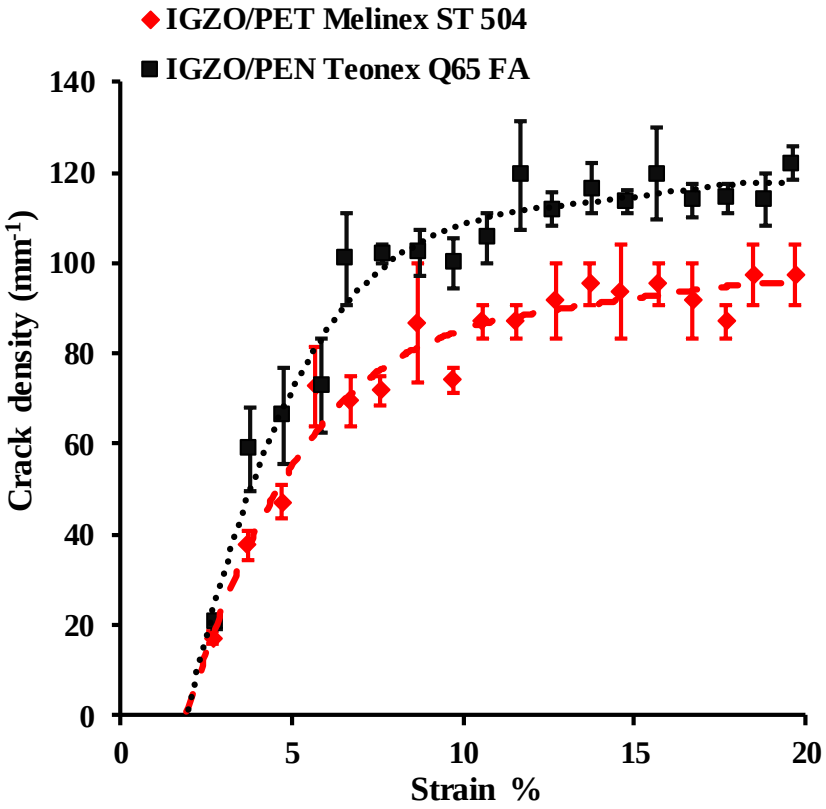

Figure 5-9 Crack density vs applied strain for IGZO (50 nm) coating on PET and PEN substrates.

Furthermore, it was found that the IGZO/PEN samples exhibit a higher value of saturated crack density of (~116 mm^{-1}) compared with the IGZO/PET specimens (~95 mm^{-1}). The quantitative measurements of the progression of crack density at saturation state indicate that the IGZO on a highly stiff polymer substrate develops more cracks to relax the applied tensile stress. On the other hand, if a less stiff polymer substrate is used the stress distribution between substrate and coating can influence the debonding formation between the polymer substrate and IGZO, hence the stress is absorbed by the polymer substrate in the debonded zone. Similar observations have been demonstrated previously by Tsubone [178] for diamond-like carbon films coated on polymer substrates.

Rehman [179] *et al*. also indicated that the onset of yielding in the substrate greatly decreased the stress transfer to the film. Following yielding the applied strain data for localised plastic

deformation in the substrate reduced the stress transfer into the coating for the equivalent substrate strain. Therefore, a low yielding substrate will delay crack development in the coating.

Also, the adhesion between IGZO films and polymer substrates which was characterized in term of interfacial shear strength (IFSS) was calculated as follows [180]:

$$\mathrm{IFSS} = 1.337\, h_f E_f \,\mathrm{COS}\, CD_{sat} \qquad 5\text{-}1$$

where CD_{sat} is crack density at saturation. The PET substrate showed lower CD_{sat} compared with the PEN substrate. IFSS of IGZO on PET will be lower (30.4 MPa) than that of IGZO on PEN (44.9 MPa). This indicated that the adhesion of the IGZO coating on the polymer substrate depends on polymer stiffness.

The above results suggest that the crack initiation and the density of channel cracks are highly related to the Young's modulus and the onset of yielding of the polymer substrates. In general, the high mechanical reliability of IGZO film coated on polymer substrate can be attributed to the following possible reason. There are many grains with preferred orientation in the IGZO coating if it exhibits a polycrystalline structure, therefore is very prone to cracking due to intergranular defects in the grains under an external force [181]. Therefore, an amorphous IGZO film delays crack initiation due to the absence of grain boundaries.

5.3.2.1. *Ex - situ* microscopical investigation of IGZO thin film after uniaxial tensile testing

Surface analysis of the IGZO films coated on both PET and PEN substrates after uniaxial fragmentation testing was performed using SEM and AFM techniques which can reveal additional fine details of the failure mechanisms of the IGZO/polymer system including delamination and buckling events. Figure 5-10 displays an SEM image of IGZO on a PEN substrate that was strained to 13%. Cohesive failure cracking perpendicular to the tensile direction and transverse buckling parallel to the tensile strain are observed. Cracks are present on the top of the buckle, parallel to the applied uniaxial loading direction, and these secondary cracks indicate open buckling zones, as Figure 5-10 (b) shows. Channel cracking and open buckling of the IGZO/PET are shown in Figure 5-11. This is similar behaviour to that observed previously for IGZO/PEN. However, the IGZO/PEN samples have fractured at the edges of the debonded zone while for the IGZO/PET delamination is continuous except for the cracks on the buckle-top, as the one-sided arrows indicate in Figure 5-10 (b). Also, a slightly higher adhesion level in IGZO/PEN systems is expected compared with IGZO/PET due to the large buckling width of IGZO/PET samples (~2.1 μm) compared with the buckling width of IGZO/PEN (~ 0.66 μm) as the double sided arrows indicate in Figure 5-10 (b) and Figure 5-11(b). This observation is consistent with results conducted in [107], where it was reported that the changes in the patterns of buckling delamination validate the highly improved adhesion between the ITO films and the PET substrate by the interlayers (Ag).

This is also consistent with previous work conducted in [182] where it was pointed out that poor interfacial adhesion of titania films on polycarbonate substrate resulted in wider buckle widths. In addition, the cross-sectional view of a channel crack in Figure 5-12 shows that the cracks originated from the top of the surface of IGZO and grew into the thickness of the film. The cracks and buckling morphology of IGZO observed in this work are similar to those of

the previous studies conducted by Frank *et al.* [183] who pointed out that the load introduced into a thin tantalum coating on a polyimide substrate during uniaxial tensile strain causes the formation of parallel cracks and at later stages led to film buckling. Moreover, buckling is initiated from the edges of the coating segment which can be clearly seen in the Figure 5-10 and Figure 5-11. This is due to the generation of high shear stress at the interface near the edges of crack compared with the centre [184]. This finding is similar to that suggested by Wojciechowski *et al*. [185] for the shear stress; the coating segment should exhibit zero shear stress at the centre and higher shear stress at the edges.

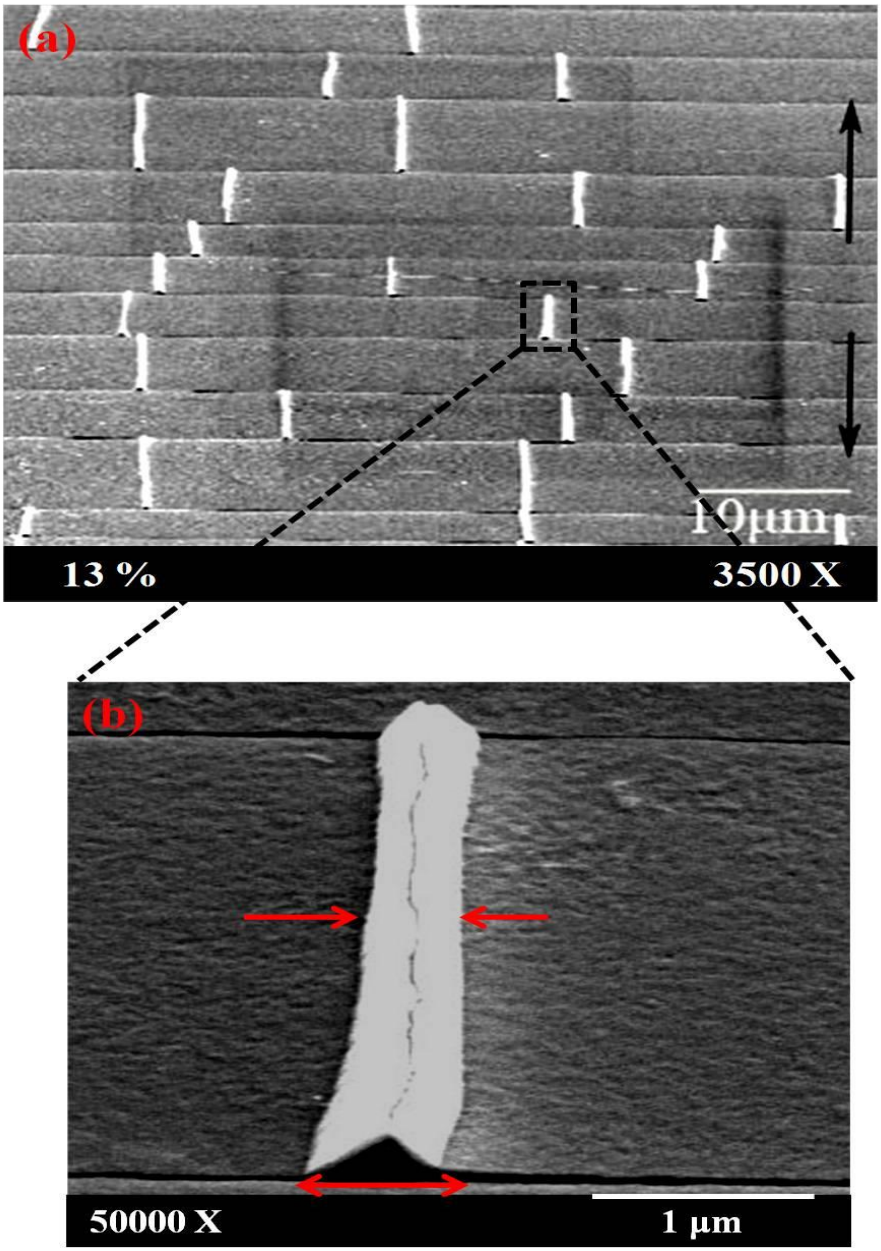

Figure 5-10 FIB-SEM image of buckling delamination of IGZO (50 nm) film deposited on PEN substrate. Note that black arrows indicate the loading direction for 13% applied strain.

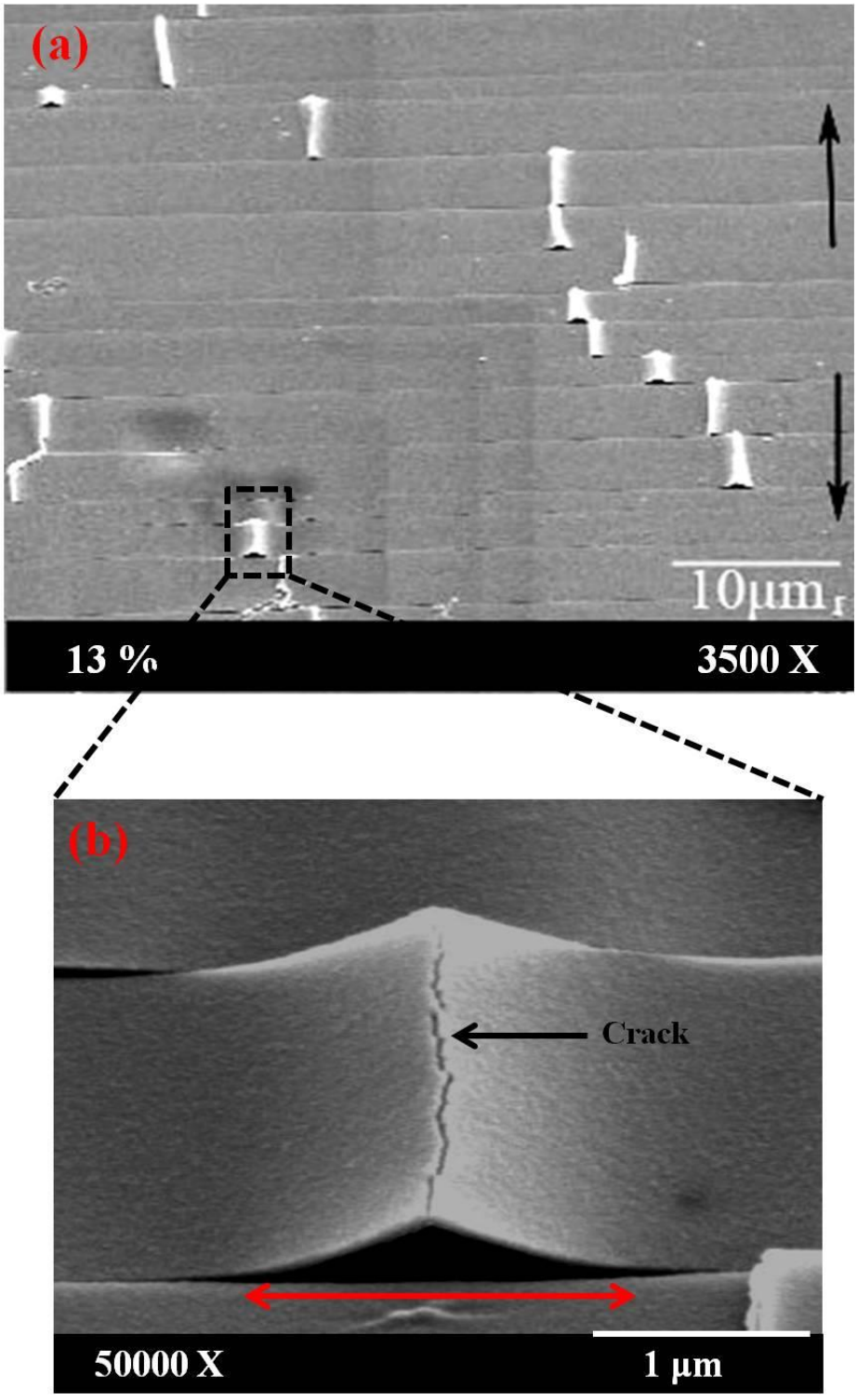

Figure 5-11 FIB-SEM image of buckling delamination of IGZO (50 nm) film deposited on PET substrate. Note that black arrows indicate the loading direction for 13% applied strain.

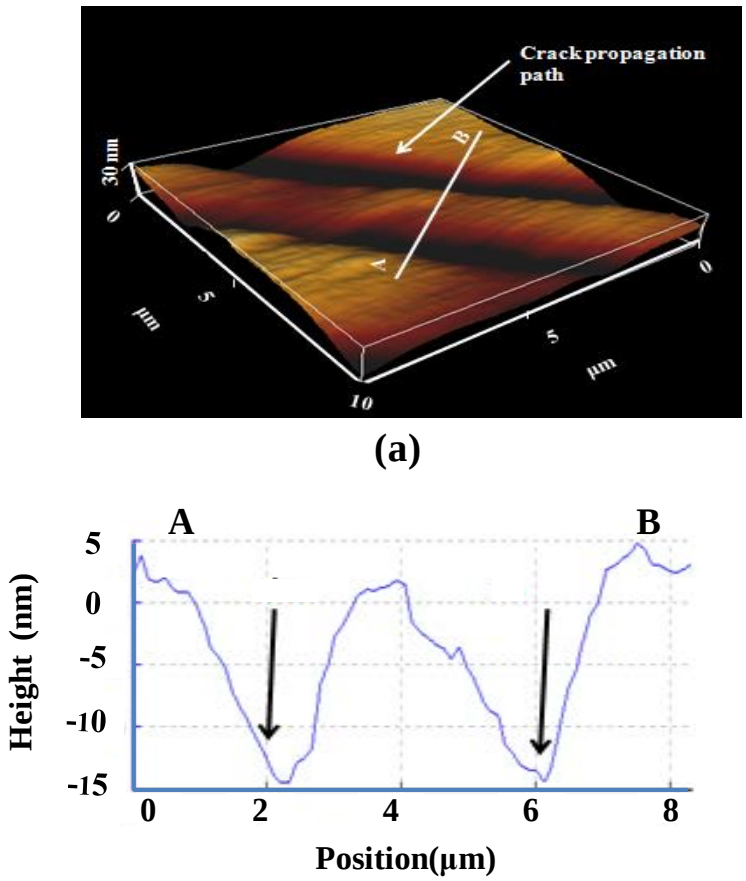

Figure 5-12 (a) 3D-AFM image of channel crack path of (50 nm) IGZO/PEN sample, white arrows show straining direction; (b) Cross section view of the channelling crack of (50 nm) IGZO/PEN.

5.3.3. *In situ* buckling test investigation

The buckling test was used to investigate the mechanical failure behaviour of IGZO films on PET substrates under both compression and tension buckling conditions. Buckling tests were coupled with *in situ* CLSM in order to evaluate the critical buckling radius, at which the cracks in the IGZO film started to initiate and to observe the film cracking behaviour above

the critical point under both compression and tension buckling mode. Figure 5-13 shows surface damage on the IGZO films deposited on a PET substrate. A high number of cracks was located in the central portion of the specimen and decreased with distance away from the centre. This indicates that the strain is not uniformly distributed throughout sample length due to the nature of the bending. This behaviour happens in samples under both compression and tension buckling modes.

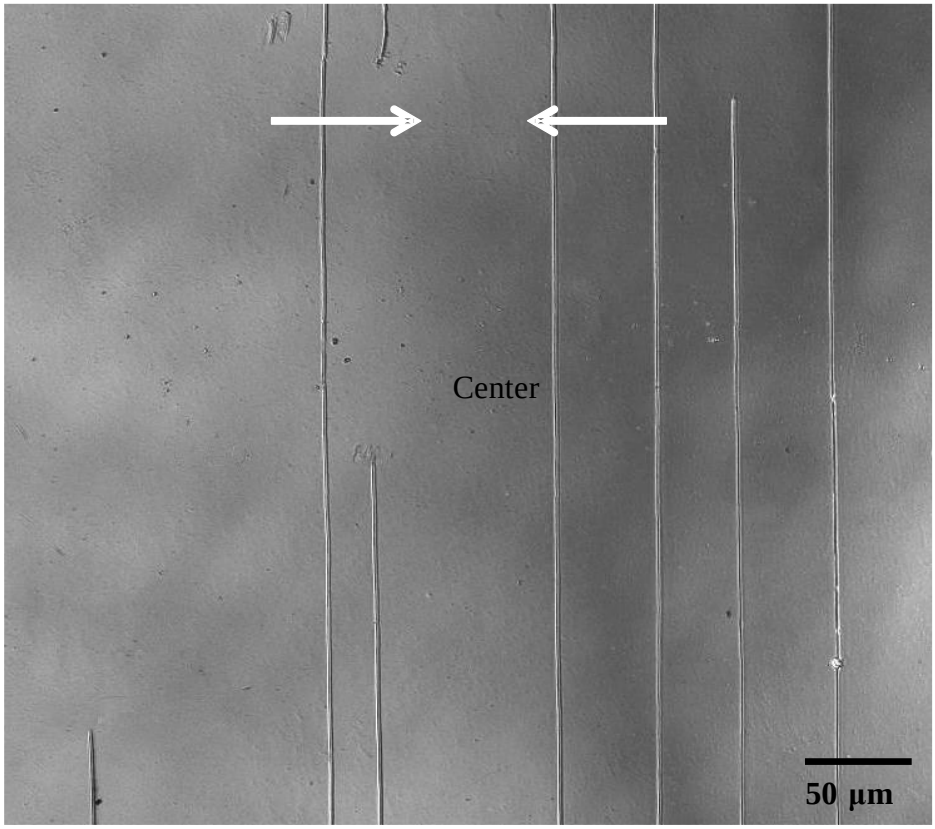

Figure 5-13 CLSM micrograph images of cracks morphology in IGZO films coated on a PET substrate under a buckling test. The white arrows indicated the loading direction.

The following discussion focusses on the centre of the bent specimen where the strain distribution is believed to be uniform. Figure 5-14 and Figure 5-15 illustrate the development of IGZO film cracking under tension and compression buckling modes

respectively. Channel cracks in IGZO/PET are observed when samples are flexed in tension down to 6.4 mm and flexed in compression down to 5.7 mm radius of curvature, which corresponds to strains of ~0.9 and 1.1%, respectively. Regardless of the type of deformation mode, it is noted that the number of cracks increased dramatically with an increase in applied strain. The cracks were initiated from surface defects for specimens in tension and then develop perpendicular to the direction of bending. These results are comparable with the results obtained from uniaxial tensile experiments.

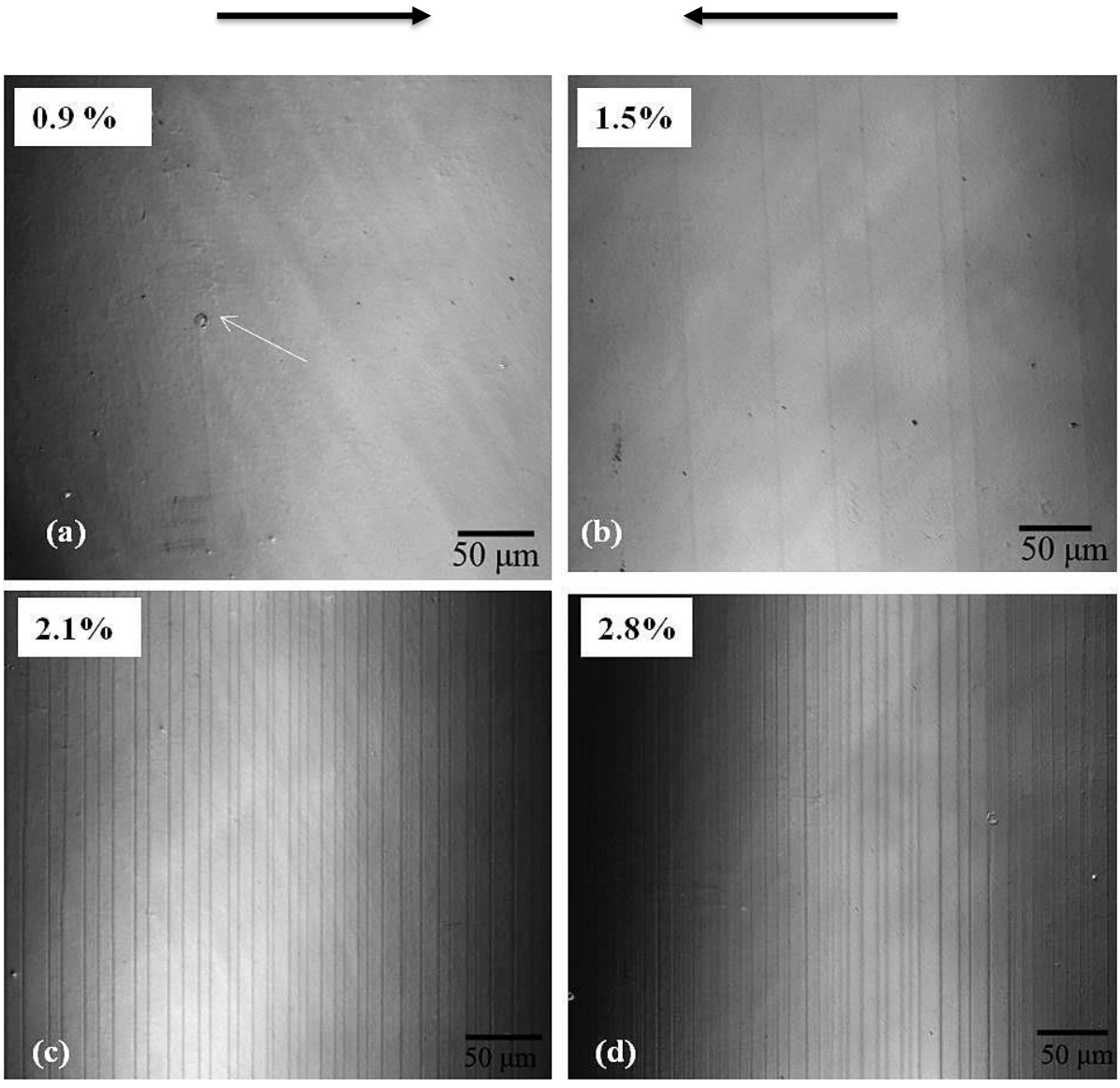

Figure 5-14 Sequence of CLSM micrograph images of crack morphology in IGZO film coated PET under (a–d) tensile buckling mode at different strain bending curvature. The white arrow at 0.9% strain indicates a crack initiating and the black arrows on the top of the images indicate the loading direction.

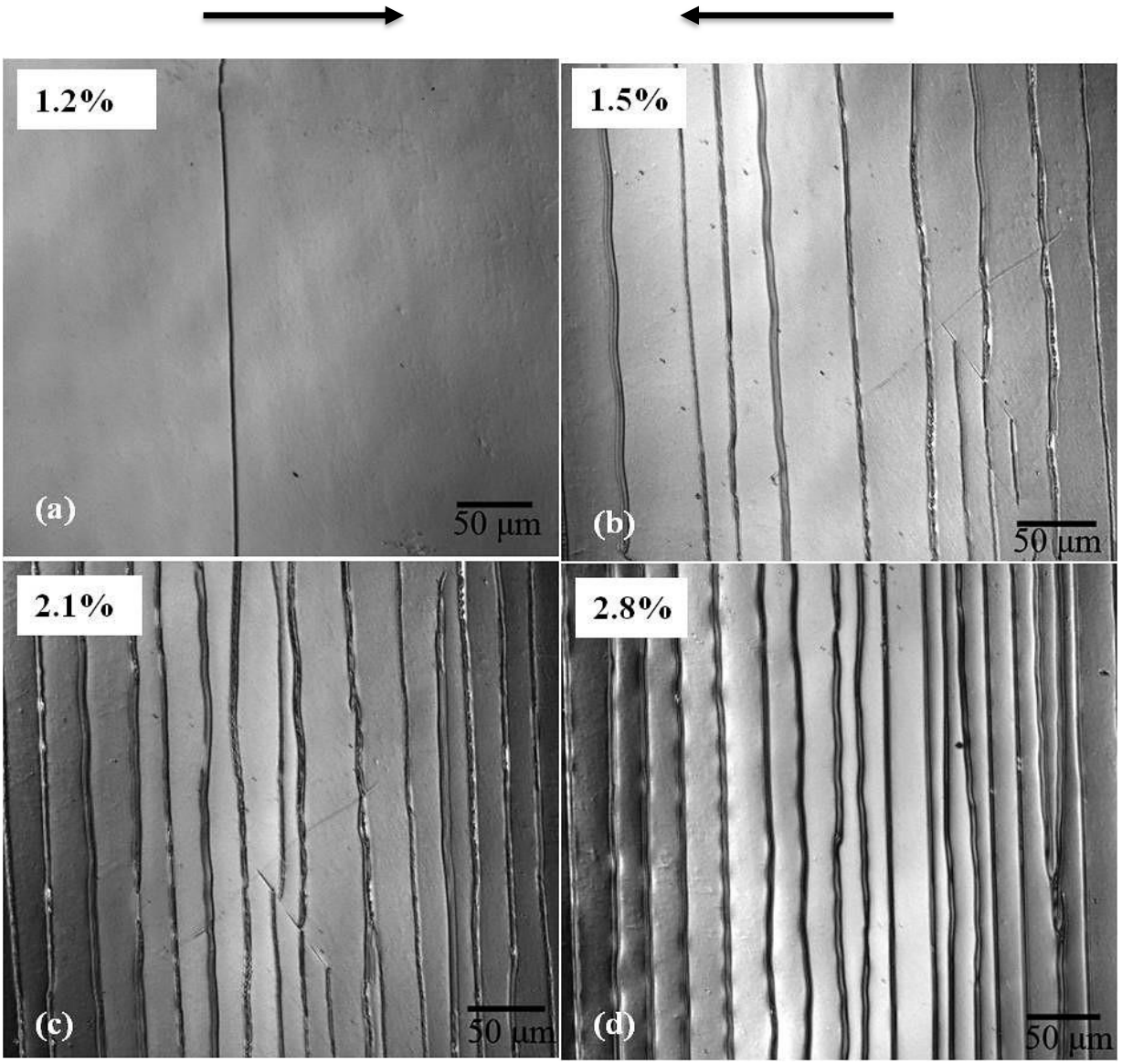

Figure 5-15 Sequence of CLSM images of cracks morphology in IGZO films coated PET under (a–d) compressive buckling mode at different strain bending curvatures. The black arrowes on the top of the images indicated the loading direction.

Based on the microscopical images, a comparison of CD of IGZO/PET under tension and compression modes is determined and presented in

Figure 5-16. It is observed that when the applied strain value exceeded the critical onset strain COS, the CD increased and correspondingly, spacing between the cracks decreased, then asymptotically approached saturation density, where cracks are no longer formed. As the applied strain increased further the cracks opened further.

In addition, it is clear to see that the saturated crack density of the film in the tension buckling mode was significantly higher than that of the film in the compression buckling mode and the discrepancy is observed to be around 58 mm^{-1}. The first reason for this might be because of surface defects such as pinholes and imperfections in the film and/or in the substrate [156]. These are also detectable in CLSM images of crack development of IGZO/PET sample as shown in Figure 5-14 (a). It illustrates crack initiation from pre-existing defects in the IGZO film under tension, which contributes to the formation of cracks in IGZO film earlier as compared with under the compression mode. Thus, it is believed that applying stresses to a specimen under compression buckling leads to closed rather than open microcracks, as also suggested by Potoczny [186]. The second reason for the discrepancy in the CD_{sat} between the film under tensile and compression buckling mode is attributed to the various failure mechanisms as can be seen in Figure 5-14 and Figure 5-15. In particular, the cracks in IGZO film under tensile bending are straighter and parallel to each other while zigzag shaped cracks are observed for the IGZO film under compression-bending. This is also confirmed by SEM images of crack morphologies of IGZO film (see Figure 5-18).

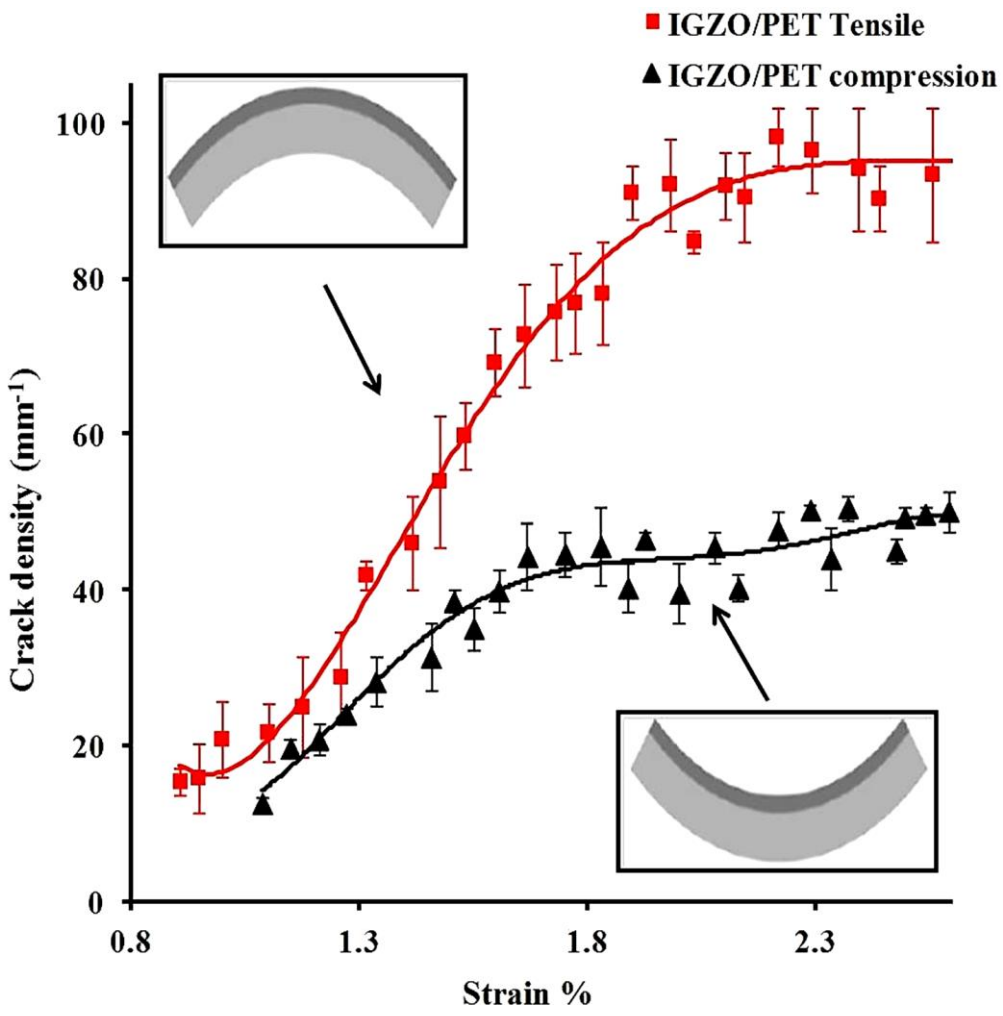

Figure 5-16 Plot of crack density of IGZO coated PET as a function of applied tensile or compressive buckling strain.

Further insight into the fracture mechanisms of the IGZO film under tension and compression modes were obtained from evaluating the fracture energy Γ , fracture toughness K_{IC} and film strength, σ_{str}. The energy and strength criterion proposed previously for the multiple cracking of thin films on compliant substrates can be used to determine the fracture energy Γ and film strength, σ_{str} respectively [187,188]. In the energy criterion, it is assumed that cracking

occurs when the change in strain energy due to cracking of a coating is in equilibrium with the energy required for film cracking. The fracture energy of the film can be expressed as [187]:

$$\Gamma = \frac{3(f_1 \epsilon_c + f_2 \Delta\epsilon)^2 f_3 f_4 + 2\Delta\epsilon(f_1\epsilon_c + f_2\Delta\epsilon)f_5}{4k} E_f' \quad 5\text{-}2$$

where ϵ_c is the strain at which the crack start to form, $\Delta\epsilon$ is the residual strain, E_f' is the biaxial modulus of the film which can be expressed as follow $E_f' = \frac{E_f}{1-\nu_f}$, where E_f and ν_f are the Young's modulus and Poisson's ratio respectively. E_f is taken as 200 GPa using the rule of mixtures [101] based on separate measurements of the substrate and composite film modulus value and ν_f is taken as 0.36 [108]. The parameters f_1, f_2, f_3, f_4,f_5 and k are given by the following equations [187]:

$$f_1 = \frac{(1+\sum\eta^3)[(1-\nu_s)(1+\nu_f) + \sum\eta(1-\nu_f\,\nu_s)}{(1+3\sum\eta^2+4\sum\eta^3+\sum\eta+\sum^2\eta^4)(1+\nu_f)} \quad 5\text{-}3$$

$$f_2 = \frac{(1+\sum\eta^3)}{(1+3\sum\eta^2+4\sum\eta^3+\sum\eta+\sum^2\eta^4)} \quad 5\text{-}4$$

$$f_3 = \frac{(1+\nu_f)(1-2\nu_f\,\nu_s+\nu_s^2)}{(1-\nu_f\,\nu_s)^2} \quad 5\text{-}5$$

$$f_4 = 1 + 3\left[\frac{\sum\eta^2(1+\eta)}{(1+\sum\eta^3)}\right]^2 \quad 5\text{-}6$$

$$f_5 = \frac{2\nu_s(1+\nu_s)(1-\nu_f^2)}{(1-\nu_f\,\nu_s{}^2)} \quad 5\text{-}7$$

$$k = \frac{1}{t_f}\sqrt{\frac{3\eta(1+3\sum\eta^2+4\sum\eta^3+\sum\eta+\sum^2\eta^4}{2(1+\nu_s)\sum(1+\sum\eta^3)}} \quad 5\text{-}8$$

where $\sum$ is the biaxial modulus ratio, η is the thickness ratio of the IGZO film and PET substrate and t_f is the film thickness. The biaxial modulus ratio can be expressed as follow $\sum = \frac{E_f(1-\nu_s)}{E_s(1-\nu_f)}$, where E_s and ν_s are the Young's modulus and Poisson's ratio of the substrate.

The residual strain is ignored as the sample after deposition was flat and the thickness of the coating was small. In such a case, the expression of fracture energy in equation 5-2 can be simplified and becomes :

$$\Gamma = \frac{3 \ f_1^2 f_3 \ f_4}{4k} \epsilon_c{}^2 E_f' \qquad 5\text{-}9$$

From this, fracture toughness, K_{IC} was determined by using the simple relation [189]:

$$\Gamma = \frac{K_{IC}{}^2}{E_f} \qquad 5\text{-}10$$

In the film strength σ_{str} criterion, it is assumed that the cracks form when the stress in the center of the film reaches the film strength. σ_{str}. By using some parameters given in equation 5-2, the film strength. σ_{str} can be quantitatively expressed as [187]:

$$\sigma_{str} = E_f' (f_1 \epsilon_c + f_2 \Delta\epsilon) \qquad 5\text{-}11$$

Then the Γ, K_{IC} and σ_{str} values of the IGZO film were determined by using the procedure as detailed above.

As observed in Figure 5-17 the IGZO film under compression mode exhibited higher fracture energy, fracture toughness and film strength compared with the IGZO film subjected to the tensile mode. The Γ, K_{IC} and σ_{str} values are ~348 J/m^2, ~8.3 MPa.m$^{1/2}$ and ~2.6 GPa respectively for thin film under tension mode, while, under compression mode the Γ , K_{IC} and

σ_{str} values are ~ 520 J/m^2, ~ 10 MPa.m$^{1/2}$ and ~ 3.2 GPa respectively. This difference is assumed to be associated with the different cracking mechanism (see Figure 5-18). Hence, the higher fracture energy of the film under compression mode observed here indicates that a much higher energy is required to develop the cracks in the films when the sample is subjected to the compression mode.

Similar observations have been reported in the literature by Ni *et al.* [113] for AZO films deposited on polymer substrates who conclude that the higher fracture energy of AZO 142.58 J. m^{-2} in compression compared to that of AZO film in tension is attributed to the difference in failure mechanisms. However, the fracture energy and fracture toughness values for IGZO obtained in this study are higher when compared with the early measurements of both Γ for AZO coated polymer substrates which was in the range of 11.7 to 142.58 J.m^{-2} [113], and K_{IC} for aluminium oxide (Al_2O_3) coated PEN substrate which was determined to be 2.3 MPa.m$^{1/2}$ [190].

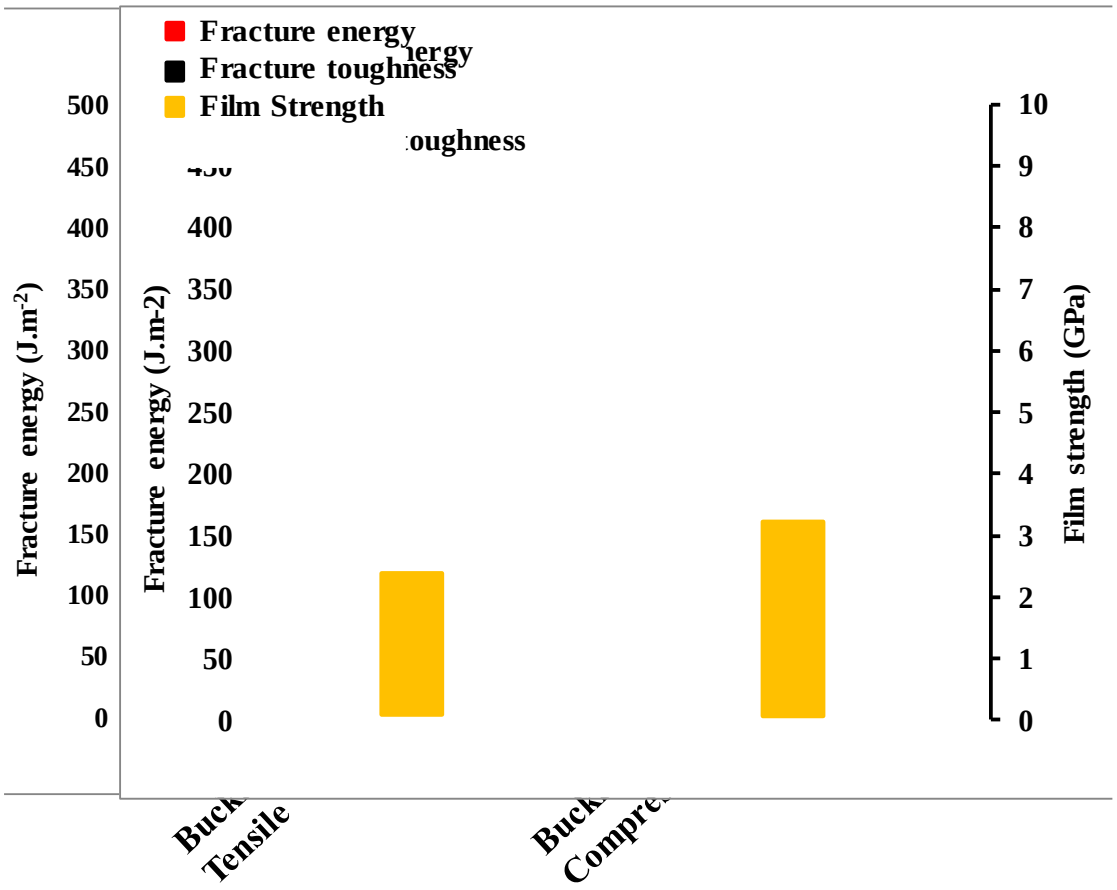

Figure 5-17 Fracture energy Γ, fracture toughness K_{IC} and σ_{str} of IGZO coated PET substrate under tensile and compressive buckling modes.

5.3.3.1. *Ex situ* microscopical investigation of IGZO thin films after buckling tests.

The SEM technique was used to characterize the crack morphology of the IGZO films grown on PET substrate after buckling in tension and compression. Further insight into the damage processes in thin films by other techniques (eg SEM) can provide the details of the failure that were not shown during *in situ* confocal laser scanning microscopy observations.

Typical SEM images of cracking morphologies of IGZO film are shown in Figure 5-18(a). This shows the IGZO/PET film after the specimen is bent in tensile bending mode to a radius of 2.7 mm, which is equivalent to a strain of 2.3%. It is observed that the IGZO film is

fractured completely due to formation of channel cracks. However, coating delamination, and channel cracking are observed when the specimen is bent in the compression buckling mode with the same radius of 2.7 mm, as shown in Figure 5-18(b). This could be due to the contraction of the polymer substrate induced by applying stress in the compressive mode.

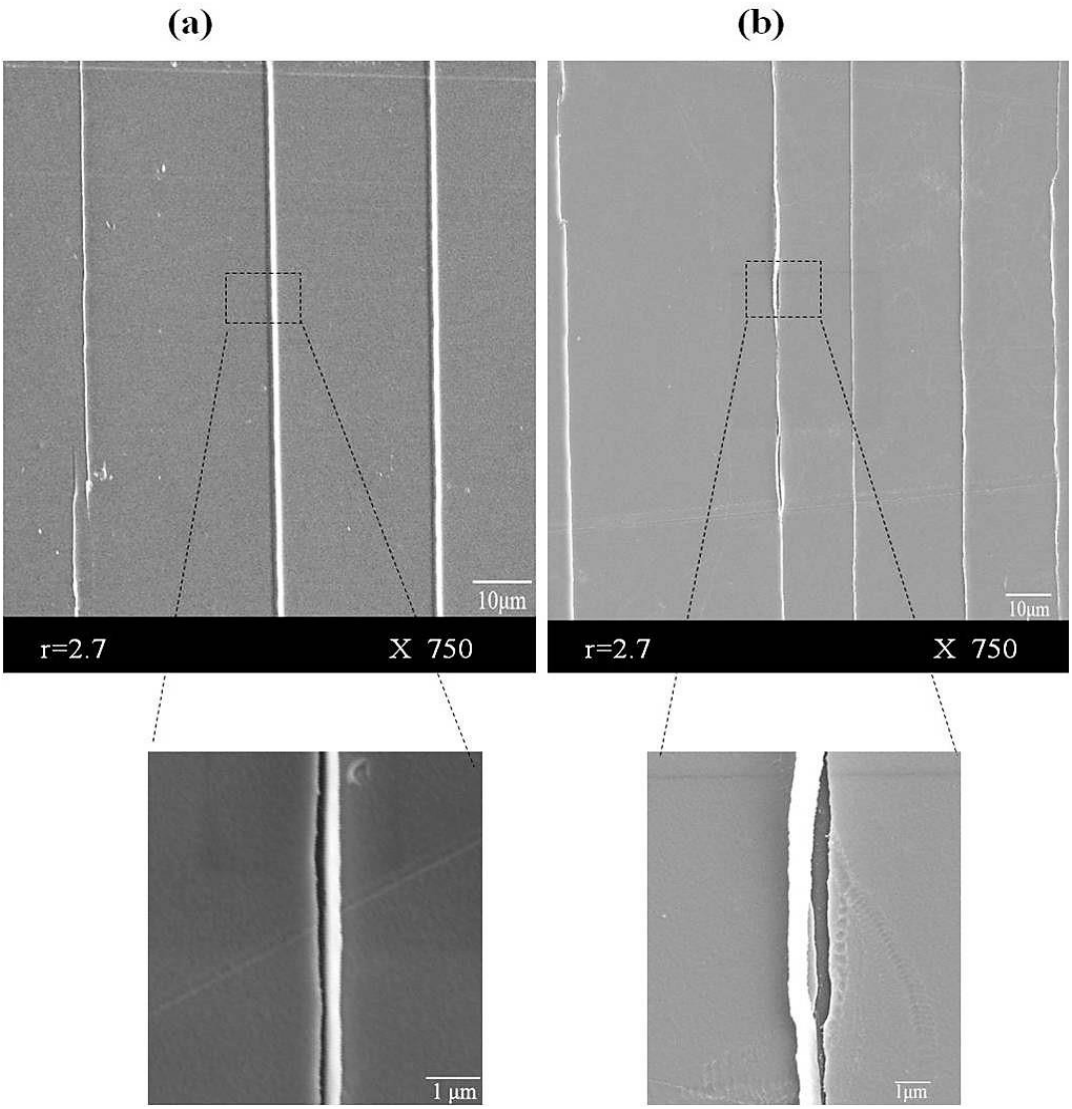

Figure 5-18 SEM micrograph showing crack morphology of IGZO after flexed down to 2.7 mm radius of curvature in (a) tensile (b) compression buckling condition.

For comparison, the coating damage, under tensile strain, is caused by the creation of channel cracks, while under compression the film specimen may first delaminate from the polymer substrate and then buckle before the initiation of a crack. This finding can be explained as follows: under the tensile strain induced by the buckling test the stored elastic energy goes solely into crack formation; however, in compression, the strain energy is distributed between crack formation and delamination. Accordingly, additional energy is required to cause the delamination of a film from a substrate under compressive buckling. This could be one of the reasons for the observation of the higher fracture energy of IGZO thin film under compression compared with that under tension in the present study.

The present findings are consistent with those found by Lu *et al*. [191] who found ITO film failures are caused by channel cracks when the sample is under tensile strain bending conditions while under compressive strain conditions the film experiences buckling delamination and cracking. The results from these experiments indicate that the film subject to tension buckling is more apt to fail than the film under compression buckling [92].

5.4. Conclusions

In summary, prior to mechanical testing, the general properties of IGZO thin film were characterized by using different techniques such as spectrophotometry, AFM and XRD in order to determine the influence of usage of different types of substrates on IGZO thin film performance.

The IGZO grown on both PET and PEN substrates has transmittance almost above 82% in the visible spectrum. In addition, the surface roughness of IGZO coated PET substrates was lower

compared with those coated on PEN substrates and this can be attributed to the surface roughness of the underling PET substrate. This suggests that it is important to control the surface roughness of the underlying substrate in order to achieve better surface roughness of thin films. XRD measurements revealed that IGZO thin film deposited at room temperature had an amorphous structure. This shows that the RF–magnetron sputtering technique can produce high quality IGZO thin film and meet the requirements for flexible electronic applications.

Furthermore, the mechanical durability of RF–magnetron sputtered IGZO thin films on PEN and PET substrates was studied by using uniaxial tensile and bending tests coupled with *in situ* CLSM.

During uniaxial tensile tests, it was found that the crack initiation strain is mostly dependent on the mechanical mismatch between the coating and substrate. Higher mechanical mismatch between IGZO thin film and PET substrates is measured as compared with IGZO on PEN substrates. Thus, a higher COS equal to ~2.9% was observed for IGZO deposited on PEN. In addition, a relatively high value of saturation crack density was observed for IGZO film coated on PEN substrates.

Furthermore, buckling test results show that thin films subject to compression buckling exhibit better bending durability than films subjected to tensile buckling. Surface defects on thin films under the tensile mode can cause IGZO film cracking to occur at strains lower than those in the film under compression buckling mode. Also, delamination of the thin film under compression from the polymer substrate can reduce the rate of crack growth.

Moreover, the value of fracture energy Γ, fracture toughness K_{IC} and the film strength. σ_{str} of IGZO films under compressive buckling were higher than those under tensile buckling. This is attributed to the different damage mechanism of the thin film. The mechanical failure of the film under tensile buckling mode was found to be due the formation of channel cracks whereas coating delamination, buckling of the film and finally channel cracking of the film were causes of mechanical failure in compressive buckling.

The results of this study may provide a better understanding of the failure processes of IGZO thin film on polyesters under different deformation stress modes. This in turn is expected to aid device designers to develop the next generation of flexible optoelectronic applications.

6. Fatigue behaviour of flexible transparent conductive multilayers films.

6.1. Introduction

In recent times, there has been a large demand in the production of flexible electronic devices, such as flexible solar cells, flexible circuits and flexible displays. However, the electrical failure of this production by mechanical deformation is one of the main reliability issues because these devices frequently work under mechanical and thermal stress caused by various mechanical deformations. Several research groups [87,191,192] have studied the electrical resistance changes under tensile and bending deformation. However, in addition to this tensile and bending deformation, twisting deformation is expected as another frequent deformation of flexible display or other flexible electronics device. Therefore, the primary objective of this chapter is to focus on flexing behaviours of TCO thin-film coated PET substrates by using a twisting and cyclic twisting device which was developed in this project. The influence of both factors including twisting angle and temperature on the fatigue behaviour of thin-film deposited on flexible PET substrates were discussed.

In the twisting test, the crack growth rate and change in electrical resistance were monitored *in situ* while during twisting fatigue test only the resistance changes were measured *in situ*. In this study ITO/Ag-alloy/ITO was chosen as an example on TCO thin film, as TCO is the main component in flexible electronic devices and it determines the flexibility and reliability of the devices.

6.2. *In situ* twisting test with confocal laser scanning microscopy investigation

Twisting tests were carried out on (200 nm) ITO/Ag-alloy/ITO films coated PET substrates by using a manually operated custom-built twisting apparatus Figure 3-9. The electrical resistance was monitored *in situ* by multi-meter and the crack development in the films was continuously monitored with CLSM.

The images were recorded from the surface and the electrical resistance was measured every 2° angle until 68° angle. These *in situ* measurements will provide critical twisting angle at which ITO/Ag-alloy/ITO film cracked and started to lose their electrical functionality.

In situ mechanical and electrical tests conducted simultaneously are highly important in correlating crack initiation and propagation with resistance change. It also helps to avoid the unloading-induced full or part closure of cracks in the thin film when performing subsequent *ex situ* tests.

The two measurement techniques are microscopy (CTA-M) and normalized electrical resistance (CTA-R) monitoring, both used to determine the critical twisting angle (CTA) for coating failure initiation. CTA-M is defined as the critical twisting angle at which the first cracks in the coating are observed, and CTA-R is defined as the critical twisting angle at which 10% increment in electrical resistance is occurring. The 10 % increases was arbitrarily selected as the criterion for crack onset initiation [87].

CLSM micrographs of the cracks, initiation and development on the ITO/Ag-alloy/ITO films at different angles are shown in Figure 6-1.

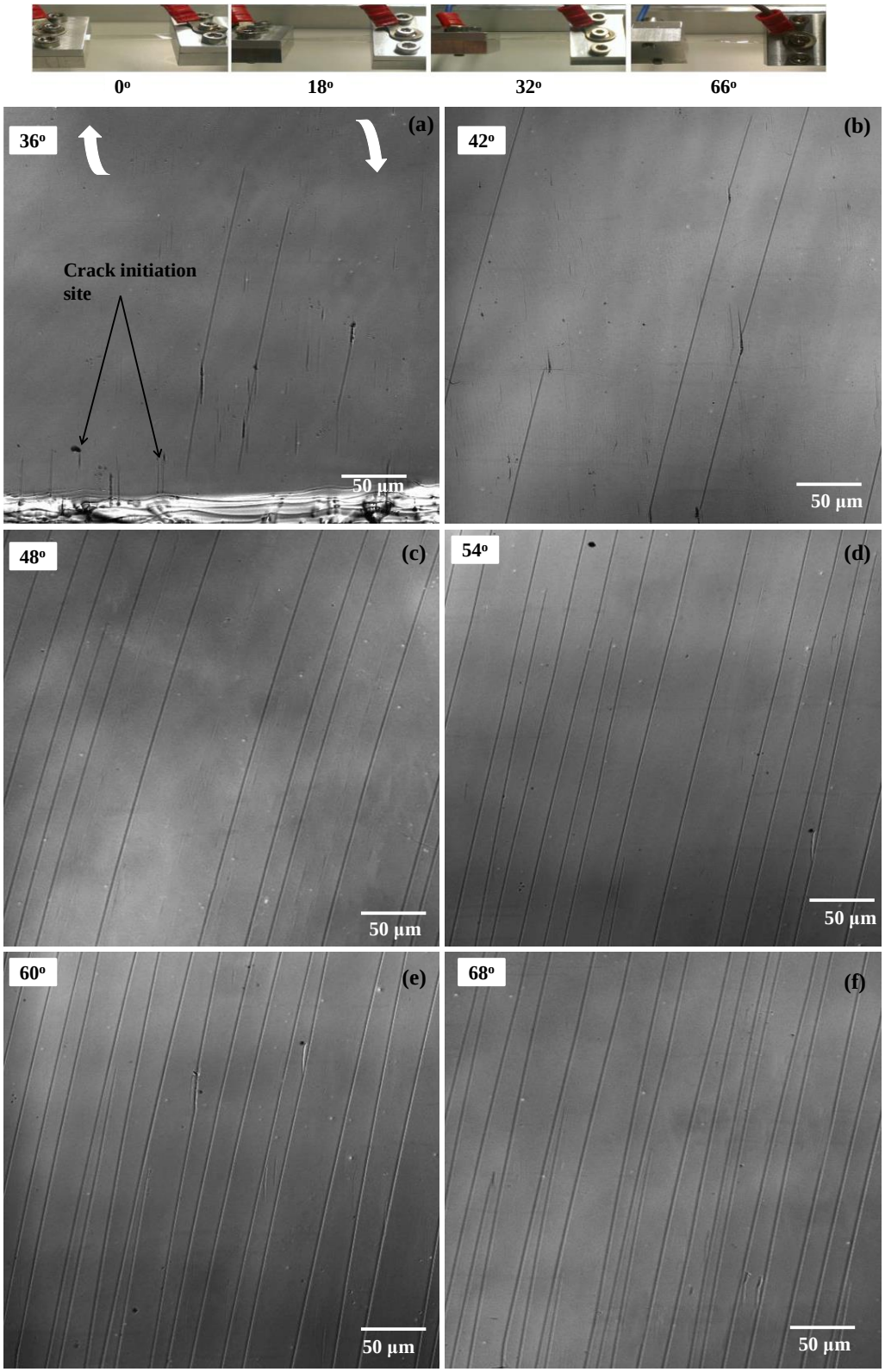

Figure 6-1 *In situ* confocal laser microscope imaging of cracks development ITO/Ag-alloy/ITO of the multilayer thin film under twisting. The corresponding twisting angle values are indicated on the images. Twisted Arrows on image (a) indicated the twisting direction. The upper panel displays the steps of the twisting test as the angles increase.

Cracking is observed to appear at CTA-M equal to 39° ± 1.7°. The imperfections or defects remaining after depositions in the layer coupled with edge defect resulting from the specimen cutting are believed to be crack-initiation sites, as can be seen in

Figure 6-1. It is suggested that this observation contributes to an increase in the energy released in the region [193]. The interface separation in the neighbourhood of an imperfection exhibits a larger energy release rate than that for a defect-free surface [193].

By increasing the applied twisting angle, the initiated channel crack starts to increase and propagate to the whole sample length. It was found that the channel crack is not grown through the whole width of the film; it is arrested at a certain distance from the middle section of the sample width, as shown in Figure 6-2.

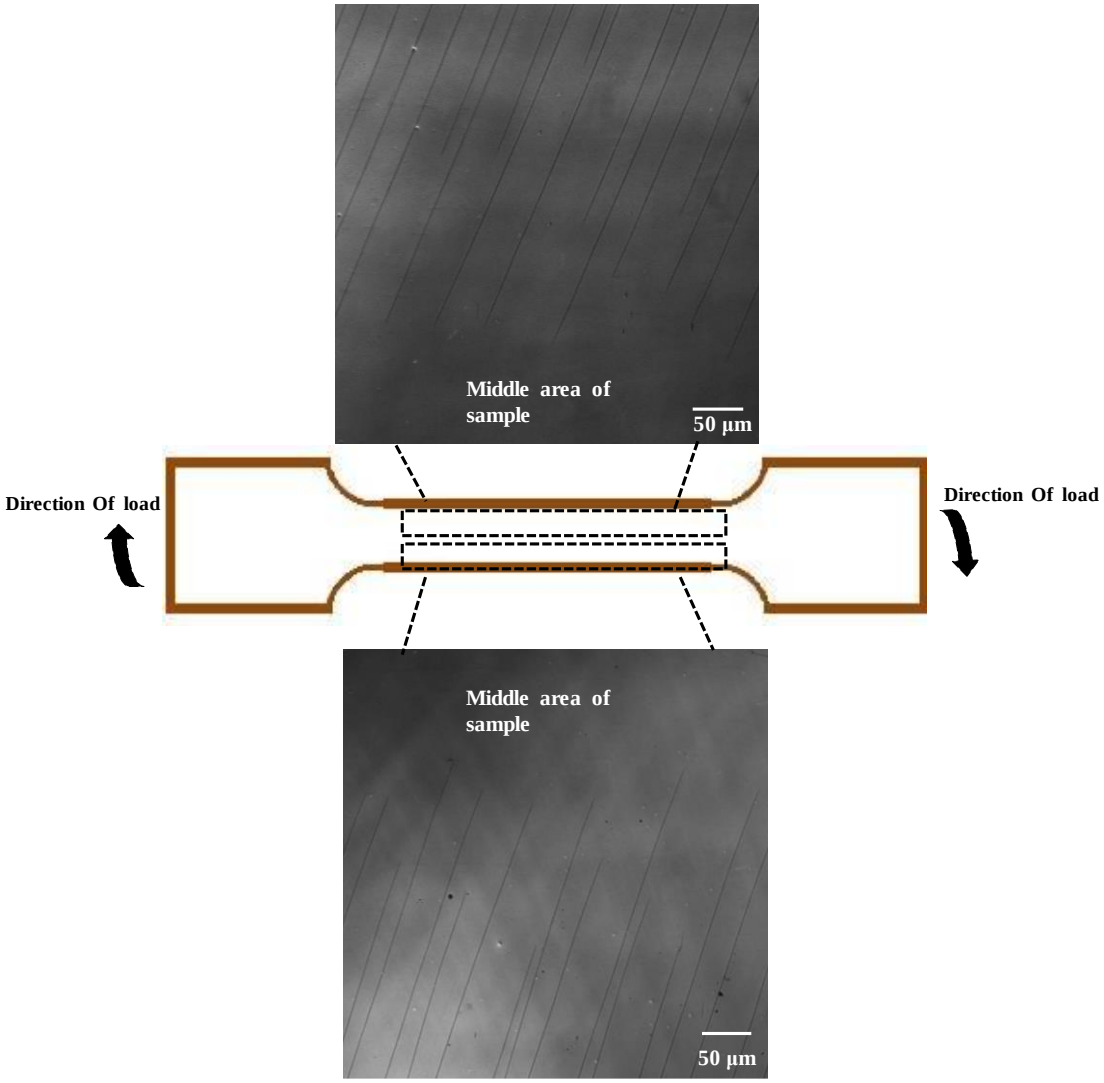

Figure 6-2 Cracks developments across the width of the sample under 68° of twisting angle.

This indicates that a maximum critical stress is produced over that specific region. It is clear to see that the cracks in the thin film are not propagating further as the applied twisting angle increase. This may be due to the substrate becoming completely plastic and not transferring the amount of stress required for further cracks to occur [105], in a similar manner to that in tensile tests.

Figure 6-3 demonstrates the results of the twisting reliability test for ITO/Ag-alloy/ITO films coated PET. It shows the crack density and the change of electrical resistance of the conductive layer, which was expressed as $\Delta R/R_o$, where $\Delta R = R - R_o$, R_o is the electrical resistance value before applying stress and R is the value after applying twisting stress. At the early stage of applying twisting angle the normalized values of electrical resistance are negative. This could be due to the shortening of the distance between adjacent atoms/grains present in the thin film, which can result in the decrease of physical barriers for moving electrons and improved mobility. These results are consistent with results reported by Potoczny [186] for ITO film on PET when subjected to compressive stress. This implies that during the twisting test the sample experienced compressive stress.

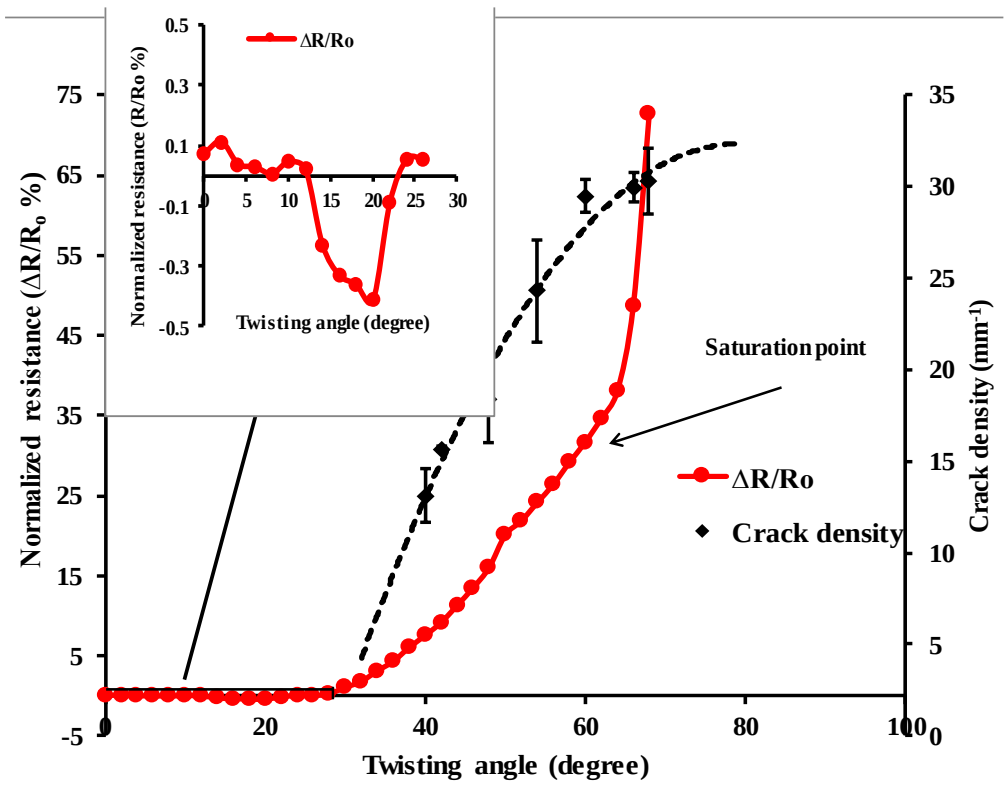

Figure 6-3 Crack density and normalized electrical resistance versus twisting angle for ITO/Ag-alloy/ITO thin film coated PET substrate.

With further twisting, the normalised electrical resistance of ITO/Ag-alloy/ITO started to increase. Then at 10% of the increase of the normalized electrical resistance, the CTA-R which promotes the first cracks in the conductive layer was observed to be 39.3° ± 3.5°. Above the CTA-R the electrical resistance was increased gradually due to the increased film crack formation [194], as the series of CLSM images show in Figure 6-1. In addition, a finite electrical resistance was observed even at high applied twisting angle of 68°.

A potential reason for finite electrical resistance in ITO/Ag-alloy/ITO thin film, even at a relatively high twisting angle, is that the channel cracks have not fully transversed across the sample width, see Figure 6-2, so that the sample remains electrically conductive. Also, any overlapping film material at the cracks after crack generation (see Figure 6-4), contributes to the formation of some conducting paths between the ITO films, which causes finite electrical resistance. This is consistent with a previous study conducted by Choa *et al*. [118] who pointed out that the overlap of the cracked IZO/Ag/IZO film, when it was twisted contributed to provide a conductive pathway through film fragmented and led to delay changes in the electrical resistance.

The CTA-R value which was determined by using normalized electrical resistance was equal to 39.3° ± 3.5° and it was in good agreement with CTA-M values determined by using the CLSM images, as shown in Table 6.1.

Leterrier *et al*. [87] also found good agreement between the initial crack growths in uniaxially strained ITO thin films measured from micrographs and the COS values which correspond to 10% increase of normalized electrical resistance.

A deeper understanding of the relationship between crack evolution density and variation in electrical resistance in the ITO/Ag-alloy/ITO film under twisting can be described in the following section.

Two distinct regions could be clearly observed in the CD and $\Delta R/R_o$ *vs* angle. In the first region, as the applied twisting increases the CD increases rapidly when channel cracks in the ITO/Ag-alloy/ITO thin film start to advance through the samples length. As a result, the electrical resistance of the thin film increases in this region; this may suggest that the applied twisting angle is proportional with number of cracks. However, above the crack saturation point, this is not applicable. In the second region (see Figure 6-3), the CD reaches a saturation point at 60°, the significant increase of the normalized electrical resistance was observed above the crack saturation point. This is possible because at large angles the material no longer overlaps at the some cracks and the conductive path is no longer present. The stress produced on the ITO/Ag-alloy/ITO films after the saturation point leads previously formed cracks to become deeper and wider and that can also be a reason for severe conduction failure when the CD is in a saturated state. This is in good agreement with previous observations of ITO deposited polymer substrates under uniaxial tension [3].

The thin film crack-initiation sites of ITO/Ag-alloy/ITO thin film observed in this study are consistent with those previously reported by Sim *et al*. [195] for ITO thin films deposited on a plastic substrate. This is also consistent with a study of Bejitual *et al*. [112] who investigated the mechanical behaviour of patterned ITO coated PET substrates. They found that the cohesive crack originated from the edges of the pattern where the thin the layer's surface is subjected to tensile buckling mode. Consequently, edge etch controlling is important and may in turn, enhance the reliability of the patterned thin film with increasing edge resolution. Furthermore, Lopez *et al*. [196] pointed out that the homogeneity of the edges has a

significant effect on the initiation and propagation of cracks and consequent bending reliability of flexible platinum lines patterned on polyimide. The increasing of CD of thin films with increasing twisting angle was also observed previously by Choa *et al*. [118] for InZnO/Ag/InZnO multilayer electrodes grown onto a flexible PET substrate.

The CTA-R of ITO/Ag-alloy/ITO thin film observed in this study is consistent with the critical twisting angle of ZTO/Ag/ZTO multilayer deposited on a PET substrate which was observed by initiating cracks at a twisting angle of 38° [117].

Table 6.1 Results of twisting test of ITO/Ag-alloy/ITO thin film deposited on PET polymer substrate.

Sample	CTA-M	CTA-R ($\Delta R/R_0 = 10\%$)
ITO/Ag-alloy/ITO	**39° ± 1.7°**	**39.3° ± 3.5°**

6.2.1. Ex - situ microscopical investigation of ITO/Ag-alloy/ITO film after twisting test.

Samples were investigated after twisting tests using *ex situ* SEM to reveal additional fine details of failure mechanisms of the ITO/Ag-alloy/ITO thin film. Figure 6-4 shows SEM micrograph of the ITO/Ag-alloy/ITO thin film coated PET after being subjected to a twisting test at a 68°of twisting angle. In some places the ITO/Ag-alloy/ITO film was in complete separation due to the formation of wide cracks, as shown in Figure 6-4 (a) However, in the

other places, overlapped film and buckling delamination of the multilayer stacking ITO/Ag-alloy/ITO thin film from the substrate are observed, as shown in Figure 6-4(b). This is in agreement with the change in electrical resistance data observed after the cracks saturation point. In addition, the existence of cohesive failure cracking is clearly visible in Figure 6-5. The investigation of an individual cracking, as Figure 6-5(b) demonstrates, reveals periodic open crack. The surface morphology of twisted ITO/Ag-alloy/ITO multilayer samples observed in this study is consistent with the morphology of cracks and buckling delamination investigated in the previous section (see section 5.3.3) for IGZO thin film under both tension and compression buckling mode. This result indicates that the twisting deformation induced tensile and compressive stress on the film simultaneously. Thus, a slight decrease in the electrical resistance was observed at early twisting stage. This result agrees with work done by Choa *et al.* [118] and Cho *et al.* [127] who have both previously found that twisting damage morphology of thin film on flexible polymer substrate is similar to the surface damage observed when the film is flexed in tension and compression buckling mode, indicating that both compression and tensile stress can be produced by the twisting motion.

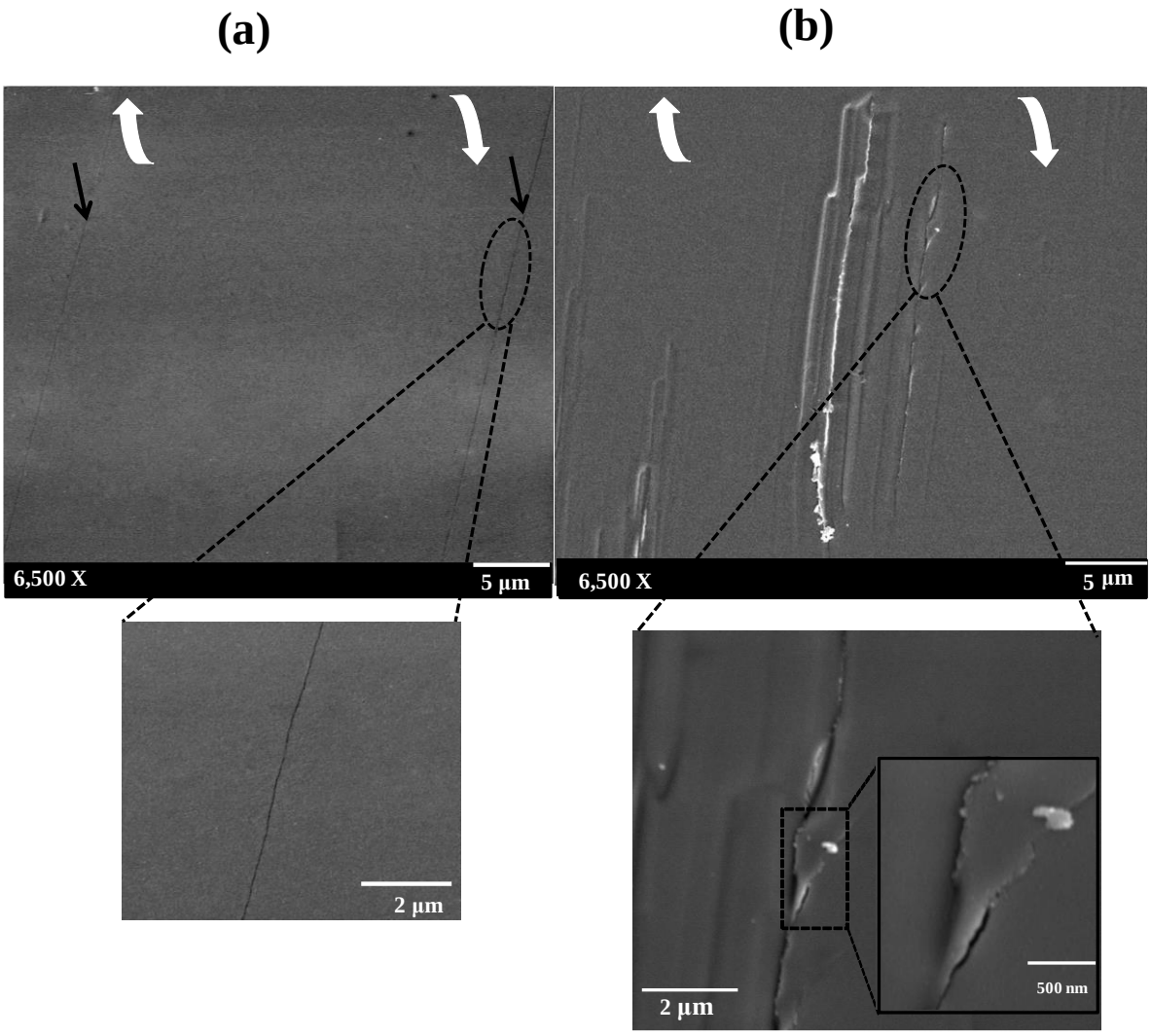

Figure 6-4 SEM micrograph with inset image showing (a) cracks on the surface (b) overlapping and buckling delamination of ITO/Ag alloy/ITO multilayer film at 68° applied angle under twisting test. Black arrows indicate the cracks and white twisted arrows on image indicate twisting direction

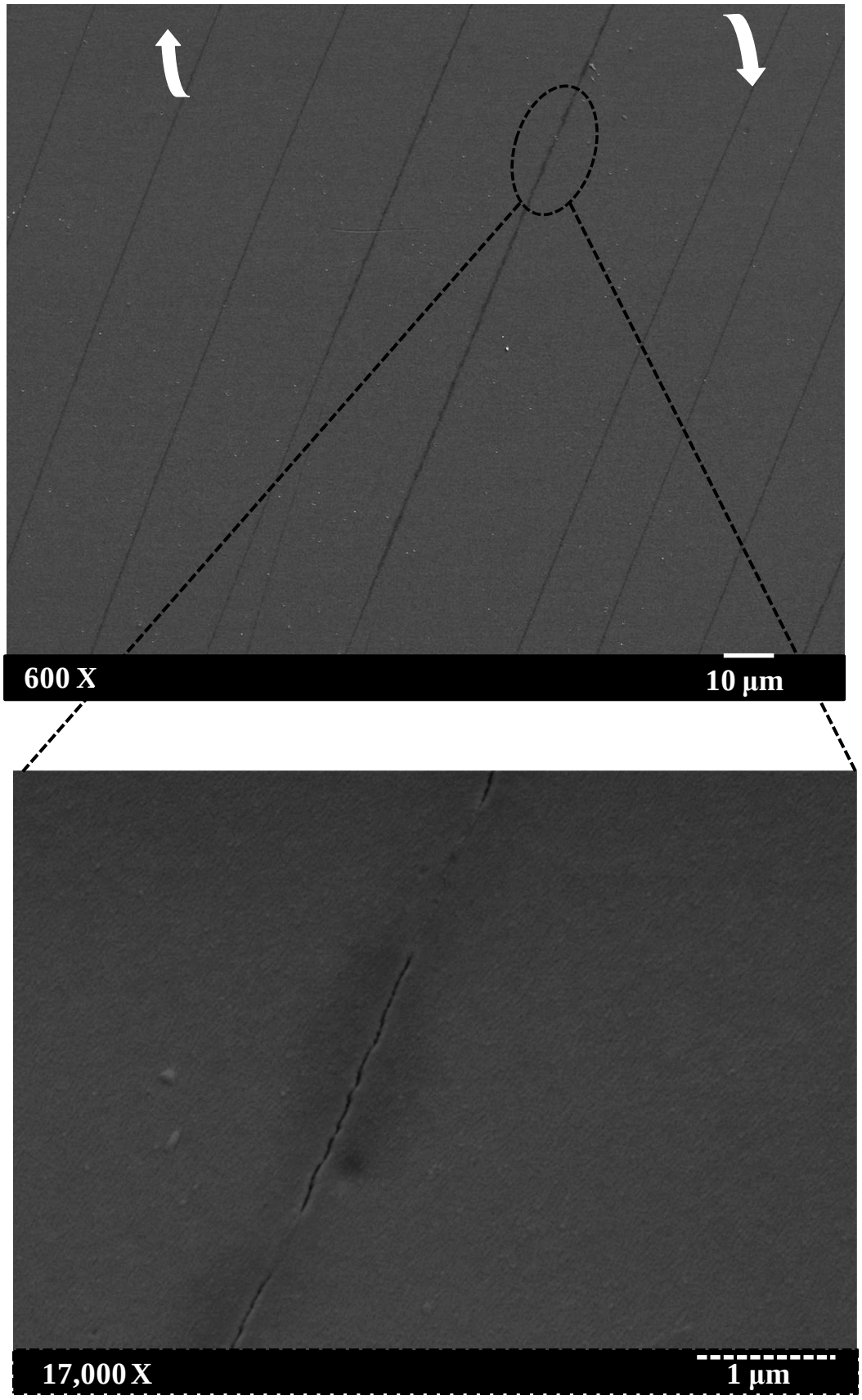

Figure 6-5 SEM micrograph image with enlarged image showing the formation of periodic crack growth of ITO/Ag-alloy/ITO multilayer film at 68° applied angle under twisting test. Twisted Arrows on image indicated the twisting direction.

6.3. Twisting fatigue tests

Twisting fatigue experiments of samples of 200 nm ITO/Ag-alloy/ITO film coated PET was conducted using a Rheometer machine. In this work two sets of experiments were performed, the first set of experiments were conducted to study the influence of various factors such as angle, temperature and frequency on electrical resistance behaviour of the thin film under twisting fatigue. The levels of angle (17.5°, 22.5°, 27.5°), frequency (10 cycles/min, 5 cycles/min) and temperature (RT, 50 °C, 100 °C) were selected (see section 3.2.3).

A second set of experiments was performed in order to assess whether the damage occurred due to the cyclic twisting or due to the temperature. Without any mechanical loading applied, the samples were subjected to the same combination of temperature for 40 minute (which is equal to the time require to perform 200 cycles at frequency of 5 cycles/min). For both sets of experiments, the electrical resistance was measured *in situ*.

6.3.1. Effect of twisting angle

The samples were tested at room temperature and a frequency of 5 cycles/min Figure 6-6 shows how the resistance changes as a function of twisting cycles for ITO/Ag-alloy/ITO film. It is clear to see the sudden increase in electrical resistance after the first few cycles. This may be attributed to the dimensional change of the polymer substrate [197]. In other words, the substrate does not appear to recover fully prior to the next cycle starting, but recovers over time. Therefore, after each cycle the gauge width of the substrate reduces up to the state of equilibrium attained between the applied load and the gauge width recovery [197]. With further increment of the number of applied twisting cycles, a gradual increase of normalized

electrical resistance is observed. This is likely to be due to progressive cracking and buckling [197], as shown in Figure 6-7. Figure 6-8 shows a comparison for three different angles. It was found that the samples tested under applied twisting angle equal to 17.5° show extremely slow increase in resistance followed by the sample tested under applied twisting angle equal to the 22.5°, while the sample tested under 27.5° shows the highest increase in normalised electrical resistance. Therefore, as the applied twisting angle increases, samples fail sooner. In addition, electrical resistances changed during loading and unloading as shown in the inset of Figure 6-8. This change is believed to result from the opening and re-closing of microcracks in the film during twisting and untwisting of the sample [198]. Furthermore, resistance modulation repeated continuously during twisting cycles as shown in Figure 6-8. The modulations in resistance of ITO/Ag-alloy/ITO multilayer film significantly depend on the twisting angle. The resistance modulation in the film with a higher twisting angle is higher than those of lower twisting angles. The resistance modulations phenomenon during the bending test was reported by Park *et al.* [199] for Ga-doped ZnO (GZO/Ag/GZO) multilayer deposited on flexible substrate. They observed that modulation in resistance becomes stronger after subjecting samples to lower bending radius. In our study, the increasing number of microcracks and growth in width and depth with increasing twisting angle, might be a primary cause of increased resistance modulation of ITO/Ag-alloy/ITO multilayer with increasing twisting angle.

The results of fatigue twisting tests at different angles of the of ITO/Ag-alloy/ITO multilayer film after 200 cycle are summarized in Table 6.2

The fatigue twisting tests were repeated at room temperature and twisting angle 27.5° at frequency of 10 cycles/min. The electrical resistance change results for this case depicted in

Figure 6-9. For comparision, the change of electrical resistance of samples tested at frequency of 5 cycles/min is also presented in Figure 6-9. There is no significant difference in the percent change of electrical resistance between the samples tested at different frequnces, for that reason the effect of the frequency is assumed to be negligible.

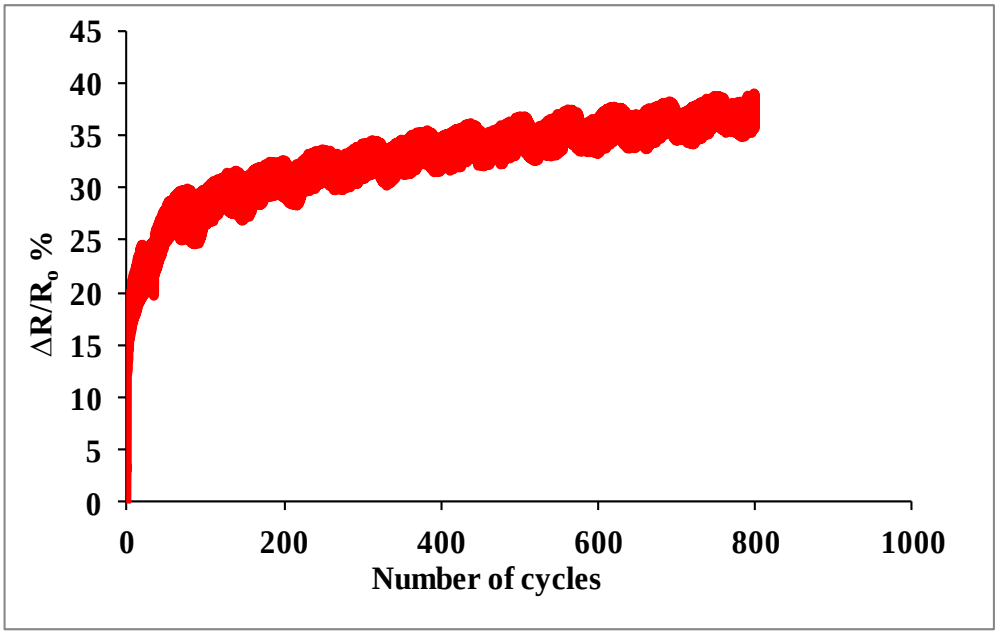

Figure 6-6 Normalized Resistance versus number of cycles for ITO/Ag-alloy/ITO multilayer coated PET substrate.

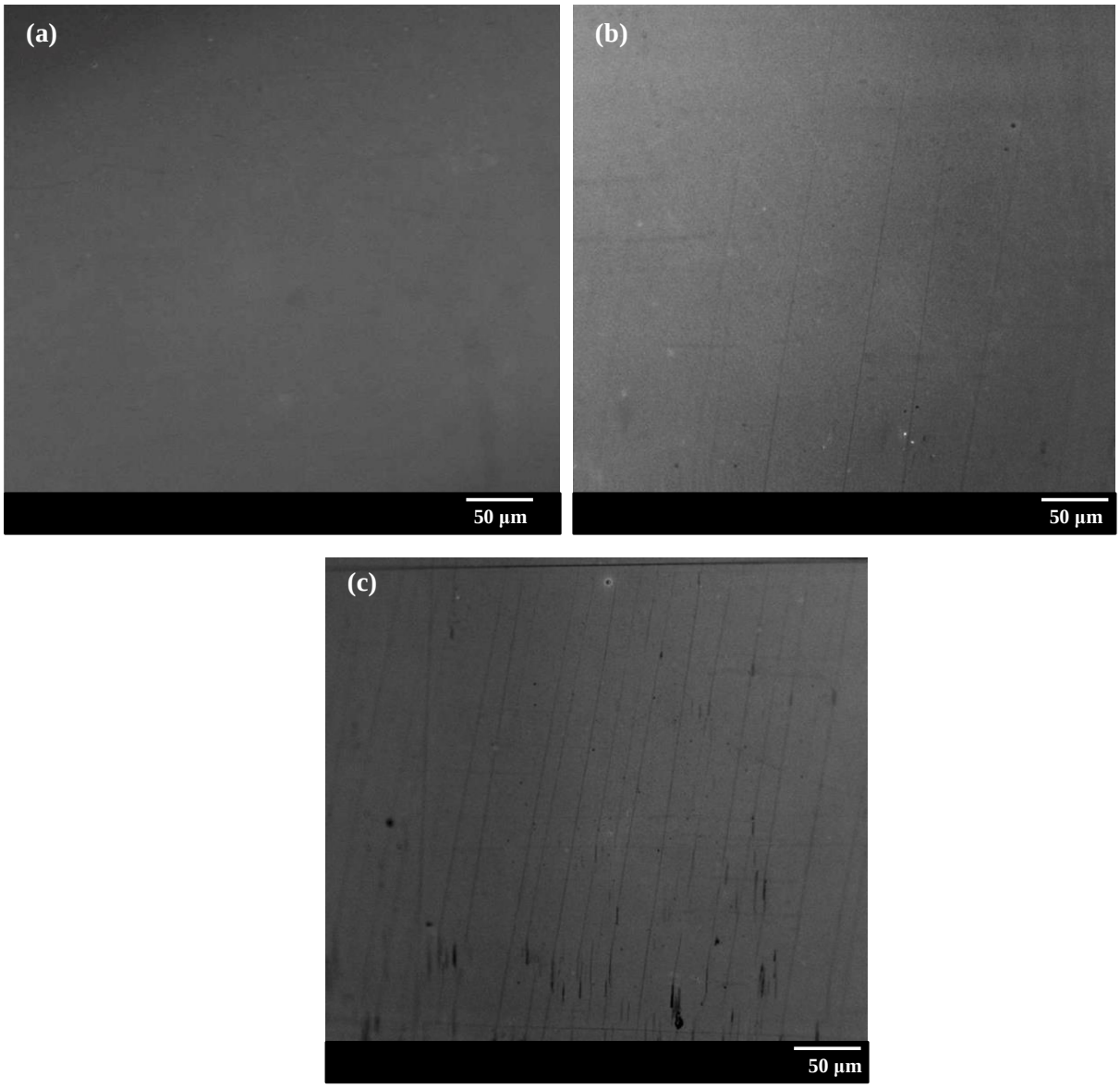

Figure 6-7 Confocal Laser microscopy images showing cracked ITO/Ag-alloy/ITO films after (a)100 (b) 300 (c) 800 twisting cycles at 27.5 °.

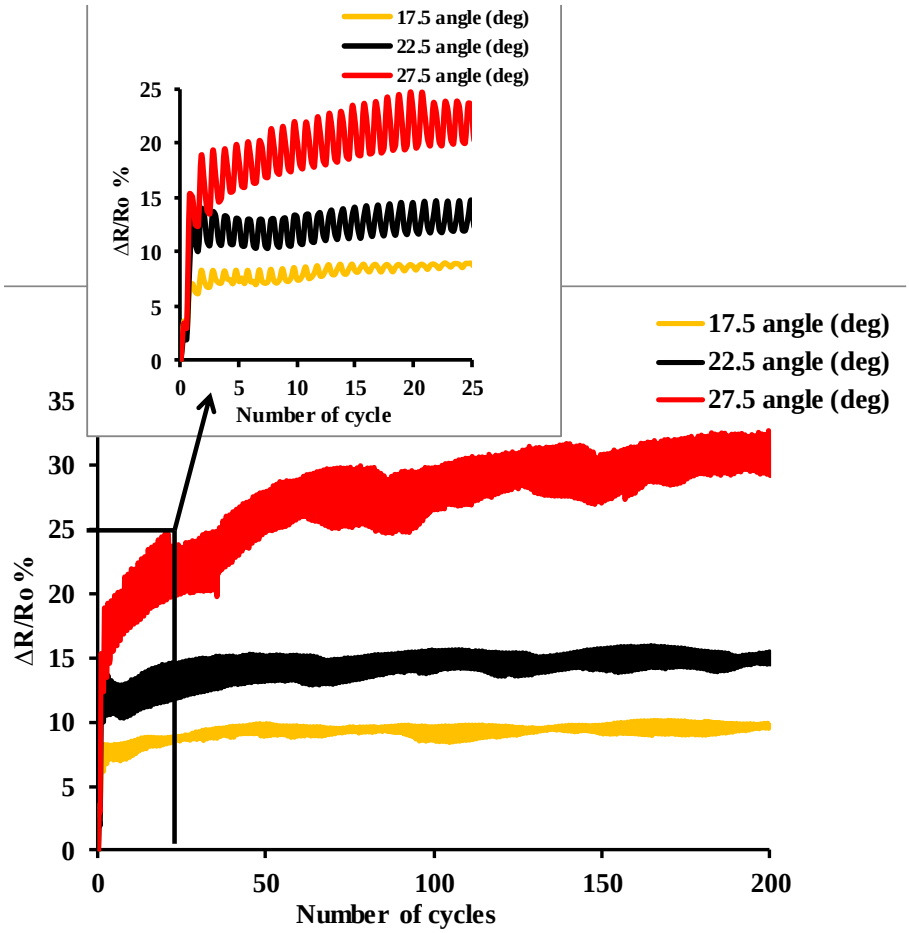

Figure 6-8 Normalized electrical resistance as function of the number of fatigue cycles during cyclic twisting of ITO/Ag-alloy/ITO under different applied angles.

Table 6.2 Summary of results from fatigue twisting test under different applied angles after 200 cycles.

Sample	($\Delta R/R_o$ %) at angle 17.5°	($\Delta R/R_o$ %) at angle 22.5°	($\Delta R/R_o$ %) at angle 27.5°
ITO/Ag-alloy/ITO	9.3 ±2.02	12.3± 0.88	28.6 ± 2.96

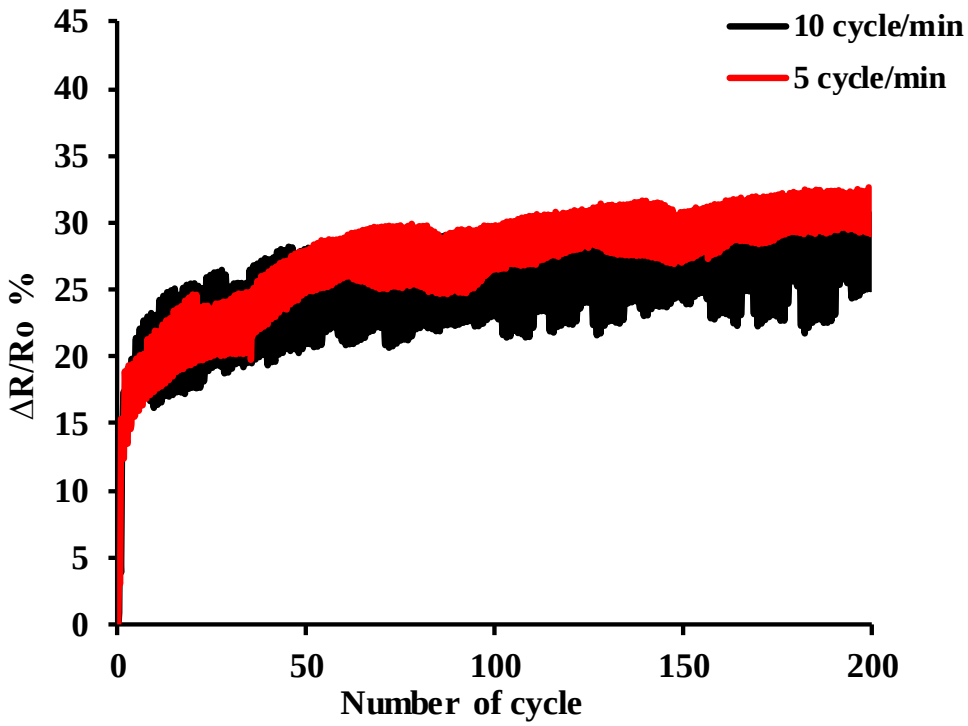

Figure 6-9 Normalized electrical resistance as function of the number of fatigue cycles during cyclic twisting of ITO/Ag-alloy/ITO under different applied frequncy.

6.3.1.1. Ex – situ SEM investigation of ITO/Ag-alloy/ITO film thin film after twisting fatigue tests under different angles

Figure 6-10 and Figure 6-11 show SEM micrographs of the ITO/Ag-alloy/ITO samples after twisting cycles at 17.5° and 22.5° applied angles respectively. The thin film did not exhibit cracking. However, a slight increase in electrical resistance with increasing number of cycles was noted. For example, we observe that at 200 cycles the change in electrical resistance is 9.3 ± 2.02% for 17.5° angle and 12.3 ± 0.88% for 22.5° .This suggests that some microcracks might have been generated in the film, and then elastic recovery of the polymer substrate occurred, thus leading to the closure of the microcracks when the sample was unloaded [198].

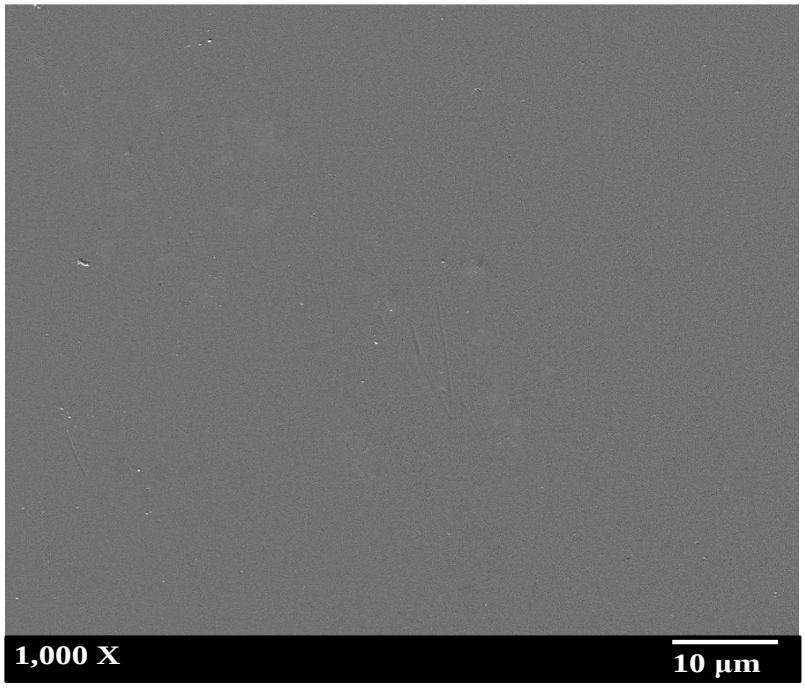

Figure 6-10 SEM micrographs of ITO/Ag-alloy/ITO films after 200 twisting cycles at 17.5° applied angle.

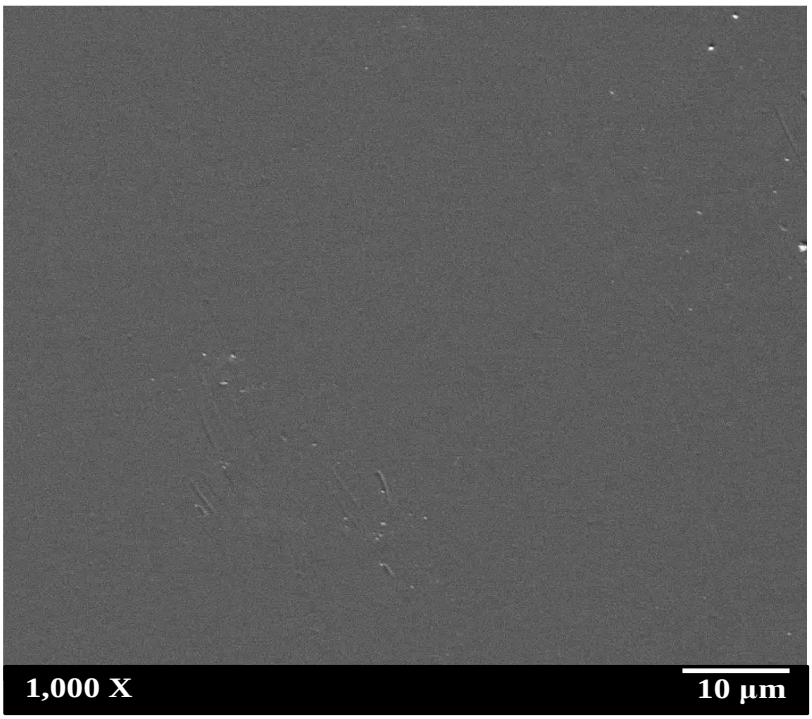

Figure 6-11 SEM micrographs of ITO/Ag-alloy/ITO films after 200 twisting cycles at 22.5° applied angle.

Figure 6-12 is depicting the surface ITO/Ag-alloy/ITO samples after twisting cycles at 27.5°. It shows a few shallow and parallel cracks to each other with finite length, which is in good agreement with results obtained from the twisting test coupled with *in situ* confocal laser scanning microscopy observations (see, Figure 6-2.). Closer observation of this image also reveals buckling formation besides the cracks. This is consistent with electrical resistance results, where the angle 27.5° shows higher change in film's electrical resistance (i.e 28.6 ± 2.9% after 200 cycles) compared to angles 17.5° and 22.5°, respectively.

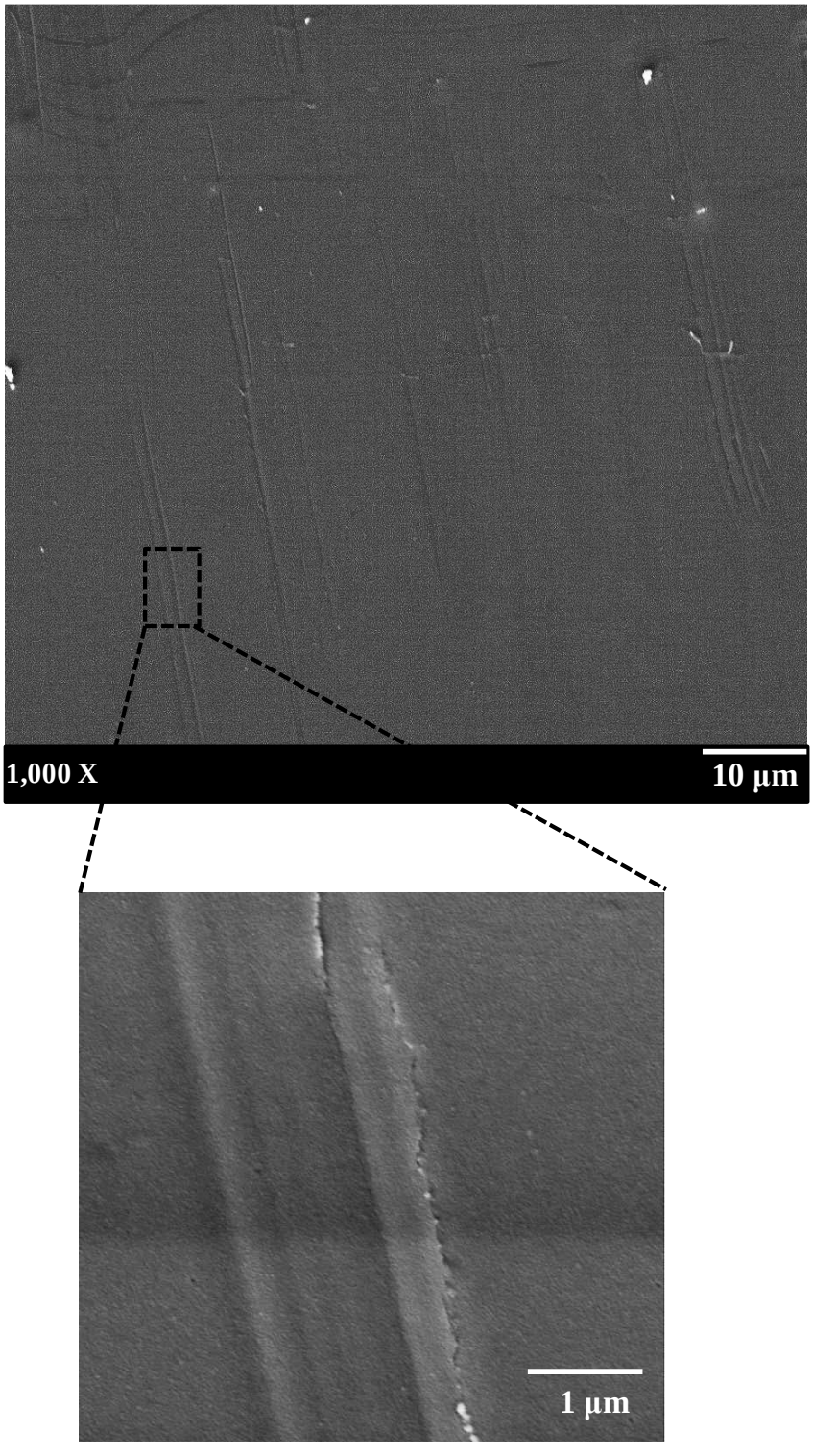

Figure 6-12 SEM micrographs of ITO/Ag-alloy/ITO films after 200 twisting cycles at 27.5 ° applied angle.

6.3.2. Effect of temperature

The influence of the temperature on the electrical resistance of ITO/Ag-alloy/ITO multilayer film on PET substrates was investigated in this work. In Figure 6-13, the normalised electrical resistance is plotted as a function of the number of twisting cycles at different temperatures and a constant twisting angle of 27.5° and constant frequency of 5 cycles/min respectively.

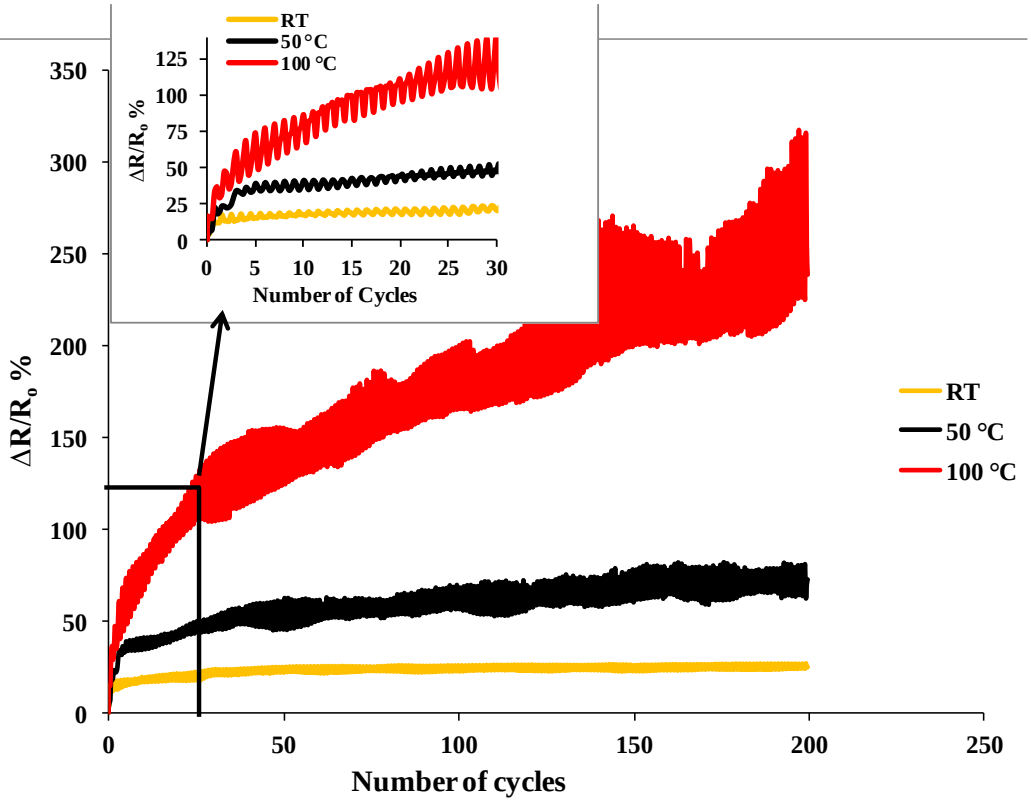

Figure 6-13 Normalized electrical resistance as a function of applied number of cycles during cyclic twisting test of ITO/Ag-alloy/ITO under different applied temperatures.

Regardless of temperature used, the electro-mechanical performance is consistent with that observed for fatigue twisting at different angles (see section 6.3.1). After the first few cycles the normalized electrical resistance increased significantly until equilibrium was reached. Above a possible equilibrium point, between the applied stress and recovery of the dimensions of the compliant substrate, a gradual linear increase of the change in resistance

with increasing number of cycles is noted. At 200 cycles, the change in electrical resistance for specimens tested at room temperature is found to be the lowest, whereas for specimens subjected to 50 °C resistance increases by about 78%, and for specimens subjected to 100 °C by about 233%, as Table 6.3 shown. Therefore, the combined action of externally applied torsional stress and temperature is considerable. The significant difference in the normalized electrical resistance for the specimens tested at 50 °C and 100 °C compared with those tested at RT could be due to the following reasons: Firstly, the internal tensile stress has a direct effect on accelerating cracking of the thin film [200]. When the temperature increases up to approximately 100 °C, the internal tensile stresses increase in the coating [97] due to the high CTE of the substrate compared to the coating and also the mechanical mismatch increases between thin film and substrate resulting from the softening of the polymer substrate. Therefore, the thin film fractures more easily, resulting in an increment in the electrical resistance. Secondly, once the crack has initiated under combined cycle stress and high temperature, it is easier for the oxygen in air to penetrate into the Ag layer and react with it thus causing the Ag layer to partially oxidize. In general, oxidation occurs at a higher rate when the temperature is high [128]. Therefore, oxidation could be another factor, which might cause increment in the electrical resistance, in addition to the externally applied twisting stress.

Table 6.3 Summary of results from fatigue twisting test under different applied temperature after 200 cycles at 27.5°.

Sample	($\Delta R/R_o$ %) at temperature RT	($\Delta R/R_o$ %) at temperature 50 °C	($\Delta R/R_o$ %) at temperature 100 °C
ITO/Ag-alloy/ITO	**28.6 ± 2.96**	**78 ± 38.3**	**233 ± 29.03**

The increase of CD with temperature is shown by the confocal micrograph images Figure 6-14. One can find that CD starts to increase as temperature increases. With further increasing temperature, the growth of cracks in the conductive layer is more pronounced and wider, see Figure 6-14(b), Figure 6-14(c) and Figure 6-17. Thus, the increment of electrical for the sample at 50 °C and 100 oC are greater than that at room temperature, see Figure 6-13.

In addition, ITO/Ag-alloy/ITO multilayer tests at higher temperature shows a larger resistance modulation when it twisted and comes back to its initial position. This may be attributed to the existence of open cracking (see Figure 6-17).

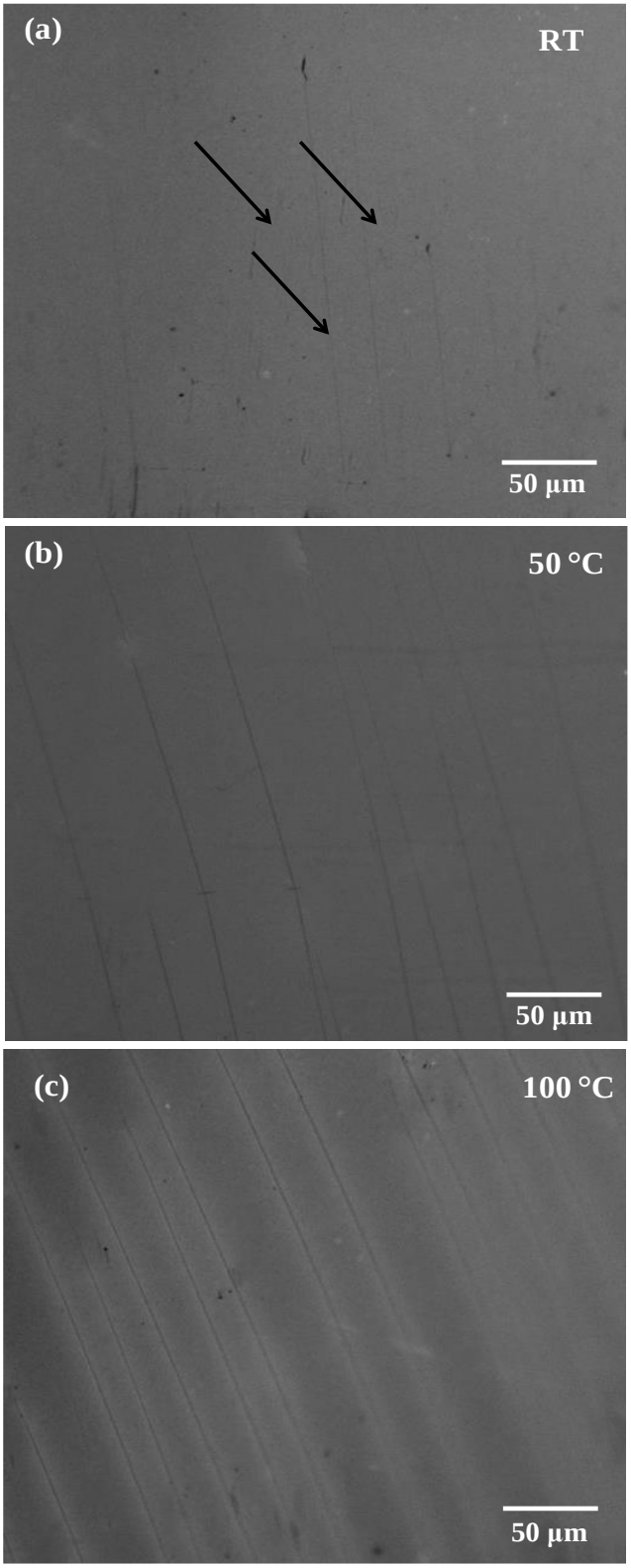

Figure 6-14 CLSM images showing surface of ITO/Ag-alloy/ITO films after 200 twisting cycles at (a) RT (b) 50 °C and (c) 100 °C subjecting temperature. The black arrows show cracks on the coating.

Similar electro-mechanical behaviour to that obtained in this work was reported for uniaxially strained ITO film coated PET substrates by Cairns *et al*. [197]. They suggested that the increase of resistance with temperature is dependent on the thermal properties of the substrate. This result is also consistent with that conducted previously by Khalid *et al*. [128] who studied the influence of temperature on the bending fatigue behaviour of copper thin film deposited on a PET substrate. They observed that the electrical resistance changes of the samples tested at higher temperatures (100 °C) is greater than that tested at both 0 °C and 50 °C temperature. It was believed that the failure of the Cu functional layer is oxidation dominated. It is noteworthy, that the electrical resistance of the material was still finite even after being subjected to temperatures of up to 100 °C. This indicates that the cracks form locally and have not propagated through the whole length and width of the sample from one edge to the other. As shown in confocal microscope image in Figure 6-15, the corner area at the end of the specimen exhibits the highest value of crack density, compared to the centre, because of the highest stress concentrated in that area. In the cases where cracks growth from one edge of sample to the other, the conductive path was reported to be severed; this means that the film lost its conductivities completely. This does demonstrate the property of an insulating material, which was not observed in our flexing test.

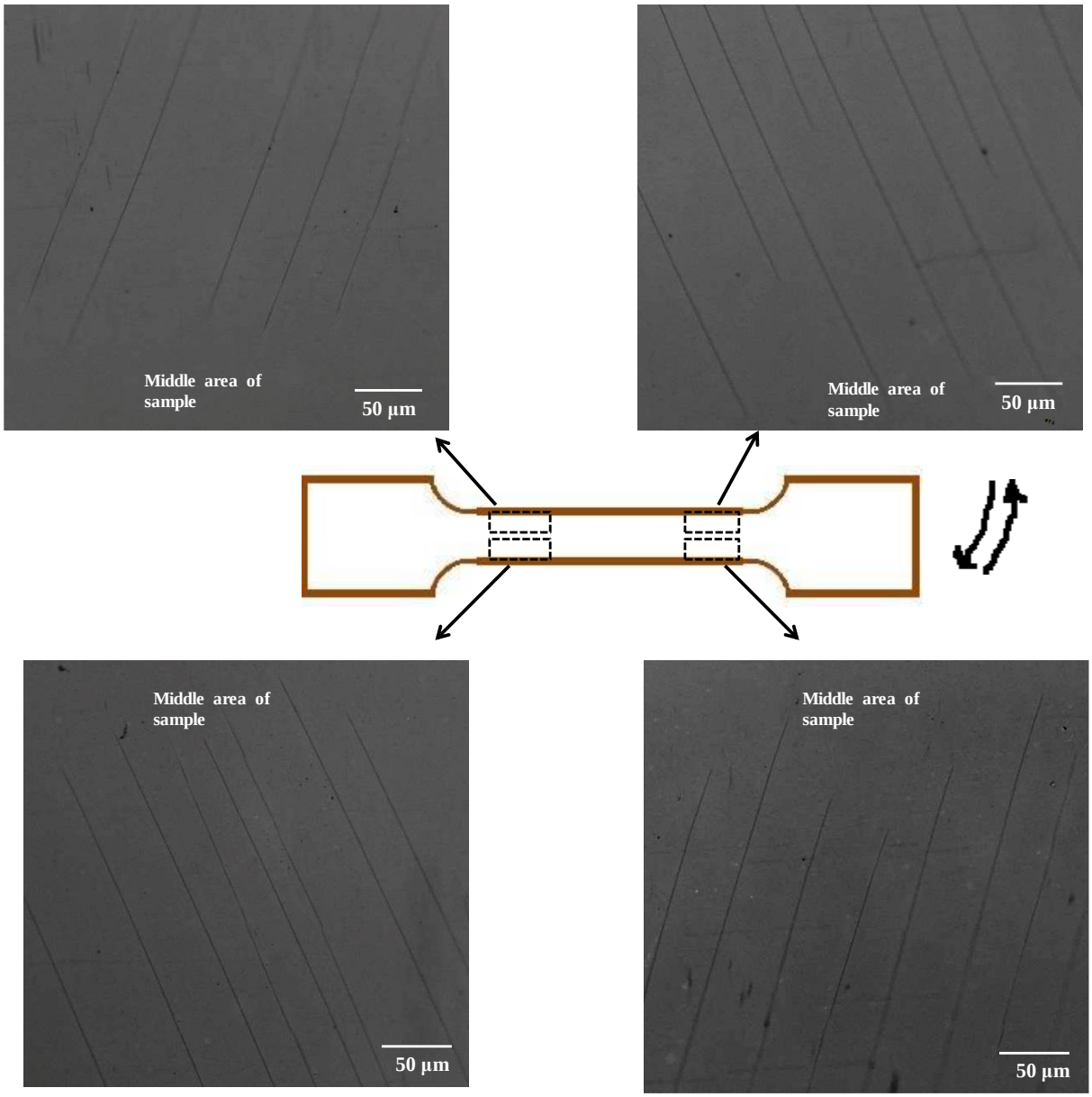

Figure 6-15 Confocal laser microscopy images showing crack distrbution in surface of ITO/Ag-alloy/ITO films after 200 twisting cycles at 100 °C.

6.3.2.1. Ex - situ microscopical investigation of ITO/Ag-alloy/ITO thin film after Twisting fatigue tests under different temperatures

The surface of the ITO/Ag-alloy/ITO after twisting fatigue is not shown here for room temperature and 27.5 ° as that result is depicted in Figure 6-12 . In the case of ITO/Ag-alloy/ITO subjected to 50°C, a crack pattern is visible, as Figure 6-16 shows. It is clear to see that this crack observation is very close to the electrical resistance results. The cracks were found in the surface, but they did not go through the film thickness, this lead to a slight increase in electrical resistance rather than a significant increase (see Figure 6-13).

Figure 6-17 shows an SEM micrographs of the ITO/Ag-alloy/ITO after 200 cycles at 100 °C. More cracks parallel to each other are found on the sample surface. Cracks opening with width of ~ 90 nm are clearly visible in the Figure 6-17 b which confirms the degradation of ITO/Ag-alloy/ITO film conductivity during twisting fatigue under high ambient temperature.

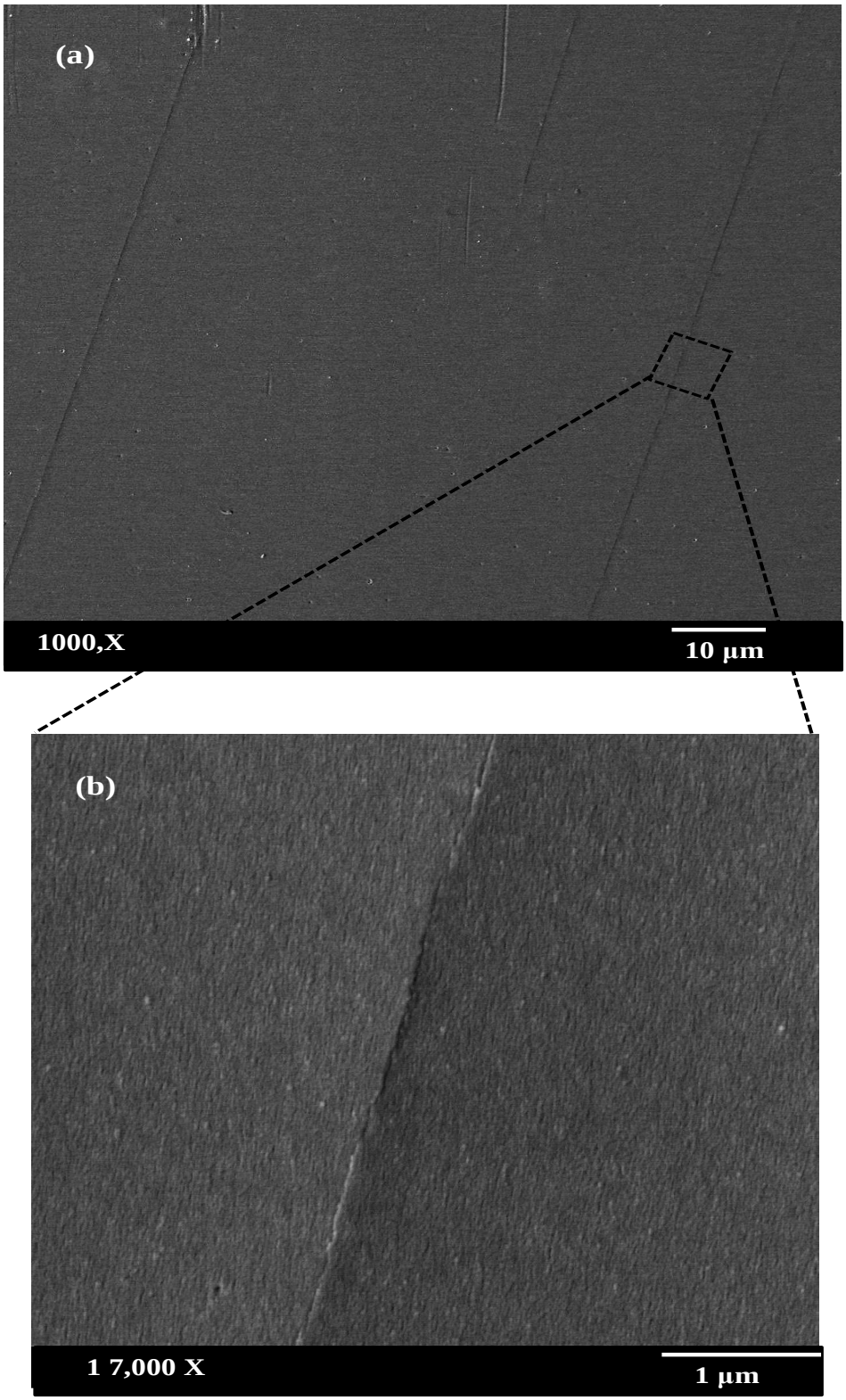

Figure 6-16 SEM images of surface of ITO/Ag-alloy/ITO films after 200 twisting cycles under 50 °C of temperature.

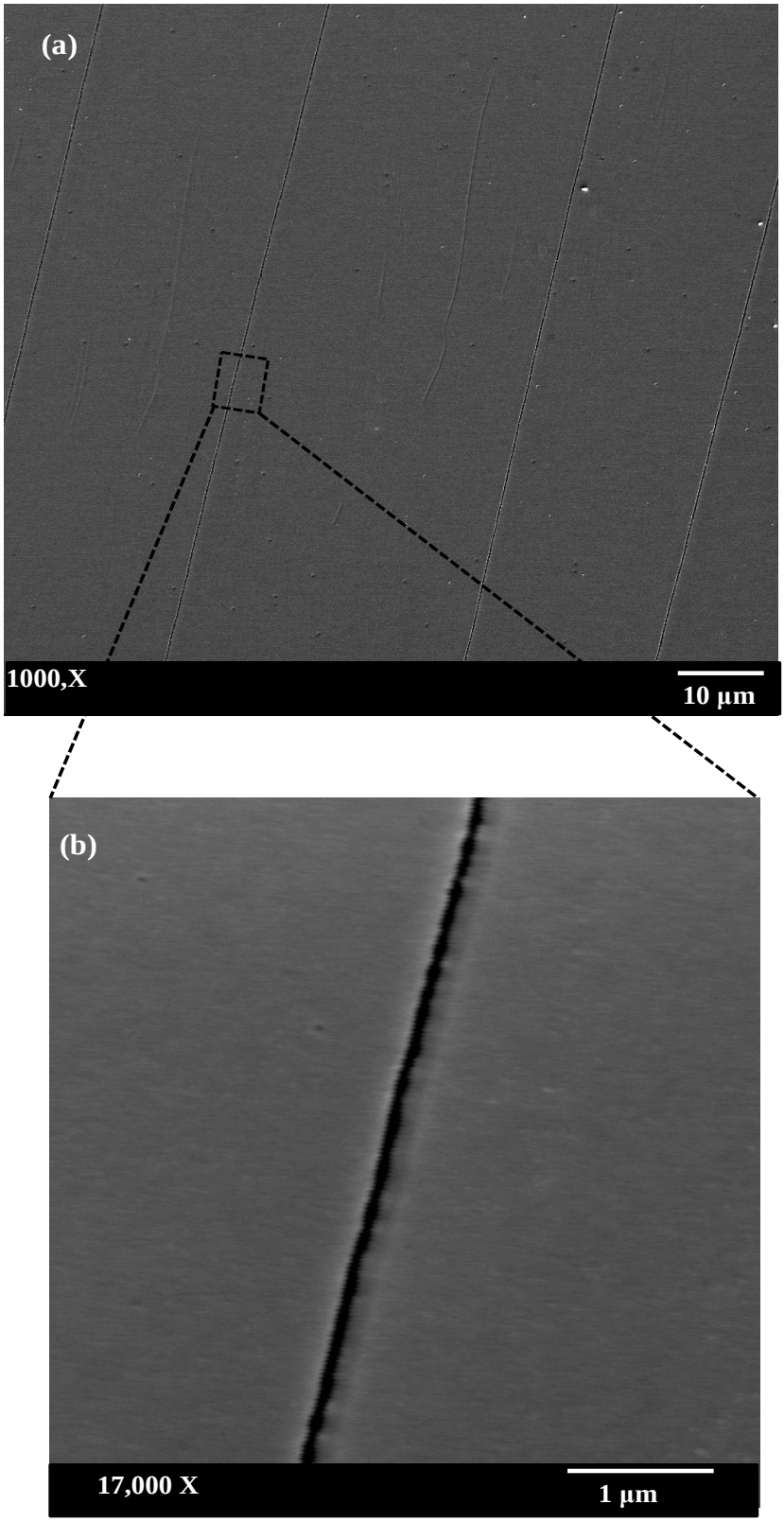

Figure 6-17 SEM images of surface of ITO/Ag-alloy/ITO films after 200 twisting cycles under 100 °C of temperature.

6.3.3. Film response characterization

The samples were subjected to the same combinations of temperature (section 6.3.2) for 40 minutes without involving cyclic twisting, in order to assess whether film damage was due to either cyclic twisting or temperature. The electrical resistance was monitored *in situ*. After the end of the exposure time, the surface morphology, crystallinity and transmittance of the films were investigated by SEM, XRD and spectrophotometer respectively.

Figure 6-18 shows no significant change in normalized electrical resistance over time for samples exposed to RT and 50 ^{o}C. However, at the early beginning of subjecting samples to high temperatures (above the T_g of PET) a slight decrease in electrical resistance is observed and then tends to stabilized after a certain period of time. This may result from rearrangements of the atoms in the ITO [201] leading to shortening of the distance between atoms and in a resulting increase of the electrical conductivity.

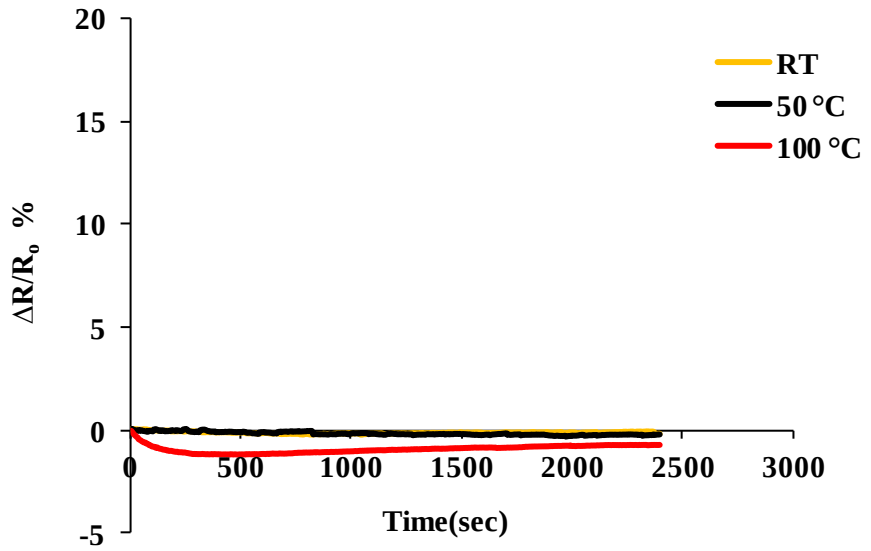

Figure 6-18 Normalized electrical resistance of ITO/Ag-alloy/ITO as function of time at different applied temperature.

In order to further understand the stability of the electrical resistance, SEM was performed on the surface of the films exposed to different temperatures. Figure 6-19 shows SEM micrographs of the surface of three different samples after being subjected to three different temperatures for 40 minute. The lack of any cracks initiating in the surface of all of the samples, confirms the electrical resistance stability.

Figure 6-20 shows diffraction peaks of ITO/Ag-alloy/ITO at different temperature. All diffraction peaks were attributed to the semi-crystalline polymer substrates (see Figure 5-4). The film did not show any additional diffraction peaks, indicating the amorphous nature of top and bottom ITO layers and Ag layer. In addition, there was no appreciable change between XRD spectra of different temperature.

As previously reported ITO films up to 100–200 nm thick are amorphous and processing temperatures above 100 °C or increasing film thickness can provide crystalline growth [202]. It was also observed by Jin *et al.* [203] that the microstructure of an inserted Ag layer between ITO layers depend on its thickness. They reported that at a thickness of 10 nm no crystalline peaks were found in XRD but above that thickness there was evidence of developing crystallinity.

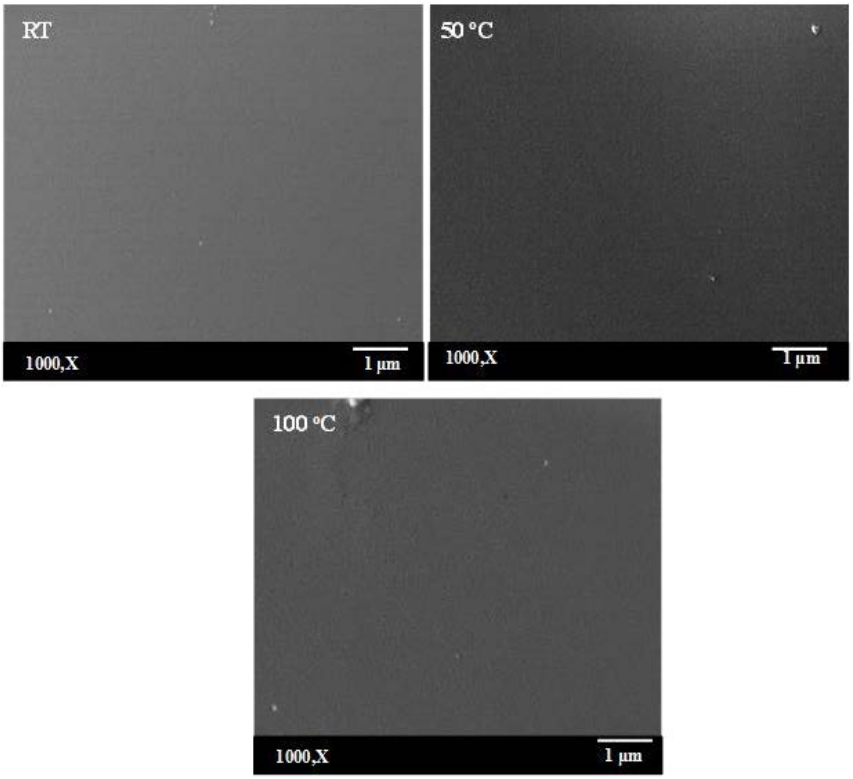

Figure 6-19 SEM images of the surface of the ITO/Ag-alloy/ITO after exposure to different temperatures for 40 minutes.

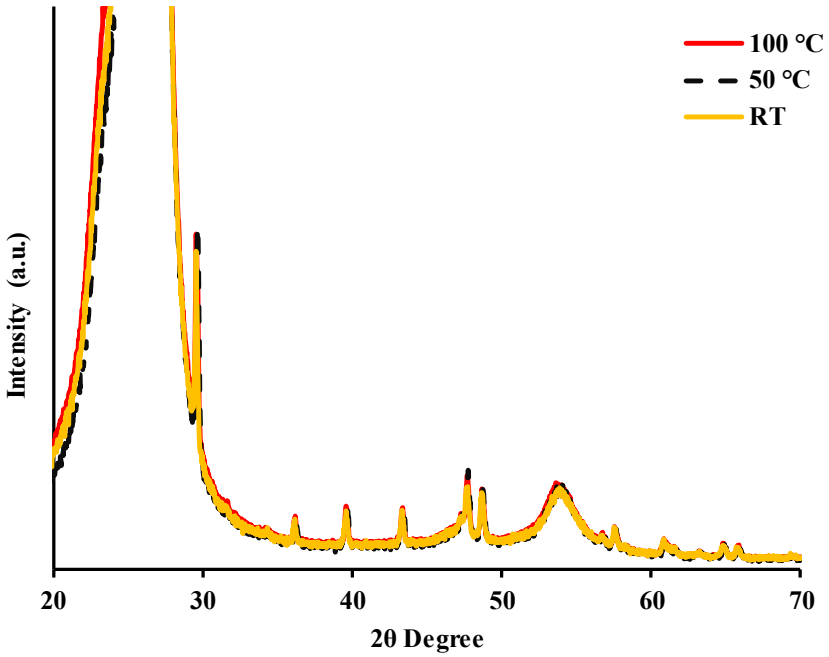

Figure 6-20 XRD diffraction patterns of the ITO/Ag-alloy/ITO film exposed to different temperatures (RT, 50 °C and 100 °C).

Figure 6-21 shows the transmittance spectra of the ITO/Ag-alloy/ITO thin film with various temperature exposures as a function of wavelength. The transmittance of all of the films was approximately 75% in the visible light region. This value was lower by around 15% in comparison to that reported by Guillen and Herrero [204] for ITO/Ag/ITO multilayer deposited on glass substrate in the visible range. This reduction in transmittance could be due to the different film thickness or differences in substrate material.

The band gap E_g was calculated by using Tauc's relation [205]:

$$(\alpha h\nu)^2 = C(h\nu - E_g) \qquad 6\text{-}1$$

where C is a constant, h is the Planck's constant, ν is the frequency of the incident light, and α is the absorption coefficient that was calculated from Lambert's law [206] :

$$\alpha = -\ln(T)/t \qquad 6\text{-}2$$

where T is the transmittance and t is thickness of the multilayer thin film. Then E_g can be obtained from the intercept of $(\alpha h\nu)^2$ versus photon energy $h\nu$ plot [207].

Figure 6-21 inset shows a plotting of $(\alpha h\nu)^2$ as a function of photon energy $h\nu$ and a linear extrapolation showing the band gap. The band gap of the ITO/Ag-alloy/ITO thin film holds at room temperature was 3.14 eV. This value was similar for the films subjected to 50 °C and 100 °C. It shows that temperature does not have to affect the optical properties.

This leads to a conclusion that combined action of an externally applied mechanical stress and temperature which promotes cracking should be taken into account for ensuring reliability.

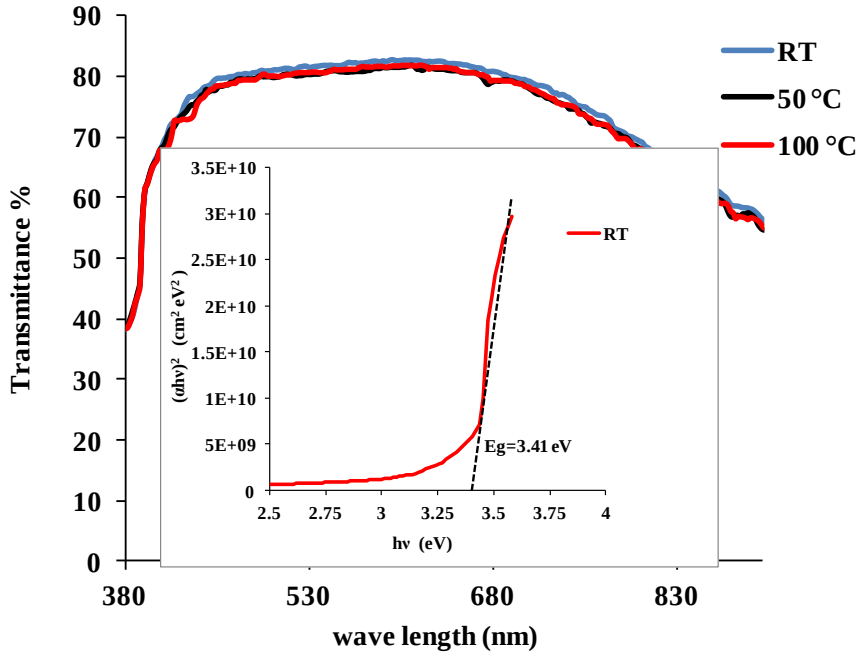

Figure 6-21 Optical transmittance spectra of ITO/Ag-alloy/ITO thin film with different temperature exposures. The inset is the Plots of $(\alpha h\nu)^2$ versus photon energy of ITO/Ag-alloy/ITO thin film with different temperature exposures.

6.4. Conclusions

In this chapter twisting test and twisting fatigue experiments were conducted on ITO/Ag-alloy/ITO thin film coated PET.

In twisting tests, crack development and electrical resistance were monitored *in situ*. Cracks started at angle of 39° ± 1.7° and propagated towards the sample length. The crack intensity increased with increasing applied angle, resulting in electrical resistance increases. The cracks were observed to initiate not only from coating defects but also from edge defects. These findings suggest that improving coating quality and sample edges can lead to preservation of the integrity of the thin film.

In addition, good correlation between the CTA-R value which was obtained by using normalized electrical resistance and CTA-M values obtained by using the CLSM images was observed. Higher CD was observed at the edge area as opposed to the centre area across the length of the specimen due to the highest stress being concentrated in that area. SEM results reveal cracking and buckling delamination failure which indicates that both tensile and compressive stresses have been induced in the films by the twisting motion.

In twisting fatigue experiments, the effect of twisting angle, twisting frequency and temperature on ITO/Ag-alloy/ITO thin film coated PET were studied. The effect of temperature without applied mechanical stress was also investigated.

The analysis of resistance has revealed that as the number of cycles increases the normalized resistance increases due to crack initiation and propagation. The highest crack density was found in the corner part of clamped samples. In addition, normalized resistance change of the samples was higher at higher applied angles. This was caused by higher stress applied which led to more thin film cracking resulting in maximum changes in electrical resistance.

Furthermore, the percent change in electrical resistance for samples during cyclic fatigue at temperature was higher compared to that at RT and 50 °C. It is believed that up to temperatures of 100 °C the internal stresses are enhanced in the coating because of a thermal expansion coefficient mismatch between the polymer substrate and thin film. Therefore, a combination of the applied external stress with internal stresses accelerates crack initiation and propagation and then leads to an increment in electrical resistance. Open cracking observed during twisting fatigue at 100 °C promoted oxidation of the Ag layer and is associated with high electrical resistance modulation.

Moreover, CLSM image showed that no crack appeared in ITO/Ag-alloy/ITO film after exposing to (RT, 50 °C and 100 °C) in the absence of cyclic twisting, which confirms the results obtained from the electrical resistance measurement.

7. Electromechanical reliability of multilayer films under harsh environmental conditions

7.1. Introduction

ITO/Ag-alloy/ITO coated polymer film is widely used as a transparent conductive electrode in many flexible electronic devices such as OLED, FPDs and photovoltaic solar cells. However, during roll- roll manufacturing processes, these electronic devices are susceptible to thermal loading combined with mechanical bending when film bends around different rolls, which can cause thin film failure as reported by Yang *et al*. [208]. In addition, during utilization of flexible electronic devices such as solar cells, they are bent around the surface that the device is laid on and can be in service in hot and humid climates for extended periods in the summer time such as deserts, which can lead to cracks in the conductive thin film and a corroded Ag layer ultimately leading to degradation of the module performance. Furthermore, the surrounding atmosphere where the flexible solar cells are sometimes used such as marine environments are rich with chlorine. Also, photolithographic patterning processes for thin films in the fabrication of electronic displays devices such as LCDs can be achieved by wet chemical etching in solutions such as HCl solutions [86] using roll-to-roll etching machines comprising incorporating etching baths [209]. The residual Cl^- after the etching processes using HCL (described above) can cause degradation of functional properties.

It is well known that chlorine deteriorates Ag-based film, therefore the electrical and optical properties of ITO/Ag-alloy/ITO film in NaCl corrosive media are investigated in this chapter. Also the effects of bending fatigue combined with aggressive environments provided by salt are studied.

So far, very little research has been done on the long term bending of transparent conductive oxide thin in various environments including temperature and humidity conditions. Therefore, in the final section in this chapter, the bending behaviour of ITO/Ag-alloy/ITO film over time under different temperature and humidity conditions was also investigated in this work. Investigation of the optical and electromechanical behaviour of multilayered films of Ag-alloy based ITO under harsh environmental condition will thus provide manufacturers important information about long-term durability.

7.2. *In situ* bending test with confocal laser scanning microscopy investigation

The controlled buckling or bending test of ITO/Ag-alloy/ITO film was conducted with the same a Fiber Sigma 2-point bend tester machine that was used in the buckling test of IGZO (

Figure 3-7). However, to enable simultaneous measurement of the change in electrical resistance *in situ*, thin polymer sheets were placed between the metal plate and the moveable arm of the machine and polymer screws were utilized to attached them together. The samples were clamped in place between two plates and the compression load was applied with the crosshead speed set at 0.5 mm/min. The compression loading was stepwise so that an image could be recorded from the surface of the ITO/Ag-alloy/ITO at each loading step during a three-minute holding period. Also, the change in electrical resistance was measured after each loading step. This test was performed in order to obtain the critical radius of curvature, at which cracks stared to occur, with a consequent increase in electrical resistance. The results from this section can provide the appropriate diameters of the mandrel and radius of curvature to

be used in the bending fatigue and long term bending experiments. Critical onset radius of curvature of coating failure (Cr-M) was measured by optical microscopy compared to the critical onset radius of curvature evaluated from the electrical resistance measurements (Cr-R), using the same 10% increment in electrical resistance criteria as in the twisting tests. Figure 7-1 displays a series of 'snap shots' of the surface of the ITO/Ag-alloy/ITO to demonstrate the development of cracks in the film as the bending load increases. It is clear to see that at a large radius of curvature (eg 8 mm, Figure 7-1 (a)), there were no signs of cracks in the surface. However, at Cr-M of 4.7 ± 0.1 mm cracks started to initiate from surface imperfections similar to the ITO/Ag-alloy/ITO sample under twisting load. As the radius of curvature decreases more cracks were observed and propagated across the width of the sample and perpendicular to the loading direction. Below approximately 3.1 mm radius curvature which corresponds to strain of 1.98%, no further development of cracks was detected. This is because plastic flow locally within the substrate will result in reduction of stress transfer to the coating segment in a similar manner to that in tensile and twisting tests.

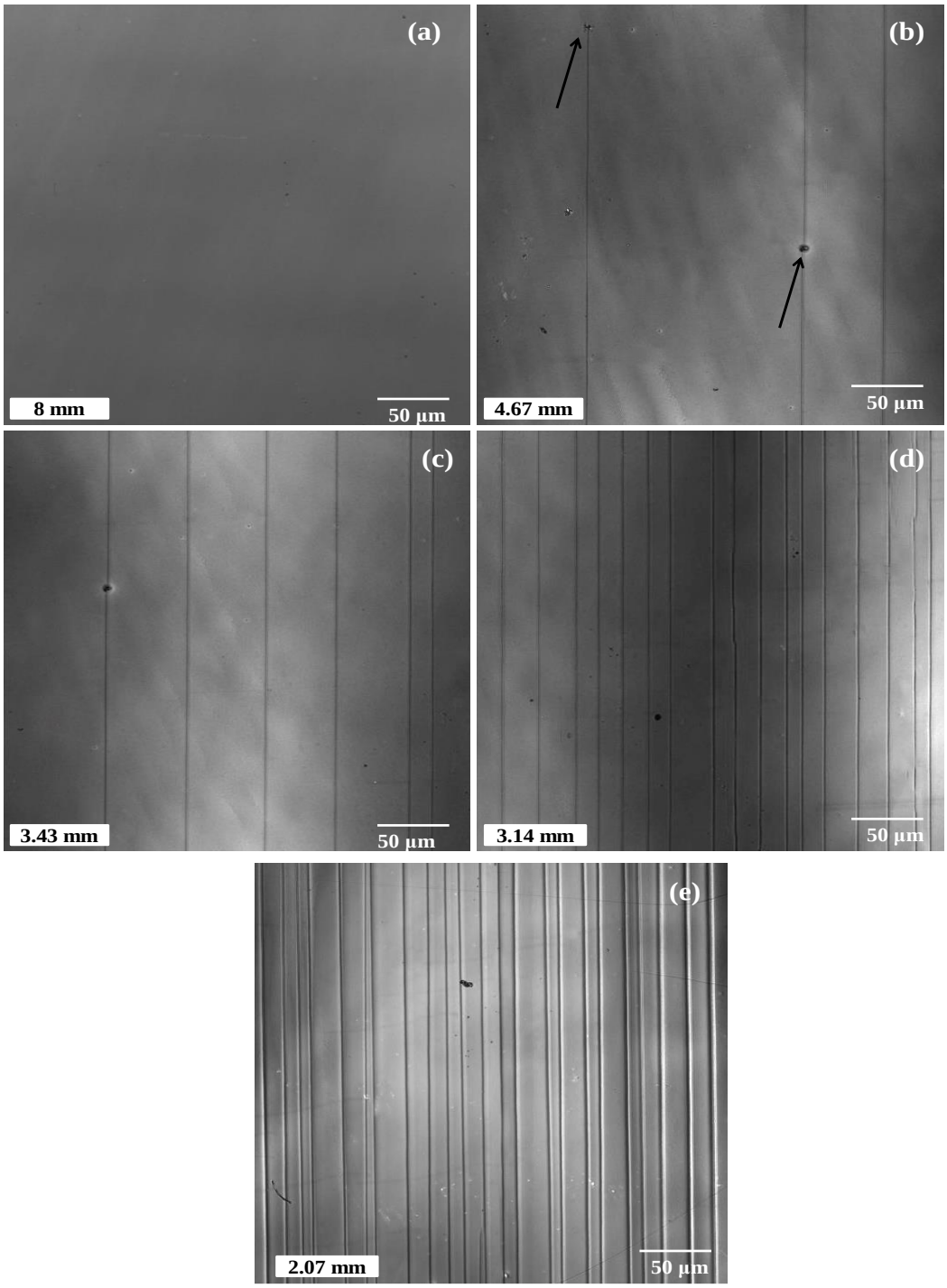

Figure 7-1 CLSM images of surface of ITO/Ag-alloy/ITO on PET taken *in situ* at different applied bending curvatures.

Figure 7-2 a and b show the change in electrical resistance and CD as a function of radius of curvature and strain of the ITO/Ag-alloy/ITO deposited PET. Initially, no increase in electrical resistance was observed, and thus no crack was investigated at the relatively high radii of curvature corresponding to low strains. Once the crack started to occur, the electrical resistance begins to increase at Cr-R equal to 4.6 ± 0.1 mm (corresponding to strain of 1.35 ± 0.02 %) and the crack density initially increases significantly as the radius of bending curvature decreases and then as radius of curvature approaches 3.1 mm corresponding to a bending strain of 1.98% the crack density gradually saturates at about 62.7 mm^{-1}.

It is interesting to note that the electrical resistance of the ITO/Ag-alloy/ITO remains conductive even after the crack spans across the whole width of the sample. It is likely that this is because the cracks have not fully developed through the whole thickness of the multilayer films and thus ITO/Ag-alloy/ITO thin film is not completely fragmentized. This can be explained by the fact that the mechanical damage of the multilayer structure of ITO/Ag-alloy/ITO starts to appear in the form of cracks in the ITO top layer while the presence of a high ductility Ag metal layer in the composite film can possible bridge cracks produced in the top layer, so these can still provide the conductivity required as the electrical resistance can flow through these bridges. This is in good agreement with work of Wang *et al*. [210] who reported that maintaining the electrical conductivity of composite thin film is a result of the cracks created in the other metal layers being bridged by a discontinuous layer of high ductility indium islands. Also, it has been reported by Lewis et al. [71] that the inserted Ag metal layer between two layers of ITO thin film can remain electrically conductive even after the ITO stretches beyond its failure strain (~0.8%). This can be attributed to the presence of a ductile Ag layer with a high failure strain which is in the range of 4 to 50% strain. However, at the saturation point and above, the film lost its conductivity completely and the

electrical resistance exceeds the meter's range. This is due to the fully developed channel crack which in turn causes large original cracks to open and be more visible as shown by thicker and sharper crack lines in Figure 7-1 (e). The critical bending radius of curvature of the cracks generated was found to be in good agreement with the critical bending radius of curvature at which the conductivity property degrades. This is because the transport path of the free carriers within the film is affected when the transparent conductive film begins to crack, which results in further deterioration of the conductive properties of the film.

Lan *et al*. [18] investigated the static mechanical bending of ITO (200 nm) coated on PET. They observed that the rapid increase in the electrical resistant occurs at bending radius of curvature equal to 17mm. The work done by Shao *et al*. [191] on ITO coated PET substrates also focused on the film's bending properties and reliability at different values of tensile bending curvature. They showed that for 200 nm thick ITO film, the critical radius of curvature was 15.9 mm, which is almost three times higher compared with that observed for the ITO/Ag-alloy/ITO multilayer in this study. This is due to the mechanical ductility of the inserted Ag layer between the ITO layers.

Table 7.1 Summarises the results of bending tests of the ITO/Ag-alloy/ITO/PET system

Sample	Critical radius of curvature Cr-M (mm)	COS-M	Critical radius of curvature Cr-R (mm), ($\Delta R/R_o$= 10 %)	COS-R ($\Delta R/R_o$= 10 %)
ITO/Ag alloy/ITO	4.7± 0.1	1.3 ±0.016	4.6 ± 0.1	1.35 ± 0.02

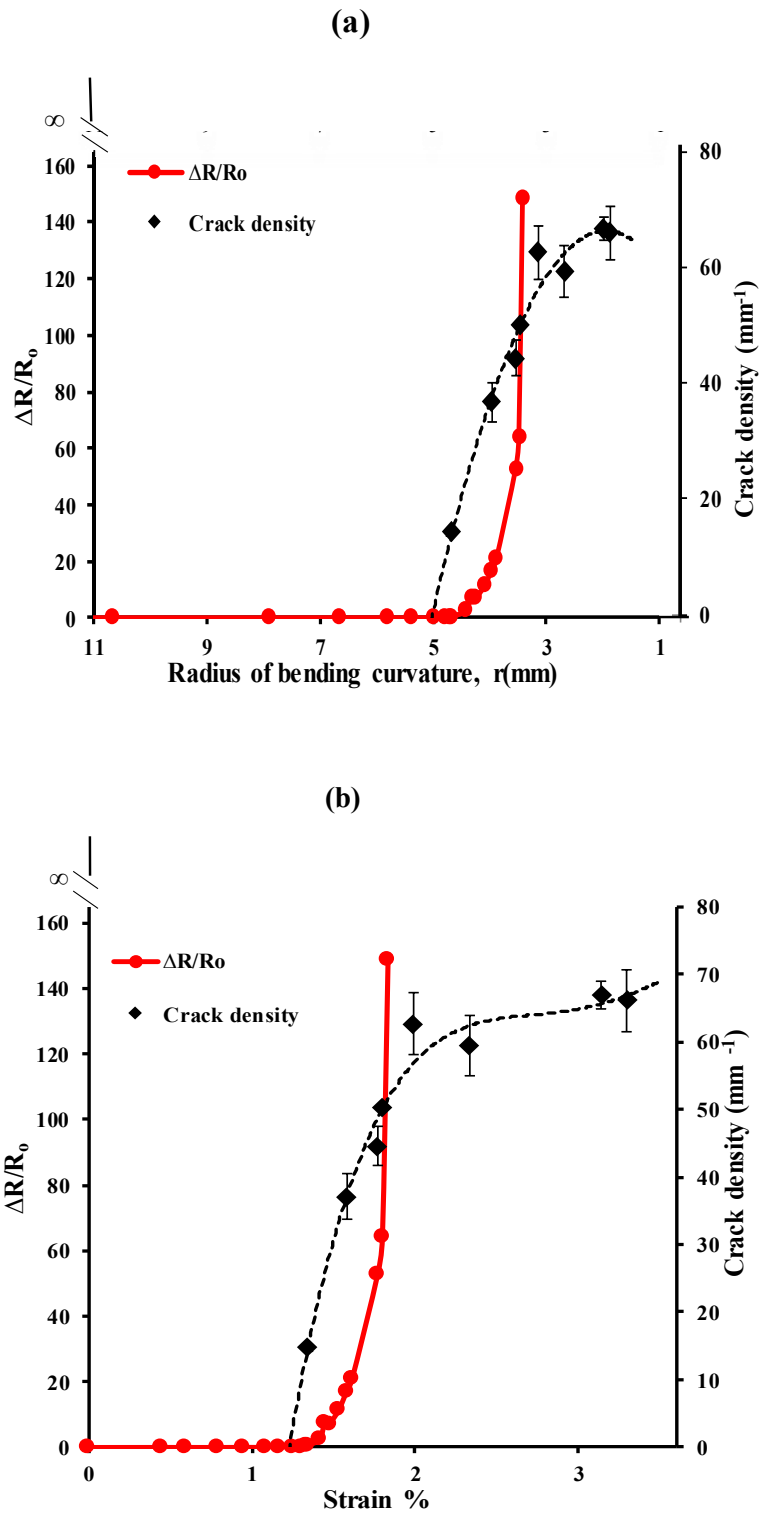

Figure 7-2 Increment in electrical resistance and crack density as a function of (a) radius of bending curvature (b) applied strain of ITO/Ag-alloy/ITO thin film coated PET substrate.

7.3. Corrosive Degradation of ITO/Ag-alloy/ITO

In this experiment the impact of aggressive salt environments on ITO/Ag-alloy/ITO films strips was investigated. The specimens were cleaned by distilled water and dried by compressed air then were put into a bath of 0.3 M, 0.5 M, 1 M, 2 M, and 3 M of NaCl solution for 16,000 seconds (4.4 hours) and 57,600 seconds (16 hours) and the electrical resistance was monitored *in situ* in order to assess the reliability of the conductive films. This is because the increment in electrical resistance can be associated with corrosion of the ITO/Ag-alloy/ITO films when immersed in NaCl solution. After the testing time the specimen was washed by distilled water and dried using compressed air. In order to observe the surface morphology, CLSM and SEM were employed. Composition information on the films was obtained from EDS. AFM has also been utilized to provide further information about surface morphology. Lastly, the spectral transmittances of the ITO/Ag-alloy/ITO films were examined using a spectrophotometer.

Figure 7-3 shows the normalized change in electrical resistance over time of the ITO/Ag-alloy/ITO films immersed in different concentrations of NaCl. For the purposes of comparison, also reported in Figure 7-3 is the normalized change in electrical resistance for 57,600 second of the as received ITO–Ag–ITO thin film. The results obtained from this investigation demonstrated that when ITO/Ag-alloy/ITO film is exposed to NaCl, over time, a loss of the function of the film will suffice which may be due to agglomeration of Ag.

For the 0.3 M and 0.5 M samples, the percent increase in electrical resistance is still close to zero until around 15,000 seconds of experimental testing and then an increase in electrical resistance is noticed. After 57,600 seconds the change in electrical resistance was 31.4% for 0.3 M and 35.2 for 0.5M, as shown in Figure 7-4. For samples immersed in 2 M NaCl, a

higher increase in electrical resistance was shown indicating faster corrosion of the ITO/Ag-alloy/ITO films as compared to the sample immersed in lower NaCl concentrations such as 0.3, 0.5 and 1 M NaCl. After 57,600 seconds ~60.7% resistance increase is observed (see Figure 7-4). The electrical resistance trace of ITO/Ag-alloy/ITO when exposed to the 3 M NaCl shows that a higher concentration of NaCl makes a ITO/Ag-alloy/ITO coating susceptible to more rapid corrosion. After 57,600 seconds of experimental testing the change in electrical resistance is observed to be ~149.5%, as shown in Figure 7-4. The gradient of the line continues to increase after the test has ended, and it was then suggested that if it was left to run for longer period of time; the ITO/Ag-alloy/ITO film would experience corrosion to the extent that it would lose all its conductivity.

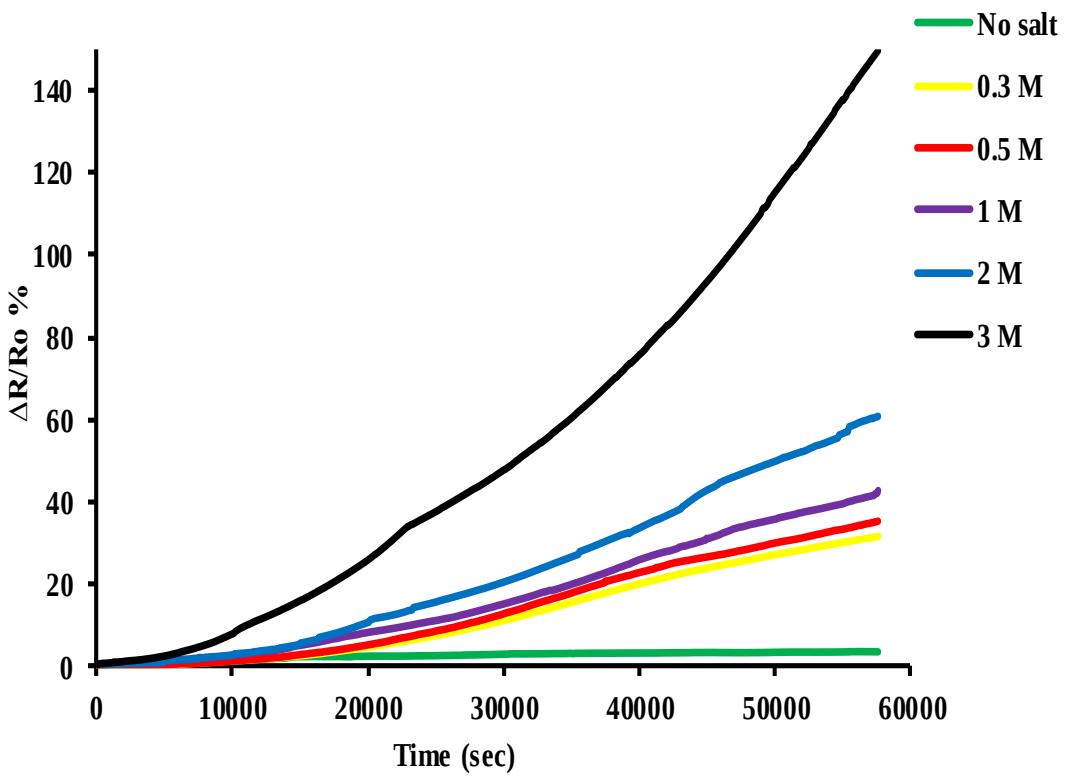

Figure 7-3 Normalised electrical resistance versus time for ITO/Ag-alloy/ITO film in different NaCl concentrations.

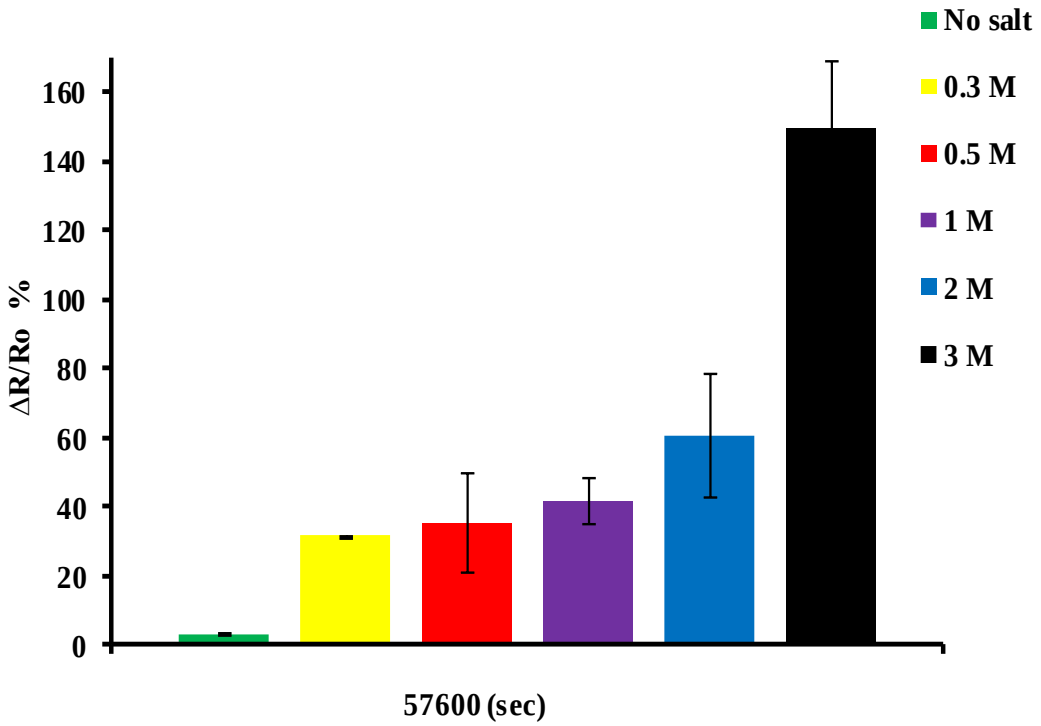

Figure 7-4 The effect of various concentrations on normalised electrical resistance of ITO/Ag–alloy/ITO film after 57,600 seconds.

Figure 7-5 displays the progressive morphological degradation for ITO/Ag-alloy/ITO immersed in NaCl of various concentrations for 16,000 and 57,600 seconds. Regardless of the amount of NaCl, ITO/Ag-alloy/ITO surfaces submerged for 57,600 seconds were observed to be more severely corroded than those for 16,000 seconds with many circular white corrosion spots. The sizes of corrosion spots after 57,600 seconds immersion were also larger than those after the 16,000 seconds immersed. Although there were some small spots, the general trend can be determined that the size of white corrosion spots increased with an increase of submersion time for all solutions. The samples immersed in 0.3 M were degraded, showing a number of white spots. By comparison with samples immersed in 0.5, 1, 2, 3 M these were less degraded, although they had a number of white spots in places. Samples immersed in 3 M were more degraded in comparison to the samples immersed in 0.3, 0.5, 1, 2 M solutions and high number of corrosion spots was observed over almost the whole surface of the sample.

These observations agree with results in term of the electrical resistance changes over time obtained for all concentrations.

(a)

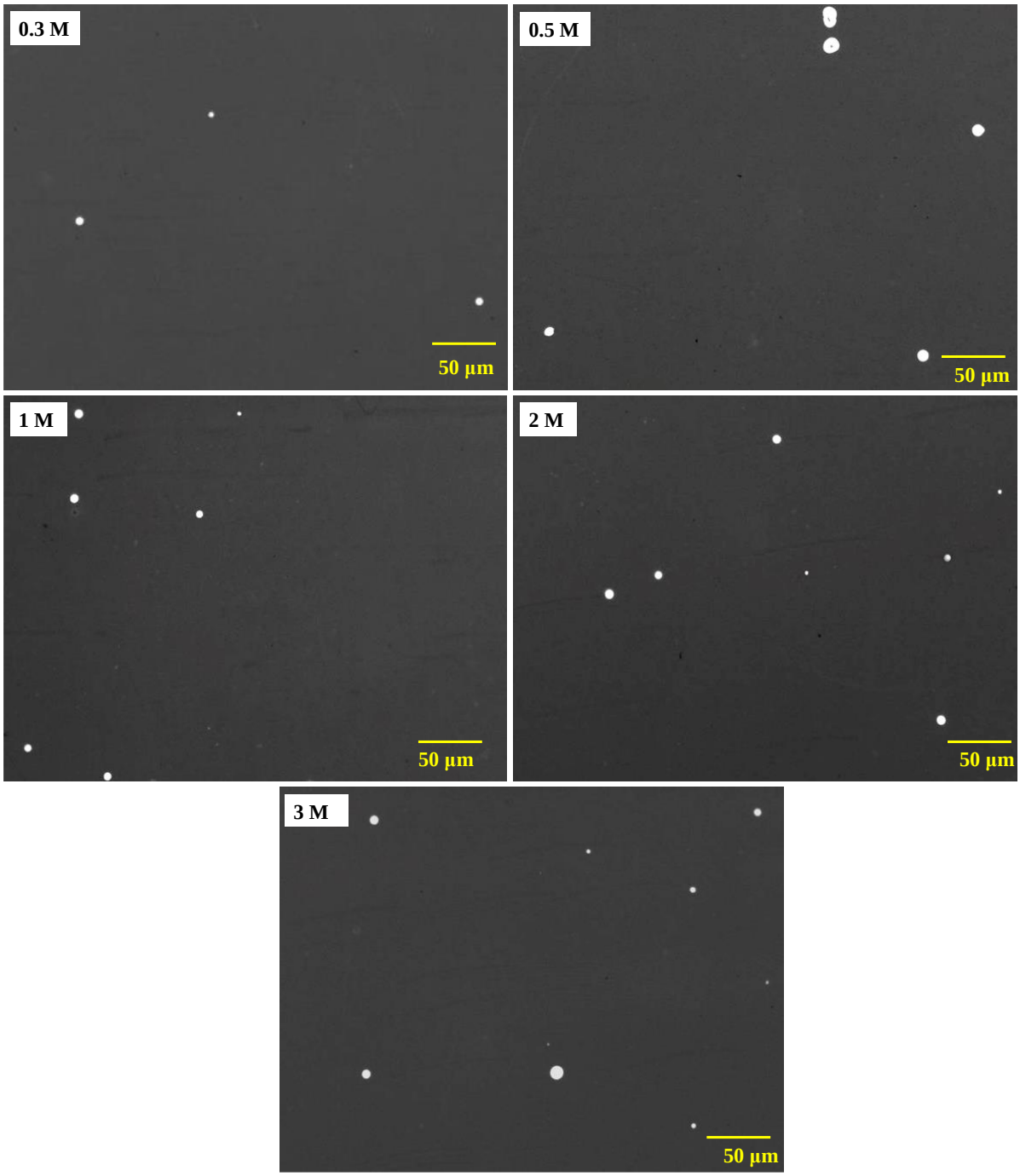

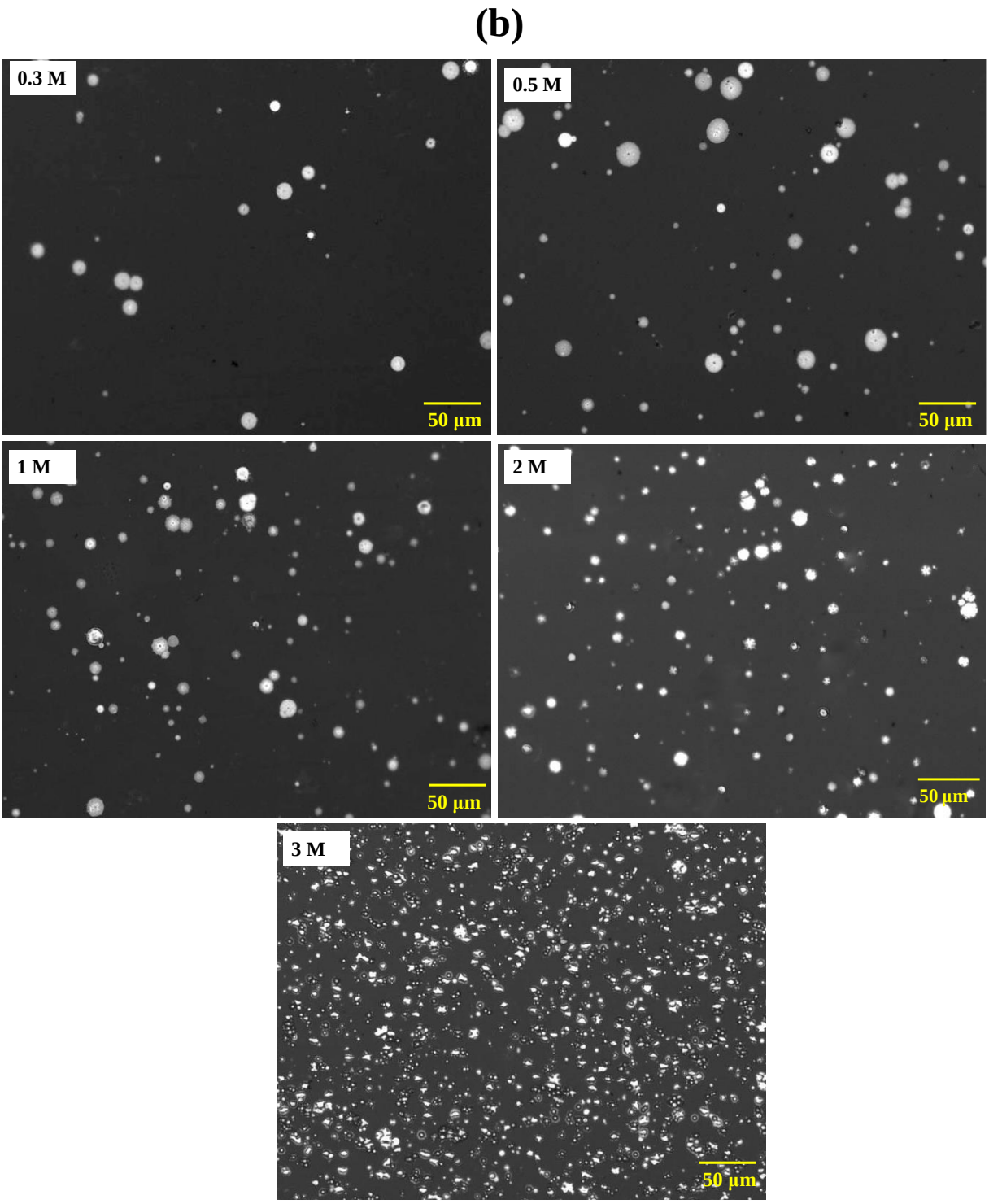

Figure 7-5 Confocal scanning microscopy images of the surface of ITO/Ag-alloy/ITO immersed in NaCl of various concentrations for (a) 16,000 seconds and (b) 57,600 seconds.

Previous studies have [131] considered that the chlorine ions (Cl^-) attacked the ITO surface, passed through the top ITO layer and reached the silver layer then the silver atoms aggregate around the chlorine atoms and form as the white clusters. Besides that, the pre-existing defects and scratches on the surface resulting from the deposition process and handling were found to serve as a point to nucleate the corrosion products or (Ag agglomerations) which appear as white areas on the CLSM image presented in Figure 7.6. Defects and scratches in the layer are believed to facilitate the movement of chlorine ion Cl^- to reach the silver layer and enhance the agglomeration of Ag.

Apart from chlorine ion Cl^- penetration through permeable defects or scratches on the coating, Cl^- ions could also penetrate by small cracks opening from the edges after sample cutting, also giving a highly hazy appearance as seen in Figure 7-7. This implies that during the cutting of specimens or fabricating of patterned electrodes in the photolithography process care must be taken to enhance edge fidelity and to avoid edge-generated micro-cracks. This will diminish corrosion spots at the edges.

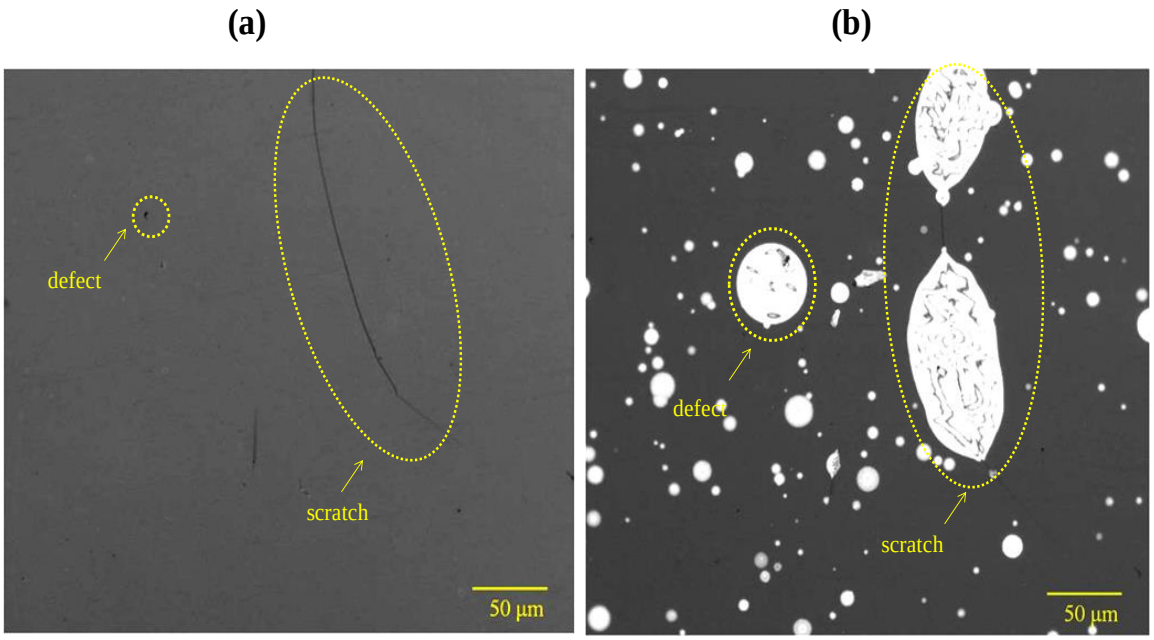

Figure 7-6 Confocal scanning microscopy images showing the coating defects and scratches on the surface of ITO/Ag-alloy/ITO surface (a) before and (b) after immersion tests in 0.5 M for 57,600 seconds.

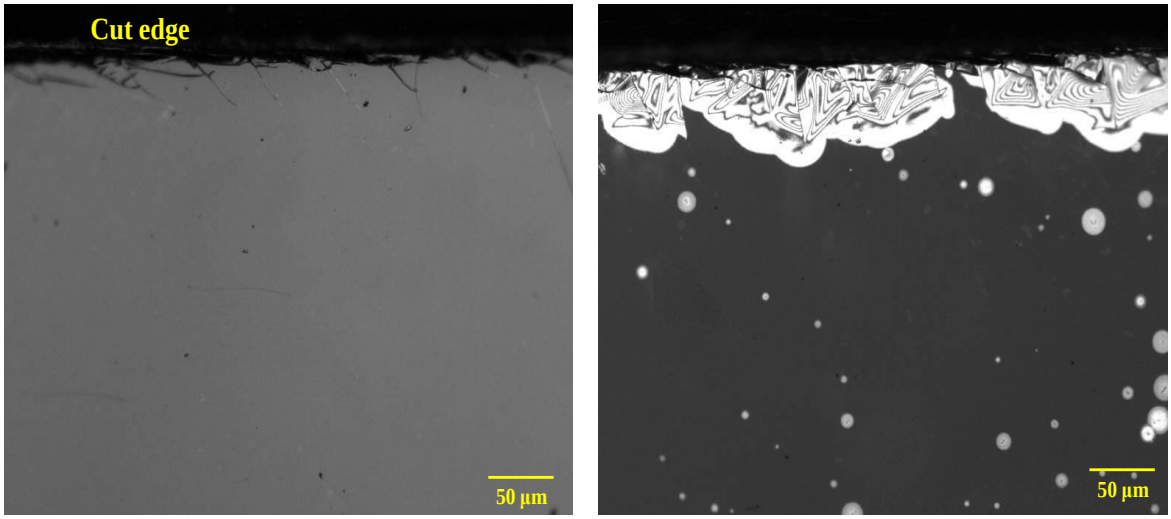

Figure 7-7 Confocal scanning microscopy images showing the edge defects initiated upon cutting of ITO/Ag-alloy/ITO (a) before and (b) after immersion tests in 0.5 M for 57,600 seconds.

Furthermore, the samples after immersion in 3M for 57600 seconds were investigated by using the EDS technique in order to investigate the corrosion product elements in ITO/Ag-alloy/ITO film. EDS spot scan analysis of surface failures and elemental mapping analysis as shown in Figure 7-8 and Figure 7-9 respectively obtained the following results: (1) The bright particles labelled A in the centre of the image, are large features that clustered in the centre of the circular shape are Ag-rich as the Ag X-ray intensity was higher than any other detectable elements apart from the peak belonging to Au that is used for SEM preparation of the sample. Along the circular edge of the area labelled B there are periodic agglomerations that are rich with Ag content as well. (2) Spectra that correspond to the area labelled B indicate a lack of Ag element and the presence of the elements from the ITO layer. (3) In all areas of the sample no removal of indium and tin was detectable; in other words the Sn/In ratio of the ITO film at damage spot area (A) is ~0.044 which is almost similar to that in the unaffected area labelled c suggesting that both top and bottom ITO layers have not been removed. Eight other damage spots from Figure 7-8 (a) have been examined and yielded similar results to those for the damage spots depicted in Figure 7-8 (b), (c) and (d). In addition, carbon and oxygen also appeared in the scan due to the PET substrate. An additional tiny amount of copper (Cu), was found in Figure 7-8 (b) and (d). The presence of this tiny amount came from the Ag alloy.

These small amounts of Cu were observed to agglomerate similar to observations in Ag, as shown in Figure 7-8(b),(c) and (d). The Cu content in the A region is 0.93 ± 39 and is higher than that of other regions. It is suggested that the white spot or agglomeration would not disappear by adding Cu metallic element alone due to the chemical instability of Cu [211]. It has been reported in [211] that an increase in thermal stability was noted when Cu with Pd

were added to the Ag alloy layer and as result the durability of the Ag alloy thin film was enhanced.

(a)

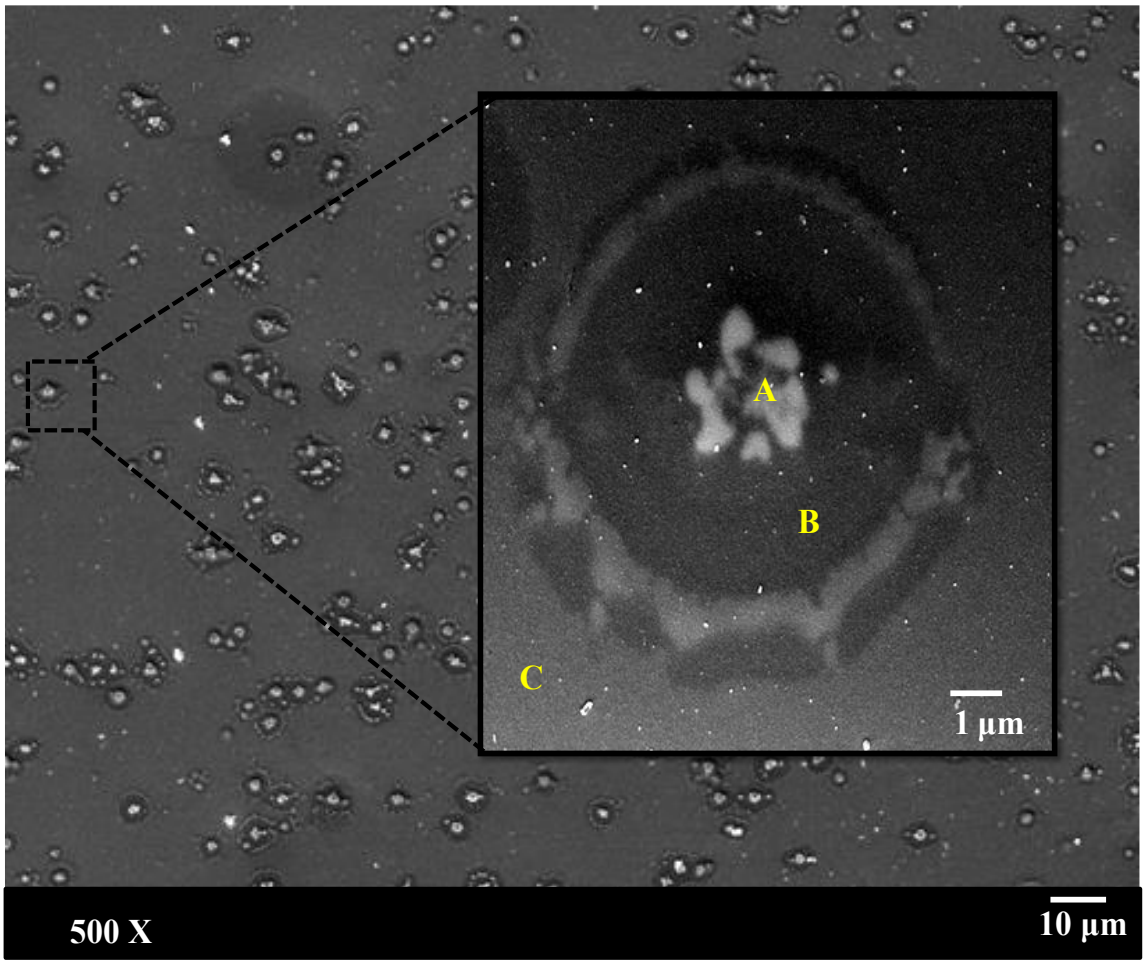

(b)

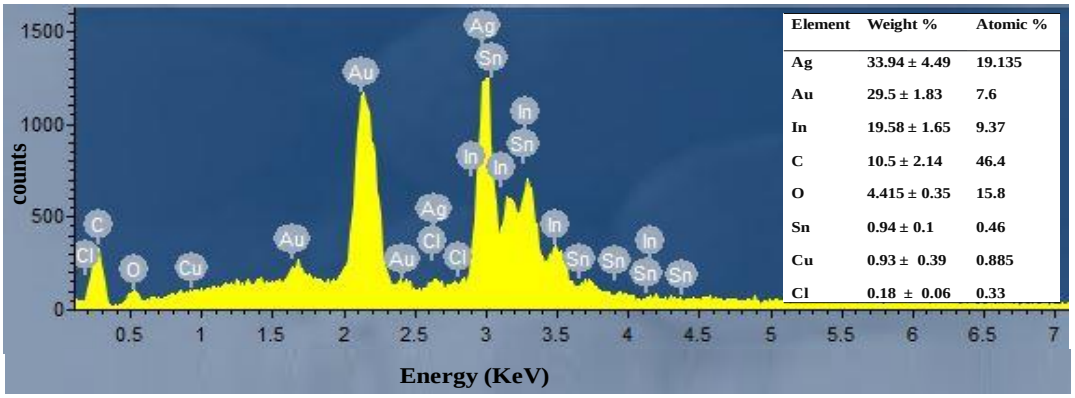

Element	Weight %	Atomic %
Ag	33.94 ± 4.49	19.135
Au	29.5 ± 1.83	7.6
In	19.58 ± 1.65	9.37
C	10.5 ± 2.14	46.4
O	4.415 ± 0.35	15.8
Sn	0.94 ± 0.1	0.46
Cu	0.93 ± 0.39	0.885
Cl	0.18 ± 0.06	0.33

(c)

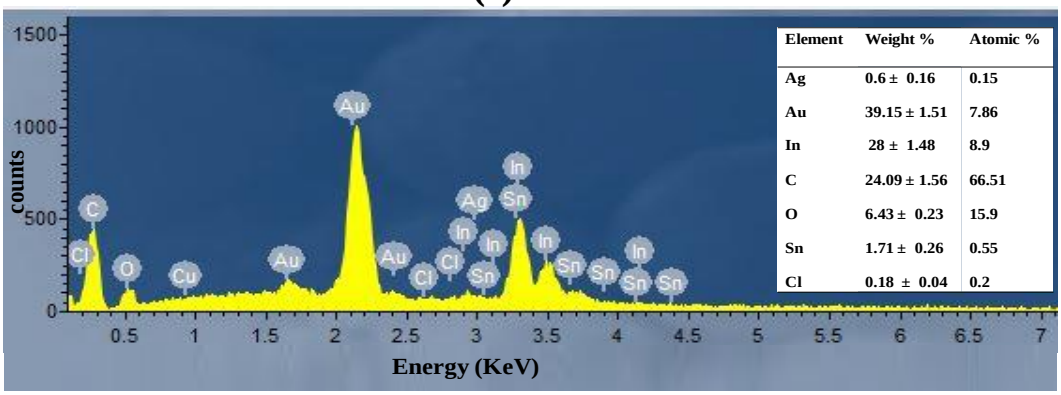

Element	Weight %	Atomic %
Ag	0.6 ± 0.16	0.15
Au	39.15 ± 1.51	7.86
In	28 ± 1.48	8.9
C	24.09 ± 1.56	66.51
O	6.43 ± 0.23	15.9
Sn	1.71 ± 0.26	0.55
Cl	0.18 ± 0.04	0.2

(d)

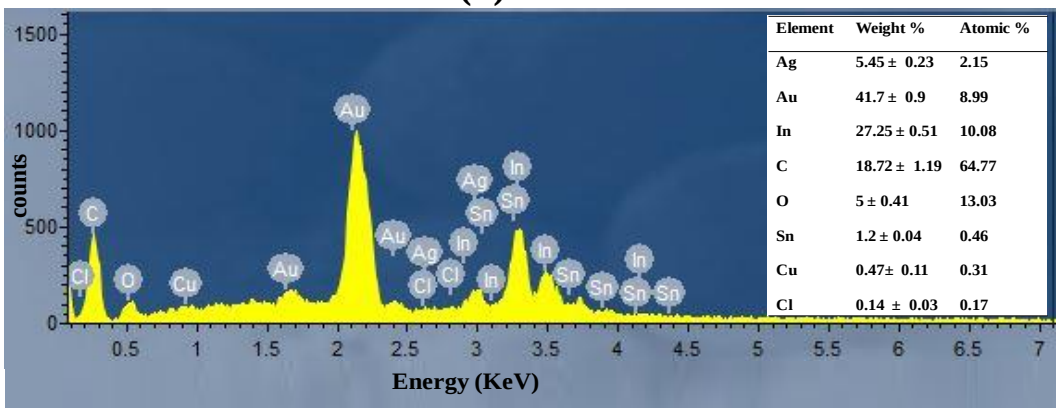

Element	Weight %	Atomic %
Ag	5.45 ± 0.23	2.15
Au	41.7 ± 0.9	8.99
In	27.25 ± 0.51	10.08
C	18.72 ± 1.19	64.77
O	5 ± 0.41	13.03
Sn	1.2 ± 0.04	0.46
Cu	0.47± 0.11	0.31
Cl	0.14 ± 0.03	0.17

Figure 7-8 (a)SEM micrographs of surface of ITO/Ag-alloy/ITO immersed in 3M NaCl for 57,600 seconds (b), (c) and (d) corresponding EDS spectra obtained in signed (A), (B) and (C) areas respectively. Inset is the table showing the percentage of each component in the film.

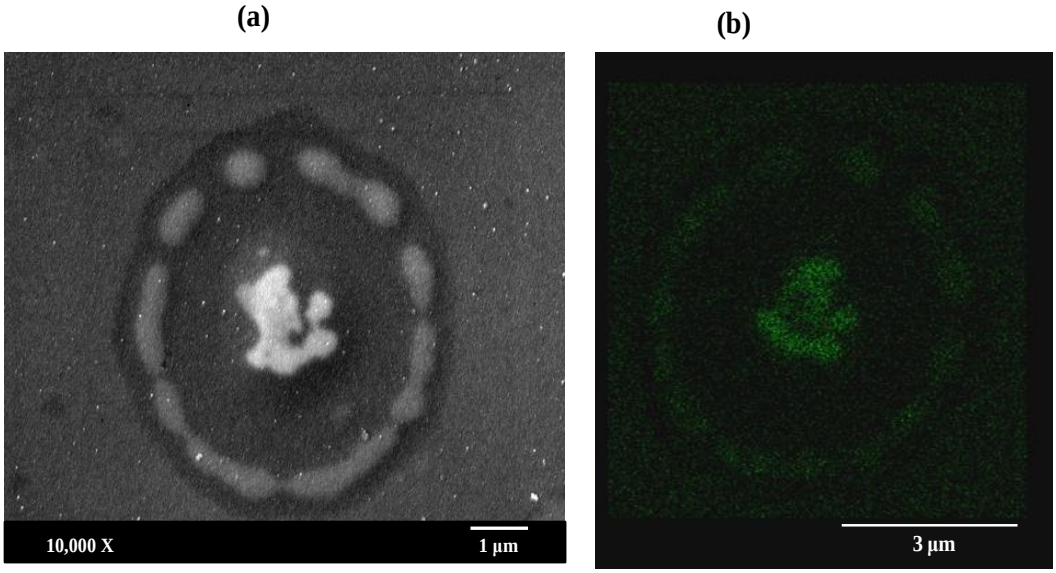

Figure 7-9 (a) SEM micrographs showing surface of ITO/Ag-alloy/ITO films after 57,600 seconds submerged in 3M of NaCl (b) EDS mapping images of Ag.

The samples submerged in 0.3M and 3 M NaCl for 57,600 seconds were also subject to atomic force microscopy (AFM) to characterize the corrosion spot behaviour of ITO/Ag-alloy/ITO film. As the 3D–AFM micrographs shown in Figure 7-10 (a) demonstrate for a sample which had been immersed in 0.3M solution, the damage area consists primarily of circular blisters that appear to be in folds in the top ITO layer. The Ag layer was clustered and its clustering or agglomeration was clearly seen all over the damaged area even though the agglomeration of the Ag film is thick at the centre, and the height of the agglomeration at the centre area is about 175 nm, as the cross–sectional AFM micrograph shows in Figure 7-10 (b). This indicates that the Ag agglomerations appear to be mobile once they are formed. However, when a sample is exposed to 3 M solution, most of the Ag has agglomerated at the centre point of the circle with height around 80 nm with some of it along the circumference with height almost equal to 15 nm, as shown in Figure 7-10 (b). Furthermore, it is clear from Figure 7-10 (b) and Figure 7-11(b) that the spot size decreases significantly with increasing

solution concentration, as approximately 37 μm and 9 μm spot diameters were observed for 0.3 M and 3 M respectively. This is because the diluted solutions are not able to be sustained, allowing growth into the spot region to continue whereas thicker solution layers remain enough to allow only deeper attack in small spot region.

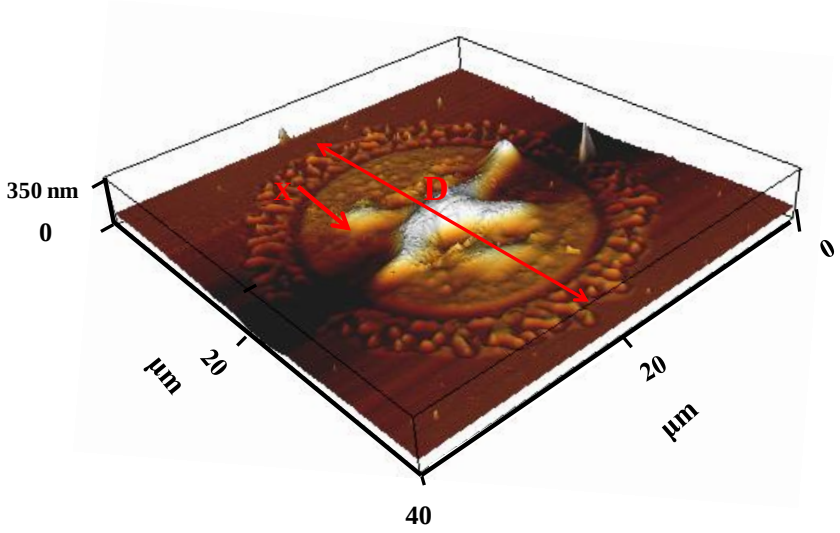

(a)

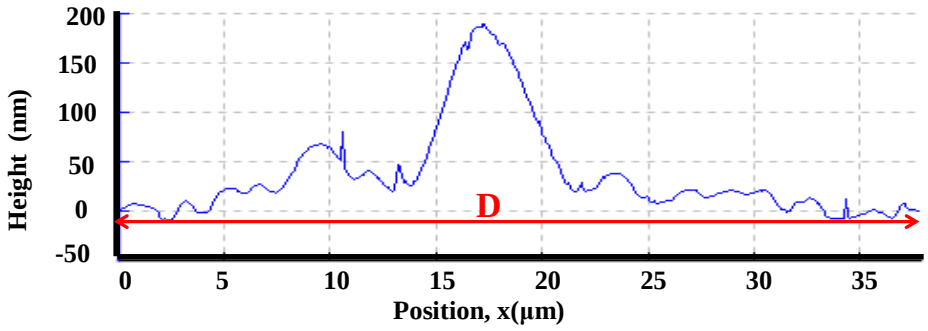

(b)

Figure 7-10 (a) 3D AFM image (b) corresponding extracted height profile scanned across the profile line for ITO/Ag- alloy/ITO films sample submerged in 0.3M for 57,600 seconds consisting damage area. Red line and red arrow in (a) indicate the position of the extracted profile and x-direction.

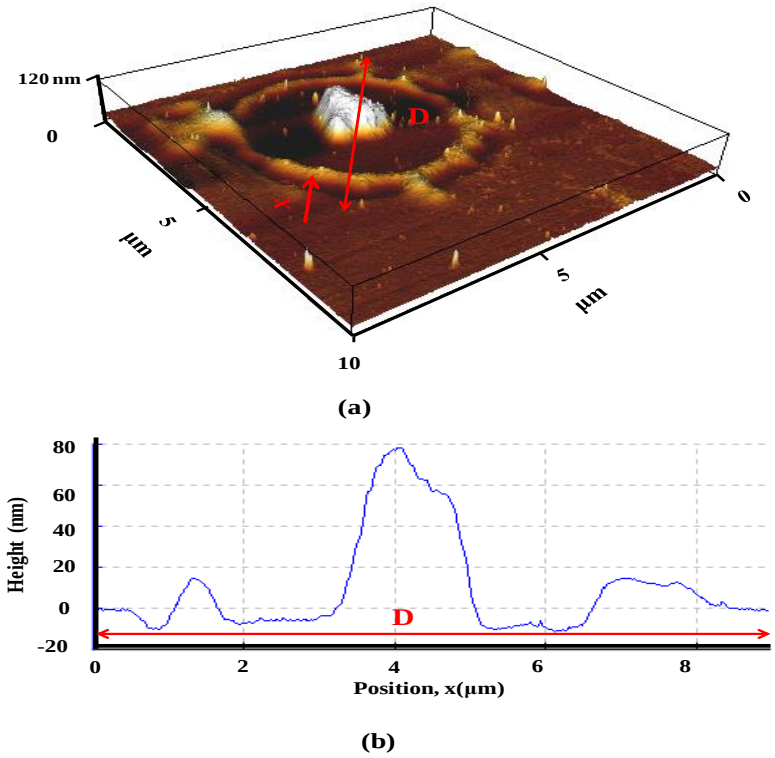

Figure 7-11 (a) 3D AFM image (b) corresponding extracted height profile scanned across the profile line for ITO/Ag-alloy/ITO films sample submerged in 3 M for 57,600 seconds consisting damage area. Red line and red arrow in (a) indicate the position of the extracted profile and x-direction.

Figure 7-12 plots the transmittance curves of ITO/Ag-alloy/ITO films immersed in various concentrations of NaCl for 57,600 seconds. For comparison, the transmittance of the as received (no salt) ITO/Ag–alloy/TO thin film is also presented in Figure 7-12. It can be seen as a general trend that the transmittance of ITO/Ag-alloy/ITO films after being submerged in NaCl solution was lower in comparison with that of the as-received ITO/Ag-alloy/ITO film. In particular, the transmittance of the ITO/Ag–alloy/ITO significantly decreased over all wavelengths after being immersed in 3M NaCl. This is due to the existence of several corrosion spots (Ag agglomeration) on the surface which cause surface roughening, and result

in an increase in the scattering of incident light [67]. Similar observations have also been reported by Sahu *et al*. [212] on Ag films exposed to 200 °C for 30 min. They attributed the decrease in transmittance of Ag film to the agglomeration of silver, and consequently enhanced scattering of light. These results are also consistent with those observed previously by Koike *et al*. [213].They found that the electrical sheet resistance was significantly increased and the transmittance was significantly decreased in the multilayer sputter coated ITO (40 nm)/Ag (10 nm)/ITO (40 nm)/glass during a 22 h salt water immersion test.

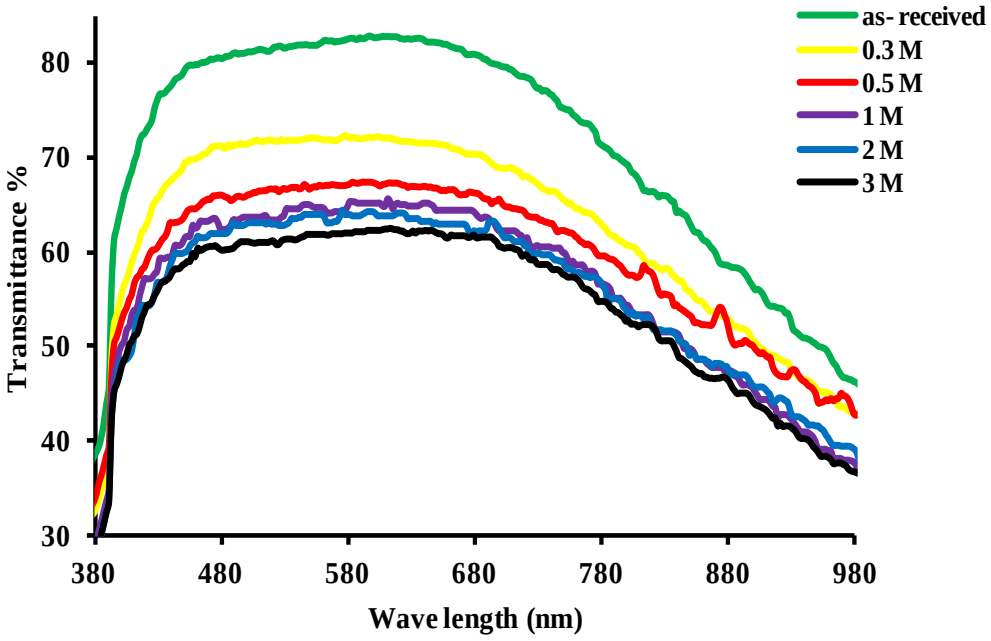

Figure 7-12 Measured optical transmittance of the flexible ITO/Ag-alloy/ITO films as a function of the NaCl concentration.

7.4. Combined corrosion and fatigue degradation of ITO/Ag-alloy/ITO

To investigate the effect of repeated loading on the structural integrity of ITO/Ag-alloy/ITO coated PET substrates under fatigue and fatigue–corrosion tests, the electrical resistance

changes were recorded *in situ*. The tests were run at a frequency of 2 Hz. A frequency any lower would take a long time to complete a higher numbers of cycles and any higher values would not be relevant to the roll-to-roll manufacturing process and in-service conditions. The combined fatigue–corrosion experiment was performed in 0.3 M NaCl since the time to corrode ITO/Ag-alloy/ITO is adequate to allow meaningful observations to be made. Using data from the bending tests; a mandrel diameter equal to 25 mm which is equivalent to a strain of 0.5% was selected for fatigue tests.

Figure 7-13 shows the percentage increase in electrical resistance as a function of number of cycles under fatigue and fatigue–corrosion. The mechanism of bending fatigue appears to be similar to that observed in the twisting fatigue test, and the observed increase in electrical resistance can be split into two distinct regions. In the first region (region I) the increment in the normalized electrical resistance is associated with the dimensional change of the compliant substrate until an equilibrium size is attained [197]. In the second region (region II), the gradually increasing resistance is likely to be due to cracking of the ITO/Ag-alloy/ITO film.

The mechanism of fatigue–corrosion in region I is not too dissimilar to the fatigue - only case. However, in the region II the high rate of electrical resistance increase was observed, as shown in Figure 7-13. For example, at the same applied strain of 0.5% and 115,200 cycles, the sample under fatigue–corrosion exhibited an increase of resistance of ~ 177% which is significantly higher than that of ~ 3.4% for the sample under fatigue only. Such phenomena may be attributed to the combined action of cracking and corrosion, since the contribution of corrosion to increase electrical resistance is significant.

Bejitual [214] reported that in the bending fatigue tests on a single ITO (200 nm) film coated on a PET substrate, at 150,000 cycles the change in electrical resistance was 50% for 0.6% strain. This means that the ITO/Ag-alloy/ITO film shows superior flexibility in compression to a single ITO layer. This is attributed to the presence of the ductile Ag middle layer. However, direct comparison of fatigue-corrosion (salt immersion) reliability of ITO/Ag-alloy/ITO with single ITO film could not be made due to lack of data available in the literature.

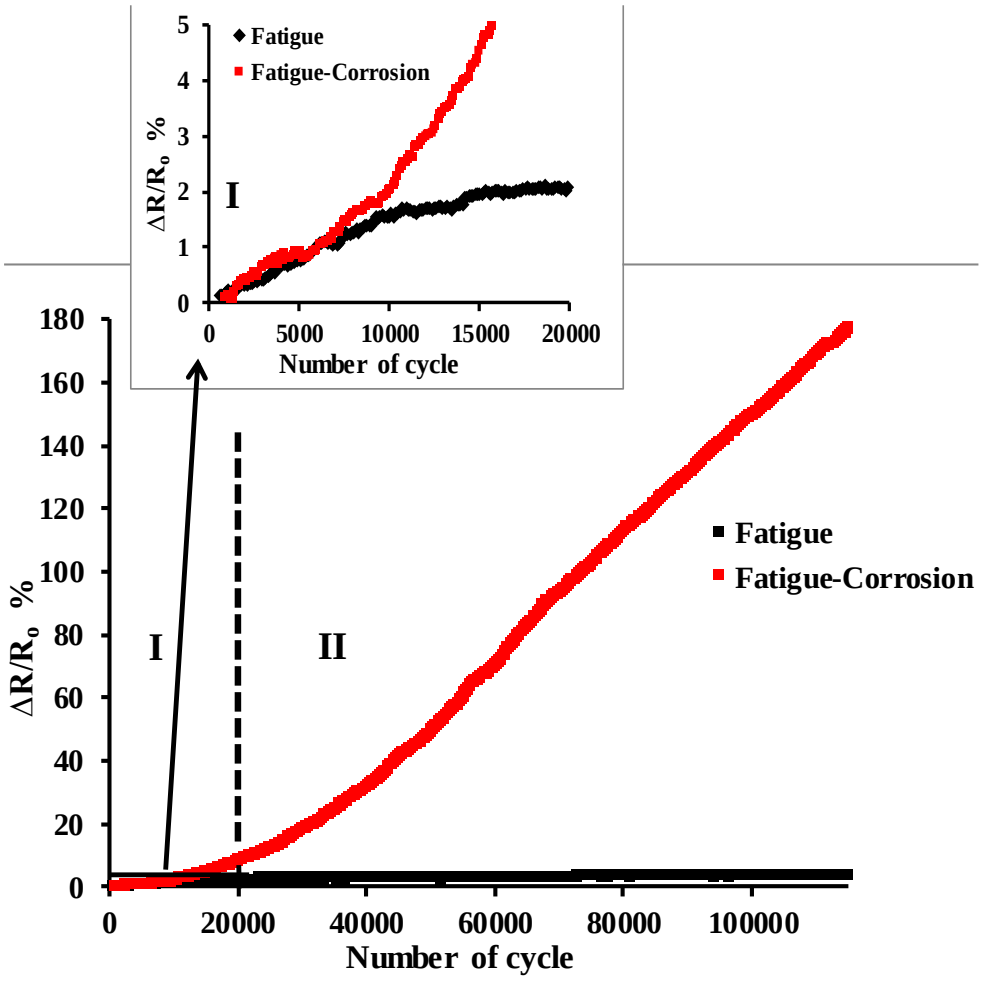

Figure 7-13 Normalized electrical resistance versus number of cycle of ITO/Ag-alloy/ITO under bending fatigue and bending fatigue-corrosion conditions.

Figure 7-14 shows an SEM micrograph of ITO/Ag-alloy/ITO samples after fatigue. Cracking was not observed on the surface of the samples. However, some submicron cracks were probably formed on the ITO/Ag-alloy/ITO film that were associated with a slight increase of electrical resistance with increasing number of cycles. Then upon un-loading the sample, the strain recovery in the polymer results in the closure of cracks and leads them to be not visible [52], in a similar manner to that in twisting fatigue test at low angles. Figure 7-15 presents an SEM image of ITO/Ag-alloy/ITO samples after fatigue–corrosion. No crack was visible; this can be due to the same reason as mentioned above in the fatigue - only case. Ag agglomeration is clearly seen to spread inside the circular spot.

At the portion where circular-blisters existed, destruction such as wrinkles or buckling features were observed. This is because an externally applied mechanical stress which induces stress in thin film combined with mechanical energy (through surface tension and capillary forces) provided by the solution can cause buckling [216].

This suggests that the presence of NaCl solution together with mechanical stress promotes electrical failure. Therefore, the effect of mechanical strain coupled with corrosion must be taken into account in the durability and lifetime prediction of ITO/Ag-alloy/ITO electrodes.

Figure 7-14 SEM images of the surface of the ITO/Ag-alloy/ITO film after the test of fatigue for 115,200 cycles.

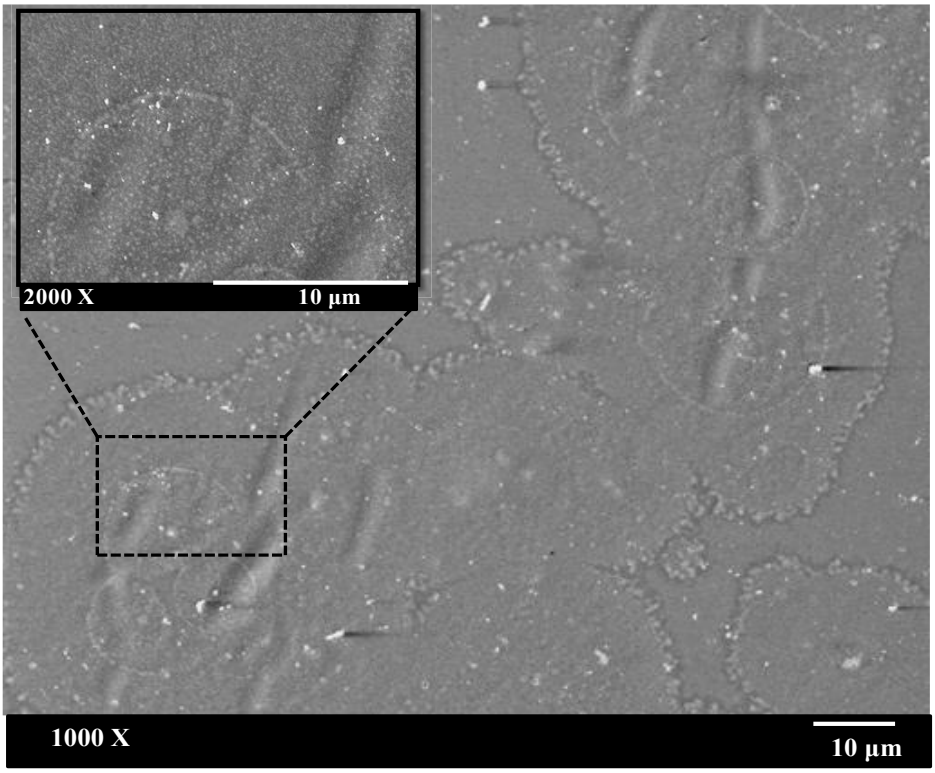

Figure 7-15 SEM images with enlarged images of the surface of the ITO/Ag-alloy/ITO film after fatigue- corrosion for 115,200 cycles.

7.5. Long term bending durability of ITO/Ag-alloy/ITO under different temperature and humidity conditions

In these experiments, ITO/Ag-alloy/ITO films were flexed in tension mode to a certain radius of curvature for 16 hours under different temperature and relative humidity conditions. Based on the data that were achieved from bending tests, two levels of bending radius (6.6 and 4.3 mm) were chosen which is equivalent to strains of 0.94% and 1.44% respectively. In order to

accelerate the failure, two levels of temperature (25, 65 °C) and humidity (25%, 80%) were selected. The maximum value of temperature (65° C) corresponded to the maximum value that our climatic chamber could achieve at a fixed value of humidity of 80%.

The electrical resistance was measured *in situ* under controlled atmospheric (temperature and humidity) conditions. CLSM images were obtained for samples under bending loads before and after exposure to different temperatures and relative humidity (RH) values in order to investigate the surface morphology while SEM images and EDS were only conducted for unloaded samples after the experiments in order to investigate the surface morphology and any change in film composition.

For the initial set of these experiments, the effects of different temperatures and low relative humidity (25% RH) on the electrical resistance of samples flexed to different radius of curvature was examined.

Figure 7-16 shows the relative changes of electrical resistance under a bending curvature of 6.6 mm and held isothermally at 25% humidity. At the very beginning, samples show a sharp decrease in change in electrical resistance and then tends to be more stable after a certain period of time. CLSM images of the surface of bent ITO/Ag-alloy/ITO films held at 25 °C and 65 °C did not show any sign of visible crack after the experiments, as Figure 7-17 shows. This indicates that samples flexed to radius of 6.6 mm over time (which corresponds to a strain of 0.94%), the surface remains undamaged upon exposure to temperature and a drop in the normalized electrical resistance is probably because the atoms rearrange in thin film and tend to get closer, and exposure to high temperature enhances this process and thus the change in electrical resistance of samples held at 65 °C decreases to a slightly greater extent than for the samples held at 25 °C.

The effects of temperature and humidity on the electrical resistance of thin film on polymer substrate under long term bending conditions have not been widely reported in the literature. However, the influence of temperature and relative humidity on unloaded single layer ITO coated PET were discussed by Hamasha [138]. They did not find any signs of cracking on the surface of the film and no increase in normalized electrical resistance was observed at the combination of low temperature of 20 °C and a low relative humidity of 20 %.

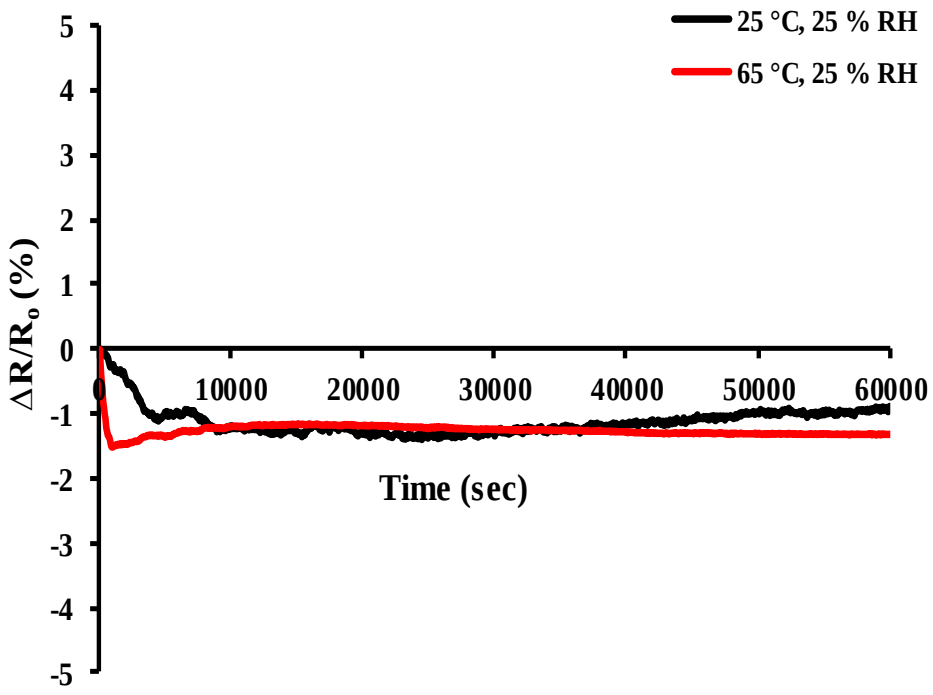

Figure 7-16 Normalized electrical resistance as a function of time for ITO/ Ag-alloy /ITO at two different temperatures and 25% of RH under 0.94% of applied strain.

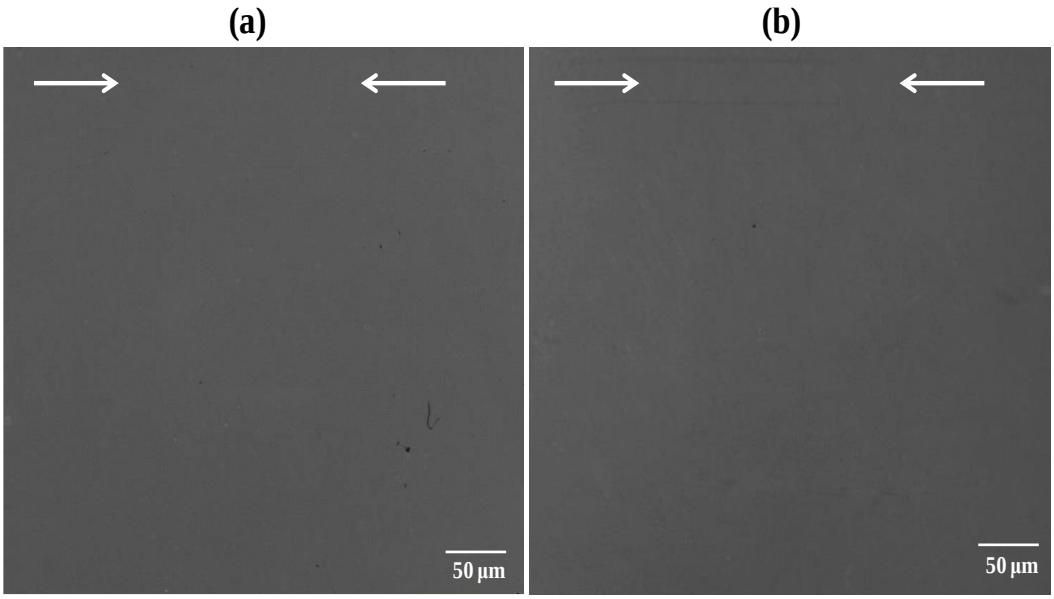

Figure 7-17 CLSM image of surface of ITO/Ag-alloy/ITO coated PET after exposed to (a) 25 °C and (b) 65 °C at 25% of RH for 16 hour. Arrows indicate the loading direction. Applied strain is 0.94%.

Figure **7-18**Figure 7-18 shows changes in electrical resistance over time for flexed specimens with 4.3 mm curvature radius (corresponding to strain 1.43%) when held at 25 °C and 65 °C under 25% RH. In this case under a high temperature of 65 °C and low humidity of 25% RH, a rapid change in electrical resistance in the first 15-25 minute was observed for 65°C. However, in both cases after a certain period of time, the electrical resistance increased linearly over time due to the development of crack growth. This could be evidenced from typical CLSM images of the flexed ITO/Ag-alloy/ITO film before and after being subjected to 25 °C and 65 °C at 25% RH for 16 hours, as shown in Figure 7-19. ITO/Ag-alloy/ITO films crack more when exposure time increases at constant bending strain. The change in electrical resistance increases at a higher rate when samples are subjected to higher temperature as shown in Table 7.2.

After around 15000 seconds, the rate of increase in normalized electrical resistance for samples held at 65 °C and 25% RH was 1.4×10^{-6} compared with 2×10^{-7} for samples held at a similar humidity, but a temperature of 25 °C. As the temperature increases, both the thermal strain caused by thermal expansion of the polymer substrate and elastic mismatch caused by softening of the polymer promoted the development of film cracking, as shown, in a similar manner to that in twisting fatigue test at high temperature. Both cause a large increase in electrical resistance.

Figure 7-20 further confirms this observation by showing the effect of different temperatures on the CD of flexed ITO/Ag-alloy/ITO thin film with 1.44% strain at 16-hours exposure time. It is observed that when exposed to 65 °C and 25% RH for 16-hours higher crack densities are seen than if exposed to 25 °C and 25% RH.

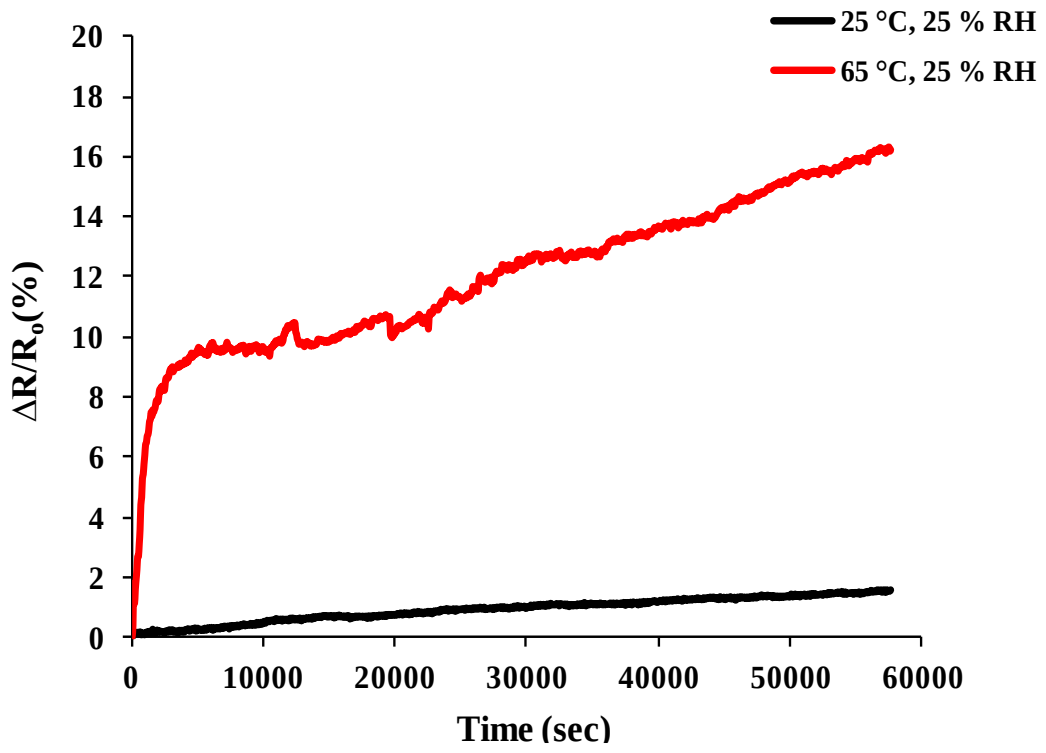

Figure 7-18 Normalized electrical resistance as a function of time for ITO/ Ag alloy /ITO at two different temperatures and 25% of RH under 1.44 % of applied strain.

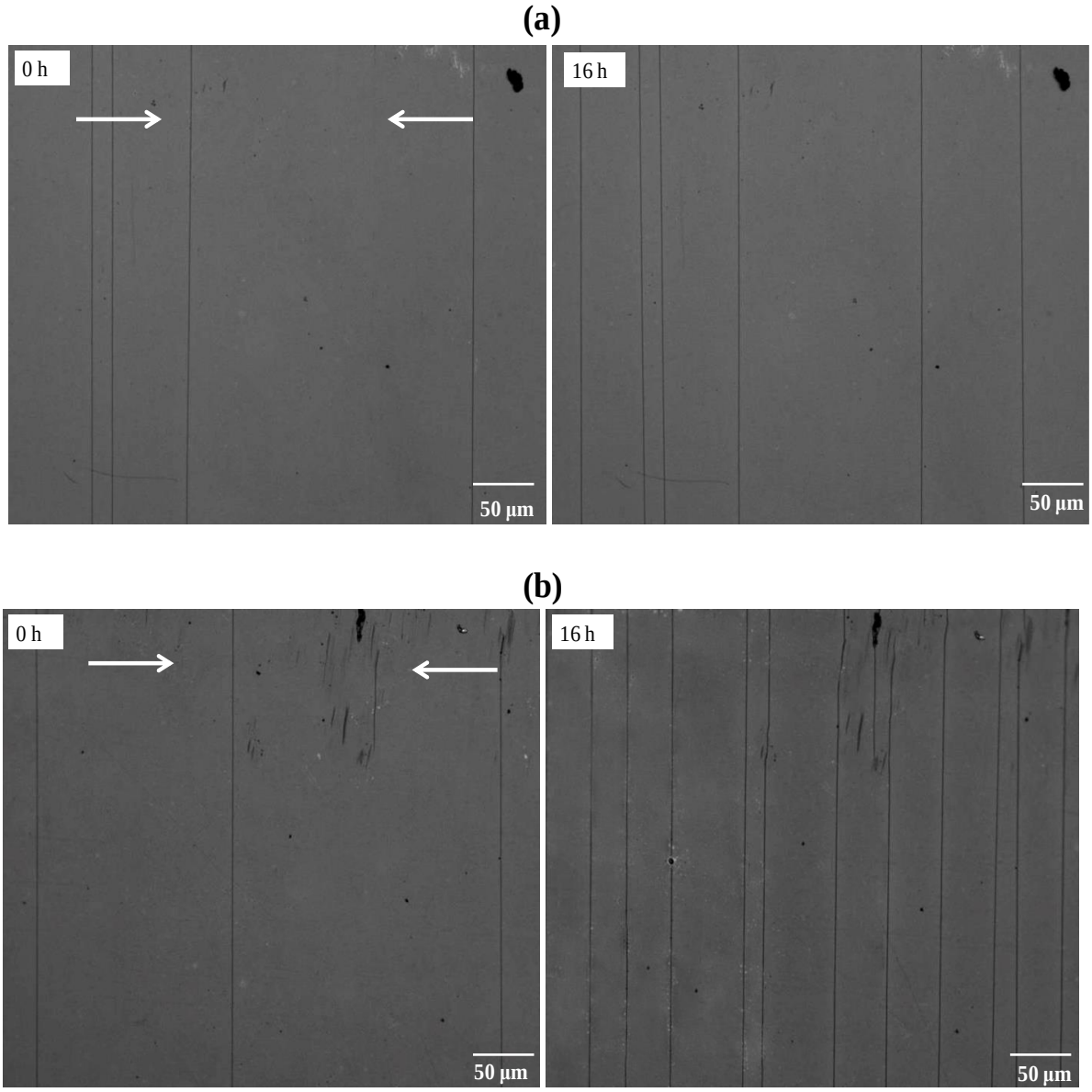

Figure 7-19(a) and (b) CLSM images of surface of ITO/Ag-alloy/ITO exposed to 25 °C and 65 °C at 25 % of RH respectively. Showing the morphological degradation as the exposure time increased. Arrows indicate the loading direction. Applied strain is 1.44%.

Table 7.2 The rate of increase in normalized electrical resistance of ITO/ Ag-alloy /ITO coated PET under varied temperature conditions at 25% RH and 1.44% of strain.

Temperature(°C)	Slope after 15000 second (sec^{-1})
25° C	2×10^{-7}
65 °C	1.4×10^{-6}

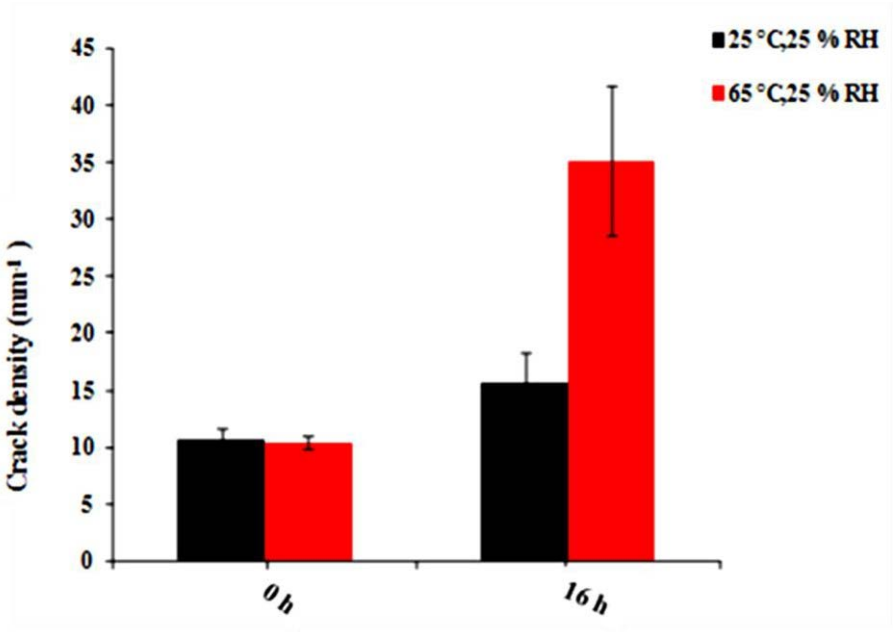

Figure 7-20 Graph showing crack density of ITO/ Ag alloy /ITO films versus exposure time of 25 °C, 25% RH and 65 ° C, 25% RH under 1.44% of applied strain.

In addition, oxidation of the Ag layer is well known when it is exposed to air [217]. The treatment was carried out under an air atmosphere; the existence of cracks on the surface of ITO/Ag-alloy/ITO make it easier for the oxygen in air to penetrate into the Ag layer and react

with it thus causing the Ag layer to be partly oxidized. In general, oxidation occurs at a higher rate when the temperatures is higher [128]. Therefore, oxidation could be a major factor which might cause a rapid increase in electrical resistance in the early stages of exposure to high temperature and low humidity. With increasing exposure time, the oxide of Ag grows thicker, and then saturates [218] and this implies that above the saturation point, crack development would contribute to decrease the electrical conductivity rather than oxidation of the Ag.

The second set of experiments was designed to study the effect of temperature and high relative humidity on the electrical resistance of ITO/Ag-alloy/ITO at two different bending radiuses 6.6 and 4.3 mm. From Figure 7-21 it can be seen that the normalized electrical resistance for flexed samples with 6.6 mm radius of curvature increases in a non-linear way up to almost 4 h at 25 °C and 65 °C of temperature and 80% of humidity exposure. This is possibly due to water reacting with more easily-accessible oxygen vacancies at the surface of the ITO film. This is followed by a decrease in reaction rate because the oxygen in the body of the material is less accessible, slowdown in reactivity due to less reactive (inaccessible) oxygen vacancies in the ITO film or another mechanism of degradation is at play [219]. Further investigation is warranted. After almost 4 h, $\Delta R/R_o$ for the samples linearly increases with the exposure time amplifying that the degradation of electrical resistance upon exposure changed from nonlinear to linear behaviour. Irrespective of temperature applied, it appeared that exposing film to high moisture conditions resulted in excessive corrosion and lowered conductivity

In general, the mechanism of moisture induced degradation of ITO/Ag-alloy/ITO is suggested to be as follows: firstly the moisture penetrates through the permeable defects of the ITO layer at the top of the multilayer because these defects act as fast vapour permeation pathways

[220]. Then the moisture would be absorbed in the intermediate metal Ag layer, and it decreased the interfacial adhesion force between silver and the top ITO layers, causing buckling of the ITO layer and agglomeration of the Ag atoms that breaks the metal layer continuity, and as a consequence, decreases the electrical conductivity of the ITO/Ag-alloy/ITO films. These failure mechanisms are schematically illustrated in Figure 7-22. Table 7.3 shows the rate of increment in electrical resistance of ITO/Ag-alloy/ITO thin film bent to 6.6 mm over time at different temperatures under a high humidity of 80% RH. Exposure to combinations of high temperature and high relative humidity causes an increase in electrical resistance faster than exposure to low temperature and high relative humidity. This is in agreement with CLSM images as shown in Figure 7-23, since at a combination of 65 °C temperature and 80% relative humidity, the density of corrosion spots on the surface appears to be higher as compared with samples exposed at a combination of 25 °C temperature and 80% relative humidity.

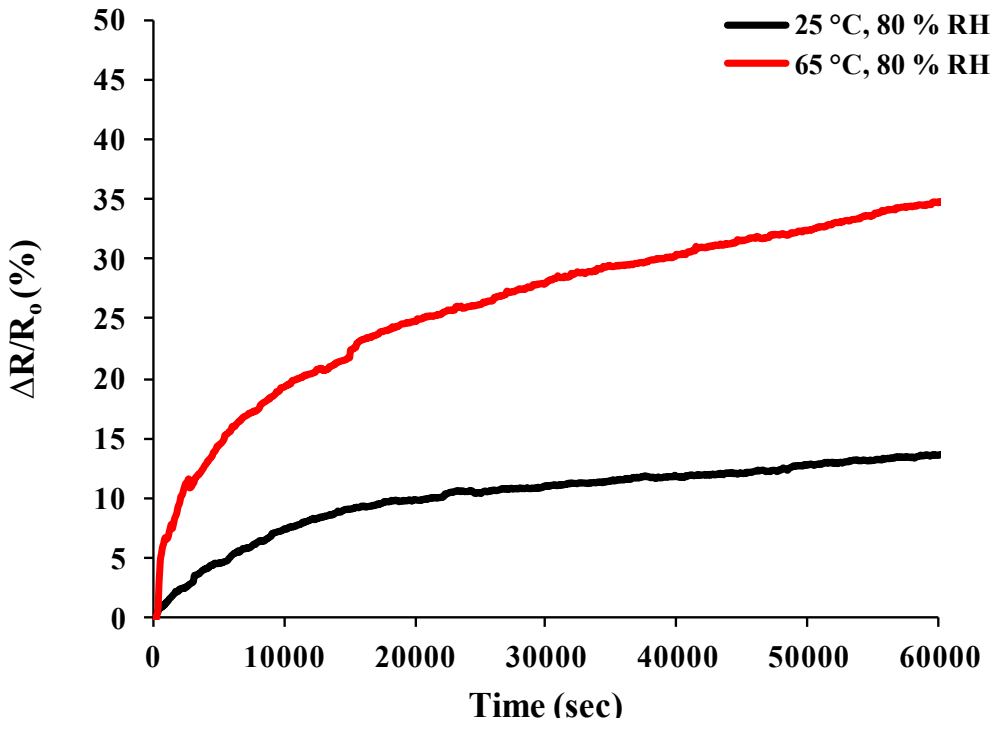

Figure 7-21 Normalized electrical resistance as a function of time for ITO/ Ag alloy /ITO at two different temperatures and 80% of RH under 0.94% of applied strain.

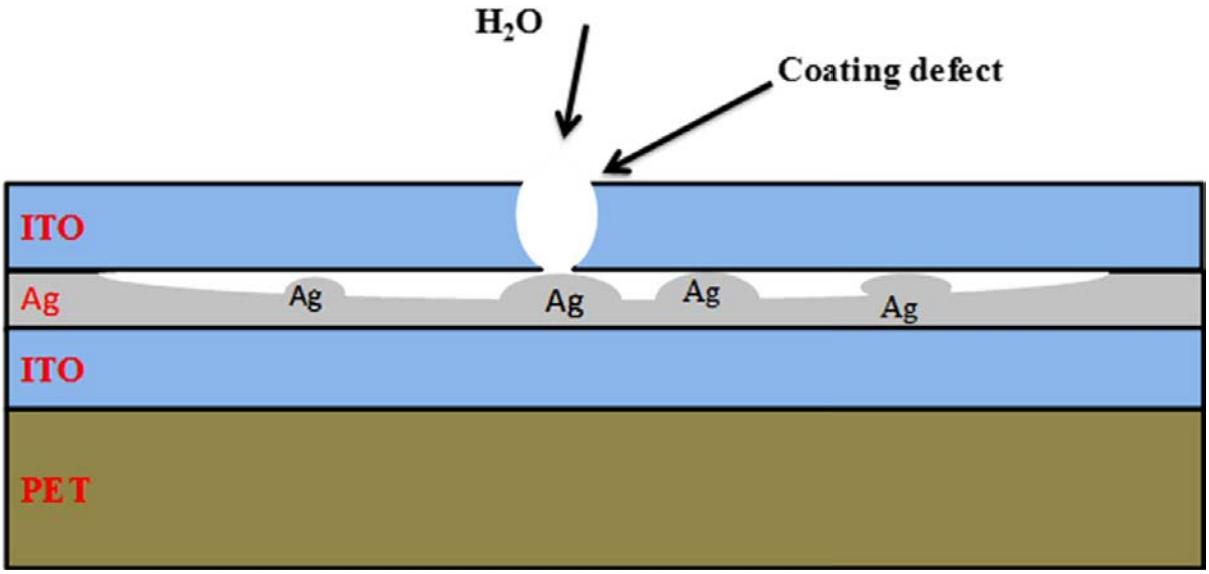

Figure 7-22 Sketch of the cross section of the ITO/ Ag alloy /ITO multilayer system showing the penetration of (H2O) moisture from the defects of top ITO layer into the Ag thin film.

Table 7.3 The rate of increase in normalized electrical resistance of ITO/ Ag alloy /ITO coated PET under varied temperature conditions at 80% RH and 0.94% of strain.

Temperature(°C)	Slope after 15000 second (sec^{-1})
25° C	0.91×10^{-6}
65 °C	25×10^{-7}

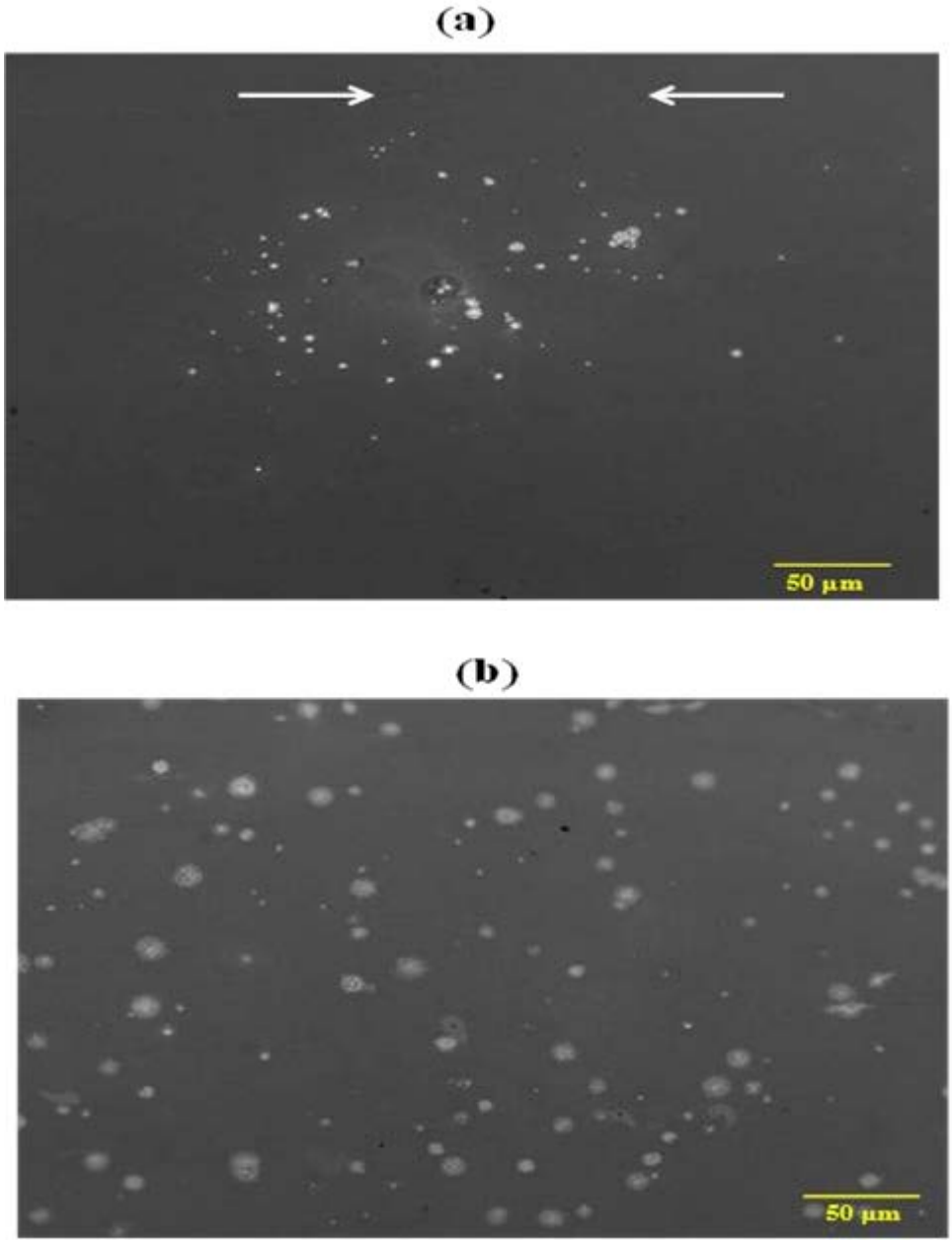

Figure 7-23 CLSM images of surface of ITO/Ag-alloy/IT exposed to (a) 25 °C and (b) 65 °C at 80% of RH respectively. Applied strain is 0.94%. Arrows indicated the loading direction.

A closer SEM examination of the corrosion spots formed on ITO/Ag-alloy/ITO coating after 57,600 seconds at 65 °C and 80% RH as shown in Figure 7-24, could be evidence for the

mechanism of the formation of corrosion spots (Ag agglomerations) as mentioned above, in which the formation of Ag clusters is visible based on EDS analysis. The clusters are similar to those observed after 57,600 seconds of NaCl immersion test (see Figure 7-8 (a)). EDS analysis on the region labelled (A) (see Figure 7-24) indicates the highest silver concentration (~25.4%) compared with other areas on the surface of the sample.

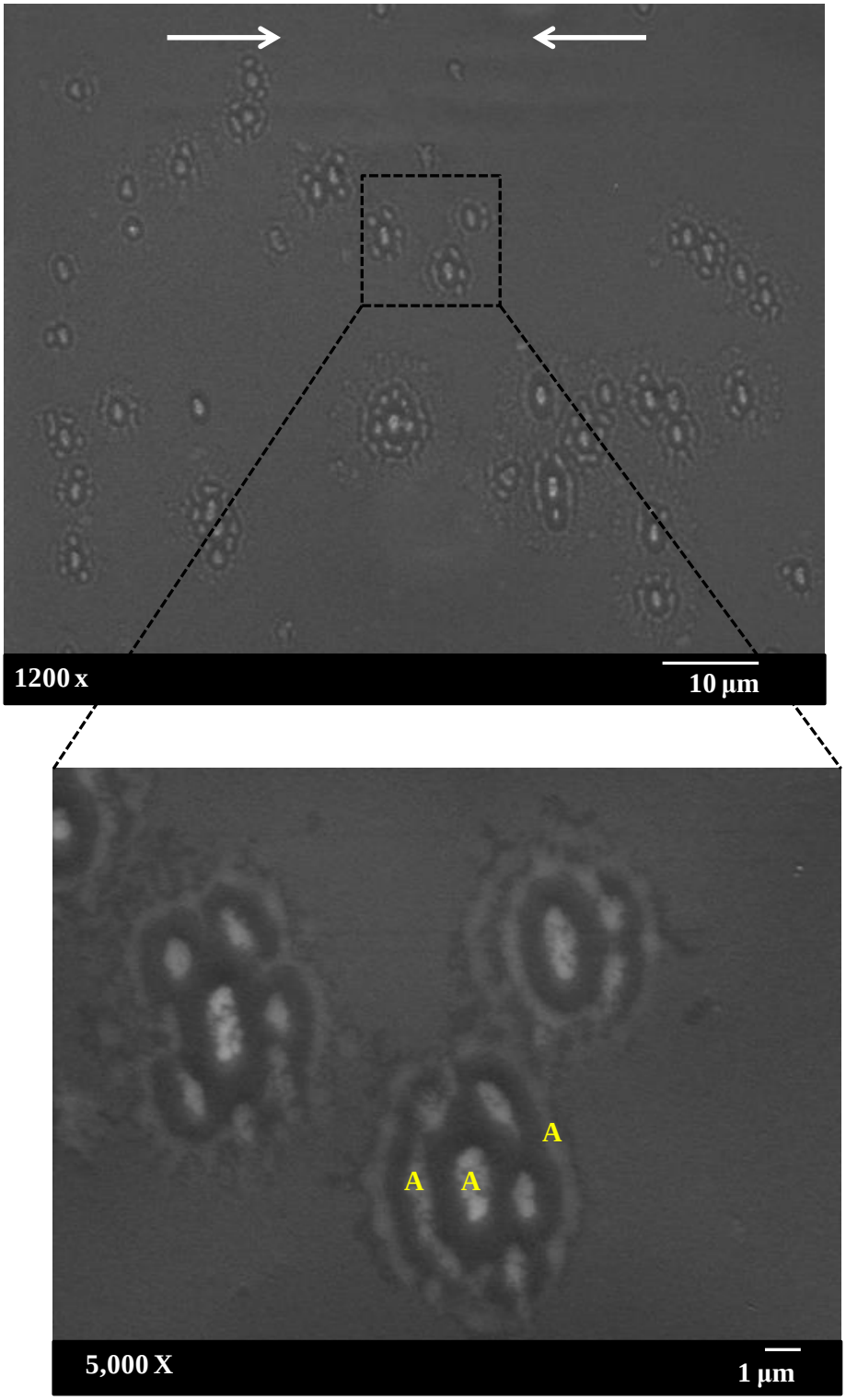

Figure 7-24 SEM images of surface of ITO/Ag-alloy/IT exposed to 65 °C at 80% of RH. Applied strain is 0.94%. Arrows indicated the loading direction.

Figure 7-25 shows the change in the electrical resistance of the films treated at different temperature and 80% RH at bending radius of 4.3 mm for 16 hours. The trend of the electrical resistance change was similar to that of the samples flexed to 6.6 mm at 25 °C, 65°C under 80 % RH. However, non-linear behaviour was not found with higher temperature exposure and a slightly higher increase in electrical resistance was observed in comparison with that under 6.6 mm bending radius (see Figure 7-21). For example, in the case of combined high temperature and humidity (65 °C, 80% RH), after 16 hours, the ITO/Ag-alloy/ITO thin flexed to 6.6 mm showed ~34.4% increase in electrical resistance while that flexed to 4.3 mm showed ~101.05% increase in electrical resistance. Two possible reasons for these discrepancies are the following: firstly, the oxidation rate of Ag will be more if the coating cracks than if the coating never cracks. The higher oxidation rate caused by the cracks leads to sharp increases in electrical resistance during the first stage of the experiment at 65 °C. Secondly cracks on the coating might accelerate the moisture or water vapour penetration that weakens the interfacial adhesion force between the upper ITO layer and the Ag layer and this enhances Ag atom migration and promotes Ag layer agglomeration. Moisture penetrate on because of cracking may also cause blistering of the ITO/Ag-alloy/ITO multilayer from the substrate and thus increase the electrical resistance, these suggestions are supported by , in which the typical ITO/Ag-alloy/ITO film buckling is revealed and also Ag layer agglomeration on the ITO/Ag-alloy/ITO multilayer after exposure to 65 °C and 80% RH under 4.3 mm of radius is presented as white clusters, based on the EDS analysis. EDS analysis of the area labelled A, B and C as shown in gave the Ag composition of ~23.25%, ~2.31% and ~5.95% respectively. The degradation rate of the electrical resistance of flexed ITO/Ag-alloy/ITO at a bending radius of 4.3 mm under different temperatures and high humidity 80% RH are listed in Table 7.4.

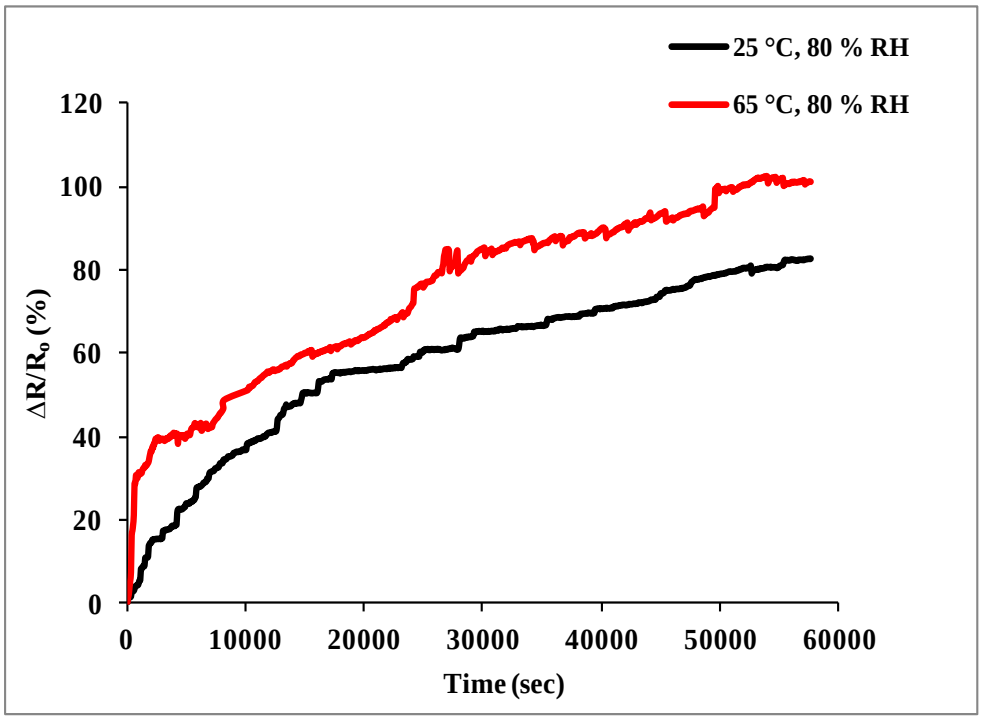

Figure 7-25 Normalized electrical resistance as a function of time for ITO/ Ag alloy /ITO at two different temperatures and 80% of RH under 1.44% of applied strain.

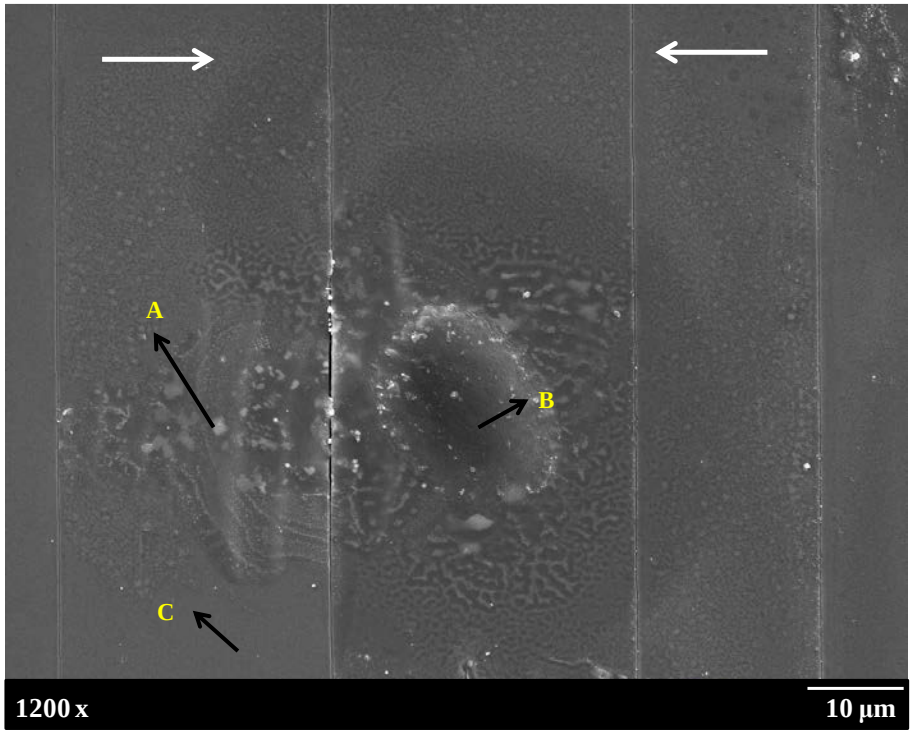

Figure 7-26 SEM image showing blistering of ITO/Ag-alloy/ITO and Ag agglomeration after 16 h of 65 °C and 80% RH exposure. White and black arrows on image indicated the loading direction and area being investigated by EDS respectively. Applied strain is 1.44%.

Table 7.4 The rate of increase in normalized electrical resistance of ITO/ Ag alloy /ITO coated PET under varied temperature conditions at 80% RH and 1.44% of strain.

Temperature(°C)	Slope after 15000 second (sec^{-1})
25° C	7.4×10^{-6}
65 °C	9.9×10^{-6}

Previous work in the literature has reported the reliability of ITO/ Ag-alloy/ITO thin film on glass substrates rather than on polymer substrates at different environmental conditions and also studied the environmental reliability of single pure Ag layer and single ITO layer coated PET substrates while being under cyclic bending fatigue rather than under long term bending. However, some analogies can be made. Across the board, whether the ITO/Ag-alloy/ITO thin film is being subjected to bending for long time or single Ag/or ITO is loaded in a cyclic manner: the exposure of high humidity at any temperature causes a severe degradation of the conductive properties ITO/Ag-alloy/ITO films. This is in good agreement with studies regarding cyclic bending fatigue stress at different temperature and humidity combinations. Yang *et al*. [208] reported that during the bending fatigue test the highest increment in electrical resistance of silver nanoparticle film on PET observed under high temperature and high humidity combination (60 °C, 90 % RH). Pre-existing cracks were found to cause larger cracks once initiated, owing to the combinational influences of the repeated bending stress and humidity, and result in the greatest increase in electrical resistance. They conclude that the reduction of defect, void, or porosity of thin film is crucial for performance of thin film under harsh mechanical stress and environmental conditions. Furthermore, the results obtained in this work for exposure to 65° C and 80% RH are consistent with those reported by Chen *et al.* [135] that the electrical resistivity of ITO–Ag–ITO thin film was increased after

being exposed to 49.8 °C temperature and 90% relative humidity for 144 hours due to formation of defects on the surface resulting from corrosion of Ag. It is also similar to those of Hee [211] who reported that severe degradation of indium zinc oxide/Ag/indium zinc oxide in humid environment 85 °C and 85% RH in air occurred by the agglomeration of Ag atoms and as a result the electrical resistance increased.

7.6. Conclusions

In order to determine the critical onset radius of curvature of ITO/Ag-alloy/ITO film failure, prior to the long-term bending reliability of ITO/Ag-alloy/ITO film and bending fatigue-corrosion experiments, buckling experiments with *in situ* microscopical and electrical resistance monitoring were conducted.

Crack onset radius values based on optical microscopy and based on an increase in electrical resistance were observed to take place at applied radius of curvature equal to 4.7 mm (corresponding to applied stain 1.35%). The better flexibility of ITO/Ag-alloy/ITO film in comparison to single ITO film was attributed to the existence of the Ag layer due to a high ductility of the Ag metal layer.

In salt immersion tests, the corrosion behaviour of ITO/Ag-alloy/ITO film coated PET substrate in the presence of 0.3, 0.5, 1, 2 and 3M NaCl was studied by *in situ* electrical measurements in order to understand its stability when in use in aggressive environments. It was observed that the normalized electrical resistance increases as the submersion time is increased and that was associated with observations of the surface of films over time. It was also noted that the rapid corrosion of the ITO/Ag-alloy/ITO film coating is promoted by high NaCl concentration. Furthermore, it is shown that the presence of defects in the deposited

films can provide a driving force to form Ag agglomerations which, in turn, degrade the conductivity of ITO/Ag-alloy/ITO film. This suggests that defects in the film should be minimized to avoid excessive corrosion.

Moreover, the ITO/Ag-alloy/ITO film submerged in high salt concentration such as 1,2,3 M exhibited high degradation of spectral transmittance. This is because an increase in chloride concentration of solution results in a higher density of spots on the surface which causes severe light scattering.

In the cyclic bending fatigue tests under aggressive salt environments, the increase in normalized electrical resistance of samples under corrosion-bending fatigue test was significantly higher than that under bending fatigue alone, which indicates that the ITO/Ag-alloy/ITO film failure is dominated by corrosion, however the external mechanical stress is an assisting failure mechanism.

In long term bending tests under different temperature and humidity conditions, CLSM images showed no signs of surface changes in the specimens bent to 6.6 mm (0.94% of strain) over time under different temperatures and low humidity. However, at an applied strain of 1.44% which is higher than crack onset strains, an increasing temperature at low humidity enhances crack initiation and propagation as well as Ag layer oxidation which causes a large increase in electrical resistance.

The results show that high humidity promotes ITO/Ag-alloy/ITO film failure, regardless whether the temperature is high or low. In particular, in the case under 4.3 mm of radius curvature at combined high temperature and high humidity, the specimen showed a high rate of increase in normalized electrical resistance, which can be attributed to crack growth and buckling of the film as well as Ag layer agglomeration. It could be concluded that when

ITO/Ag-alloy/ITO is subjected to a harsh environment together with the presence of cracks on the surface, the cracks act as a tunnel for easy permeation of moisture and oxygen. Therefore, an external applied stress with moisture and/or harsh environments as well as moisture and/or harsh environments alone should be avoided in both manufacturing processes and applications.

8. Conclusions and further work

8.1. Conclusions

The main focus of this work was on the investigation of mechanical and electro-mechanical reliability of IGZO and ITO/Ag-alloy/ITO thin films that are commonly used throughout the field of flexible optoelectronic devices. PET and PEN are the most promising substrate candidates for flexible electronic applications, therefore, they were characterised in order to understand the differences in performance and behaviour between PET and PEN substrates and their impact on mechanical reliability of IGZO and other oxide films.

Better thermal properties of PEN, as compared with those of PET, indicate that PEN can withstand higher temperatures during both device manufacturing as well as in end-use applications. High transmittance in the visible range was observed for both substrates. However, PET showed slightly lower surface roughness and lower Young's modulus. A strong dependence of the elastic modulus of this semicrystalline polymer on the biaxial orientation of the polymer chains was observed.

The lower surface roughness of the IGZO film grown on PET emphasizes the importance of smooth substrates for achieving lower surface roughness of the thin oxide films. The structure of sputtered 50 nm thick IGZO film on polymer substrates was found to be amorphous; accordingly, the RF – magnetron sputtering technique can be chosen for applications where a high quality amorphous structure is required.

Mechanical reliability of IGZO film on different polymer substrates was investigated using uniaxial tensile tests. It was observed using *in situ* optical microscopy that IGZO film deposited on PEN exhibits higher crack onset values due to its lower mechanical mismatch. In

addition, a high crack density at saturation was found for IGZO deposited on PEN substrates. The failure pattern under uniaxial tensile stress is characterized by cohesive cracking perpendicular to the loading direction and adhesive failure with buckling in a parallel direction.

During buckling tests, IGZO film under compression buckling showed better bending durability than under tensile buckling. Higher critical radius of curvature values (6.4 mm) were observed for thin films under tensile buckling compared with those under compression buckling. This suggests that surface defects on the films induce crack initiation when the film is under tensile buckling. Also, the results showed that the difference in saturation crack density, fracture energy, fracture toughness and film strength between the IGZO film under tensile and compression buckling were due to the different fracture mechanisms. Channel cracks were the major failure mode when the film was in a tensile buckling mode while when the coating was under compressive buckling a delamination-buckling-cracking was the failure mode.

In twisting tests, the onset of cracking was observed at a twisting angle equal to 39° ± 1.7°. Both coating defects and edge defect were believed to promote crack initiation. Results suggest that improving coating quality and sample edges is effective in improving the twisting reliability of thin film. In addition, critical twisting angle values based on CLSM images were in good agreement with those calculated based on an normalized electrical resistance. Also, twisting damage morphology of thin films indicated that both tensile and compressive stresses can be induced in the film when it is subjected to twisting stress.

In twisting fatigue experiments, the normalized electrical resistance was found to be higher at higher applied angles and higher number of cycles and that is associated with high crack

density. Also, it was observed that the increase in applied temperature led to a higher percentage change in electrical resistance.

In controlled buckling experiments, ITO/Ag-alloy/ITO film demonstrated excellent flexibility in comparison with single ITO film as the ITO/Ag-alloy/ITO film can tolerate a 4.7 mm bending radius without cracking and or losing its functionality. This indicates that ITO/Ag-alloy/ITO is a strong candidate to substitute for ITO anodes for high performance in flexible electronic devices.

The corrosion studies of ITO/Ag-alloy/ITO showed that the presence of aggressive salt environments increased the electrical resistance of such films over time. Increased NaCl concentration caused a more rapid degradation of the ITO/Ag-alloy/ITO surface and of transmittance. Furthermore, it was observed that the chlorine ion penetrated primarily through coating defects and /or edge defects, which can provide a driving force for Ag agglomerations and thus degrade the conductivity of ITO/Ag-alloy/ITO film. This finding suggests that reduction of defects will be critical for improving the corrosion resistance of such structures. The combined action of corrosive environmental NaCl and repeated bending stress was found to lower the performance of ITO/Ag-alloy/ITO film considerably. This indicated that the combined effect of corrosion and fatigue must be taken into account for electrodes that might experience both during manufacture and in service conditions.

In long term bending tests, the results showed that the conditions of high temperature and low humidity at low bending radius cause a large increase in electrical resistance due to the enhancement of crack initiation and propagation. However, high humidity was found to promote ITO/Ag-alloy/ITO film failure regardless of the bending radius and temperature applied.

8.2. Overall conclusions

It is believed that this work provides fundamental background knowledge for understanding the mechanical and electro-mechanical properties of flexible optoelectronics components under under different mechanical and environmental loads. It was found that the crack initiation strain is mostly dependent on the elastic mismatch between the brittle coating and polymer substrate. This work showed that the twisting reliability and corrosion resistnace of ITO/Ag-alloy/ITO coated PET substrates can be improved by a improving coating quality and sample edges. Also, higher change in electrical resistance for specimens subjected to bending fatigue–corrosion was observed as compared with the ones under bending fatigue alone. These findings underline the importance of the combined action of bending fatigue and corrosion. In this study ITO/Ag-alloy/ITO film showed higher flexibility in comparison with single ITO film. ITO/Ag-alloy/ITO films should be ideal candidates for flexible devices with a moderate degree of bending. Understanding the bending behaviour of multilayers under various environmental condition can lead to increasing long term reliability of flexible devices.

8.3. Further work

In this dissertation, a number of mechanical tests were developed to investigate the properties of brittle thin oxide films on polymer substrates. However, the following work is recommended for further study and in understanding the reliability of such material for other flexible electronic applications such as solar cells.

Sputtering IGZO on different polymer thicknesses should be attempted in order to investigate its impact on the mechanical properties of the coating. As has been reported recently by Hsu et al. [125] increasing the PET thickness causes the number of microcracks of ITO coating to increase under both tensile and compressive bending stress.

In addition, as well as further work on sputtering of IGZO on polymer substrates it will be interesting to sputter IGZO film on pre-strained polymer substrates. Polymer substrates can be elongated or bent to produce various strains before coating by using the apparatus which was used in this study for the long term bending tests Figure 3-13. The parallel plates designed to hold the specimen under strain could be installed in the RF magnetron sputtering chamber. Once deposition is achieved, the mechanical, electrical, optical and structural properties of IGZO film could be examined to investigate the effect of pre-loading the substrate.

In order to support the twisting and bending experiment, a finite element model could be developed to simulate the stress on the structure and to predict the stress distribution across the coating as the structure is subjected to different radius of curvature and angles. With regards to the twisting fatigue test it would be interesting to find the effects of sample width and ITO coating thickness on crack development and electrical properties of the ITO/Ag-alloy/ITO. The effect of the continuous heat on ITO/Ag-alloy/ITO has been investigated in this work. However, in real applications, heat fluctuations between day and night to which flexible devices (in particularly solar cells) may be subject, could damage and crack ITO/Ag-alloy/ITO films. Therefore, the influence of fluctuating temperatures on the conductivity, material constituents and surface morphology of ITO/Ag-alloy/ITO and other films could be investigated.

In the bending behaviour of ITO/Ag-alloy/ITO film over time under different temperature and humidity conditions, the effects on the polymer substrates could also be considered.

In this study during various experiments including buckling, twisting, corrosion (aggressive salt), etc, the impact of coating defects and edge effect on the electro mechanical reliability of thin films was observed. Since the IGZO and ITO/Ag-alloy/ITO that were used in this study were coated on polymer by magnetron sputtering, it may be worth to deposit such thin film by other techniques such as pulsed laser deposition to improve coating quality. The comparison of electro-mechanical performance of sputtered and pulsed laser deposited film on polymer substrate should be a good contribution.

Also, in order to better understand edge effects, ITO/Ag-alloy/ITO can be patterned by photolithography. Then the electro-mechanical and corrosion test can be performed under different conditions of stresses and compared with unpatterned ITO/Ag-alloy/ITO. The stability of the patterned film could be also studied in term of transmittance after being subjected to environments rich with NaCl concentration.

Furthermore, structure optimization and material improvement is a good opportunity to improve the product qualities. Therefore, it will be interesting to optimise multilayered films of Ag based aluminum doped zinc oxide (AZO)/polymer in terms of high transmittance and electrical conductivity. AZO film is a viable alternative to ITO electrodes because it inexpensive and abundant material. All techniques and equipment used in this study can be used to investigate the influence of various factors such as twisting angle, fatigue loading, bending strain, NaCl concentration, temperature and humidity on electrical performance of AZO/Ag/AZO film and then to compare their performance with ITO/Ag-alloy/ITO and ITO. Moreover, carbon nanotube films have been reported [221] as promising to replace TCOs due

to their mechanical robustness. Therefore, it would be valuable to see the electrical resistance response under a variety of mechanical deformation.

9. References

[1] K. A. Ray, Flexible Solar Cell Arrays for Increased Space Power, Trans. Aerosp. Electron. Syst. AES-3 (1967) 107–115.

[2] R.L. Crabb, F.C. Treble, Thin Silicon Solar Cells for Large Flexible Arrays, Nature. 213 (1967) 1223–1224.

[3] J.I. Han, Stability of Externally Deformed ITO Films, in: G.P. Crawford (Ed.), Flex. Flat Panel Displays, John Wiley & Sons Ltd, Chichester, 2005: pp. 121–132.

[4] https://prohardver.hu/hir/elektronikus_papir_a_fujitsutol.html, (2014).

[5] https://www.flickr.com/photos/marufish/2720185982/, (2008).

[6] http://www.phonearena.com/news/Here-is-a-closer-look-at-the-flexible-display-battery-and-more-on-the-LG-G-Flex_id49981, (2013).

[7] http://www.led-billboard-display.com/sale-245904-aluminum-or-iron-flexible-modular-outdoorcurved-led-display-screen-p16-2r1g1b.html, (2012).

[8] A. Martin, A physics of failure based qualification process for flexible display interconnect materials, PhD thesis, University of Maryland, 2011.

[9] K.H. Cherenack, Fabricating silicon thin-film transistors on plastic at 300 °c, PhD thesis, Princeton University, 2009.

[10] Kalluri R. S., Amorphous Silicon: Flexible Backplane and Display Application, in: Tuller H.L. (Ed.), Flex. Electron. Appl., Springer Science+Business Media, New York, 2009: pp. 75–105.

[11] E. Morton, D. Forsythe, Flexible-Display development for army applications, Inf. Displays. (2007).

[12] S. Fumio, Research on Flexible Display Systems, Broadcast Technol. (2005) 10–15.

[13] N. Lu, Mechanics of Hard Films on Soft Substrates, PhD thesis, Harvard University, 2009.

[14] D.Y. Cho, K. Eun, S.H. Choa, H.K. Kim, Highly flexible and stretchable carbon nanotube network electrodes prepared by simple brush painting for cost-effective flexible organic solar cells, Carbon N. Y. 66 (2014) 530–538.

[15] M.C. Choi, Y. Kim, C.S. Ha, Polymers for flexible displays: From material selection to device applications, Prog. Polym. Sci. 33 (2008) 581–630.

[16] R. Eveson, W.A. Macdonald, D. Mackerron, A. Hodgson, K. Rakos, K. Rollins, et al., P-65 : Optimising Polyester Films For Flexible Electronic Applications, SID Symp. Dig. Tech. Pap. (2008) 1431–1434.

[17] P.E. Burrows, G.L. Graff, M.E. Gross, P.M. Martin, M.K. Shi, M. Hall, et al., Ultra barrier fexible substrates for flat panel displays, Displays. 22 (2001) 65–69.

[18] Y.F. Lan, W.C. Peng, Y.H. Lo, J.L. He, Durability under mechanical bending of the indium tin oxide films deposited on polymer substrate by thermionically enhanced sputtering, Org. Electron. 11 (2010) 670–676.

[19] B.K. Sharma, B. Jang, J.E. Lee, S.H. Bae, T.W. Kim, H.J. Lee, et al., Load-Controlled Roll Transfer of Oxide Transistors for Stretchable Electronics, Adv. Funct. Mater. 23 (2013) 2024–2032.

[20] G. Woo, J. Park, J. Wang, H.W. Lee, Z. Li, J. Koo, Amorphous Indium Gallium Zinc Oxide Thin-Film Transistors with a Low-Temperature Polymeric Gate Dielectric on a Flexible Substrate, Jpn. J. Appl. Phys. 071102 (2013) 1–5.

[21] M. Girtan, Comparison of ITO/metal/ITO and ZnO/metal/ZnO characteristics as transparent electrodes for third generation solar cells, Sol. Energy Mater. Sol. Cells.

100 (2012) 153–161.
[22] X.T. Hao, F.R. Zhu, K.S. Ong, L.W. Tan, Colour tunability of polymeric light-emitting diodes with top emission architecture, Semicond. Sci. Technol. 21 (2006) 19–24.
[23] C. Guillen, J. Herrero, ITO/metal/ITO multilayer structures based on Ag and Cu metal films for high-performance transparent electrodes, Sol. Energy Mater. Sol. Cells. 92 (2008) 938–941.
[24] K. a. Sierros, A.J. Kessman, R. Nair, N.X. Randall, D.R. Cairns, Spherical indentation and scratch durability studies of transparent conducting layers on polymer substrates, Thin Solid Films. 520 (2011) 424–429.
[25] E.H. Kim, C.W. Yang, J.W. Park, Designing interlayers to improve the mechanical reliability of transparent conductive oxide coatings on flexible substrates, J. Appl. Phys. 111 (2012) 093505.
[26] K.A. Sierros, D.S. Hecht, D.A. Banerjee, N.J. Morris, L. Hu, G.C. Irvin, et al., Durable transparent carbon nanotube films for flexible device components, Thin Solid Films. 518 (2010) 6977–6983.
[27] D.M. Bagnall, M. Boreland, Photovoltaic technologies, Energy Policy. 36 (2008) 4390–4396.
[28] N. Kenji, O. Hiromichi, T. Akihiro, K. Toshio, H. Masahiro and H. Hideo, Room-temperature fabrication of transparent flexible thin-film transistors using amorphous oxide semiconductors., Nature. 432 (2004) 488–92.
[29] A. Weber, S. Deutschbein, A. Plichta, A. Habeck, 6.3: Thin Glass-Polymer Systems as Flexible Substrates for Displays, SID Symp. Dig. Tech. Pap. 33 (2002) 53.
[30] J.S. Park, T.W. Kim, D. Stryakhilev, J.S. Lee, S.G. An, Y.S. Pyo, et al., Flexible full color organic light-emitting diode display on polyimide plastic substrate driven by amorphous indium gallium zinc oxide thin-film transistors, Appl. Phys. Lett. 95 (2009) 013503.
[31] T. Scheirs J. and Long, Modern Polyesters : Chemistry and Technology of Polyesters and Copolyesters, John Wiley & Sons Ltd, 2003.
[32] W.A. Macdonald, K. Rollins, R. Eveson, R.A. Rustin, M. Handa, P-17 : Plastic Displays - New Developments in Polyester Film for Plastic Electronics, SID Symp. Dig. Tech. Pap. (2003) 264–267.
[33] S. Logothetidis, Flexible organic electronic devices: Materials, process and applications, Mater. Sci. Eng. B. 152 (2008) 96–104.
[34] W.A. Macdonald, D.T. Films, P.O.B. Wilton, U.K. Ts, Engineered films for display technologies, J. Mater. Chmistry. 14 (2004) 4–10.
[35] W.A. MacDonald, M.K. Looney, D. MacKerron, R. Eveson, K. Rakos, Designing and manufacturing substrates for flexible electronics, Plast. Rubber Compos. 37 (2008) 41–45.
[36] W.A. MacDonald, M.K. Looney, D. MacKerron, R. Eveson, R. Adam, K. Hashimoto, et al., Latest advances in substrates for flexible electronics, J. Soc. Inf. Disp. 15 (2007) 1075.
[37] a. Laskarakis, S. Logothetidis, Study of the electronic and vibrational properties of poly(ethylene terephthalate) and poly(ethylene naphthalate) films, J. Appl. Phys. 101 (2007).
[38] D.J. MCCLURE, Polyester (PET) Films as a Substrate: a Tutorial, 50th Annu. Tech. Conf. Proc. Soc. Vac. Coaters. (2007) 692– 699.
[39] A.J. DE Vries, C. Bonnebat, Uni- and biaxial orientation of polymer films and sheets, J. Polym. Sci. Polym. Symp. 58 (1977) 109–156.

[40] K. A. Sierros, Mechanical properties and Characterisation of Substrates for Flexible Displays, PhD thesis,University of Birmingham, 2006.
[41] J.C. Kim, M. Cakmak, X. Zhou, Effect of composition on orientation, optical and mechanical properties of bi-axially drawn PEN and PEN/PEI blend films, Polymer (Guildf). 39 (1998) 4225–4234.
[42] M. Cakmak, Y.D. Wang, M. Simhambhatla, Processing characteristics, structure development, and properties of uni and biaxially stretched poly(ethylene 2,6 naphthalate) (PEN) films, Polym. Eng. Sci. 30 (1990) 721–733.
[43] C.W. Bauer, Effects of degree of stretching on the properties of heat set biaxially stretched naphthalate-containing polyester films, J. Plast. Film Sheeting. 13 (1997) 336–347.
[44] S. K. Sharma andA. Misra, The effect of stretching conditions on properties of amorphous polyethylene terephthalate film, J. Appl. Polym. Sci. 34 (1987) 2231–2247.
[45] Y. Maruhashi, T. Asada, Structure and Properties of Biaxially Stretched Poly(Ethy1ene Terephthalate) Sheets, Polym. Eng. Sci. 36 (1996) 483–494.
[46] R. Mody, E. a. Lofgren, S. a. Jabarin, Shrinkage Behavior of Orientedpoly(Ethylene Terephthalate), J. Plast. Film Sheeting. 17 (2001) 152–163.
[47] W.A. Macdonald, K. Rollins, D. Mackerron, R. Eveson, R.A. Rustin, K. Rakos, et al., P-46 : Plastic Displays – Latest Developments in Polyester Film for Plastic Electronics, SID Symp. Dig. Tech. Pap. 12 (2004) 420–423.
[48] W.Y. Teng, S.C. Jeng, J.M. Ding, C.W. Kuo, W.K. Chin, Flexible Homeotropic Liquid Crystal Displays Using Low-Glass-Transition-Temperature Poly(ethylene terephthalate) Substrates, Jpn. J. Appl. Phys. 49 (2010) 3.
[49] D. Nicholls, Physical Ageing In Semi-Crystalline Polyethylene Terephthalate, MRes thesis,University of Birmingham, 2009.
[50] R.J. Young, P.A. Lovell, Introduction to polymers, Second edi, Cambridge University Press, Cambridge, 1991.
[51] B. Demirel, A. Yaras, H. Elcicek, Crystallization Behavior of PET Materials, BAu Fen Bil. Enst. Derg. Cilt. 13 (2011) 26–35.
[52] J.R. Isasi, L. Mandelkern, A.J. Galante, R.G. Alamo, The Degree of Crystallinity of Monoclinic Isotactic Poly (propylene), J. Polym. Sci. Part B Polym. Phys. 37 (1999) 323–334.
[53] B.A.MacDonald, K. Rollins, D. MacKerron, K. Rakos, R. Eveson, K. Hashimoto, et al., Engineered Films for Display Technologies, in: G. P. Crawford (Ed.), Flex. Flat Panel Displays, John Wiley & Sons Ltd, Chichester, 2005: pp. 11–33.
[54] J.S. Lewis, M.S. Weaver, Thin-Film Permeation-Barrier Technology for Flexible Organic Light-Emitting Devices, IEEE J. Sel. Top. Quantum Electron. 10 (2004) 45–57.
[55] E.M. Abdel-bary, Handbook of Plastic Films, 2003.
[56] J.D. Affinito, S. Eufinger, M.E. Gross, G.L. Graff, P.M. Martin, PML/oxide/PML barrier layer performance differences arising from use of UV or electron beam polymerization of the PML layers, Thin Solid Films. 308-309 (1997) 19–25.
[57] K. Leppanen, B. Augustine, J. Saarela, R. Myllyla, T. Fabritius, Breaking mechanism of indium tin oxide and its effect on organic photovoltaic cells, Sol. Energy Mater. Sol. Cells. 117 (2013) 512–518.
[58] M.M. Hamasha, K. Alzoubi, S. Lu, S.B. Desu, Durability study on sputtered indium tin oxide thin film on Poly Ethylene Terephthalate substrate, Thin Solid Films. 519 (2011) 6033–6038.

[59] K. Sierros, N.J. Morris, S.N. Kukureka, D.R. Cairns, Dry and wet sliding wear of ITO-coated PET components used in flexible optoelectronic applications, Wear. 267 (2009) 625–631.
[60] A. Kleiman, M. Tagawa, Y. Kimoto, Protection of Materials and Structures From the Space Environment, Springer- Verlag Berlin Heidelberg, 2013.
[61] Nisha M., Growth and Characterisation of Radio Frequency Magnetron Sputtered Indium Tin Oxide Thin Film, PhD thesis,Cochin University of Science And Technology, 2006.
[62] S.O. Yoon, H.J. Jung, K.H. Yoon, Contact resistance of the electrodes on semiconducting ceramics, Solid State Commun. 64 (1987) 617–619.
[63] W.F. Wu, B.S. Chiou, Deposition of indium tin oxide films on polycarbonate substrates by radio-frequency magnetron sputtering, Thin Solid Films. 298 (1997) 221–227.
[64] Q. Xu, W. Shen, Q. Huang, Y. Yang, R. Tan, K. Zhu, et al., Flexible transparent conductive films on PET substrates with an AZO/AgNW/AZO sandwich structure, J. Mater. Chem. C. 2 (2014) 3750.
[65] L. Minseong, D. Joonghoe, Controlling the Electrical and the Optical Properties of Amorphous IGZO Films Prepared by Using Pulsed Laser Deposition, J. Korean Phys. Soc. 58 (2011) 492.
[66] C.C. Lo, T.E. Hsieh, Preparation of IGZO sputtering target and its applications to thin-film transistor devices, Ceram. Int. 38 (2012) 3977–3983.
[67] C. Guillen, J. Herrero, TCO/metal/TCO structures for energy and flexible electronics, Thin Solid Films. 520 (2011) 1–17.
[68] B. Szyszka, ITO Replacements:Insulator-Metal-Insulator Layers, in: Handb. Vis. Disp. Technol., Springer-Verlag Berlin Heidelberg, 2012.
[69] Lide D. R., The Handbook of Chemistry and Physics, 84th ed., CRC Press LLC, 2004.
[70] Y.S. Park, K.H. Choi, H.K. Kim, Room temperature flexible and transparent ITO/Ag/ITO electrode grown on flexile PES substrate by continuous roll-to-roll sputtering for flexible organic photovoltaics, J. Phys. D. Appl. Phys. 42 (2009) 235109.
[71] J. Lewis, S. Grego, B. Chalamala, E. Vick, D. Temple, Highly flexible transparent electrodes for organic light-emitting diode-based displays, Appl. Phys. Lett. 85 (2004) 3450.
[72] D. Jang, S. jae Jung, J. joong Lee, Al doped zinc oxide thin films on polymer substrates deposited by inductively coupled plasma assisted reactive sputtering, Curr. Appl. Phys. 12 (2012) S118–S122.
[73] G.J. Exarhos, X.-D. Zhou, Discovery-based design of transparent conducting oxide films, Thin Solid Films. 515 (2007) 7025–7052.
[74] P.J. Kelly, R.D. Arnell, Magnetron sputtering: a review of recent developments and applications, Vacuum. 56 (2000) 159–172.
[75] http://www.pfonline.com/articles/vacuum-deposition-and-coating-options, (2013).
[76] A. Antony, M. Nisha, R. Manoj, M.K. Jayaraj, Influence of target to substrate spacing on the properties of ITO thin films, Appl. Surf. Sci. 225 (2004) 294–301.
[77] H. Han, D. Adams, J.W. Mayer, T.L. Alford, Characterization of the physical and electrical properties of Indium tin oxide on polyethylene napthalate, J. Appl. Phys. 98 (2005).
[78] H. Yabuta, M. Sano, K. Abe, T. Aiba, T. Den, H. Kumomi, et al., High-mobility thin-film transistor with amorphous InGaZnO4 channel fabricated by room temperature rf-magnetron sputtering, Appl. Phys. Lett. 89 (2006) 10–13.
[79] F. Shi, L. Chen, Q. Li and F. Li, Dependence of electrical and optical properties of

IGZO film on oxygen flow, J Shanghai Univ (Engl Ed). 15 (2011) 242–244.
[80] C. Guillen, J. Herrero, Transparent conductive ITO/Ag/ITO multilayer electrodes deposited by sputtering at room temperature, Opt. Commun. 282 (2009) 574–578.
[81] E. Schwartz, Roll to Roll Processing for Flexible Electronics MSE 542 : Flexible Electronics, 2006.
[82] G. Abbie, L. York, M. Strnad, Roll-to-Roll Manufacturing of Flexible Displays, in: G. P. Crawford (Ed.), Flex. Flat Panel Displays, John Wiley & Sons Ltd, Chichester, 2005: pp. 409–447.
[83] K. Alzoubi, Experimental and analytical studies of the high cycle bending fatigue of thin films on flexible substrates for flexible electronics applications, PhD thesis, Binghamton University, 2010.
[84] T.P. Nguyen, P. Jolinat, P. Destruel, R. Clergereaux, J. Farenc, Degradation in organic light-emitting diodes, Thin Solid Films. 325 (1998) 175–180.
[85] K.H. Choi, J.A. Jeong, J.W. Kang, D.G. Kim, J.K. Kim, S.I. Na, et al., Characteristics of flexible indium tin oxide electrode grown by continuous roll-to-roll sputtering process for flexible organic solar cells, Sol. Energy Mater. Sol. Cells. 93 (2009) 1248–1255.
[86] G. Folcher, H. Cachet, M. Froment, J. Bruneaux, Anodic corrosion of indium tin oxide films induced by the electrochemical oxidation of chlorides, Thin Solid Films. 301 (1997) 242–248.
[87] Y. Leterrier, L. Medico, F. Demarco, J. a. E. Manson, U. Betz, M.F. Escola, et al., Mechanical integrity of transparent conductive oxide films for flexible polymer-based displays, Thin Solid Films. 460 (2004) 156–166.
[88] M. Ohring, The materials science of thin films, Academic Press, San Diego, 1992.
[89] P. Tsung, T. Chang, B. Hsiung, C. Jen, J. Fin, Structural and mechanical properties of pre-strained transparent conducting oxide films on fl exible substrate, Surf. Coat. Technol. 231 (2012) 443–446.
[90] Y.C. Lin, W.Q. Shi, Z.Z. Chen, Effect of deflection on the mechanical and optoelectronic properties of indium tin oxide films deposited on polyethylene terephthalate substrates by pulse magnetron sputtering, Thin Solid Films. 517 (2009) 1701–1705.
[91] P.C.P. Bouten, P.J. Slikkerveer, Y. Leterrier, Mechanics of ITO on Plastic Substrates for Flexible Displays, in: G. P. Crawford (Ed.), Flex. Flat Panel Displays, John Wiley & Sons Ltd, Chichester, 2005: pp. 99–120.
[92] Z. Chen, B. Cotterell, W. Wang, The fracture of brittle thin films on compliant substrates in flexible displays, Eng. Fract. Mech. 69 (2002) 597–603.
[93] Z. Suo, Fracture in Thin Films, Encycl. Mater. Sci. Technol. 2nd Ed. Elsevier Sci. (2001) 1–17.
[94] R. Huang, J.H. Prevost, Z.Y. Huang, Z. Suo, Channel-cracking of thin films with the extended finite element method, Eng. Fract. Mech. 70 (2003) 2513–2526.
[95] Z. Chen, B. Cotterell, W. Wang, E. Guenther, S. Chua, A mechanical assessment of flexible optoelectronic devices, Thin Solid Films. 394 (2001) 202–206.
[96] K. a. Sierros, D. a. Banerjee, N.J. Morris, D.R. Cairns, I. Kortidis, G. Kiriakidis, Mechanical properties of ZnO thin films deposited on polyester substrates used in flexible device applications, Thin Solid Films. 519 (2010) 325–330.
[97] J.H. Waller, L. Lalande, Y. Leterrier, J. a. E. Manson, Modelling the effect of temperature on crack onset strain of brittle coatings on polymer substrates, Thin Solid Films. 519 (2011) 4249–4255.

[98] Y. Leterrier, A. Pinyol, D. Gillieron, J. a. E. Manson, P.H.M. Timmermans, P.C.P. Bouten, et al., Mechanical failure analysis of thin film transistor devices on steel and polyimide substrates for flexible display applications, Eng. Fract. Mech. 77 (2010) 660–670.
[99] G. Rochat, Y. Leterrier, P. Fayet, J. a. . Manson, Mechanical analysis of ultrathin oxide coatings on polymer substrates in situ in a scanning electron microscope, Thin Solid Films. 437 (2003) 204–210.
[100] M.J. Cordill, O. Glushko, B. Putz, Electro-Mechanical Testing of Conductive Materials Used in Flexible Electronics, Front. Mater. 3 (2016) 1–11.
[101] Y. Leterrier, L. Boogh, J. Andersons, J. a. E. Manson, Adhesion of silicon oxide layers on poly(ethylene terephthalate). I: Effect of substrate properties on coating's fragmentation process, J. Polym. Sci. Part B Polym. Phys. 35 (1997) 1449–1461.
[102] Y. Leterrier, J. Andersons, Y. Pitton, J.A.E. Manson, Adhesion of Silicon Oxide Layers on Poly (ethylene terephthalate). II : Effect of Coating Thickness, J. Polym. Sci. Part B Polym. Phys. 35 (1997) 1463–1472.
[103] Kelly A., W.R. Tyson, Tensile properties of fibre-reinforced and metals: copper/tungsten and copper/molybdenum, J. Mech. Phys. Solids. 13 (1965) 329–350.
[104] D.R. Cairns, R.P. Witte, D.K. Sparacin, S.M. Sachsman, D.C. Paine, G.P. Crawford, et al., Strain-dependent electrical resistance of tin-doped indium oxide on polymer substrates, Appl. Phys. Lett. 76 (2000) 1425.
[105] H. Changji, H. Zhenhui, F. Weichun, Z. Qi, Influence of deposition pressure on the adhesion of ZnO thin films deposited by cathodic vacuum arc deposition on polyimide foil substrates, J. Phys. D. Appl. Phys. 42 (2009) 185303.
[106] E.H. Kim, C.W. Yang, J.-W. Park, Improving the delamination resistance of indium tin oxide (ITO) coatings on polymeric substrates by O2 plasma surface treatment, Curr. Appl. Phys. 10 (2010) S510–S514.
[107] C.W. Yang, J.W. Park, The cohesive crack and buckle delamination resistances of indium tin oxide (ITO) films on polymeric substrates with ductile metal interlayers, Surf. Coatings Technol. 204 (2010) 2761–2766.
[108] B.J. Kim, K.Y. Park, J.H. Ahn, Y.J. Kim, Numerical Design of SiO2 Bridges in Stretchable Thin Film Transistors, Jpn. J. Appl. Phys. 51 (2012) 01AG–10.
[109] S. Zhang, D. Sun, Y. Fu, H. Du, Toughness measurement of thin films: a critical review, Surf. Coatings Technol. 198 (2005) 74–84.
[110] H. Gleskova, S. Wagner, Z. Suo, a-Si : H thin film transistors after very high strain, J. Non. Cryst. Solids. 269 (2000) 1320–1324.
[111] K. Ramji, D.R. Cairns, K. a. Sierros, S.N. Kukureka, 65.4: Stress Corrosion Cracking of Patterned Indium Tin Oxide Electrodes for Flexible Displays, SID Symp. Dig. Tech. Pap. 38 (2007) 1790.
[112] T.S. Bejitual, N.J. Morris, D.R. Cairns, K. a. Sierros, Controlled buckling behavior of patterned oxide structures on compliant substrates for flexible optoelectronics, Thin Solid Films. 549 (2013) 268–275.
[113] J.L. Ni, X.F. Zhu, Z.L. Pei, J. Gong, C. Sun, G.P. Zhang, Comparative investigation of fracture behaviour of aluminium-doped ZnO films on a flexible substrate, J. Phys. D. Appl. Phys. 42 (2009) 175404(7pp).
[114] K.H. Cherenack, N.S. Munzenrieder, G. Troster, Impact of mechanical bending on ZnO and IGZO thin-film transistors, IEEE Electron Device Lett. 31 (2010) 1254–1256.
[115] N. Munzenrieder, K.H. Cherenack, G. Troster, S. Member, A.I. Tfts, The Effects of Mechanical Bending and Illumination on the Performance of Flexible IGZO TFTs,

IEEE Trans. Electron Devices. 58 (2011) 2041–2048.
[116] S.A. Khan, Amorphous Metal-Oxide Based Thin Film Transistors on Metal Foils : Materials , Devices and Circuits Integration Amorphous Metal-Oxide Based Thin Film Transistors on, PhD thesis, Lehigh University, 2012.
[117] J.W. Lim, S.I. Oh, K. Eun, S.H. Choa, H.W. Koo, T.W. Kim, et al., Mechanical Flexibility of ZnSnO/Ag/ZnSnO Films Grown by Roll-to-Roll Sputtering for Flexible Organic Photovoltaics, Jpn. J. Appl. Phys. 51 (2012) 115801.
[118] S.H. Choa, C.K. Cho, W.J. Hwang, K.T. Eun, H.K. Kim, Mechanical integrity of flexible InZnO/Ag/InZnO multilayer electrodes grown by continuous roll-to-roll sputtering, Sol. Energy Mater. Sol. Cells. 95 (2011) 3442–3449.
[119] S. Jung, K. Lim, J.W. Kang, J.K. Kim, S.I. Oh, K. Eun, et al., Electromechanical properties of indium–tin–oxide/poly(3,4-ethylenedioxythiophene): Poly(styrenesulfonate) hybrid electrodes for flexible transparent electrodes, Thin Solid Films. 550 (2014) 435–443.
[120] J.W. Lim, D.Y. Cho, K. Eun, S.H. Choa, S.I. Na, J. Kim, et al., Mechanical integrity of flexible Ag nanowire network electrodes coated on colorless PI substrates for flexible organic solar cells, Sol. Energy Mater. Sol. Cells. 105 (2012) 69–76.
[121] J.M. Gere, S.P. Timoshenko, Mechanics of Materials, Stanley Thornes, Cheltenham, 1999.
[122] C. LeChat, A. Bunsell, P. Davies, A. Piant, Mechanical behaviour of polyethylene terephthalate and polyethylene naphthalate under cyclic loading, J. Mater. Sci. 41 (2006) 1745–1756.
[123] S.P. Gorkhali, D.R. Cairns, G.P. Crawford, Reliability of transparent conducting substrates for rollable displays: A cyclic loading investigation, J. Soc. Inf. Disp. 12 (2004) 45–49.
[124] K. Alzoubi, M.M. Hamasha, S. Lu, B. Sammakia, Bending Fatigue Study of Sputtered ITO on Flexible Substrate, J. Disp. Technol. 7 (2011) 593–600.
[125] J.S. Hsu, C.C. Lee, B. j. Wen, P.C. Huang, C. k. Xie, Experimental and Simulated Investigations of Thin Polymer Substrates with an Indium Tin Oxide Coating under Fatigue Bending Loadings, Materials (Basel). 9 (2016) 1–13.
[126] Q. Chen, L. Xu, A. Salo, G. Neto, G. Freitas, Reliability study of flexible display module by experiments, in: 2008 Int. Conf. Electron. Packag. Technol. High Density Packag., Ieee, 2008: pp. 1–6.
[127] C.K. Cho, W.J. Hwang, K. Eun, S.H. Choa, S.I. Na, H.K. Kim, Mechanical flexibility of transparent PEDOT:PSS electrodes prepared by gravure printing for flexible organic solar cells, Sol. Energy Mater. Sol. Cells. 95 (2011) 3269–3275.
[128] K. Alzoubi, S. Lu, B. Sammakia, M. Poliks, Experimental and Analytical Studies on the High Cycle Fatigue of Thin Film Metal on PET Substrate for Flexible Electronics Applications, IEEE Trans. Components, Packag. Manuf. Technol. 1 (2011) 43–51.
[129] C.-T. Chu, P.D. Fuqua, J.D. Barrie, Corrosion characterization of durable silver coatings by electrochemical impedance spectroscopy and accelerated environmental testing., Appl. Opt. 45 (2006) 1583–93.
[130] E. Ando, S. Suzuki, N. Aomine, M. Miyazaki, M. Tada, Sputtered silver-based low-emissivity coatings with high moisture durability, Vacuum. 59 (2000) 792–799.
[131] K. Koike, F. Yamazaki, T. Okamura, S. Fukuda, Improvement of corrosion resistance of transparent conductive multilayer coating consisting of silver layers and transparent metal oxide layers, J. Vac. Sci. Technol. A Vacuum, Surfaces, Film. 25 (2007) 527.
[132] S. J. Nadel, Durability of Ag based low emissivity coatings, J. Vac. Sci. Technol. A. 5

(1987) 2709–2713.
[133] E. Ando, M. Miyazaki, Moisture degradation mechanism of silver-based low-emissivity coatings, Thin Solid Films. 351 (1999) 308–312.
[134] E. Ando, M. Miyazaki, Moisture resistance of the low-emissivity coatings with a layer structure of Al-doped ZnO/Ag/Al-doped ZnO, Thin Solid Films. 392 (2001) 289–293.
[135] S.W. Chen, C.H. Koo, H.E. Huang, C.H. Chen, Ag–Ti Alloy Used in ITO–Metal–ITO Transparency Conductive Thin Film with Good Durability against Moisture, Mater. Trans. 46 (2005) 2536–2540.
[136] S.W. Chen, C.Y. Bai, C.C. Jain, C.-J. Zhan, C.-H. Koo, Durability of Indium Tin Oxide-Silver-Indium Tin Oxide Films against Moisture Investigated Through The Wettability of The Top Oxide Layer, Mater. Trans. 48 (2007) 2230–2234.
[137] K.A. Sierros, N.J. Morris, K. Ramji, D.R. Cairns, Stress–corrosion cracking of indium tin oxide coated polyethylene terephthalate for flexible optoelectronic devices, Thin Solid Films. 517 (2009) 2590–2595.
[138] M.M. Hamasha, Reliability of Thin Films for Solar Photovoltaic Applications, PhD thesis, Binghamton University, 2011.
[139] T.S. Bejitual, D. Compton, K.A. Sierros, D.R. Cairns, S.N. Kukureka, Electromechanical reliability of flexible transparent electrodes during and after exposure to acrylic acid, Thin Solid Films. 528 (2013) 229–236.
[140] DuPont Teijin Films, Wilton, Middlesbrough, UK, TS90 8JF. (n.d.).
[141] A. Kiani, D.G. Hasko, W.I. Milne, A.J. Flewitt, Analysis of amorphous indium-gallium-zinc-oxide thin-film transistor contact metal using Pilling-Bedworth theory and a variable capacitance diode model, Appl. Phys. Lett. 102 (2013) 1–5.
[142] N.M. Alves, J.L. Gomez Ribelles, J.F. Mano, Study of the viscoelastic properties of PET by thermally stimulated recovery, Plast. Rubber Compos. 32 (2003) 281–290.
[143] http://www.kazuli.com/UW/4A/ME534/lexan2.htm, (2003).
[144] C.K. Huang, W.M. Lou, C.J. Tsai, T.C. Wu, H.Y. Lin, Mechanical properties of polymer thin film measured by the bulge test, Thin Solid Films. 515 (2007) 7222–7226.
[145] R. A. Alizadeh, Nanostructure and Engineering Properties of Basic and Modified Calcium-Silicate-Hydrate Systems, PhD thesis,University of Ottawa, 2009.
[146] R. Verdejo, Gas Loss and Durability of EVA foams used in Running Shoes, PhD thesis,University of Birmingham, 2003.
[147] D.M.Pnnico, Novel flexible pvc compounds characterized by improved sustainability and reduced plasticizer migration, PhD thesis,University of Naples, 2010.
[148] X. Zhu, B. Zhang, J. Gao, G. Zhang, Evaluation of the crack-initiation strain of a Cu–Ni multilayer on a flexible substrate, Scr. Mater. 60 (2009) 178–181.
[149] B. Balakrisnan, C.C. Chum, M. Li, Z. Chen, T. Cahyadi, Fracture toughness of Cu-Sn intermetallic thin films, J. Electron. Mater. 32 (2003) 166–171.
[150] S.J. Britvec, The Stability of Elastic Systems, Pergamon Press, New-York, NY, 1973.
[151] A.Rajakutty, Static and dynamic mechanical properties of amorphous recycled poly-(ethylene terepthalate), Master thesis, Anna University, 2010.
[152] Seawater, (2016). https://en.wikipedia.org/wiki (accessed July 28, 2016).
[153] http://www.arduino.cc, (2016).
[154] J. M. Boyea, Polystyrene composites filled with multi-wall carbon nanotubes and indium tin oxide nanopowders: properties, fabrication, characterization, Master thesis, Georgia Institute of Technology, 2010.
[155] https://www.jic.ac.uk/microscopy/more/T5_8.htm, (2016).

[156] L.E. Nielsen, Mechanical Properties of Polymers and Composites, Second Edi, New York: Dekker., 1974.
[157] G. Schoukens, P. Samyn, S. Maddens, T. Van Audenaerde, Shrinkage behavior after the heat setting of biaxially stretched poly(ethylene 2,6-naphthalate) films and bottles, J. Appl. Polym. Sci. 87 (2003) 1462–1473.
[158] B.D. Beake, G.J. Leggett, P.H. Shipway, Tapping mode and phase imaging of biaxially oriented polyester films, Surf. Interface Anal. 31 (2001) 39–45.
[159] M. Benmalek, H.M. Dunlop, Inorganic coatings on polymers, Surf. Coatings Technol. 76-77 (1995) 821–826.
[160] F. Dinelli, H.E. Assender, K. Kirov, O. V Kolosov, Surface morphology and crystallinity of biaxially stretched PET films on the nanoscale, Polymer (Guildf). 41 (2000) 4285–4289.
[161] D.W.H. Ian Macmillan Ward, An introduction to the mechanical properties of solid polymers, Wiley & Sons, 1993.
[162] D. Lukkassen, A. Meidell, Advanced Materials and Structures and their Fabrication Processes, 2007.
[163] C.S. Lin, T.L. Horng, J.H. Chen, K.H. Chen, J.J. Wu, C.Y. Chen, et al., Mechanical Properties Measurement of Polymer Films by Bulge Test and Fringe Projection, Adv. Mater. Sci. Eng. (2014) 1–12.
[164] J. Scheirs, Compositional and Failure Analysis of Polymers: A Practical Approach, John Wiley & Sons Ltd, Chichester, 2000.
[165] A. Kiani, D.G.Hasko, W. I. Milne and A. J. Flewitt., Analysis of amorphous indium-gallium-zinc-oxide thin-film transistor contact metal using Pilling-Bedworth theory and a variable capacitance diode model, Appl. Phys. Lett. 102 (2013) 0–5.
[166] A. Dhar and T. L. Alford, High Mobility IGZO/ITO Double-layered Transparent Composite Electrode: A Thermal Stability Study, Mater. Res. Soc. 1577 (2013) 0–5.
[167] C.J. Chiu, S.P. Chang, S.J. Chang, High-performance amorphous indium–gallium–zinc oxide thin-film transistors with polymer gate dielectric, Thin Solid Films. 520 (2012) 5455–5458.
[168] N. Nomuram, T. Akihiro, K. Toshio, O. Hiromichi, H. Masahiro and H. Hideo, Amorphous oxide semiconductors for high-performance flexible thin-film transistors, Jpn. J. Appl. Phys. 45 (2006) 4303–4308.
[169] H. Klauk, M. Halik, U. Zschieschang, F. Eder and G. Schmid, Pentacene organic transistors and ring oscillators on glass and on flexible polymeric substrates, Appl. Phys. Lett. 82 (2003) 4175.
[170] A. Dhar, Z. Zhao and T. alford., Effect of Different Substrates on the Wettability and Electrical Properties of Au Thin Films Deposited by Sputtering, J. Miner. Mater. Soc. 67 (2015) 845–848.
[171] C. Ji-Hyuk, S. Hyun and, M. Jae-Min, Dual-Gate InGaZnO Thin-Film Transistors with Organic Polymer as a Dielectric Layer, Electrochem. Solid-State Lett. 12 (2009) H145.
[172] Y. Leterrier, P. Sutter, J. a. E. Manson, Thermodynamic and Micromechanical Approaches to the Adhesion between Polyethylene Terephthalate and Silicon Oxide, J. Adhes. 69 (1999) 13–30.
[173] D. Compton, Effects of acrylic acid on ITO coated polymer substrates for flexible displays, MRes thesis,University of Birmingham, 2012.
[174] L. Rebouta, L. Rubio Pena, C. Oliveira, S. Lanceros-Mendez, C.J. Tavares, E. Alves, Strain dependence electrical resistance and cohesive strength of ITO thin films deposited on electroactive polymer, Thin Solid Films. 518 (2010) 4525–4528.

[175] E. Fortunato, P. Nunes, A. Marques, D. Costa, H. Aguas, I. Ferreira, et al., Transparent , conductive ZnO : Al thin film deposited on polymer substrates by RF magnetron sputtering, Surf. Coatings Technol. 152 (2002) 247–251.
[176] G. Rochat, A. Delachaux, Y. Leterrier, J. a E. Manson, P. Fayet, Influence of substrate morphology on the cohesion and adhesion of thin PECVD oxide films on semi-crystalline polymers, Surf. Interface Anal. 35 (2003) 948–952.
[177] L. B Freund and S. Suresh, Thin Film Materials Stress, Defect Formation and Surface Evolution, Cambridge: Cambridge University Press, 2003.
[178] D. Tsubone, T. Hasebe, A. Kamijo, A. Hotta, Fracture mechanics of diamond-like carbon (DLC) films coated on flexible polymer substrates, Surf. Coatings Technol. 201 (2007) 6423–6430.
[179] H.U. Rehman, F. Ahmed, C. Schmid, J. Schaufler, K. Durst, Study on the deformation mechanics of hard brittle coatings on ductile substrates using in-situ tensile testing and cohesive zone FEM modeling, Surf. Coatings Technol. 207 (2012) 163–169.
[180] Y. Leterrier, A. Mottet, N. Bouquet, D. Gillieron, P. Dumont, A. Pinyol, et al., Mechanical integrity of thin inorganic coatings on polymer substrates under quasi-static, thermal and fatigue loadings, Thin Solid Films. 519 (2010) 1729–1737.
[181] Y. S. Kim, S. I. oh, and S. H. Choa, Mechanical Integrity of Flexible In – Zn – Sn – O Film for Flexible Transparent Electrode, Jpn. J. Appl. Phys. 52 (2013) 05DA17.
[182] D. Bernoulli, K. Fliger, K. Thorwarth, G. Thorwarth, R. Hauert, R. Spolenak, Cohesive and adhesive failure of hard and brittle films on ductile metallic substrates: A film thickness size effect analysis of the model system hydrogenated diamond-like carbon (a-C:H) on Ti substrates, Acta Mater. 83 (2015) 29–36.
[183] S. Frank, U. a. Handge, S. Olliges, R. Spolenak, The relationship between thin film fragmentation and buckle formation: Synchrotron-based in situ studies and two-dimensional stress analysis, Acta Mater. 57 (2009) 1442–1453.
[184] F. Ahmed, Deformation and Damaging Mechanisms in Diamond Thin Films Bonded to Ductile Substrates, PhD thesis,University Erlangen-Nürnberg, 2012.
[185] Wojciechowski p. H. and Mendolia M. S., On the multiple fracture of low elongation thin films deposited on high elongation substrates, J. Vac. Sci. Technol. A. (1989) 1282.
[186] G. A. potoczny, Electro-Mechanical Behaviour of Indium Tin Oxide Coated Polymer Substrates for Flexible Electronics by, PhD thesis, University of Birmingham, 2011.
[187] X.C. Zhang, C.J. Liu, F.Z. Xuan, Z.D. Wang, S.T. Tu, Effect of residual stresses on the strength and fracture energy of the brittle film: Multiple cracking analysis, Comput. Mater. Sci. 50 (2010) 246–252.
[188] C.H. Hsueh, a. a. Wereszczak, Multiple cracking of brittle coatings on strained substrates, J. Appl. Phys. 96 (2004) 3501.
[189] H.R. Choi, S.K. Eswaran, S.M. Lee, Y.S. Cho, Enhanced Fracture Resistance of Flexible ZnO:Al Thin Films in Situ Sputtered on Bent Polymer Substrates, ACS Appl. Mater. Interfaces. 7 (2015) 17569–17572.
[190] S.H. Jen, J. a. Bertrand, S.M. George, Critical tensile and compressive strains for cracking of Al2O3 films grown by atomic layer deposition, J. Appl. Phys. 109 (2011) 084305.
[191] S. kai Lu, J. ting Huang, T. hsin Lee, J. jie Wang, D. shan Liu, Flexibility of the Indium Tin Oxide Transparent Conductive Film Deposited Onto the Plastic Substrate, Smart Sci. 2 (2014) 7–12.
[192] S.K. Park, J.I. Han, D.G. Moon, W.K. Kim, Mechanical Stability of Externally

Deformed Indium–Tin–Oxide Films on Polymer Substrates, Jpn. J. Appl. Phys. 42 (2003) 623–629.
[193] A.A. Abdallah, P.C.P. Bouten, J.M.J. den Toonder, G. De With, Buckle initiation and delamination of patterned ITO layers on a polymer substrate, Surf. Coatings Technol. 205 (2011) 3103–3111.
[194] M.M. Hamasha, K. Alzoubi, J.C. Switzer, S. Lu, S.B. Desu, M. Poliks, A study on crack propagation and electrical resistance change of sputtered aluminum thin film on poly ethylene terephthalate substrate under stretching, Thin Solid Films. 519 (2011) 7918–7924.
[195] B. Sim, E.H. Kim, J. Park, M. Lee, Highly enhanced mechanical stability of indium tin oxide film with a thin Al buffer layer deposited on plastic substrate, Surf. Coatings Technol. 204 (2009) 309–312.
[196] F.M. Lopez, R.E. De Araujo, M. Jarrier, J. Courbat, D. Briand, N.F. De Rooij, Study of bending reliability and electrical properties of platinum lines on flexible polyimide substrates, Microelectron. Reliab. 54 (2014) 2542–2549.
[197] D.R. Cairns, G.P. Crawford, Electromechanical Properties of Transparent Conducting Substrates for Flexible Electronic Displays, Proc. IEEE. 93 (2005) 1451–1458.
[198] T. Koniger and H. Munstedt, Coatings of indium tin oxide nanoparticles on various flexible polymer substrates: Influence of surface topography and oscillatory bending on electrical properties, J. Soc. Inf. Disp. 16 (2008) 559–568.
[199] Y.S. Park, H.K. Kim, S.W. Kim, Thin Ag Layer Inserted GZO Multilayer Grown by Roll-to-Roll Sputtering for Flexible and Transparent Conducting Electrodes, J. Electrochem. Soc. 157 (2010) J301.
[200] K. Hu, Z.H. Cao, L. Wang, Q.W. She, X.K. Meng, The Anomalous Temperature Effect on the Ductility of Nanocrystalline Cu Films Adhered to Flexible Substrates, Chinese Phys. Lett. 30 (2013) 076201.
[201] K. Alzoubi, M.M. Hamasha, L. Wang, H. Zhang, J. Yin, J. Luo, et al., Stability of interdigitated microelectrodes of flexible chemiresistor sensors, IEEE/OSA J. Disp. Technol. 8 (2012) 377–384.
[202] Y. Shigesato, R. Koshiishi, T. Kawashima, J. Ohsako, Early stages of ITO deposition on glass or polymer substrates, Vacuum. 59 (2000) 614–621.
[203] J. Jeong, H. Kim, Low resistance and highly transparent ITO–Ag–ITO multilayer electrode using surface plasmon resonance of Ag layer for bulk-heterojunction organic solar cells, Sol. Energy Mater. Sol. Cells. 93 (2009) 1801–1809.
[204] C. Guillen, J. Herrero, Transparent conductive ITO/Ag/ITO multilayer electrodes deposited by sputtering at room temperature, Opt. Commun. 282 (2009) 574–578.
[205] Y. Kim, W. Lee, D.-R. Jung, J. Kim, S. Nam, H. Kim, et al., Optical and electronic properties of post-annealed ZnO:Al thin films, Appl. Phys. Lett. 96 (2010) 171902.
[206] E. X. Zou, Sol-gel Processed Zinc Oxide for Third Generation Photovoltaics, PhD thesis, University of Oxford, 2012.
[207] M.S. Tokumoto, A. Smith, C. V. Santilli, S.H. Pulcinelli, A.F. Craievich, E. Elkaim, et al., Structural electrical and optical properties of undoped and indium doped ZnO thin films prepared by the pyrosol process at different temperatures, Thin Solid Films. 416 (2002) 284–293.
[208] M. Yang, M.W. Chon, J.H. Kim, S.H. Lee, J. Jo, J. Yeo, et al., Mechanical and environmental durability of roll-to-roll printed silver nanoparticle film using a rapid laser annealing process for flexible electronics, Microelectron. Reliab. 54 (2014) 2871–2880.

[209] F.C. Krebs, S.A. Gevorgyan, J. Alstrup, A roll-to-roll process to flexible polymer solar cells: model studies, manufacture and operational stability studies, J. Mater. Chem. 19 (2009) 5442.
[210] D.P. Wang, F.Y. Biga, A. Zaslavsky, G.P. Crawford, Electrical resistance of island-containing thin metal interconnects on polymer substrates under high strain, J. Appl. Phys. 98 (2005) 48–51.
[211] S.H. Cho, W.J. Lee, Effect of added metallic elements in Ag alloys on the durability against heat and humidity of indium zinc oxide/Ag alloy/indium zinc oxide transparent conductive multilayer system, Jpn. J. Appl. Phys. 49 (2010).
[212] D.R. Sahu, J.L. Huang, Design of ZnO/Ag/ZnO multilayer transparent conductive films, Mater. Sci. Eng. B. 130 (2006) 295–299.
[213] K. Koike, K. Shimada, S. Fukuda, Aggregation in thin-film silver: Induced by chlorine and inhibited by alloying with two dopants, Corros. Sci. 51 (2009) 2557–2564.
[214] T.S. Bejitual, Reliability of flexible optoelectronic device electrodes, PhD thesis, West Virginia University, 2013.
[215] Y. Leterrier, Durability of nanosized oxygen-barrier coatings on polymers, Prog. Mater. Sci. 48 (2003) 1–55.
[216] A.A. Volinsky, P. Waters, Mechanical Self-Assembly, Springer New York, New York, NY, 2013.
[217] S. Nam, M. Song, D.H. Kim, B. Cho, H.M. Lee, J.D. Kwon, et al., Ultrasmooth, extremely deformable and shape recoverable Ag nanowire embedded transparent electrode., Sci. Rep. 4 (2014) 4788.
[218] M. Yang, M.W. Chon, J.H. Kim, S.H. Lee, J. Jo, J. Yeo, et al., Mechanical and environmental durability of roll-to-roll printed silver nanoparticle film using a rapid laser annealing process for flexible electronics, Microelectron. Reliab. (2014).
[219] M. a Yaklin, D. a Schneider, K. Norman, J.E. Granata, C.L. Staiger, Impacts of Humidity and Temperature on the Performance of Transparent Conducting Zinc Oxide, Photovolt. Spec. Conf. (PVSC), 2010 35th IEEE. (2010) 002493–002496.
[220] M.L. and M.R.W. A. S. da Silva Sobrinho, G. Czeremuszkin, Defect-permeation correlation for ultrathin transparent barrier coatings on polymers, J. Vac. Sci. Technol. 18 (2000) 149.
[221] D.S. Hecht, L. Hu, G. Irvin, Emerging transparent electrodes based on thin films of carbon nanotubes, graphene, and metallic nanostructures., Adv. Mater. 23 (2011) 1482–513.

10. Appendix A - Publications

1. Published in *Thin Solid Films,* 594 (2015) 197–204

Journal manuscript

Mechanical properties of amorphous indium–gallium–zinc oxide thin films on compliant substrates for flexible optoelectronic devices

D. W. Mohammed [a*], R. Waddingham [b], A. J. Flewitt [b], K. A. Sierros [c], J. Bowen [d] and S. N. Kukureka[a]

[a] University of Birmingham, School of Metallurgy and Materials, Edgbaston, Birmingham, B15 2TT, United Kingdom.

[b] University of Cambridge, Electrical Engineering Division, Department of Engineering, J J Thomson Avenue, Cambridge CB3 0FA, United Kingdom.

[c] West Virginia University Mechanical & Aerospace Engineering, Morgantown, WV 26506, USA.

[d] Open University, Department of Engineering and Innovation, Walton Hall, Milton Keynes, MK7 6AA, United Kingdom.

Corresponding author:

Dilveen Mohammed

E-mail: DWM172@bham.ac.uk, Dilveen@uod.ac

Abstract

Amorphous indium–gallium–zinc-oxide (a-IGZO) thin films were deposited using RF magnetron sputtering on polyethylene naphthalate (PEN) and polyethylene terephthalate (PET) flexible substrates and their mechanical flexibility investigated using uniaxial tensile and buckling tests coupled with *in situ* optical microscopy. The uniaxial fragmentation test demonstrated that the crack onset strain of the IGZO/PEN was ~2.9%, which is slightly higher than that of IGZO/PET. Also, uniaxial tensile crack density analysis suggests that the saturated crack spacing of the film is strongly dependent on the mechanical properties of the underlying polymer substrate. Buckling test results suggest that the crack onset strain (equal to ~ 1.2%, of the IGZO/polymer samples flexed in compression to ~ 5.7 mm concave radius of curvature) is higher than that of the samples flexed with the film being in tension (convex bending) regardless whether the substrate is PEN or PET. The saturated crack density of a-IGZO film under the compression buckling mode is smaller than that of the film under the tensile buckling mode. This could be attributed to the fact that the tensile stress encouraged this crack formation originating from surface defects in the coating. It could also be due to the buckling delamination of the thin coating from the substrate at a lower strain than that at which a crack initiates during flexing in compression. These results provide useful information on the mechanical reliability of a-IGZO films for the development of flexible electronics.

Keywords: Polymer substrates, IGZO, PEN, PET, flexible optoelectronic devices, mechanical properties

1. Introduction

Electronic devices fabricated on flexible plastic substrates are expected to find a variety of new applications due to their attractive advantages, such as being mechanically robust, light weight and potentially having simple roll-to-roll-based fabrication and mass production [1,2]. Transparent oxide semiconductors, such as zinc oxide (ZnO), gallium-doped zinc oxide (GZO), indium tin oxide (ITO), zinc tin oxide (ZTO), and indium gallium zinc oxide (IGZO) have attracted many researchers with their large potential in flexible optoelectronic applications, such as transparent electrodes in solar cells, rollable displays, and channel layers in transparent thin film transistors TTFTs [1,3], because of the capability of large-area, uniform deposition at low temperatures [4]. In particular, IGZO has drawn considerable attention as an extremely promising alternative to hydrogenated amorphous silicon (a-Si:H) for thin-film transistors (TFTs) due to its high electron mobility, processing compatibility with plastic substrates, good-uniformity and high transparency in the visible wavelength region (400 - 700 nm) [4,5]

Polyethylene terephthalate (PET) and polyethylene naphthalate (PEN) have been widely used as the base substrates in the fabrication of flexible optoelectronic devices. This is due to their satisfactory optical transmittance, mechanical flexibility, light weight, transparency, low cost and ability to be manufactured through roll-to-roll processing. However, due to the low melting point of the polymers, transparent oxides must be fabricated on polymer substrates at a lower deposition temperature. The RF magnetron sputtering technique is one of the most commonly used methods to deposit a-IGZO thin films on flexible substrates at room temperature [6]. Many research groups have reported using radio frequency (r.f.) sputtering to fabricate a-IGZO layers for use in thin film transistors (TFTs) on flexible substrates [6].

However, transparent conducting oxide films are brittle by nature, and susceptible to cracking and/or buckling delamination under externally applied mechanical deformation, which significantly limits the flexibility of the devices [7]. Consequently, failure behaviour of the films under various loading modes such as stretching, bending, or twisting becomes a critical issue during both manufacturing processes and in service conditions [8]. Hence, this gives rise to the motivation for predicting the onset of failure such as critical strain and critical radius of curvature to provide this information to optoelectronic device designers.

Uniaxial tensile and buckling tests, coupled with *in situ* optical microscopy are commonly used to determine the failure strains of thin coatings adhering to a compliant substrate, where cracks first initiate, as well as any subsequent buckling and delamination that may occur [9]. For example, the mechanical behaviour of ZnO coated polymer substrates was investigated under compression tests by Sierros *et al*. and the critical onset strain for cracking was found to be approximately 2% [10]. Chen *et al.* [11] reported buckling experiments carried out on ITO, reporting that the crack onset strain (COS) of the film under tension at 1.1% was less than its value under compression. In addition, Ni *et al.* [12] investigated the fracture properties of AZO-coated on PET substrates under simple-support bending conditions. It was reported that the coating damage, under tensile strain, is caused by the creation of channel cracks, while under compression the film specimen may first delaminate from the polymer substrate and then buckle before the initiation of a crack. They explained that in tension, on the outer surface, the stored elastic energy went solely into crack formation; however, in compression the elastic energy was distributed between crack formation and delamination, so the crack density is usually lower for bend-testing on the compression side.

However, relatively little research to date has been reported about the mechanical behaviour of a-IGZO coated on polymers. Cherenack *et al.* [2] Investigated the performance of amorphous thin film transistors (a-IGZO) under mechanical bending. It was pointed out that the films can be flexed down to 10 mm radius of bending curvature and, still, can remain functional. Also Munzenrieder [13] investigated the behaviour of a-IGZO TFTs on flexible substrates under tensile and compressive stress conditions. It was found that the mechanical stress has considerable impact on the TFT mobility and threshold voltage. Gleskova *et al.* [14], demonstrated that the amorphous silicon TFTs fabricated on polyimide foil can be strained more in compression than in tension. No mechanical failure was noted in compression for strains smaller than 2%, while in tension, mechanical failure was found at a strain of 0.5%. They also pointed out that the failure mode was the formation of periodic cracks perpendicular to the straining direction. Such cracks interrupt the current path if the source-drain current path and the strain direction are parallel.

In this work, we report on the mechanical flexibility of a-IGZO thin film grown on PET and PEN substrates via RF magnetron sputtering at room temperature for use in flexible optoelectronics. We utilize two different polyesters in an effort to elucidate the effect(s) of the underlying substrate on the resulting mechanical performance of the sputtered films since the applied stresses are transferred from the substrate to the coating through the interface. We examined the mechanical integrity of a-IGZO by using uniaxial tensile fragmentation and buckling tests coupled with *in situ* optical microscopy to further understand the failure mechanism under different mechanical deformation modes. Although the performance of the coated substrates will be modified once they are in a complete device, with potentially several other layers above or below, an understanding of the mechanical properties of the IGZO/polymer layers remains of fundamental importance.

2. Experimental Procedure

The polymer substrates used were two semi-crystalline polyesters, 0.125 mm thick polyethylene terephthalate (PET Melinex ST 504) and 0.125 mm thick polyethylene naphthalate (PEN Teonex Q65FA). Samples of both were supplied in the form of A4 sheet (DuPont Teijin Films, UK). Thermal and mechanical properties of both substrates were measured by using differential scanning calorimetry and uniaxial tension (Instron 4410) respectively. a-IGZO film of thickness ~50nm was deposited on to polymer substrates using RF magnetron sputtering from a In_2O_3:Ga_2O_3:ZnO (1:1:1) target (99.99% purity), the samples having a dog-bone shape (50 mm length , with 18 mm gauge length and 4 mm gauge width). The substrates were cut from sheets using a Moore Hydraulic Press. Prior to introduction inside the sputtering chamber, the polymer substrates were ultrasonically cleaned in acetone, ethanol, and then in deionized water for 5 min each. Deposition was performed (without heating the substrate) in an argon atmosphere and without an oxygen feed. A 4-inch diameter ceramic target, 20 cm from the substrate, was used under a base pressure of $5.1x10^{-6}$ Pa; constant RF power of 55 W; deposition pressure of 0.5 Pa; power density of 0.7 W/cm^2; Ar flow rate of 50 sccm (sccm denotes standard cubic centimeter per minute at STP conditions) and deposition rate of ~3.3 nm/min. In order to remove contaminant on the surface of the target, the a-IGZO target was pre-sputtered for 5 min before the deposition of the film. The optical transmittance of the films was measured in the visible range from 400 to 800 nm using a Jenway 6310 spectrophotometer. Moreover, X-ray diffraction was used to examine the structural properties of the a-IGZO films. The IGZO deposition conditions were previously optimised to produce thin film transistors with a high mobility, low threshold voltage and large switching ratio. Examples of TFT characteristics have been reported previously in [15].

The mechanical flexibility of the a-IGZO films deposited on the polymer substrate was evaluated by uniaxial tensile and buckling tests. The uniaxial fragmentation test was performed using a Miniature Materials testing machine. The test was coupled with *in situ* optical microscopy; images were taken every 3 seconds during the test in order to monitor the critical onset strain and development of the cracking of thin film as the applied tensile strain increases. Equipment originally designed to determine the critical failure strain of optical fibres was slightly modified to test the a-IGZO/polymer samples. Fig. 1 shows the experimental set-up used in this case. The sample is clamped between the two parallel plates, where one plate is movable, while the other plate is fixed. The distance between the two parallel plates was measured using a side-view digital imaging system and image analysis software (Image J). Crack initiation and propagation were carefully monitored by using confocal microscopy. *In situ* optical observation was used as a simple and effective way to determine the crack-initiation strain of thin film, particularly as the film is non electrically conductive [16]. The values of the resulting strain from buckling were calculated using the following equation [17].

$$\frac{h_s}{2R} \qquad 1$$

Where R is the radius of curvature and h_s is substrate thickness.

Scanning electron microscopy (SEM) was performed to investigate the microstructure of the IGZO coatings and to characterize the cracking morphology of the a-IGZO films after testing. (The specimens were coated with a 5 nm thick Au layer before SEM investigation in order to increase their conductivity).

Atomic Force Microscopy (AFM) was employed in order to examine the coating fragmentation as a result of uniaxial straining. The atomic force microscope (JPK Instruments, UK) was operated in contact-mode conditions. Si cantilevers with a spring constant of 0.3 N/m were used with an operating frequency of 330 Hz.

3. Results and discussion

3.1 Characterisation of polymer substrate and IGZO thin film

Table 1 shows that the glass transition temperature and Young's modulus of PEN are slightly higher than those of PET due to the substitution of the phenyl ring of PET by the naphthalene double ring of PEN [18]. This indicates that the first Dundur's parameter α for PEN (~0.96) will be slightly lower than that of PET (~0.97) as determined according to Eq (2), indicating also a lower mismatch in mechanical properties of the oxide coating on a PEN substrate compared with a PET substrate.

$$\alpha = \frac{E_f + E_s}{E_f - E_s} \qquad 2$$

where E is the Young's modulus, the subscripts f and s stand for the film and the substrate, respectively. E_f is taken as 200 GPa using the rule of mixtures [19] based on separate measurements of the substrate and composite film modulus.

It is observed that both films exhibit high transparency equal to ~82% in the visible region. Fig. 2 illustrates the XRD patterns for IGZO/PEN and PEN substrate. Strong diffraction peaks in the range of 24 to 29 degrees were observed for both IGZO/PEN and PEN substrates and

corresponds to the semi-crystalline polymer substrate. The lack of any other peaks confirms the amorphous nature of the IGZO.

Inset Fig. 2 shows AFM pictures of IGZO thin films deposited on polymer substrate. The root mean square (RMS) roughness of the films was approximately 1.12 nm, the surface appearing smooth and featureless, which contributes to the high electrical performance of the proposed device [20], since surface defects are primary candidates for inducing cracks in the film under application of external stresses [21].

3.2 Uniaxial fragmentation test

Uniaxial fragmentation tests were performed in order to investigate the critical onset strain (COS) at which the IGZO-coated PET and PEN started to crack. Fig. 3 (a) and (b) show a series of representative optical microscopy images of crack progression for the IGZO coating on PEN and PET substrates, respectively. These were optically monitored *in situ* during the tensile tests. The cracks can channel across the film and may arrest at the film-substrate interface. The channel crack initiation and evolution processes in the IGZO/PEN films are quite similar to those in the IGZO/PET samples. Upon loading, the initial channel cracks begin to initiate from microscopic defects such as pinholes in the coating and surface defects on the underlying polymer substrates. The cracks then grow to span the whole sample width direction, and are propagating perpendicular to the loading direction. However, the IGZO/PEN sample exhibits a higher crack onset strain (COS) of ~ 2.9% than that IGZO/PET at ~ 2.4%. Such a slight difference in critical strain for the IGZO layer deposited on the two types of substrates may be due to the lower mechanical mismatch between the (IGZO) coating

and the PEN. Cracks grew into the thickness of the film, as can be seen in the cross-sectional view of a channel crack in Fig. 4 (b).

As the strain level increases, at almost ~6.8% and ~5.4% strain of IGZO coated PEN and PET respectively, an adhesion-related failure appears in the form of buckling of the IGZO film. Cracks on the buckle top were not visible during *in situ* optical microscopy observations indicating closed buckle delamination. However, SEM analysis confirm that there are cracks present on the top of the buckle, parallel to the applied tensile strain, and these secondary crack indicating open buckling zones, as Fig. 5(a) and (b) show. The secondary cracks and buckling of the film appear to be due to the lateral contraction mismatch between the substrate and thin film [22,23]. It is important to note that the IGZO/PEN samples have fractured at the edges of the debonded zone while for the IGZO/PET delamination is continuous except for the cracks on the buckle-top, as double sided arrows indicate in Fig. 5 (a) and (b). Also, a slightly higher adhesion level in IGZO/PEN systems is expected compared with IGZO/ PET due to the large buckling width of IGZO/PET sample, as shown in Fig. 5(b).

The cracks and buckling morphology of IGZO observed in this work are consistent with a study conducted by Frank *et al*. [24] who pointed out that the load introduced into a thin tantalum coating on a polyimide substrate during uniaxial tensile strain causes the formation of parallel cracks and at later stages lead to film buckling. The IGZO cracking was quantitatively characterized under tensile strain, in terms of crack density, defined as the number of channel cracks per unit length in the straining direction.

Fig. 6 shows the evolution of the coating crack density as a function of the applied strain for both IGZO/PEN and IGZO /PET samples. It is observed that there is a significant increase in crack density as the applied strain increases. However, with further increases in strain, the

crack density gradually saturates at certain value, above which no new cracks can form. Furthermore, it was found that the IGZO/PEN samples exhibit a higher value of saturated crack density compared with the IGZO/PET specimens. The quantitative measurements of the progression of crack density at saturation state indicate that the IGZO on a highly stiff polymer substrate develops more cracks to relax the applied tensile stress. On the other hand, if a less stiff polymer substrate is used the stress concentration can influence the debonding formation between the polymer substrate and IGZO, hence the stress is absorbed by the polymer substrate in the debonded zone. Similar observations have been demonstrated previously by Tsubone [25] for diamond-like carbon films coated on polymer substrates. The above results suggest that the crack initiation and the density of channel cracks are highly related to the Young's modulus of the polymer substrates. In general, the high mechanical reliability of a-IGZO film coated on polymer substrate is attributed to the following possible reason. There are many grains with preferred orientation in the thin film when it exhibits a polycrystalline structure, therefore is very prone to cracking due to intergranular defects in the grains under an external force [26]. However, an amorphous IGZO film delays crack initiation due to the absence of grain boundaries.

3.3 Buckling test analysis

The buckling test was used to evaluate the mechanical failure behaviour of a-IGZO films on PET substrates under both compression and tension buckling conditions. Fig.7 and Fig. 8 illustrate the development of IGZO film cracking under tension and compression buckling modes respectively. Channel cracks in IGZO/PET are observed when samples are flexed in tension down to 6.4 mm and flexed in compression down to 5.7 mm radius of curvature,

which correspond to strains of ~ 0.9 and 1.1%, respectively. Regardless of the type of deformation mode, it is noted that the number of cracks increased dramatically with an increase in applied strain. The cracks were initiated from surface defects for specimens under tension mode and then develop perpendicular to the direction of bending, which are comparable with the results obtained from uniaxial tensile experiments.

Based on the optical images, a comparison of crack density of IGZO/PET under tension and compression modes is determined and presented in Fig. 9 It is observed that the saturated crack density of the film in the tension buckling mode was significantly higher than that of the film in the compression buckling mode and the discrepancy is observed to be around 58 mm^{1}. The first reason for this might be because of surface defects such as pinholes and imperfections in the film and/or in the substrate [27]. These are also detectable in optical images of crack development of IGZO/PET sample as shown in Fig. 7(a). It illustrates crack initiation from pre-existing defects in the IGZO film under tension, which contributes to the formation of cracks in IGZO film earlier as compared with that under compression mode. Thus, it is believed that applying stresses to a specimen under compression buckling leads to closed rather than open microcracks, as also suggested by Potoczny [28]. The second reason for the discrepancy in the saturated crack density between the film under tensile and compression buckling mode is attributed to the various failure mechanisms as can be seen in Fig. 7 and Fig. 8. In particular, the cracks in IGZO film under tensile bending mode are straighter and parallel to each other while zigzag shaped cracks are observed for the IGZO film under the compression-bending mode. This is also confirmed by SEM images of cracking morphologies of IGZO film shown in Fig. 10. Fig. 10 (a) shows the IGZO/PET film after the specimen is bent in tensile bending mode to a radius of 2.7mm, which is equivalent

to a strain of 2.3%. It is observed that the IGZO film is fractured completely due to formation of channel cracks. However, coating delamination and channel cracking are observed when the specimen is bent in the compression buckling mode with the same radius of 2.7 mm, as shown in Fig. 10(b). This can be due to the contraction of the polymer substrate induced by applying stress in the compressive mode. The present findings are consistent with those found by Lu *et al*. [29] who found ITO film failures are caused by channel cracks when the sample is under tensile strain bending conditions while under compressive strain conditions the film experiences buckling delamination and cracking. The results from these experiments indicate that the film subject to tension buckling mode is more apt to fail than the film under compression buckling mode (see Section 1 and [13].)

4. Conclusions

In summary, the mechanical durability of RF–magnetron sputtered a-IGZO thin films on PEN and PET substrates was studied by using uniaxial tensile and bending tests coupled with *in situ* optical microscopy. During uniaxial tensile tests, it was found that the crack initiation strain is mostly dependent on the mechanical mismatch between the coating and substrate. High COS was observed for IGZO deposited on PEN. In addition, a relatively high value of saturation crack density was observed for IGZO film coated on PEN substrates. Furthermore, bending test results show that thin films subject to the compression buckling mode exhibit better bending durability than the films subjected to tensile buckling mode. Surface defects on thin films under the tensile mode can cause the a-IGZO film cracking to occur at strains less than those of the film under the compression buckling mode. Also, delamination of the thin film under compression from the polymer substrate can reduce the rate of crack growth.

The results of this study may provide a better understanding of the failure processes of IGZO thin films on polyesters under different deformation stress modes. This in turn is expected to aid device designers to develop the next generation of flexible optoelectronic applications.

Acknowledgments

The authors would like to thank DuPont-Teijin for donating polymer samples. We would also like to thank Mr Frank Biddlestone for his technical support and Mr Warren Hay for his help in the workshop. Financial support from the Kurdistan Regional Government HCDP program is gratefully acknowledged. The atomic force microscope used in this research was obtained, through Birmingham Science City: Innovative Uses for Advanced Materials in the Modern World (West Midlands Centre for Advanced Materials Project 2), with support from Advantage West Midlands (AWM) and partly funded by the European Regional Development Fund (ERDF). R.W. gratefully acknowledges funding from the EPSRC Centre for Doctoral Training in Photonic Systems Development.

[1] K.C. Sanal, M. Majeesh, M.K. Jayaraj, Growth of IGZO thin films and fabrication of transparent thin film transistor by RF magnetron sputtering, Proc. SPIE. 8818 (2013) 881814–3.

[2] K.H. Cherenack, N.S. Munzenrieder, G. Troster, Impact of mechanical bending on ZnO and IGZO thin-film transistors, IEEE Electron Device Lett. 31 (2010) 1254–1256.

[3] E. Fortunato, P. Barquinha, R. Martins, Oxide semiconductor thin-film transistors: A review of recent advances, Adv. Mater. 24 (2012) 2945–2986.

[4] L. Minseong, D. Joonghoe, Controlling the Electrical and the Optical Properties of Amorphous IGZO Films Prepared by Using Pulsed Laser Deposition, J. Korean Phys. Soc. 58 (2011) 492.

[5] B.K. Sharma, B. Jang, J.E. Lee, S.H. Bae, T.W. Kim, H.J. Lee, et al., Load-Controlled Roll Transfer of Oxide Transistors for Stretchable Electronics, Adv. Funct. Mater. 23 (2013) 2024–2032.

[6] H. Yabuta, M. Sano, K. Abe, T. Aiba, T. Den, High-mobility thin-film transistor with amorphous InGaZnO4 channel fabricated by room temperature rf-magnetron sputtering, Appl. Phys. Lett. 89 (2006) 112–123.

[7] E.H. Kim, C.W. Yang, J.W. Park, Designing interlayers to improve the mechanical reliability of transparent conductive oxide coatings on flexible substrates, J. Appl. Phys. 111 (2012) 093505.

[8] H.R. Choi, B.C. Mohanty, J.S. Kim, Y.S. Cho, AlN passivation layer-mediated improvement in tensile failure of flexible ZnO:Al thin films., ACS Appl. Mater. Interfaces. 2 (2010) 2471–2474.

[9] Y. Leterrier, É. Polytechnique, F. De Lausanne, C. Fischer, L. Médico, F. Demarco, et al., Mechanical Properties of Transparent Functional Thin Films for Flexible Displays, in: 46th Annu. Tech. Conf. Proceedings,Society Vac. Coaters, 2003: pp. 169–174.

[10] K. a. Sierros, D. a. Banerjee, N.J. Morris, D.R. Cairns, I. Kortidis, G. Kiriakidis, Mechanical properties of ZnO thin films deposited on polyester substrates used in flexible device applications, Thin Solid Films. 519 (2010) 325–330.

[11] Z. Chen, B. Cotterell, W. Wang, The fracture of brittle thin films on compliant substrates in flexible displays, Eng. Fract. Mech. 69 (2002) 597–603.

[12] J.L. Ni, X.F. Zhu, Z.L. Pei, J. Gong, C. Sun, G.P. Zhang, Comparative investigation of fracture behaviour of aluminium-doped ZnO films on a flexible substrate, J. Phys. D. Appl. Phys. 42 (2009) 175404(7pp).

[13] N. Münzenrieder, K.H. Cherenack, G. Tröster, S. Member, A.I. Tfts, The Effects of Mechanical Bending and Illumination on the Performance of Flexible IGZO TFTs, IEEE Trans. Electron Devices. 58 (2011) 2041–2048.

[14] H. Gleskova, S. Wagner, Z. Suo, Failure resistance of amorphous silicon transistors under extreme in-plane strain, 75 (1999) 3011–3013.

[15] A. Kiani, D.G. Hasko, W.I. Milne, A.J. Flewitt, Analysis of amorphous indium-gallium-zinc-oxide thin-film transistor contact metal using Pilling-Bedworth theory and a variable capacitance diode model, Appl. Phys. Lett. 102 (2013) 1–5.

[16] X. Zhu, B. Zhang, J. Gao, G. Zhang, Evaluation of the crack-initiation strain of a Cu–Ni multilayer on a flexible substrate, Scr. Mater. 60 (2009) 178–181.

[17] Z. Chen, B. Cotterell, W. Wang, E. Guenther, S. Chua, A mechanical assessment of flexible optoelectronic devices, Thin Solid Films. 394 (2001) 202–206.

[18] A. Douillard, L. Hardy, I. Stevenson, G. Boiteux, G. Seytre, T. Kazmierczak, et al., Texture and Morphology of Biaxially Stretched Poly (ethylene naphthalene-2, 6-dicarboxylate), J. Appl. Polym. Sci. (2002).

[19] Y. Leterrier, L. Boogh, J. Andersons, J. a. E. Manson, Adhesion of silicon oxide layers on poly(ethylene terephthalate). I: Effect of substrate properties on coating's fragmentation process, J. Polym. Sci. Part B Polym. Phys. 35 (1997) 1449–1461.

[20] C.J. Chiu, S.P. Chang, S.J. Chang, High-performance amorphous indium–gallium–zinc oxide thin-film transistors with polymer gate dielectric, Thin Solid Films. 520 (2012) 5455–5458.

[21] B. Sim, E.H. Kim, J. Park, M. Lee, Highly enhanced mechanical stability of indium tin oxide film with a thin Al buffer layer deposited on plastic substrate, Surf. Coatings Technol. 204 (2009) 309–312.

[22] C.W. Yang, J.W. Park, The cohesive crack and buckle delamination resistances of indium tin oxide (ITO) films on polymeric substrates with ductile metal interlayers, Surf. Coatings Technol. 204 (2010) 2761–2766.

[23] E. Fortunato, P. Nunes, A. Marques, D. Costa, H. Aguas, I. Ferreira, et al., Transparent, conductive ZnO : Al thin film deposited on polymer substrates by RF magnetron sputtering, Surf. Coatings Technol. 152 (2002) 247–251.

[24] S. Frank, U. a. Handge, S. Olliges, R. Spolenak, The relationship between thin film fragmentation and buckle formation: Synchrotron-based in situ studies and two-dimensional stress analysis, Acta Mater. 57 (2009) 1442–1453.

[25] D. Tsubone, T. Hasebe, A. Kamijo, A. Hotta, Fracture mechanics of diamond-like carbon (DLC) films coated on flexible polymer substrates, Surf. Coatings Technol. 201 (2007) 6423–6430.

[26] Y. S. Kim, S. I. oh, S.H. Choa, Mechanical Integrity of Flexible In – Zn – Sn – O Film for Flexible Transparent Electrode, Jpn. J. Appl. Phys. 52 (2013) 05DA17.

[27] L.E. NIELSEN, Mechanical Properties of Polymers and Composites, second Edi, New York: Dekker., 1974.

[28] G.A. Potoczny, Electro-Mechanical Behaviour of Indium Tin Oxide Coated Polymer Substrates for Flexible Electronics by, PhD thesis, University of Birmingham, 2011.

[29] S. Lu, J. Huang, T. Lee, J. Wang, D. Liu, Flexibility of the Indium Tin Oxide Transparent Conductive Film Deposited On to the Plastic Substrate, Smart Sci. 2 (2014) 7–12.

Table captions

Table 1Thermal and mechanical properties of PET and PEN.

Figure Captions

Fig. 1 The bending test set-up used in this study.

Fig. 2. XRD patterns of the bare PEN substrate and IGZO films deposited on PEN at room temperature. Inset shows AFM images of IGZO on PEN substrate.

Fig. 3 Progressive cracking in the IGZO (50 nm) coating on PEN Substrate (a) and on PET substrate (b) at different applied tensile strains. The arrows show failure initiation on the coating.

Fig. 4 (a)3D - AFM image of channel crack path of (50 nm) IGZO/PEN sample, white arrows show straining direction; (b) Cross section view of the channelling crack of (50nm) IGZO/PEN.

Fig. 5 FIB-SEM image of buckling delamination of IGZO (50 nm) film deposited on PEN substrate (a) and on PET substrate (b). Note that black arrows indicate loading direction for 13% applied strain in both cases.

Fig. 6 density vs applied strain for IGZO (50 nm) coating on PET and PEN substrates.

Fig. 7 Sequence of optical micrograph images of cracks morphology in a-IGZO films coated PET under (a-d) tensile buckling mode at different strain bending curvature. The white arrow at 0.9% strain indicates a crack initiation.

Fig. 8 Sequence of optical micrograph images of cracks morphology in a-IGZO films coated PET under (a-d) compressive buckling mode at different strain bending curvature.

Fig. 9 Plot of crack density of a-IGZO thin film coated PET as a function of applied tensile and compression buckling strain.

Fig. 10 SEM micrograph showing crack morphology of a-IGZO after flexed down to 2.7 mm radius of curvature in (a) tensile (b) compression buckling condition.

Table 5

Property	PET Melinex ST 505	PEN Teonex Q65 FA
Glass transition temperature, Tg (°C)	78	119
Melting point, Tm (°C)	257	263
Young's modulus, E (GPa)	3	3.5

Fig. 1

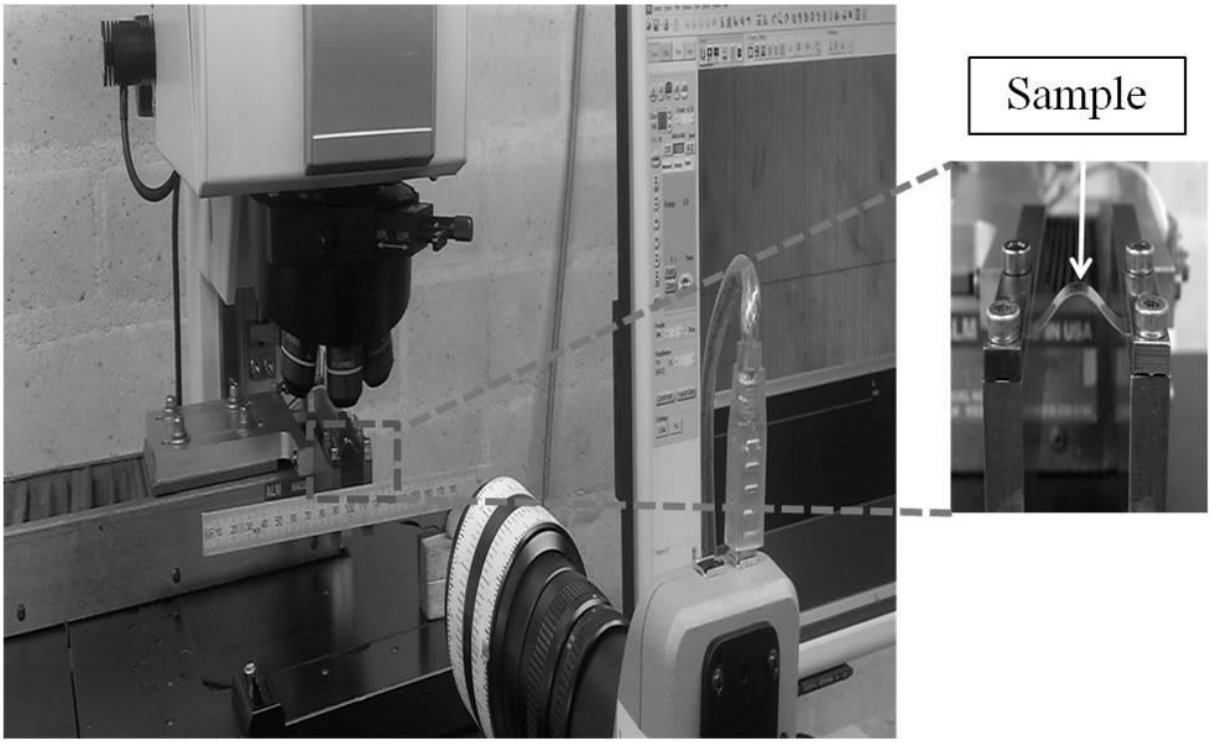

Fig. 2

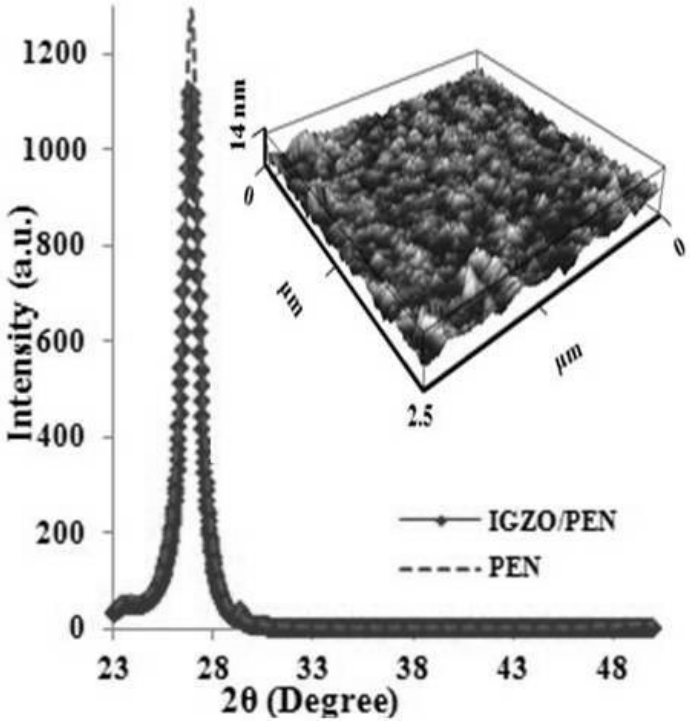
1200
1000
800
600
400
200
0
Intensity (a.u.)
23
28
33
38
43
48
2θ (Degree)
14 nm
0
μm
2.5
μm
0
IGZO/PEN
PEN

Fig. 3

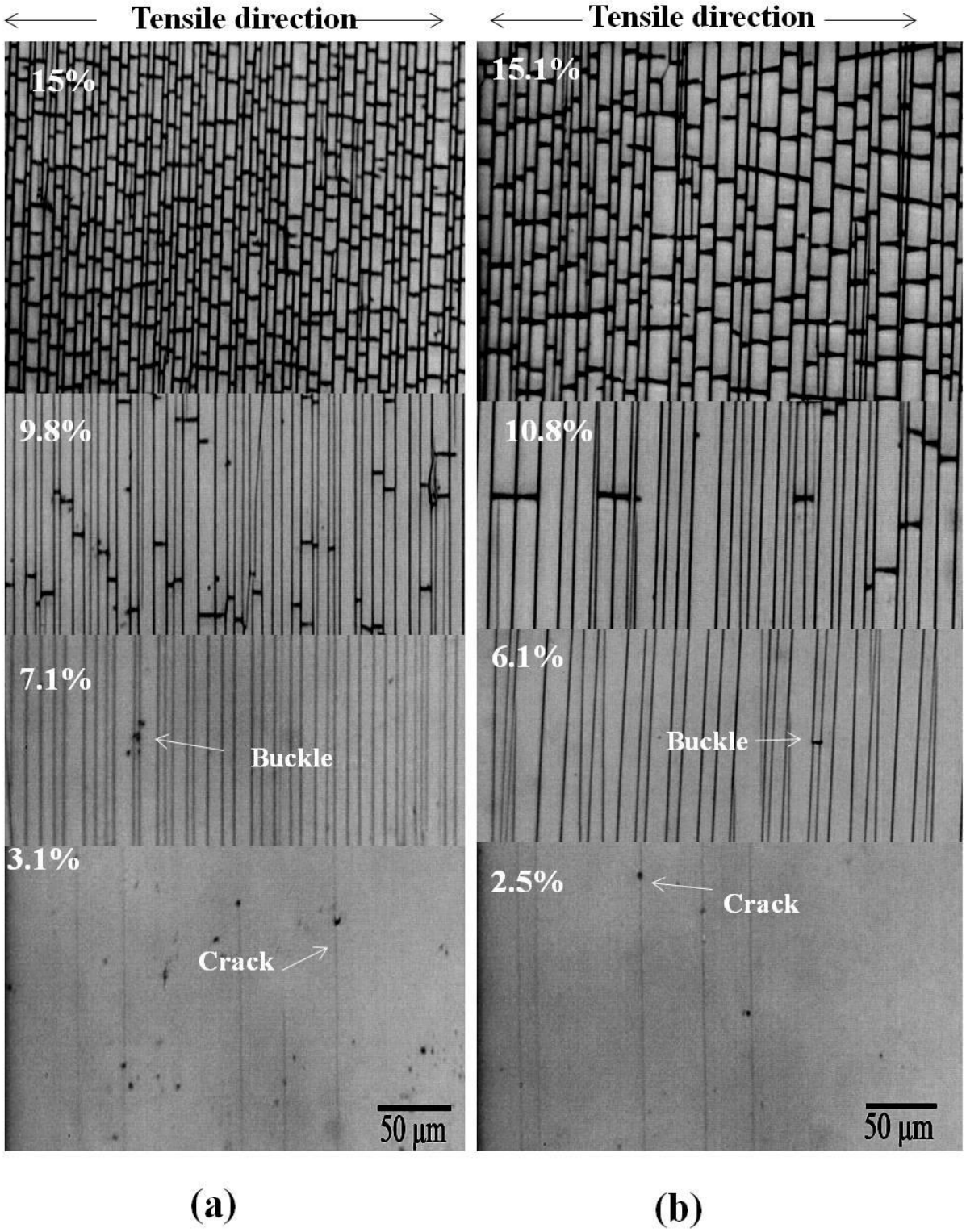
Tensile direction
Tensile direction
15%
15.1%
9.8%
10.8%
7.1%
Buckle
6.1%
Buckle
3.1%
Crack
2.5%
Crack
50 μm
50 μm
(a)
(b)

Fig. 4

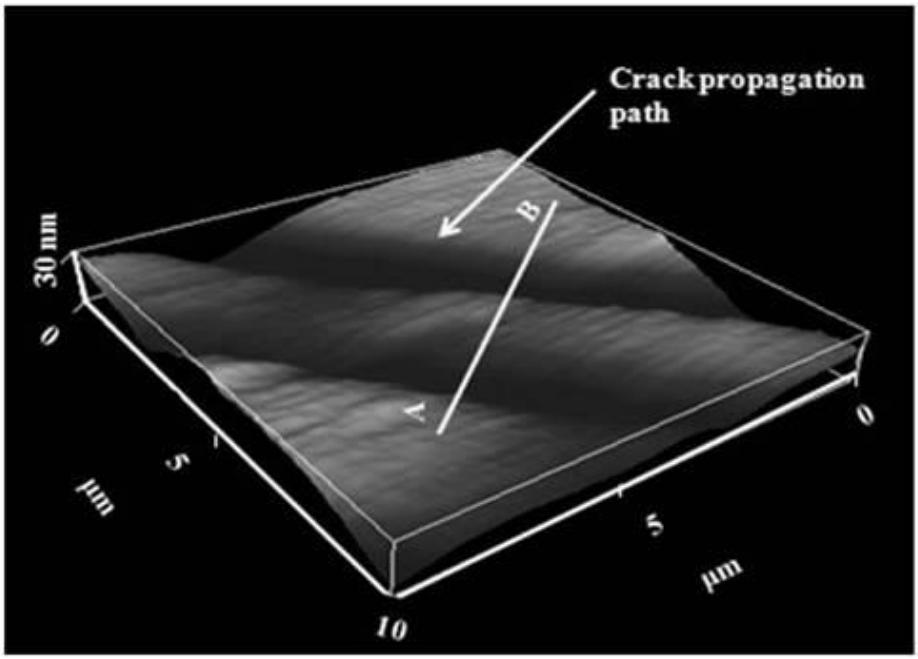
Crack propagation path
B
A
30 nm
0
0
5
μm
5
μm
10

(a)

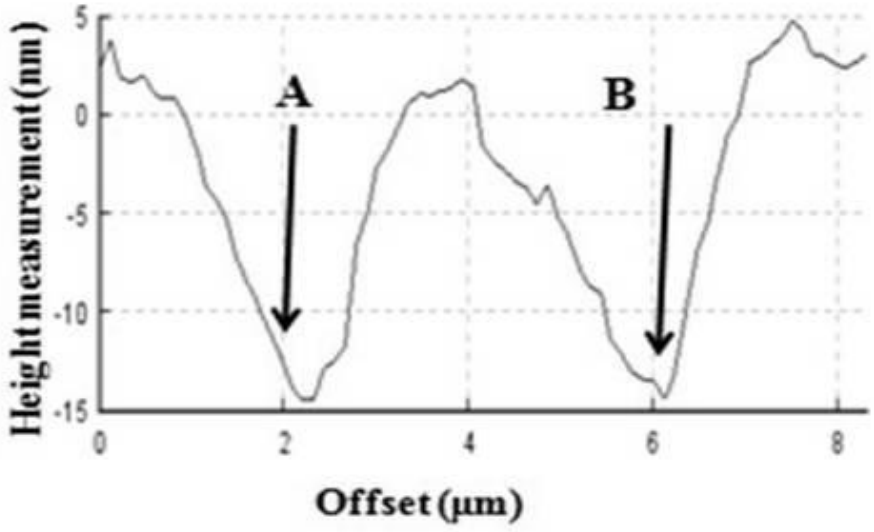
Height measurement (nm)
5
0
-5
-10
-15
A
B
0
2
4
6
8
Offset (μm)

(b)

Fig.5

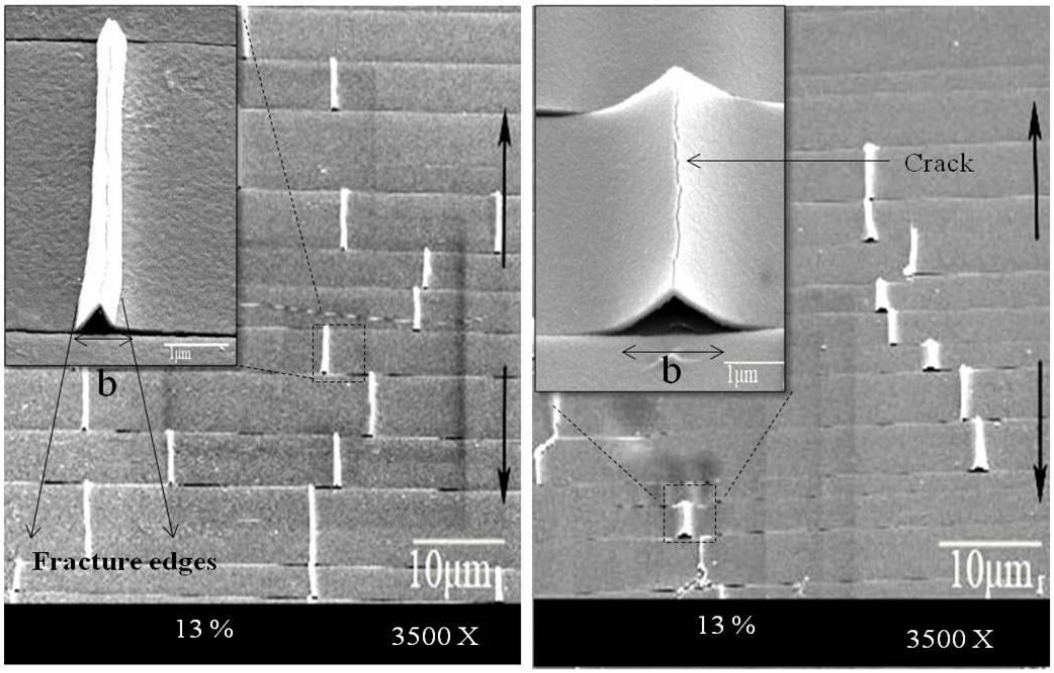
b
1μm
Fracture edges
10μm
13 %
3500 X
(a)
Crack
b
1μm
10μm
13 %
3500 X
(b)

Fig.6

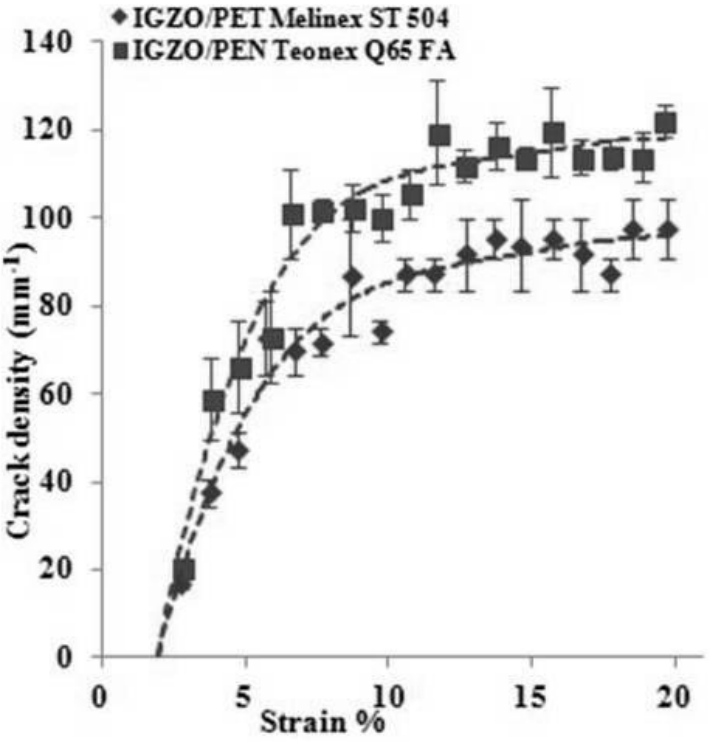
IGZO/PET Melinex ST 504
IGZO/PEN Teonex Q65 FA
Crack density (mm-1)
Strain %
0
20
40
60
80
100
120
140
0
5
10
15
20

Fig.7

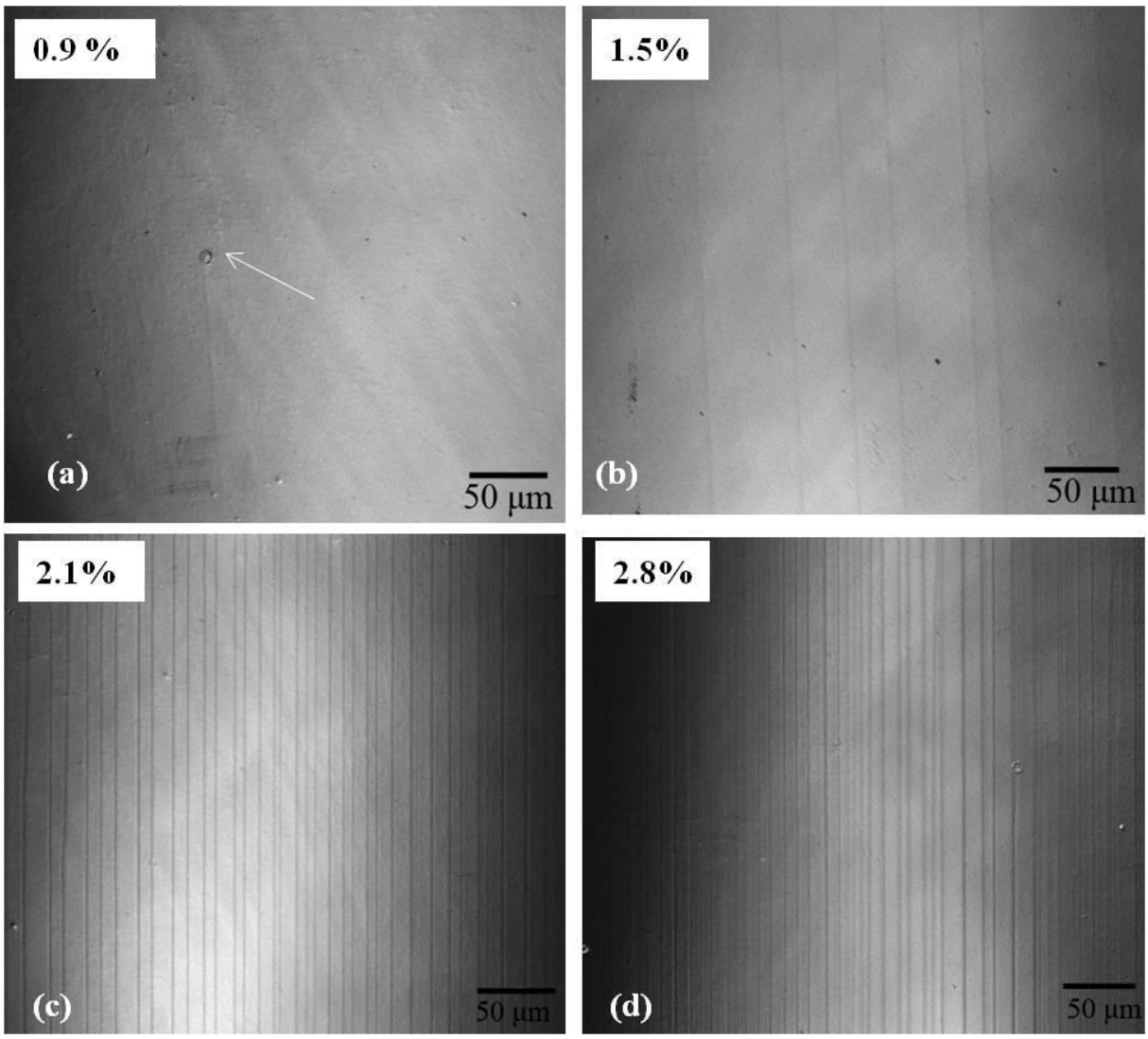

Fig. 8

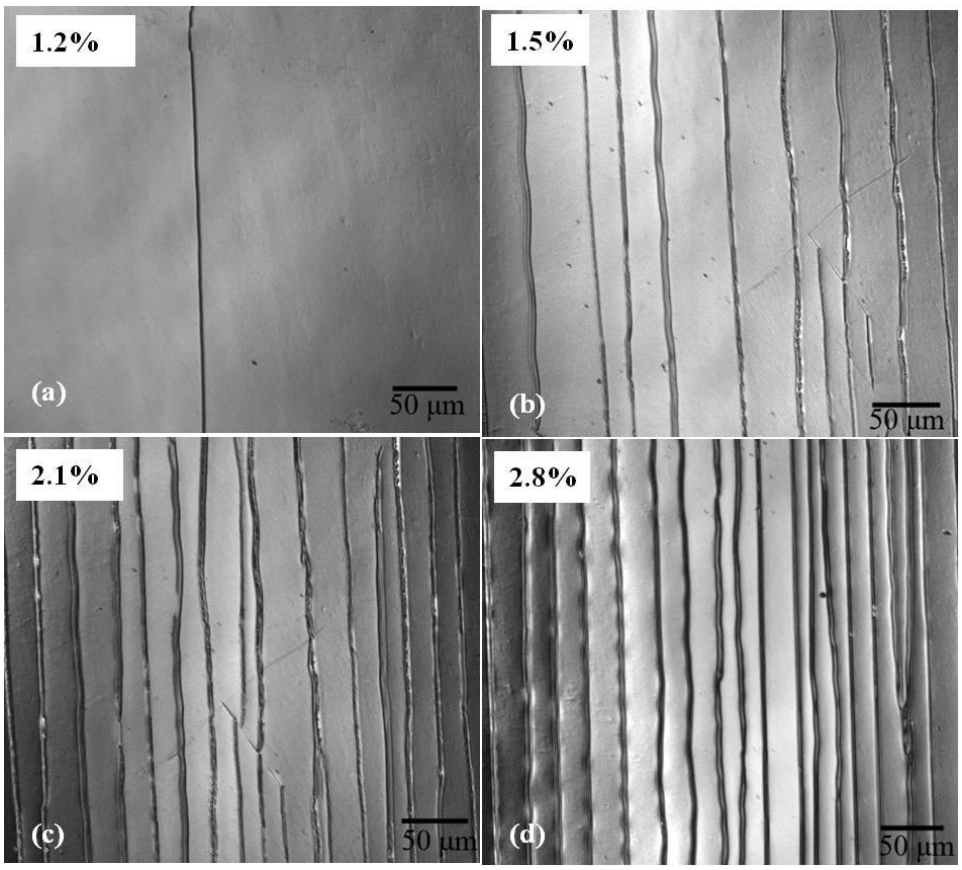
1.2%
(a)
50 μm
1.5%
(b)
50 μm
2.1%
(c)
50 μm
2.8%
(d)
50 μm

Fig. 9

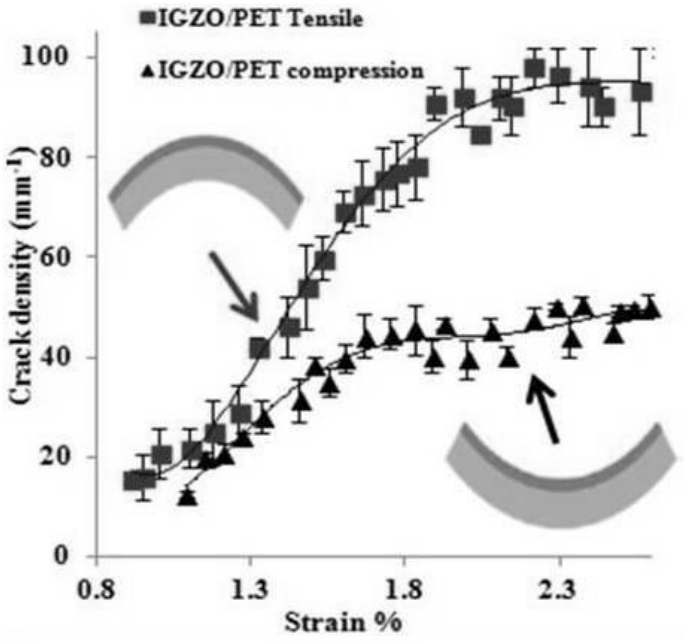
IGZO/PET Tensile
IGZO/PET compression
Crack density (mm-1)
100
80
60
40
20
0
0.8
1.3
1.8
2.3
Strain %

Fig. 10

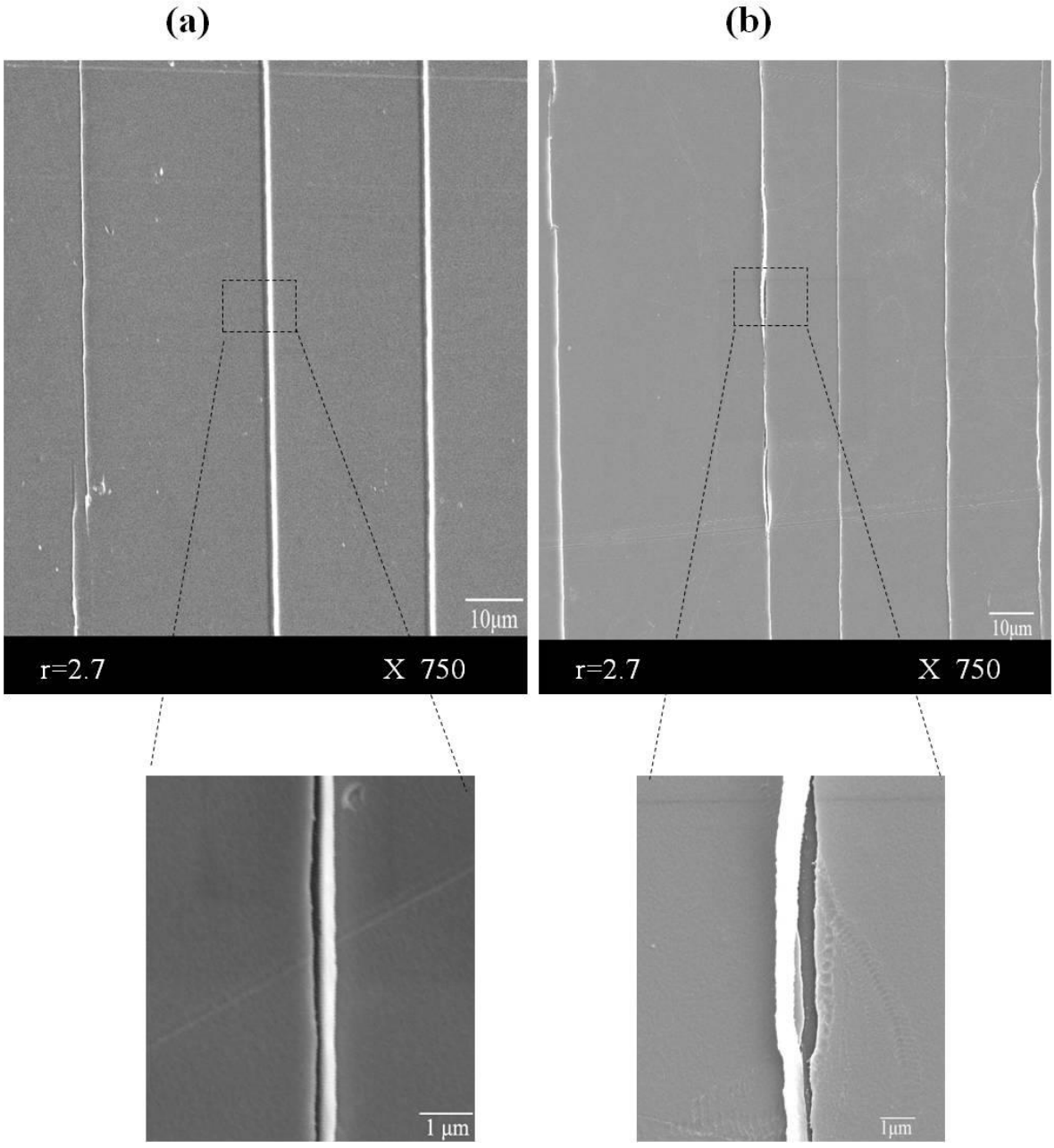

2. Submitted to *Thin Solid Films*

D. W. Mohammed, R. B. Ameen, K. A. Sierros, J. Bowen and S. N. Kukureka. Twisting and twisting fatigue of ITO/Ag/ITO multilayer films on PET substrates used in flexible electronic applications.

11. Appendix B – Conferences

1. Dilveen W. Mohammed, Rob Waddingham, Andrew J. Flewitt, Stephen N. Kukureka: Mechanical properties of a-IGZO thin films on compliant substrates for flexible optoelectronic devices. Poster presented at 10th International Thin–Film Transistor Conference. On January 23-24th, 2014 in Delft University, Netherland.

2. Dilveen W. Mohammed, Konstantinos A. Sierros, Stephen N. Kukureka: Electromechanical Properties of ZnO:Al Thin Films on Polymer Substrates for Optoelectronics Applications. Oral presentation at The International Conference on Metallurgical Coatings and Thin Films or ICMCTF. On April 28-May 2, 2014 at the Town and Country Hotel in San Diego, California, USA.

3. Dilveen W. Mohammed, James Bowen, Stephen N. Kukureka: Electromechanical reliability of ITO/Ag/ITO multilayer coated pet substrate for optoelectronic application. Oral presentation at International Conference on Advanced Materials Science and Technology (ICAMST), on April, 13-14th, 2015 in Venice, Italy.

1. Dilveen W. Mohammed, Konstantinos A. Sierros, James Bowen, Stephen N. Kukureka: The effects of corrosion, fatigue and fatigue corrosion on ITO/Ag/ITO-coated polymer substrates used in solar cell applications. Poster presented at 2nd Asian-European Symposium on Organic Optoelectronics. October 27-29th, 2015 Edinburgh, UK.